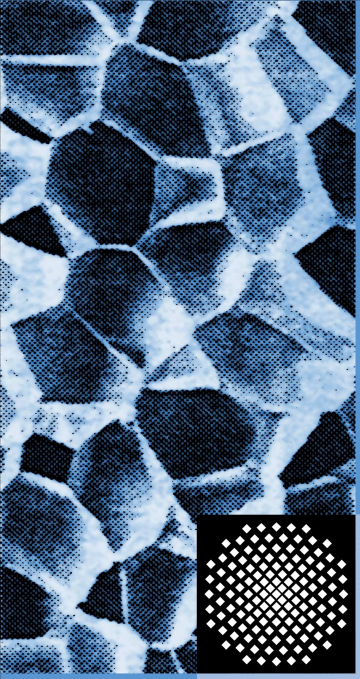

Universität Stuttgart
Germany

Institut für Mechanik (Bauwesen)
Lehrstuhl für Kontinuumsmechanik
Prof. Dr.-Ing. W. Ehlers

Coupled Problems in the Mechanics of Multi-Physics and Multi-Phase Materials

Seyedmohammad Zinatbakhsh

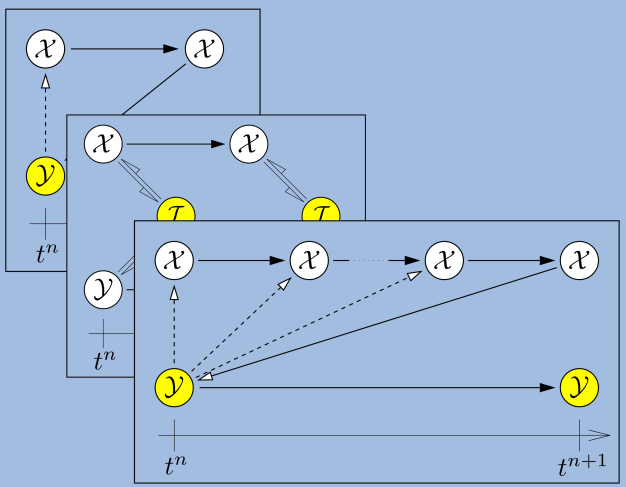

Report No.: II-30 (2015)

Coupled Problems in the Mechanics of Multi-Physics and Multi-Phase Materials

Von der Fakultät Bau- und Umweltingenieurwissenschaften
der Universität Stuttgart zur Erlangung der Würde
eines Doktor-Ingenieurs (Dr.-Ing.)
genehmigte Abhandlung

vorgelegt von

Seyedmohammad Zinatbakhsh, M. Sc.

aus
Shiraz, Iran

Hauptberichter:	Prof. Dr.-Ing. Wolfgang Ehlers
1. Mitberichter:	Prof. Dr.-Ing. Bernd Markert
2. Mitberichter:	Prof. Dr. rer. nat. Barbara Wohlmuth

Tag der mündlichen Prüfung: 7. August 2015

Institut für Mechanik (Bauwesen) der Universität Stuttgart
Lehrstuhl für Kontinuumsmechanik
Prof. Dr.-Ing. W. Ehlers
2015

Report No. II-30
Institut für Mechanik (Bauwesen)
Lehrstuhl für Kontinuumsmechanik
Universität Stuttgart, Germany, 2015

Editor:
Prof. Dr.-Ing. W. Ehlers

© Seyedmohammad Zinatbakhsh
Institut für Mechanik (Bauwesen)
Lehrstuhl für Kontinuumsmechanik
Universität Stuttgart
Pfaffenwaldring 7
70569 Stuttgart, Germany

All rights reserved. No part of this publication may be reproduced, stored in a retrieval system, or transmitted, in any form or by any means, electronic, mechanical, photocopying, recording, scanning or otherwise, without the permission in writing of the author.

Printed by DIP – Digital Print, Witten, Germany, 2015

ISBN 978 – 3 – 937399 – 30 – 5
(D 93 – Dissertation, Universität Stuttgart)

Acknowledgements

The work presented in this doctoral thesis was carried out between the years 2008 and 2015, while I was working as a teaching assistant and a research associate at the Institute of Applied Mechanics (Civil Engineering), Chair of Continuum Mechanics, University of Stuttgart, Germany. Numerous people contributed in many ways to the realisation of this work - all their support is most gratefully acknowledged.

First of all, I would like to sincerely thank my supervisor, Professor Wolfgang Ehlers, for giving me the opportunity to work at his institute, and for his constant support in various aspects of my scientific as well as personal life. I also thank him for the outstanding friendly atmosphere and the companionable relationships at the institute. I would like to express my gratitude to my co-supervisor, Professor Bernd Markert, for inspiring me to start working on this project, and for his direct contribution to the development of a substantial portion of this thesis. My sincere thanks go to the rest of the committee, Professor Barbara Wohlmuth and Dr. rer. nat. Bernd Flemisch, for taking the co-chairs in my promotion procedure and for carefully reading the manuscript. I am also very grateful to Professor Kwang-Chun Park from the Center for Aerospace Structures of the University of Colorado at Boulder, USA, for his supports during and after my visit to the CU Boulder in 2012.

I would like to warmly thank all of my fellow colleagues at the institute, who always shared their experience and knowledge with me. In particular, I am very thankful to Dr.-Ing. Arndt Wagner for many long and fruitful discussions we had, to my long-time roommate Dr.-Ing. Yousef Heider for his goodwill and kindness, and to Maik Schenke, Kai Häberle, Chenyi Luo, Patrick Schröder, Thomas Heidlauf, Michael Sprenger, Lukas Eurich, Davina Fink and all other colleagues for their wonderfully friendly and kind attitude. My appreciations and sincere thanks go to David Koch for his unlimited support within and without the university, for sharing his astonishing open-minded vision and critical viewpoints, and for his selfless and untiring cooperation in the development of final parts of this thesis. I further owe my gratitude to Dr.-Ing. Joffrey Mabuma, Dr. rer. nat. Michael Mayer, Sami Bidier and Faris Bidier for the careful, time-consuming linguistic proofreading of the manuscript.

I would like to deeply thank my parents for always trusting in me and giving me the freedom to make my own choices, and for their limitless encouragement throughout my studies. Last, but by no means the least, my love and most heartfelt thanks go to my adorable wife and my best friend Maryam, without her support and motivation, this journey would not have been possible. I would like to thank her for her everlasting love and continuous belief in me, and for her patience in sharing the frustration as well as the joy of my studies.

Stuttgart, September 2015 Seyedmohammad Zinatbakhsh

Ars longa, vita brevis, occasio praeceps, experimentum periculosum, iudicium difficile.
Hippocrates of Kos (460 B. C. – 370 B. C.)

Contents

List of Figures

Deutschsprachige Zusammenfassung

Motivation und Zielsetzung

Viele ingenieurwissenschaftliche, physikalische, biologische und chemische Fragestellungen erfordern eine umfassende Betrachtung von Systemen mit dynamischer Interaktion zwischen mehreren heterogenen Komponenten. Einige der bekanntesten Beispiele hierfür sind die Interaktion zwischen Deformation und Temperatur bei thermomechanischen Problemen, die gegenseitige Abhängigkeit von Flüssigkeitsdruck und Strukturverschiebung in Konsolidierungsprozessen, der Kräfteaustausch zwischen dem Körper eines Unterseebootes mit dem umgebenden Wasser und Knochenverdichtung als Reaktion auf körperliche Beanspruchungen.

Die mathematische Beschreibung solcher Phänomene mit Hilfe von Kontinuumstheorien, wie beispielsweise der Theorie Poröser Medien (TPM) [77–79, 81, 82], führt häufig auf gekoppelte differential-algebraische Gleichungen (DAE) oder partielle Differentialgleichungen (PDE), die prinzipiell analytisch oder auch numerisch gelöst werden können. Die analytischen Verfahren liefern die exakten Lösungen der Gleichungen. Dennoch können diese Methoden meist nur auf eine eingeschränkte Klasse von Problemen angewandt werden (z. B. lineare Gleichungen mit konstanten Koeffizienten). Darüber hinaus führen analytische Verfahren oftmals zu sehr komplexen Ausdrücken [72], weshalb in vielen Fällen auf numerische Lösungsverfahren zurückgriffen werden muss. Mit Hilfe von numerischen Verfahren kann zwar nicht die exakte Lösung berechnet werden, sie lässt sich jedoch approximieren. Dabei werden die kontinuierlichen Differentialgleichungen durch diskrete ersetzt. Dieses Verfahren wird üblicherweise in zwei Schritten durchgeführt: der räumlichen Diskretisierung und der zeitlichen Integration. Durch die Ortsdiskretisierung werden die räumlichen Ableitungen eliminiert, und es verbleiben nur noch gewöhnliche Differentialgleichungen (ODE), welche zeitlich integriert werden müssen. Diese Integration geschieht gewöhnlich mit Hilfe einer monolitischen oder einer entkoppelten Strategie.

Im Rahmen einer monolithischen Vorgehensweise gilt das gesamte Problem als eine Einheit, für die alle Komponenten simultan, d. h. unter Verwendung identischer zeitlicher Integrationsverfahren und ähnlicher Zeitschrittgröße, aktualisiert werden. Solche Löser sind besonders dann zu bevorzugen, wenn die Kopplung zu hochgradig nichtlinearen Gleichungssystemen führt [188] oder wenn die interagierenden Felder vergleichbare Längenskalen oder Entwicklungsraten aufweisen [100]. Darüber hinaus sei erwähnt, dass monolithische Methoden, die auf impliziten Zeitintegrationsverfahren basieren, zu unbedingt stabilen numerischen Lösungen führen [4]. Monolithische Lösungsmethoden wurden erfolgreich auf verschiedene gekoppelte Probleme angewendet, zum Beispiel Mehrkomponentenmodelle mit chemischen Wechselwirkungen [189, 274], Fluid-Struktur-Interaktion [13, 25] sowie zur Modellierung inelastischer und dynamischer poröser Medien [6, 85, 137, 174, 175, 190].

Die Verwendung monolithischer Lösungsmethoden ist jedoch tendenziell nicht empfeh-

lenswert, wenn das System Komponenten mit stark unterschiedlichen Entwicklungsraten enthält, spezialisierte Löser für die interagierenden Komponenten bereits existieren, oder ein anwendungsorientiertes Problem mit sehr vielen Freiheitsgraden berücksichtigt werden muss. Die Unzulänglichkeit monolithischer Löser in solchen Fällen hat zur Entwicklung entkoppelter Lösungsmethoden geführt.

Entkoppelte Lösungsmethoden lassen sich durch Verwendung unterschiedlicher Techniken, wie räumliche Partitionierung, Zerlegung von Differentialoperatoren, oder einer Kombination aus beidem, entwickeln. Diese Techniken ermöglichen eine Zerlegung des Problems in kleinere Teilprobleme, welche mit Hilfe individuell angepasster Lösungs- und Diskretisierungsalgorithmen für die interagierenden Komponenten parallel oder sequentiell gelöst werden können. Derartige Möglichkeiten haben zur Entwicklung diverser entkoppelter Lösungsmethoden beigetragen. In diesem Zusammenhang seien hier die Anwendungen in Bereichen der Fluid-Struktur-Interaktion [63, 92, 152, 192, 193, 225], Simulation fluidgesättigter poröser Medien [137, 138, 190], Thermoelastizität [4, 252] und Advektions-Diffusions-Kopplung [45, 264] als typische Beispiele genannt. Die Entkopplung der Gleichungen erhöht allerdings das Risiko einer nur bedingt stabilen Lösungsmethode, selbst wenn für jedes Teilproblem unbedingt stabile, implizite Zeitintegrationsmethoden verwendet werden [86, 101, 192]. Die Stabilitätsanalyse ist daher ein äußerst wichtiger Schritt bei der Entwicklung neuer, entkoppelter Lösungsmethoden.

Aus den oben genannten Gründen kann gefolgert werden, dass für die erfolgreiche Einführung einer effizienten Lösungsstrategie je nach Problemstellung zwei Voraussetzungen wesentlich sind: die Bestimmung der Eigenschaften des zu lösenden Problems einerseits und die Kenntnis vorhandener Lösungsoptionen andererseits. Es werden daher in dieser Arbeit wichtige Aspekte der mathematischen Simulation gekoppelter Phänomene im Rahmen der Kontinuumsmechanik untersucht, die Kopplungsmechanismen in verschiedenen Fällen geprüft und die Optionen für eine monolithische oder entkoppelte Lösung der Gleichungssysteme untersucht. Darüber hinaus wird basierend auf der von-Neumann-Methode [48] ein Algorithmus zur Stabilitätsanalyse numerischer Lösungsstrategien eingeführt. Abschließend wird die Anwendbarkeit der vorgestellten Lösungsmethoden auf typische gekoppelte Probleme überprüft und die Übereinstimmung zwischen den Ergebnissen des Stabilitätsanalyse-Algorithmus und den numerisch berechneten Resultaten gezeigt.

Gliederung der Arbeit

Kapitel 1 beinhaltet die Einleitung, den Stand der Forschung und die Ziele dieser Arbeit.

In **Kapitel 2** werden die für diese Arbeit notwendigen Begriffe eingeführt, und es wird die allgemeine Problemstellung erklärt. Insbesondere erfolgt die Definition und die Klassifizierung der sogenannten gekoppelten Probleme. Diese werden anhand von Beispielen aus unterschiedlichen Bereichen erarbeitet.

Nach einem kurzen historischen Überblick zur Frage der mathematischen Modellierung physikalischer Phänomene folgen in **Kapitel 3** die notwendigen Grundlagen der Kontinuumsmechanik und außerdem die benötigten Konzepte der Theorie Poröser Medien (TPM). Insbesondere werden differential-algebraische Gleichungen, partielle Differentialgleichun-

gen und die Besonderheit der steifen Differentialgleichungen erörtert. Im Weiteren wird der Begriff der algebraischen Nebenbedingungen genauer untersucht. Es folgen Methoden zur Überwindung der durch diese Bedingungen entstehenden numerischen Schwierigkeiten.

Kapitel 4 beschäftigt sich mit Lösungsmethoden von Differentialgleichungen im Allgemeinen und mit der numerischen Behandlung gekoppelter Differentialgleichungssyteme im Speziellen. In diesem Zusammenhang werden die monolithischen und entkoppelten Lösungsstrategien betrachtet und ihre jeweiligen Vor- und Nachteile erläutert. Hierbei werden zunächst unterschiedliche Methoden für räumliche Partitionierung vorgestellt und die Gemeinsamkeiten zwischen diesen verdeutlicht. Im Anschluss wird der Prozess der Zerlegung von Differentialoperatoren betrachtet und die daraus resultierenden Lösungsstrategien in einen größeren Zusammenhang gestellt.

Kapitel 5 konzentriert sich auf die Stabilitätsanalyse der numerischen Zeitintegrationsverfahren. In einem ersten Schritt werden die grundlegenden Begriffe, Definitionen und die Notation eingeführt. Anschließend werden spezifische Kriterien für die Stabilität der numerischen Lösungen und ihre Beziehung zueinander erläutert. Zum Schluss wird ein pragmatischer Algorithmus für die Stabilitätsanalyse numerischer Verfahren entwickelt.

Die nächsten zwei Kapitel beinhalten die praktische Anwendung der vorgestellten Lösungsmethoden und des entwickelten Stabilitätsanalyse-Algorithmus. Es werden mehrere volumen- und oberflächengekoppelte Probleme betrachtet. Die Ergebnisse dazu sind in **Kapitel 6**, bzw. in **Kapitel 7** dargestellt.

Zum Schluss gibt **Kapitel 8** eine kurze Zusammenfassung und Vorschläge zur Weiterarbeit auf diesem Gebiet.

Darüber hinaus wird in **Anhang A** eine detaillierte Stabilitätsanalyse einer entkoppelten Lösungsmethode auf das volumengekoppelte Problem der Thermoelasitizät angewendet. In **Anhang B** erfolgt die Anwendung der Stabilitätsanalyse auf das oberflächengekoppelte Problem der Interaktion zwischen porösem Medium und Fluid.

List of Acronyms

Acronym	Description
1-d	one-dimensional
2-d	two-dimensional
3-d	three-dimensional
a. m.	above mentioned
m.o.m.	moment of momentum
w.r.t.	with respect to
ADI	alternating direction implicit method
ALE	arbitrary-Lagrangean-Eulerian
B. C.	before Christ
BC	boundary conditions
BDD	balancing domain decomposition
BDF	backward differentiation formulae
BEM	boundary element method
BGS	block-Gauss-Seidel
BJ	block-Jacobi
CD	central difference
CFL	Courant, Friedrichs and Lewy (the convergence condition)
CSI	control-structure interaction
CSS	conventional serial staggered
DAE	differential algebraic equations
DD	domain decomposition
DE	differential equations
DOF	degrees of freedom
EEM	explicit Euler method
ERK	explicit Runge-Kutta method
FD	finite difference
FDE	finite-difference equations
FDM	finite-difference method
FEM	finite-element method
FETI	finite-element tearing and interconnect
FPMI	fluid-porous-media interaction
FSI	fluid-structure interaction
FVM	finite-volume method

GLM	global Lagrange multipliers
IBVP	initial-boundary-value problem
IC	initial conditions
IEM	implicit Euler method
IPS	improved parallel staggered
IRK	implicit Runge-Kutta
ISS	improved serial staggered
LBB	Ladyzhenskaya-Babuška-Brezzi
LHS	left-hand side
LLM	localised Lagrange multipliers
MED	modified Eulerian description
NSC	necessary stability condition
ODE	ordinary differential equations
OSS	operator-splitting scheme
PANDAS	porous media adaptive nonlinear finite element solver based on differential algebraic systems
PDE	partial differential equations
PMD	porous-media dynamics
REV	representative elementary volume
RHS	right-hand side
SCM	Schur complement method
SSI	structure-structure interaction
TED	thermo-elastodynamics
TM	theory of mixtures
TPM	theory of porous media
TR	trapezoidal rule

Chapter 1:
Introduction and Overview

In this monograph, the important aspects regarding the mathematical simulation of coupled multi-field phenomena in the framework of continuum mechanics are studied. To this end, the coupling mechanisms in various cases are investigated, and the options for the numerical solution of the corresponding governing equations are explored. In particular, different monolithic and decoupled solution approaches are scrutinised. It is endeavoured to answer the question whether it is necessary to solve a system of coupled equations monolithically including the numerical complexity of the coupled problems, or if decoupling methods can be applied yielding almost the same quality of results but at lower numerical costs. Moreover, a framework for the stability analysis of numerical solution strategies is introduced, and an easy-to-use procedure to find the necessary stability condition, based on the method of von Neumann, is provided. Subsequently, the applicability of the presented strategies for the numerical treatment of representative coupled problems is demonstrated, and the consistency of the outcomes of the stability analysis algorithm with results obtained from numerical solution of the problems is investigated.

1.1 Motivation

Many problems in engineering, physics or other disciplines require an integrated treatment of coupled heterogeneous fields. Some of the typical examples are the deformation of a bimetallic strip as a response to the alteration of the temperature (coupled problem of thermoelasticity), the interdependence of the pore pressure and the deformation of the solid skeleton in the processes of soil liquefaction and consolidation (porous-media dynamics), the interchange of the forces between the body of a submarine with water (fluid-structure interaction), and bone densification in response to physical exercises (process of bone remodelling). The mathematical modelling of such phenomena often results in systems of coupled partial differential equations (PDE) or differential algebraic equations (DAE) in space and time, which could, in principle, be solved employing an analytical or a numerical scheme.

The analytical approaches are based on calculating the exact solution of differential equations in their continuous form. Nevertheless, these schemes can only be applied to a restricted class of problems (e. g. linear, constant-coefficient equations) and, moreover, the expressions for them are often very complicated, cf. DuChateau & Zachmann [72]. Therefore, considerable progress has been made in the development of schemes for an approximate solution of coupled systems of equations. It has resulted in a wide spectrum of numerical approaches. Here, the idea is to replace the continuous differential equations by discrete algebraic ones, which could be solved much easier. This process is usually performed in two steps, namely spatial discretisation and temporal integration of the equations.

The spatial discretisation of the equations eliminates the spatial derivatives. It transforms a coupled PDE system to a system of coupled ordinary differential equations (ODE) in time, which should be temporally integrated. The temporal integration is commonly done following a monolithic or a decoupled strategy.

Following a monolithic strategy, the whole problem is considered as a monolithic entity. Thus, the time integration of all components is performed simultaneously, using identical time-advancing scheme and time-step size. Such a procedure, provided exploiting an implicit time-stepping method, produces unconditionally stable numerical results. However, the holistic approach of the monolithic schemes has certain disadvantages. In particular, using an identical time-step size for the time integration of a system containing components with very different evolution rates proves to be inefficient. Furthermore, the monolithic schemes generally prohibit using the existing solvers in a modular manner and, thus, require a special solution algorithm for each individual coupled system. Apart from that, the spatial discretisation of problems defined on large spatial domains produced huge ODE systems, the simultaneous treatment of which can be computationally too expensive. To break down the problem into several subproblems is a promising approach to overcome these limitations. This is the main motivation behind the development of decoupled solution schemes.

Decoupled solution strategies are usually based on the partitioning of the spatial domain into smaller subdomains, the splitting of the differential operators into simpler sub-operators, or a combination of both techniques. The resulting smaller or simpler subproblems may be solved in a parallel or in a sequential manner, using tailored discretisation and solution algorithms for individual subsystems. Nevertheless, assembling a decoupled solver is a rather technical procedure that should be done very carefully. In particular, selection of the decoupling strategy and, as well, the sequence of time integration of the subsystems are not trivial. This is mainly because a decoupled solution of a coupled system of equations produces some errors, that may result in conditional stability of the scheme, cf., for example, Ehlers *et al.* [86] or Felippa *et al.* [101]. This can be the case even if each subproblem is treated by unconditionally stable, implicit time-stepping methods as stated by Matthies *et al.* [192]. Consequently, to execute an appropriate stability analysis in order to establish the stability criterion for the partitioned algorithms becomes a pertinent step in studying this class of solution strategies.

In conclusion, to choose or to design an efficient solution strategy for each problem has to be done based on the characteristics of that specific case. To this end, the characteristics of coupled systems and the differences between various types of coupled phenomena must be firstly clarified. Moreover, the miscellaneous monolithic and decoupled solution strategies have to be investigated. It is essential to achieve a good understanding of these solution schemes in order to be able to compare them with each other and, hence, to select an appropriate strategy for the solution of the problem at hand. Apart from that, and as it was already mentioned, each decoupled solution scheme should be accompanied by a thorough stability analysis. This urges a careful exploration of different stability criteria in order to propose an applicable algorithm, which can be employed to reveal the necessary stability conditions for numerical solution methods. To cover these topics and to investigate their relevant issues highlight the main contributions of this thesis.

1.2 State of the art

Preliminaries: terminologies and classifications

The term "coupled problems", or more precisely "coupled multi-field problems", is used as an umbrella covering a plethora of phenomena in science and engineering. These phenomena describe an inherent dynamic interaction[1] among two or more heterogeneous components. The interaction may happen on the common boundaries separating the adjacent subdomains, or within the same spatial domains, in which cases one respectively encounters a *surface-coupled* or a *volume-coupled* problem. Famous examples include the surface-coupled problems of fluid-structure interaction (FSI) studied by Bathe *et al.* [14], Degroote *et al.* [63], Hübner *et al.* [145], Joosten *et al.* [152], Matthies *et al.* [192], Matthies & Steindorf [193], Morand & Ohayon [202], Piperno *et al.* [225], and its variations as aeroelasticity presented by Farhat & Lesoinne [92], Lin & Farhat [178], Piperno & Farhat [224], and the volume-coupled problems of poroelasticity discussed by Heider [137], Heider *et al.* [138], Markert *et al.* [190], Zienkiewicz *et al.* [288], and thermo-elastodynamics and thermoelasticity studied by Argyris *et al.* [3], Armero & Simo [4], Simo & Miehe [252].

According to Felippa & Park [100], the heterogeneity is commonly due to the physical distinction between the components (multi-physics problems), the diversity of the exploited computational methods (multi-processing problems), or the difference in the physical scales of the interacting systems (multi-scale problems). A reinterpretation of this classification has been presented by Markert [188]. Following his proposition, every coupled problem is per se a coupled-multi-field problem, wherein the individual field equations are functions also of the other field variables. Furthermore, he modifies the concept of multi-physics problems to be the ones comprising either different computation techniques for interacting components, or different field variables representing various physical phenomena. Thus, the multi-scale and multi-processing problems in the sense of Felippa & Park [100] lie within the category of multi-physics problems in the sense of Markert [188]. This, however, leads to some contradiction between these classifications. To make the point clear, consider the problem of consolidation with the solid displacement and the pore-fluid pressure as the coupled field variables. Then, proceeding from the definitions proposed by Felippa & Park [100] and considering that the solid displacement and the pore-fluid pressure are different physical properties, consolidation should lie in the category of the coupled multi-physics problems. Nevertheless, this problem comprises only one physical phenomenon and, hence, this is a multi-field, but no multi-physics problem in the sense of Markert [188].

What was mentioned is not the only diversity in the terminologies presented in the coupled-phenomena-related publications. This is mainly because the broad domain of research areas in which coupled systems are seen has attracted specialists from different disciplines, who study the problem from different angles. Therefore, the initial essential steps in exploring the coupled phenomena is to get familiar with the different nomenclatures and, consequently, to choose a rigorous terminology that best suits the nature of the project at hand. In this regard, some of the consistent reference works are presented

[1] "Dynamic" in the sense of "active", opposed to "passive".

by Felippa & Geers [99], Felippa & Park [100], Hameyer *et al.* [133], Lewis [173], Markert [188], Matthies *et al.* [192] and Matthies & Steindorf [193]. In this thesis, a modified version of the terminology presented by Markert [188] is suggested. This terminology accompanied by several illustrating examples are presented in Chapter 2.

Simulation and mathematical modelling

After identification of coupled systems, it is of utmost interest to establish sound mathematical models for them. These models are utilised in order to predict the response of the systems due to changes in the external conditions. Focusing on the transient multi-field coupled systems arising in the engineering applications, the mathematical modelling could usually be done in the framework of continuum theories. Therein, the evolution of the field variables, or degrees of freedom (DOF), is governed by some conservation principles or balance laws combined with thermodynamically admissible constitutive relations. This combination, when complemented by sets of initial and boundary conditions, builds a closed partial differential equations (PDE) or differential algebraic equations (DAE) system in space and time, the solution of which deterministically reveals the response of the system to the external excitations.

The roots of the theory of continuum mechanics can be traced back to the classic works of René Descartes, Isaac Newton, Leonhard Euler and other outstanding figures of the 17th, 18th and early years of the 19th centuries. In the modern age, further extension of the classical theories towards more enhanced methods for macroscopic description of the motion of the mutli-phasic materials has led to the development of the Theory of Mixtures (TM) by Truesdell [269], the augmentation of which, through inclusion of the concept of volume fractions by Bowen [30, 31], followed by the several treatises of de Boer & Ehlers [27] and Ehlers [77–79, 81, 82] has led to rise of the modern Theory of Porous Media (TPM). In this regard, comprehensive reviews of the development of the classical continuum mechanics are presented by Truesdell [265, 266], Truesdell & Noll [267] and Truesdell & Toupin [268]. A brief review is also presented in Section 3.1 of this thesis. Furthermore, Ehlers [83] provides a historical account of development of the TPM.

In this monograph, selected fundamental concepts of the theory of continuum mechanics, and also of the TPM will be presented in Chapter 3. It will be discussed that, in the framework of continuum mechanics, the mathematical models corresponding to the coupled phenomena happen to be coupled systems of differential equations, which have to be solved. The solution may, in principle, be performed following either an analytical or a numerical approach.

Solution methods

Exploiting an analytical solution method, one aims to treat the differential equations in their continuous form, such that the exact solution of the system can be found. Some of the most popular techniques used in this context are based on separation of variables, Fourier series, Fourier transform, Laplace transform, and the method of characteristics, cf. DuChateau & Zachmann [72]. Focusing on the coupled multi-field problems as the

main concern of this contribution, the analytical approaches have been successfully implemented for treatment of porous media problems, both in quasi-static situation, cf. Cheng & Detournay [51], and also poroelastodynamics, see, e. g., de Boer *et al.* [28] and Schanz & Cheng [241]. The interested reader may also refer to Schanz [240] and the references therein for an overview on poroelastodynamic models and their analytical solutions. See also the review article by Selvadurai [249] presenting more analytical solutions of the porous media problems, especially in geomechanics.

Nevertheless, usage of the analytical solvers is restricted to fairly simple cases, for instance, one-dimensional (1-d) problems with linear, constant-coefficient equations. This is mainly due to the complexity of the analytical methods and their rather complicated expressions. In particular, analytical solution of a coupled PDE system generally proves to be too cumbersome, if not entirely impossible. This has contributed to the development of a vast number of numerical solution schemes that are specialised to solve various coupled problems.

Employing a numerical solution method, the computational treatment of a coupled PDE system is done after spatial and temporal discretisation of the continuous equations. Apart from some special solution approaches like the space-time Galerkin method discussed by Donea & Huerta [67], and the characteristic method presented by Pironneau [226], where the spatial and temporal discretisations are done simultaneously, the discretisations are commonly performed separately, within consecutive steps.

The spatial semi-discretisation is commonly done by the finite-element method (FEM), cf., e. g., Bathe [12], Belytschko *et al.* [17], Hughes [146] or Zienkiewicz & Taylor [290], the finite-difference method (FDM), cf., e. g., Mitchell & Griffiths [200], Morton & Mayers [203] or Thomas [263], the finite-volume method (FVM), cf., e. g., LeVeque [172] or Versteeg & Malalasekera [273] or the boundary-element method (BEM), cf., e. g., Banerjee [8], Gaul *et al.* [113] or Wrobel & Aliabadi [283]. This process results in a coupled system of ordinary differential equations (ODE) in time that should be numerically integrated. In this conjunction, the strategies for the time integration of transient coupled systems of equations can be assigned to three major groups, namely the field variable elimination strategies, the monolithic schemes, and the decoupled solution approaches.

In the variable elimination, exploiting different techniques such as integral transforms or model reduction reduces the number of dependent variables and, hence, the number of equations, without altering the solvability of the problem, cf. Zienkiewicz [287]. A typical example is the formulation of a heat diffusion problem, which depicts a coupled problem with two variables, namely the heat flux and the temperature. There, an explicit interpretation of the heat flux in terms of the temperature facilitates the elimination of the former, and facilitates a reformulation of the equation system in terms of one single variable, i. e., the temperature [287]. Artificial intelligence and computer science are other fields of application where the variable elimination method is used for constraint processing [170] and production of the constraint elimination algorithm [29, 62, 170]. The interested reader may also refer to Coelho *et al.* [53] for more practical cases in the multi-disciplinary optimisation problems.

Nevertheless, the feasibility of variable elimination at the differential equation level is

restricted to special linear problems as stated by Felippa & Park [100][2]. Moreover, the process of field elimination often introduces fully populated unsymmetric coefficient matrices or higher order temporal derivatives and, therefore, cause numerical difficulties, cf. Felippa & Park [100] and Markert [188, 189]. In this regard, the monolithic and decoupled treatments are more general in nature.

Monolithic schemes

The monolithic solution methods, also known as simultaneous, coupled, or direct schemes, are based on a holistic treatment of the coupled PDE system. Such a process entails a simultaneous integration of all components using a unique time-stepping scheme and time-step size. These solvers are especially preferred when the coupled field interaction is highly nonlinear [188], or the interacting fields possess comparable length scales or evolution speeds [100]. Furthermore, employing an implicit time integration, monolithic schemes result in unconditionally stable numerical solutions independent of the machine accuracy and occurring errors, cf. Armero & Simo [4].

The monolithic solution methods have been successfully applied to different coupled problems. Some of these applications include multicomponent porous media problems with chemical interactions, cf., e. g., Markert [189] and Wagner [274], fluid-structure interaction, cf., e. g., Bathe *et al.* [13] and Blom [25], multi-field problems in structural dynamics, cf. Kuhl [163], and inelastic and dynamic porous media problems describing consolidation and deformation of elastoplastic porous media, see Avci [6], Ehlers & Wagner [85], Heider [137], Lewis *et al.* [174, 175] and Markert *et al.* [190]. The interested reader can consult Hübner *et al.* [145], Michler *et al.* [197] and references therein for more examples.

However, discrete equation systems of real-size problems may contain millions of evolution equations. Thus, monolithic solution of such problems incurs huge computational cost, such that the computational burden can quickly become prohibitively large for multidimensional simulations. Moreover, monolithic integration is performed without distinguishing between different subsystems and regardless of the specialised solvers that may exist for them. As a consequence, each coupled problem requires a special unified simulator, which can be applied to the overall system. It, on the one hand, makes the monolithic solvers very case-specific and often only semi-optimal. On the other hand, to develop a global structure for simultaneous treatment of the coupled PDE systems is a tedious task, involving complicated code management that at best could be done with the facilities available in the industrial rather than academic environments, as is presented, for example, by Padula *et al.* [209] and Weston *et al.* [280]. Apart from that, exploiting identical time-step sizes for all processes within the problem may be disadvantageous. In particular, using identical time-step sizes for time integration of the problems including processes with drastically different evolution speeds causes redundant calculations.

Attempts to overcome these flaws have given rise to the development of various solution schemes based on the domain decomposition (DD), the spatial partitioning, and the

[2]It is interesting to note that following the nomenclature proposed by Zienkiewicz [287], a coupled formulation is one, in which neither set of dependent variables can be explicitly eliminated. Instead, he places these problems under the category of mixed formulation problems.

operator splitting, as we shall see next.

Domain decomposition and partitioning

The roots of domain decomposition methods can be traced back to the second half of the 19th century. By that time, it appeared that a specific differential equation, nowadays known as the Laplace's equation, plays an important role in a wide spectrum of applications in physics and mathematics, ranging from the fluid mechanics of Euler [88] and the theory of heat transfer of Fourier [105] to the complex analysis of Riemann [232]. Because of that, to solve the Laplace's equation on bounded domains attracted a lot of interest amongst researchers. It was especially due to the fact that the solution methods available by then were only able to solve the Laplace's equation on geometrically simple circular and rectangular domains, cf. Gander & Wanner [111]. More crucially, even to prove the existence and uniqueness of the solution of the Laplace's equation on arbitrary domains appeared to be formidable. In this regard, and in an attempt to verify the validity of the Dirichlet's principle[3] in geometrically complex domains, the first domain decomposition method was designed and published by H. A. Schwarz in his classic work of 1870 [248].

In its original form, the so-called Schwarz alternating method provides a framework for iterative solution of the Laplace's equation in a complex domain subjected to arbitrary Dirichlet boundary conditions. To this end, the domain is firstly broken down into two (or more) simpler "overlapping" subdomains, for which the problem could readily be solved. The overlapping should be such that the boundary of each subdomain consists of two parts: an external boundary belonging to the original complex domain, and an internal boundary which lies within another subdomain. Then, the problem is solved within the subdomains in a sequential iterative manner by passing data from one subdomain to the other as Dirichlet boundary conditions through the respective internal boundaries. Schwarz showed that following this procedure, the iterative solutions found within subdomains eventually converge to one unique function: the solution of the Laplace's equation within the original complex domain. Based on this, he inferred the existence and the uniqueness of the solution for the Laplace's equation within a complex domain subjected to arbitrary Dirichlet boundary conditions, and deduced the validity of the Dirichlet's principle.

During the next decades, the potential of Schwarz's idea in treating the partial differential equations within complex domains inspired the development of dozens of DD strategies: to overcome the serial nature of the alternating method, a parallel version of the scheme was introduced by Lions [179], applying the idea to the discretised version of the Laplace's equation led to multiplicative (Gander [110]), additive (Dryja [68], Dryja & Widlund [71]), and restricted additive (Cai & Sarkis [44]) Schwarz methods. Further, noticing the deficiency of the method in being restricted to overlapping subdomains, a modified version

[3]The Dirichlet's principle, named by Bernhard Riemann (1826 – 1866) after Peter Gustav Lejeune Dirichlet (1805 – 1859), addresses the existence and uniqueness of the solution of the Laplace's equation on arbitrary domains with Dirichlet boundary conditions, cf. Courant [56]. The Dirichlet's principle was assumed valid until 1869, as it was put under question by Karl Theodor Wilhelm Weierstrass (1815 – 1897), cf. Kudryavtsev [162]. This critique was challenged one year later by Karl Hermann Amandus Schwarz (1843 – 1921), cf. Gustafson [125].

for handling "non-overlapping" subdomains was also proposed by Lions [180], wherein the data transmission between the subdomains could take place via Dirichlet, Neumann or Robin conditions. An interpretation of this method using Lagrange multipliers was later performed by Glowinski & Le Tallec [115]. Moreover, in an effort to enhance the convergence properties of the scheme, the so-called optimised Schwarz methods were proposed by Gander [109].

Focusing on the surface interaction among non-overlapping subdomains, the ideas of DD also provide a suitable framework for decoupled solution of surface-coupled problems via partitioning schemes. Note that within this report, the process of partitioning addresses a certain class of decoupling method, accomplished via field-by-field decomposition of the spatial domain of a surface-coupled problem into several non-overlapping subdomains. Doing so, one wishes to separate the "distinct" governing equations of the subdomains from one another, such that each resulting subproblem could be solved using optimal, tailored solution methods, possibly by individual time steps. On the contrary, the domain decomposition methods aim at simplifying the task of the solution of "one same" differential equation which governs the process within the whole domain by splitting a complex domain into several simpler subdomains. Consequently, following the DD methods, one ends up with simpler subdomains governed by "similar" differential equations. However, whether utilising a DD strategy or following a partitioning scheme, the mathematical model would comprise the governing equations of the subdomains subjected to some interface consistency constraints. In this regard, employing a staggered solution method based on the block-Gauss-Seidel (BGS) or the block-Jacobi (BJ) data transfer strategy has proved to be a practical procedure for decoupled solution of the problem, see Joosten *et al.* [152], Matthies *et al.* [192] and Matthies & Steindorf [193]. These staggered time-marching algorithms are introduced in Section 4.3.1. Apart from that, the problem can be seen as a constrained optimisation problem, which, depending on the strategy chosen for enforcement of the constraints, may be tackled in different ways. In particular, explicit or implicit enforcement of the constraints has resulted in the development of the primal and the dual Schur complement methods, respectively.

The first member of the family of Schur complement methods was introduced in 1963 by Przemieniecki [228] as a tool for elastic analysis of aircraft structures. Originally named substructuring, Przemieniecki designed his method to facilitate different types of analyses on different subdomains (substructures) in order to cope with inadequate capacity of the available computers. To realise this goal, the complex structure is firstly divided into simpler substructures. Following that,

> *"... each substructure is first analyzed separately, assuming that all common boundaries (joints) with the adjacent substructures are completely fixed; these boundaries are then relaxed simultaneously and the actual boundary displacements are determined from the equations of equilibrium of forces at the boundary joints. The substructures are then analyzed separately again under the action of specified external loading and the previously determined boundary displacements."* [228]

As will be demonstrated in Section 4.3.2, the second step of this procedure to determine the boundary displacements entails the solution of a reduced equation system which con-

tains the Schur complement[4] of the matrix of coefficients; hence the name of the method. Furthermore, due to fact that this formulation is based on an explicit enforcement of the consistency of boundary displacements (the primary variable), the Przemieniecki's substructuring lies in the category of primal Schur complement methods.

Solution of the interface reduced system is sometimes done iteratively as presented by Bjørstad & Widlund [24], Bryant *et al.* [37] and Dryja & Widlund [70]. There, considering the symmetry and the positive definiteness of the Schur complement, the iteration is performed following the preconditioned conjugate gradient algorithm described by Hestenes & Stiefel [141]. In this regard, using a "balanced" preconditioner, as firstly introduced by Mandel [184], enhances the scheme and increases the rate of convergence of the iterations. This idea has led to the development of the family of balancing domain decomposition (BDD) methods, cf., e. g., Dryja & Proskurowski [69], Mandel [184], Mandel & Brezina [185] and Pavarino & Widlund [219].

Another large group of DD and partitioning strategies could be put under the umbrella of dual Schur complement methods. These schemes are based on an implicit enforcement of the interface consistency constraints through force-like Lagrange multipliers.

Global and localised Lagrange-multiplier methods

Since firstly introduced by Joseph-Louis Lagrange (1736 – 1813) in Mécanique analytique [166], the nowadays called method of Lagrange multipliers has been one of the favourite strategies used to find the arguments of the extrema of a function subjected to one or more constraints. In the most basic way, this is done by multiplying each constraint by a Lagrange multiplier, adding the resultant to the original function, and eventually finding the stationary condition for this newly found augmented Lagrange function. In this regard, the method provides also an appropriate framework for the treatment of constrained problems arising from partitioning and domain decomposition. Therein, the total energy of the system plays the role of the objective function that should be minimised, and the kinematic conditions at the interface specify the constraints. Consequently, the Lagrange multipliers in these cases have a direct physical meaning and represent the interaction forces between subsystems. Following that, using common (global) or individual (local) multipliers for the interacting subsystems, one ends up with a global or a localised Lagrange-multipliers method, herein referred to as the GLM and the LLM methods, respectively.

From a practical perspective, following the GLM method, also called by Park *et al.* [216] the classical method of Lagrange multipliers, one does not distinguish between the forces applied on the interacting subdomains. This is physically motivated and is the case in many partitioning and DD schemes that differ from one another in the way of time integration and data transfer between the subsystems. In the realm of finite-element methods, this idea has led to the development of the finite-element tearing and interconnect (FETI) methods, originally designed by Farhat & Roux [97] as a structural domain decomposition

[4] Named by Emilie Virginia Haynsworth (1916 – 1985) after a determinant lemma of Issai Schur (1875 – 1941), cf. Haynsworth [135].

solver and later presented in different variants [90, 93–95, 98], and the mortar method of Bernardi *et al.* [21] and its variants [20, 104, 282].

However, using common Lagrange multipliers (force vectors) implies a tight coupling between the subsystems and yields a lack of modularity of such solution schemes. Employing a localised version of the Lagrange-multipliers method is a plausible way to overcome this flaw. Following the idea of the LLM method presented by Park & Felippa [214], Park *et al.* [216] and Ross *et al.* [235], which is also called the three-field domain decomposition method, cf. Brezzi & Marini [36] and Farhat *et al.* [94], one loosens the coupling by considering the interface as an additional subsystem that acts like a medium or a membrane that prohibits a direct interaction between the adjacent subsystems. Consequently, and unlike the GLM methods, one ends up with local sets of Lagrange multipliers, each acting between the interface and one of the meeting subsystems. It yields an automatic partitioning of the problem that can conveniently be solved in a parallel manner.

The vast field of applicability of the partitioning methods, in particular the modularity provided by these schemes, has resulted in emergence of numerous variants. This versatility of applications has motivated an enormous amount of research ongoing in this area, such that a comprehensive study of all available partitioning schemes becomes prohibitive. Restricting ourselves to the methods presented above, explanations regarding different formulations are provided in Section 4.3.2, and demonstrative examples are presented in Chapter 7.

Operator-splitting schemes

The operator-splitting and fractional-step methods have been originally developed as a technique for transforming a complicated problem into a sequence of simpler ones, cf., e. g., Marchuk [186], Strang [258] and Yanenko [284]. Here, the idea is to split a complex differential operator into several simpler sub-operators. This process replaces the task of integration of the original problem by a sequence of integrations of simpler subproblems. The integration of the subproblems is then performed individually and in consecutive fractional steps, possibly by using individual step sizes, discretisation methods and, more importantly, different computer codes on different machines, cf. Barry *et al.* [11] and McLachlan & Quispel [195]. Hence, in contrast to the partitioning methods that usually imply a spatial field-by-field decomposition, operator splitting is commonly based on a decomposition of the time discretisation of a field within its time-step interval as explained by Markert [188].

Operator-splitting schemes (OSS) have been successfully used in a wide spectrum of applications. Initial usages proposed by Yanenko [284] include splitting a multi-dimensional spatial operator into several 1-d operators. It yields a solution strategy, also known as the alternating direction implicit (ADI) method [188], which aims at preserving the computational benefits of the related 1-d problem also for the multi-dimensional counterpart. Furthermore, the OSS are excessively used for the treatment of equations comprising various differential operators, for instance linear and non-linear, or stiff[5] and non-stiff

[5] See Section 3.4.2 for a review over the concept of stiff differential equations.

components. In particular, separating the stiff and non-stiff components facilitates an efficient solution of the equation via applying an explicit method to the non-stiff and an implicit method to the stiff part as stated by Burrage [39] and Hofer [143]. Employing such schemes, which, according to Hairer [130], are also known as "mixed", "partially implicit", "compound", and also "partitioned differential" methods, opens new opportunities for the numerical integration of systems including processes of different evolution speeds, as in the problems of advection-diffusion studied by Timmermans *et al.* [264], reaction-diffusion presented by Karlsen & Lie [157], and reaction-transport investigated by Miller & Rabideau [198]. Other examples in this regard include the porous media flow problems involving advection-diffusion as discussed by Cao *et al.* [45], and coupled chemical transport and reaction processes as scrutinised by Barry *et al.* [11].

Splitting methods have also shown a good performance for treatment of the incompressible fluid problems, where the algebraic incompressibility constraint transforms the governing equations to a coupled DAE system, the solution of which entails certain difficulties, cf. Section 3.4.1. To overcome this concern, various splitting schemes based on pseudo-compressibility methods, pressure stabilisation-like schemes, and also projection schemes have been developed. An overview of the related methods and practical examples can be found in the treatises of Chorin [52], Gresho [120], Guermond *et al.* [121], Guermond & Quartapelle [122], Heider [137], van Kan [154], Maday *et al.* [183], Prohl [227], Rannacher [229] and the references therein.

Similar numerical difficulties are observed in the porous media problems. In particular, in the framework of the TPM, the mathematical model of a fluid-saturated porous medium with materially incompressible constituents comprises the mixture volume balance, which also acts as an algebraic constraint. In this conjunction, operator splitting provides a chance to decouple this algebraic constraint from the rest of the model. This process also separates the pore-pressure solution from the kinematic primary unknowns and, thus, removes the burden of using mixed finite elements and its related issues, namely checking for fulfilment of the Ladyzhenskaya-Babuška-Brezzi (LBB) condition [35] or the patch test of Zienkiewicz [289]. To this end, various schemes are developed, which differ in the way that the pore-pressure variable is treated. In this regard, Markert *et al.* [190] and Heider [137] have provided a thorough explanation of such solution strategies for the dynamic porous medium problems. See also Section 6.2 for a brief presentation and the stability analysis of the splitting method of Markert *et al.* [190].

Another operator-splitting method for solving the coupled consolidation problem has been introduced by Lewis *et al.* [175]. Therein, proceeding from mathematical modelling of the porous media using the Biot's theory [23], a two-step solution method has been proposed, where via solving a fluid flow equation the pressure distribution is firstly obtained, and then, assuming 1-d consolidation, the land subsidence is calculated.

The OSS have also been applied to the coupled problem of thermoelasticity. In this regard, some innovative decoupled solution methods have been proposed by Armero & Simo [4], Farhat *et al.* [96] and Simo & Miehe [252]. The so-called isothermal splitting scheme of Armero & Simo [4] has also been adopted by Schrefler *et al.* [244] for decoupled solution of the problem of thermo-hydro-mechanics. The isothermal OSS and its stability analysis are presented in Section 6.1 of this contribution.

The application of decoupled solution strategies is, certainly, not limited to the above cases. In fact, the appealing possibilities offered by such strategies have made them a strong tool to treat coupled systems of different types, for instance fluid-particle systems, cf. Glowinski *et al.* [116], magneto-hydrodynamics, cf. Ryu & Jones [239], image processing, cf. Weickert *et al.* [277], combustion chemistry, cf. Yang & Pope [285], fluid flow in porous media, cf. Barry *et al.* [10] and Kim *et al.* [158], geothermal reservoir analysis, cf. Schrefler [243], electro-thermo-magnetics, cf. Schuler & Felippa [245] and Schuler & Felippa [246], control-structure interaction, cf. Belvin & Park [16] and Park & Belvin [213], etc. The convenience of decoupled solvers, however, comes at a price: decoupling of the equation system causes a delay in the information transfer that introduces an error to the system. Therefore, selection of the way of decoupling and the sequence of time integration of the subsystems can be detrimental to the stability of the scheme and can lead to conditional stability as stated, e. g., by Felippa *et al.* [101], Joosten *et al.* [152] and Matthies *et al.* [192]. This can be the case even if each subproblem is treated by unconditionally stable, implicit time-stepping methods, cf. Kim *et al.* [158] and Schrefler [243]. This problem can, however, be diminished via iterating across the subsystems. In fact, the combination of the decoupled solution methods with the iteration schemes is so common that the decoupled schemes are also sometimes called the iterative solution methods as mentioned by Matthies *et al.* [192] and Markert [188]. The iteration is usually done following a block-Gauss-Seidel, or a block-Jacobi strategy, cf. Section 4.3.1. It can be shown that, provided there are infinite stable iterations, the errors produced by the decoupled schemes become identical to the one belonging to the monolithic methods as argued by Matthies *et al.* [192] and Turska *et al.* [271]. See the works of Barry *et al.* [10] and Turska *et al.* [271], where iterative schemes are used in combination with the operator splitting schemes, and also refer to Joosten *et al.* [152] and Matthies *et al.* [192], where the combination with the partitioning schemes is demonstrated. Also see Schrefler *et al.* [244], where the design of staggered solution methods with iteration is explained in an excellent way.

Nevertheless, stability analysis and establishing the stability condition are still pertinent steps in studying the decoupled and iterative solution strategies. This is because, firstly, in many cases the decoupled schemes are used without iteration and, secondly, even combined with an iteration scheme, the stability of the iteration should be established. Therefore, to delve into the issues regarding the stability analysis of the numerical solution methods applied to coupled systems of equations composes another major part of this report. The goal is to obtain the conditions under which the numerical treatment of the system of governing equations corresponding to a physically stable phenomenon results in stable solutions.

Stability analysis

Studying the stability and convergence of the numerical schemes has a long history. Courant, Friedrichs and Lewy [57] showed in their pioneering work of 1928 that

> *"the convergence of a finite-difference scheme used to solve an initial-value problem for a hyperbolic partial differential equation is obtained only if the ratio of the mesh*

widths in different directions satisfies certain inequalities."

Since then, these "inequalities" are known as the CFL condition. However, considering the Lax equivalence theorem [171],

> *"given a properly posed initial-value problem together with a finite-difference approximation to it that satisfies the consistency condition, stability is the necessary and sufficient condition for convergence."*

Therefore, bearing in mind that only well-posed initial-value problems can be used to model the evolution of physical processes as stated by Strikwerda [260], the CFL condition for a consistent discretisation scheme, which originally ascertains the convergence of the scheme, becomes identical to the stability condition. This is the reason why the necessary stability condition of a scheme is commonly introduced as the CFL condition as done, for instance, by Armero & Simo [4]. Nevertheless, to obtain a direct convergence condition is usually difficult and, therefore, it is commonly preferred to find the CFL condition of a consistent finite-difference (FD) scheme by performing a stability analysis [260]. To this end, different procedures for analysing the stability of the solutions obtained via numerical schemes have been proposed, some of which are briefly outlined in what follows.

The energy method is one of the oldest stability analysis tools and is firstly introduced by the Russian mathematician Aleksandr Mikhailovich Lyapunov[6] (1857 – 1918) in 1892 [182]. This scheme is based on the direct observation of the mechanical systems, for which an equilibrium state is where the total energy of the system reaches a local or a global minimum. This equilibrium state is then stable, if after a perturbation the state of the system remains in a bounded neighbourhood of the equilibrium state. Inspired by this observation, the basic procedure for the stability analysis via the energy method is to assemble a scalar "energy-like" functional, called the Lyapunov functional, and then to examine the variations of this functional as a response to a perturbation. Following that, the system is stable, if its total energy remains bounded as the time elapses.

The energy method is vastly used in the control of nonlinear systems, cf., e. g., Mohandas [201]. It has also been employed for the stability analysis of decoupled solution methods, applied to coupled problems, for instance, by Belytschko & Mullen [18] for the problem of FSI and by Armero & Simo [4] for the problem of thermoelasticity. Furthermore, Hughes & Liu [148] employed the energy method for the stability analysis of the element-by-element partitioning schemes. Nevertheless, to assemble a suitable energy-like Lyapunov function usually proves difficult. Moreover, even after choosing a functional, the region of stability, also called the "domain of attraction", is not unique and depends on the chosen functional, such that sometimes the region may be too small to be of any practical use, cf. Mohandas [201]. In this regard, to study the Lyapunov stability analysis method is out of the scope of this contribution. The interested reader may consult Ascher [5], Hafstein [129], Hairer *et al.* [131], Richtmyer & Morton [230], Yeh & Lu [286] and the references therein for more details. Instead, here the focus is on the method of von Neumann, which is an alternative way to study the stability behaviour of the numerical solution strategies.

The von Neumann stability analysis method has been firstly introduced by Charney, Fjörtoft and von Neumann in 1950 [48], as they faced the question of how to prevent

[6] Also written Ljapunov, Liapunov and Ljapunow.

the amplification of a disturbance that may be introduced to a system. This question led them to base their studies on the method of Courant *et al.* [57] and to derive the criteria which insure that no such amplification occurs for linear difference equations with constant coefficients. This attempt resulted in a rigorous method for investigating the stability behaviour of numerical schemes based on a Fourier mode analysis, which, in the literature, is often referred to as the von Neumann stability analysis as stated by Richtmyer & Morton [230]. Following this, the state of the system obtained via a numerical scheme is called stable, if it always remains in a bounded neighbourhood of the initial state. Nevertheless, considering the Parseval's identity (cf. Strikwerda [260] or Thomas [263]), it could be shown that the boundness of the Fourier transform of the state vector is equivalent to the boundness of the state itself. To determine the conditions under which this prerequisite is satisfied, one has to firstly assemble the so-called amplification matrix, which is a matrix relating the Fourier transform of the state vectors of the system in two consecutive time steps. Subsequently, it can be shown that the solution may be stable, only if the spectral radius corresponding to the amplification matrix remains smaller than unity. Hence, to keep the spectral radius smaller than unity becomes the necessary stability condition for the scheme. In this regard, among the large number of references available, one may refer to Strikwerda [260] and Richtmyer & Morton [230] for a more mathematically oriented, and to Bažant & Cedolin [15] for a more practically oriented introduction. The interested reader can also refer to Gantmacher [112] Chapter XV, and Felippa & Park [100] for a historical review. More details can also be found in the contributions of Burrage [39], Hairer *et al.* [131], Hairer & Wanner [132] and Thomas [263].

The handiness and the capability of the von Neumann method makes it also a strong tool for the stability analysis of numerical solution schemes applied to coupled PDE systems. In this context, the details of the procedure are presented by Ehlers *et al.* [86], Felippa & Park [100] and Park [210]. For a case-specific application, the interested reader may also refer to Park [211] and Zienkiewicz *et al.* [288], where the stability analysis of staggered solution algorithms applied to pore-fluid-soil interaction problems is investigated. Furthermore, Schrefler [243] and Simoni & Schrefler [253] have used the method proposed by Park [210] to study the stability of the decoupled solution schemes proposed for the coupled problems of geothermal reservoir analysis, and water and gas flow in deforming porous media, respectively. Moreover, Armero & Simo [4] have employed the von Neumann stability analysis method to provide the necessary stability condition for the isothermal operator-splitting scheme, and Degroote *et al.* [63] have exploited the Fourier error analysis to achieve the stability condition of a partitioned solution scheme applied to the coupled problem of an unsteady flow in a tube. Furthermore, Kim *et al.* [158] have presented the von Neumann stability analysis of two operator-splitting schemes for fluid flow in a porous medium.

Matrix analysis is another alternative for determining the stability condition of numerical schemes. Similar to the von Neumann method, following the matrix analysis, one firstly assembles the amplification matrix and then determines the conditions under which the spectral radius remains smaller than unity, see, for instance, Peet & Fischer [220]. Thus, this scheme also usually yields a necessary stability condition for the numerical solution

method as stated by Rivera-Gallego [233]. Nevertheless, the difference between the von Neumann and matrix stability analysis schemes lies in the way of assembling the amplification matrix; contrary to the von Neumann method that relies on the relation between the Fourier transform of the state vectors, following the matrix method, the amplification matrix relates the state vectors including all DOF of all spatial nodes in consecutive time steps. This, of course, yields very big equation systems for multi-dimensional problems, and makes the investigation of the eigenvalues and consequently the spectral radii formidable. Nevertheless, this method has been used by Peet & Fischer [220] for the stability analysis of the iterative solution algorithms.

Investigating the truncation errors is another way for analysing the stability of results obtained by a numerical scheme. This is due to the fact that the boundness of the truncation errors is the necessary and sufficient condition for the boundness of the numerical solution. The logic behind this statement is rather simple, as described in what follows: Consider an "admissible" set of governing equations corresponding to a physically stable phenomenon. The exact solution of these governing equations "must be" essentially stable. Nevertheless, results obtained via a numerical solution may be stable or unstable. In this connection, the truncation error depicts the amount of deviation of the numerical solution from the exact one. Thus, one concludes that the numerical solution would be bounded in a neighbourhood around the analytical solution and, hence, the scheme would be stable, if and only if the truncation errors are bounded. See Hirt [142], Schrefler *et al.* [244], Turska & Schrefler [270] and Turska *et al.* [271] for the stability and convergence analysis of solution methods via error propagation analysis.

The theory proposed by Gustaffson, Kreiss, Sundstrøm, and Oliger [126, 127] provides a more general method of establishing the necessary and sufficient stability condition for the numerical schemes. Usually called the GKSO method, this form of the stability analysis is very similar to the von Neumann method, except that it is compatible with the discrete Laplace instead of the Fourier transform, cf. Rivera-Gallego [233]. The GKSO analysis has been used by Berger [19] to investigate the stability of numerical solutions obtained for hyperbolic equations and by Rivera-Gallego [233] to look at stability properties of an explicit predictor method for solving the heat equation. However, the drawback of this method consists in its difficulty of application, particularly because it is difficult to apply the GKSO systematically to the algorithms applied to the 2- and 3-d problems as stated by Rivera-Gallego [233] and Peet & Fischer [220].

What was said represents only a small portion of the works done in the field of stability analysis. To read more about the issues related to the stability and the convergence of the numerical methods, one may also refer to Dekker & Verwer [64], Felippa & Park [100], Hairer *et al.* [131], Hairer & Wanner [132], Kim *et al.* [158], Morton & Mayers [203], Süli & Mayers [262] and the references therein. It should, however, be noted that in this thesis, we talk about the stability of the solutions of the differential equations (DE) found via numerical solution procedures. In this regard, the methods for determining the stability of continuous data systems, such as the Nyquist criterion and the Bode diagram are excluded. These methods are mostly used in the field of automatic control, cf. any standard textbook, for instance, Golnaraghi & Kuo [118]. Furthermore, we limit our attention only to the linear DE with constant coefficients. This decision has been made

considering that although the linear stability is not a sufficient condition for guaranteeing the nonlinear stability, it is still a necessary condition for achieving the nonlinear stability as argued by Shi [251]. Thus, the von Neumann stability analysis method has been chosen, and various criteria for locating the spectral radius of the amplification matrix have been studied. In this regard, in Section 5.4.2, the methods of Schur & Cohn [153, 247], Hurwitz [149], Routh [237] and Liénard & Chipart [176] are introduced, and the relations between them are established. The focus has been on providing related definitions and theorems in an application-friendly style and on presenting the procedure such that the algorithm can be employed to find the critical grid sizes in different scenarios with minimum difficulty and without any need to solve the whole problem.

1.3 Outline

In **Chapter 2**, the terminologies used in this monograph are presented, and a framework for classification of the coupled problems is proposed. To support the explanations, several examples from different fields are presented.

To explore coupled systems of equations resulting from the mathematical modelling of the coupled phenomena is the objective of **Chapter 3**. In this regard, after a short historical overview, the fundamental concepts of continuum mechanics, and also the related concepts of the TPM, are briefly introduced. Identifying the mathematical models of coupled systems as coupled systems of PDE or DAE, different strategies for dealing with the numerical difficulties caused by the algebraic constraints are introduced. At the end of this chapter, the controversial concept of the stiffness of the differential equations is discussed, and a feasible definition for stiff problems is presented.

Having coupled systems of equations introduced, **Chapter 4** is devoted to the procedures for the numerical solution of the differential equations in general, and the coupled PDE or DAE systems in particular. Therein, in order to build a foundation for the upcoming stability analysis of the numerical schemes, the families of the Runge-Kutta methods and the backward differential formulae are initially introduced. After that, the focus is directed towards the numerical integration strategies for coupled systems of equations. In this regard, the monolithic and decoupled strategies are demonstrated and the advantages and disadvantages of such integration schemes are examined. In particular, several partitioning techniques are studied and the relation between them is established. Moreover, a convenient framework for presentation of operator-splitting schemes is proposed, and the process of time integration in the methods belonging to this class of solution strategies is described.

Driven by the fact that decoupling of a physically stable problem may generate computationally unstable subproblems, **Chapter 5** is assigned to stability analysis of the numerical schemes. To this end, the related notions are introduced and the definitions regarding the numerical stability are presented. After that, several stability criteria are presented and the relations between them are investigated. Subsequently, a pragmatic stability analysis algorithm is established.

Using the knowledge acquired from the last parts, numerical solution and stability analysis

of several benchmark examples are accomplished. The examples are grouped into the classes of volume- and surface-coupled problems, respectively presented in **Chapter 6** and **Chapter 7**. These chapters especially serve to illustrate the way the decoupled solution schemes shall be employed, and to investigate the capabilities of the stability analysis algorithm introduced in Chapter 5.

Finally, the conclusions and discussions including suggestions on conceivable further developments of the present study are given in **Chapter 8**.

For further elucidation, the detailed stability analysis procedures for decoupled solution strategies applied to the volume-coupled problem of thermo-elastodynamics and the surface-coupled problem of fluid-porous-media interaction are presented in **Appendix A** and **Appendix B**, respectively.

Chapter 2:
Definitions and Classifications

In this chapter, the terminology used within this report is presented and a framework for classification of coupled systems is proposed. We basically stick to a modified version of the definitions of Felippa & Park [100] and Markert [188, 189]. Alternative nomenclatures can be found, inter alia, in [133, 173, 192, 193]. Note that the main focus in the following is on coupled problems in the field of engineering, especially on those which can be modelled within the framework of continuum theories.

To start off, consider the motion of a submarine within the surrounding water, blood within a blood vessel wall, or a wind turbine blade in the surrounding air. In all those situations, the pressure applied by a fluid body on a flexible structure causes a deformation in the structure which, in its turn, changes the profile of the fluid flow and, hence, the fluid pressure. In these cases, two naturally distinct properties of the system, i. e., the fluid pressure and the structural deformation, are *coupled* to each other. Considering this, similar systems, in which heterogeneous components are interacting with each other, are known as physically coupled systems, or simply *coupled systems*.

The interaction between the components may be with or without feedback, in which cases one ends up with a *one-way* or a *multi-way* interaction, respectively. Considering this, the above examples lie in the category of the multi-way coupled systems. An alternative one-way coupled version is imaginable for the cases where, e. g., the changes in the profile of the fluid flow in response to the structural deformation are negligible.

A second look at the above examples also shows that in those cases, the interaction takes place on common boundaries between geometrically distinct subdomains. Thus, such coupled systems are commonly referred to as *surface-* or *geometrically coupled* systems. In some other coupled systems, however, the interaction between the heterogeneous components occurs within the same spatial domain. This phenomenon can be seen, for instance, in thermodynamics, where the interaction between the mechanical quantity (deformation) and the thermal quantity (temperature) essentially happens at each material point. Such systems are referred to as *volume-* or *materially coupled* systems.

Having coupled systems introduced, the mathematical models corresponding to the coupled phenomena are investigated in the next step.

From a simulation point of view, one aims at describing the behaviour of physical systems via mathematical models. These models are normally generated in two main steps: i) choosing suitable physical theories for describing the phenomenon at hand and, ii) establishing the set of governing equations within the framework of the chosen theories. The governing equations are commonly presented in the form of partial differential or differential algebraic equations in space and time. They govern the response of the system to the external excitations, hence their name. Considering coupled systems, the corresponding mathematical models also happen to be coupled systems of equations. This sort of "computational" coupling is in the sense that at least some of the field equations are functions

of several unknown field variables. Such computationally coupled systems, together with the initial and boundary conditions (IC and BC) corresponding to a specific external excitation, form a certain class of mathematical problems, herein are called *multi-field coupled problems* or simply *coupled problems*.

Coupled problems can be categorised in different ways. This could be with respect to the nature of the heterogeneity in the coupled systems. Thus, one ends up with two main categories, namely *single-* and *multi-physics coupled problems*. The term *physics* in this context refers to a physical phenomenon and its corresponding mathematical model in the system. Following that, a *multi-physics coupled problem* is a coupled problem containing several physically distinct phenomena, which are essentially described by distinct mathematical models. In this context, the distinction between the phenomena and their corresponding models may be due to different reasons. First of all, it is well known that there are various physical theories on the market, each of which specialised for the description of processes in a specific range of relative length and time scales. Employing these theories yields different families of simulation methods. Therefore, the presence of physical heterogeneities, in the sense of having drastically different length and time scales, calls for the process of *multi-scale* modelling, i. e., simultaneous exploitation of modelling methods specialised for different scales. Thus, the mathematical models produced in this way belong to the class of multi-physics coupled problems.

The multi-scale modelling is seen, for instance, in the micro-macro modelling of complex polymeric fluids, which are composed of molecules of very different sizes [177]. In this case, the macroscopic continuum model of the problem is complemented by constitutive relations calculated from microscopic models, e. g., molecular or atomic models [208]. Another example is the modelling of locally large deformations in granular matter, where the multi-scale approach facilitates a concurrent usage of a microscopic, discrete particle model in domains of large and possibly discontinuous deformation in conjunction with a macroscopic continuum model for the description of the remaining domain [279]. Multi-scale modelling has also been employed in biomechanics, e. g., in order to simulate the intervertebral disc. In this regard, Karajan *et al.* [156] use a homogenisation technique to couple the continuum-mechanical model for the intervertebral disc (smaller length scale) to a discrete multi-body system model, which is used for the simulation of the rest of the body (larger length scale). The interested reader is referred to [256, 278] and the references therein for more details about the multi-scale modelling.

Multi-physics coupled problems are also seen in the field of automatic control, where a common task is to force a dynamic structure to maintain a predefined status despite disturbances. This goal is achieved within three main steps, namely i) measure the state of the system by a sensor, ii) send the collected data to a controller, iii) if necessary, correct the behaviour of the system by applying a load via an actuator. The mathematical simulation of such a process entails the development of one model for the physical subsystem and another one for the controlling unit. Nevertheless, the distinction between the natures of subsystems yields a heterogeneity in the model building strategy, such that the resulting problem, which is usually called a *control-structure interaction* (CSI) problem, also falls into the category of multi-physics problems. More details about this class of coupled problems can be found in [16, 100, 213] and the references therein.

Electro-thermodynamical processes build another group of coupled multi-physics problems. These processes are modelled benefiting from two distinct, yet related, physical theories, namely continuum thermodynamics and electrodynamics. The mathematical model is then realised by coupling the thermodynamical balance laws presented in Section 3.2.4, to the Maxwell's equation of electrodynamics [194]. To this end, the fusion of the equations can be done by following a continuum-like approach, where the electromagnetic effects are inserted into the thermodynamical balance laws as actions from the distance. A neat representation of the problem, a detailed review of the approach and the resulting equation systems, as well as a list of references for other approaches are presented by Markert [188].

Modelling a diffusion-reaction process also yields a multi-physics coupled problem. Usually seen in chemistry, these problems describe the changes in the concentration of the substances in response to two physically distinct phenomena, namely spatial diffusion and chemical reaction. The spatial diffusion of the substance in the domain is typically a slow process, trying to retain the overall homogeneity of the system[1]. In contrast, the chemical reaction yields local production (or consumption) of the substance that occurs with a relatively higher speed and leads to destruction of the homogeneity [65]. Consequently, a sound governing equation corresponding to such a *multi-rate process* should also contain two differential operators, one of which causing a fast variation of the quantity, and the other one causing a slow variation. This is the characteristic of a special class of the differential equations, usually called *stiff differential equations*, cf. Section 3.4.2.

The process of bone remodelling embodies a more complex multi-physics coupled phenomenon, incorporating mechanical, chemical, and biological processes. It describes the gradual adaptation of the bone tissue structure in response to cycles of mechanical loading, which usually take place with higher pace in relatively short time periods, for instance, during sport sessions. Consequently, due to the significant difference in the speeds of the contributing processes, this problem also lies within the category of multi-rate problems, cf. [161] and the references therein for more details regarding this problem and its corresponding solution strategies.

Modelling of the surface interaction among heterogeneous media also yields a multi-physics coupled problem. It is found, for instance, in the fluid-structure interaction (FSI), where the set of governing equations comprises distinct mathematical models corresponding to the fluid and the structure subsystems. Other similar examples include surface-coupled problems of fluid-porous-media interaction (FPMI), describing the coupling between the deformation of a porous medium and the fluid pressure, possibly accompanied by fluid mass exchange between subsystems, acoustic-structure interaction, describing the coupling between the structural displacement field and the acoustic pressure field, and structure-structure interaction (SSI), describing the surface interaction between solid structures, with different physical properties. Consult Section 4.3.2, where different solution strategies for numerical treatment of the surface-coupled problems are presented. Also see Chapter 7 for several numerical examples.

It should be noted that the coexistence of heterogeneous mathematical models in multi-

[1] Homogeneity in the sense of having homogeneous concentration of the substances within the domain.

physics coupled problems is sometimes accompanied by mutual application of distinct numerical solution strategies. This is another type of computational heterogeneity seen, for instance, in the FSI, where the spatial discretisation of the fluid subdomain is usually done via the FVM, whereas the spatial discretisation of the solid subdomain is commonly done employing the FEM. Considering this, the coexistence of different discretisation methods is usually a "consequence" of, rather than an "indicator" for, having a multi-physics coupled problem. However, the unlikely case of concurrent exploitation of different methods for the spatial discretisation of a physically homogeneous domain can also be recognised as a multi-physics coupled problem. An example would be the simultaneous application of the FDM and the FEM for spatial discretisation of different parts of a homogeneous solid domain.

Bearing in mind that all of the above-mentioned examples belong to the category of multi-physics and multi-field coupled problems, the class of single-physics multi-field coupled problems is briefly reviewed in the next step.

A single-physics multi-field coupled problem comprises "one" mathematical model describing immanent interaction among "several" distinct physical quantities. In this case, the corresponding set of governing equations is composed solely of one single set of coupled PDE or DAE in space and time. Considering the modelling of thermomechanical systems in the framework of the theory of continuum thermodynamics, it means that the whole domain of the problem can be simulated using the same set of balance equations, constitutive relations and material parameters. In this regard, some of the typical single-physics coupled problems are incompressible fluid flows described by the Navier-Stokes equations, containing two physical quantities, namely the fluid velocity and the fluid pressure (cf. Sections 7.3), dynamics of saturated porous media, describing the relation between the solid displacement, the pore-fluid pressure and the pore-fluid velocity (cf. Section 6.2 and 7.3), and the problem of thermo-elastodynamics, describing the alteration of the temperature in a solid in response to deformation and vice versa (cf. Section 6.1).

Remarks:

- Clearly, the problems of thermo-elastodynamics as well as porous-media dynamics comprise several physical phenomena. Nevertheless, the process of modelling for both examples can be done within the unique framework of continuum thermodynamics. It yields only one physical model for each of these problems and, hence, they do not fall in the category of multi-physics problems.
- Application of specific time integration schemes, e. g. implicit Runge-Kutta methods (IRK), demand the differential equations (DE) to be of first order. To this end, order reduction is commonly used to convert the higher-order differential equations to systems of lower-order equations. This, however, entails the introduction of auxiliary variables resulting in heterogeneity and, therefore, in a coupled system of equations, cf. [132] and, furthermore, Chapters 6 and 7 for several examples of order reduction.

Chapter 3:
Mathematical Framework

Mechanics is the paradise of mathematical science,
because here we come to the fruits of mathematics.
Leonardo da Vinci (1452 – 1519) [2]

In this chapter, we take a short look on the scientific achievements of ancient civilisations in the field of mathematics, and briefly review the history of mechanics, from early years until today's modern theory of continuum mechanics. Subsequently, the fundamental concepts of continuum mechanics, in particular those exploited in this contribution are presented and, furthermore, the basics of the Theory of Porous Media (TPM) are concisely demonstrated. After that, the classes of PDE and DAE systems are studied. In particular, the numerical difficulties caused by algebraic constraints are discussed, and selected strategies to eliminate these constraints are presented. Furthermore, the concept of stiffness in connection with differential equations is investigated.

3.1 A brief historical sketch

Ever since getting familiar to the concept of "causality", men have been trying to explain how the universe works, and whether there is a way to predict the natural events. Nevertheless, first attempts to satisfy this curiosity were rather unsuccessful. Above all, limited experience and the absence of a proper framework for rational reasoning misled the initial quests and resulted in explanations, which were mostly concentrated around myths and superstitious stories. After thousands of years, the initial "explanations" transformed to "beliefs" that built some kind of theological world view, which was based on holding supernatural agencies responsible for natural phenomena. In fact, the Ionian Greek physiologoi[1], as Aristotle called them [128], were the first ones who dared to question and criticise this type of mythology, and strived to propose natural explanations for the natural phenomena. Therefore, it makes perfect sense to seek the roots of modern science in the early Greek philosophy.

The dawn

The branch of science today called "mathematics" has very old roots. Anthropological findings have shown the familiarity of neolithic men (10000 B. C. – 2000 B. C.) with the concepts of geometry and numbers. The Egyptian papyri and Babylonian clay tablets are other evidences which prove the practical use of mathematics by those very old civilisations since at least 5000 years ago [32]. Nevertheless, the Ionian Greek physiologoi were the pioneers of employing mathematics instead of mythology to describe the laws of "physis" ($\phi\acute{\upsilon}\sigma\iota\varsigma$), which means "nature". Amongst prominent natural philosophers, one may name Thales (624 B. C. – 546 B. C.), who is sometimes called the first philosopher of history

[1] In English, physical or natural philosophers.

[32], and Pythagoras (570 B. C. – 495 B. C.) who is the first person that called himself a philosopher, i. e. the lover of wisdom [231]. It were also Pythagoreans who coined the term "mathematics" from the ancient Greek "mathema" ($\mu\acute{\alpha}\theta\eta\mu\alpha$), meaning "subject of instruction" [136]. Later, this knowledge was brought to Athens, where the discovery of the laws of nature was pursued by a very long chain of pre-Soctratic philosophers, amongst others Heraclitus, Empedocles, Parmenides, Leucippus and his student Democritus, who is the last natural philosopher and, due to his ground-breaking doctrine of atomism, has been considered by many to be the "father of modern science" [119].

The post-Socrates era started with the appearance of Socrates (469 B. C. – 399 B. C.) and his successor Plato (427 B. C. – 347 B. C.) at Athens. Nevertheless, in spite of heroic contributions of these two legendary figures to philosophy, they were both more concerned with political issues rather than mathematics or natural sciences [32, 73]. However, the Plato Academy played a central role in the inspiration of mathematical activity and development, such that Plato has been sometimes called "the maker of mathematicians" [218]. Amongst others, Aristotle (384 B. C. – 322 B. C.) is with no doubt the most prominent scholar of the Academy. Although Aristotle also made no original contributions to mathematics, in his "Prior Analytics", or "Analytical Priora", he introduced the principles of deductive reasoning and formal logic for the very first time [55].

Euclid (325 B. C. – 265 B. C.), Archimedes (287 B. C. – 212 B. C.) and Ptolemy (90 – 168) were the next most outstanding thinkers before the end of the scientific glory of the ancient Greece [32]. With the "Elements" Euclid indeed authored one of the most successful and probably the oldest mathematics textbooks in geometry. Nevertheless, his aspiration was mostly around pure theoretical aspects of mathematics rather than its practical use. In opposition, Archimedes is thought to be one of the pioneers of using mathematical models for solving physical problems. And the last but not the least was Ptolemy, whose hypothesis of the central Earth and the circular motion of heavenly objects ruled for more than a millennium.

The decline of the Greek science and philosophy which was started by the conquest of Greece by the Romans in 146 B. C., reached its nadir by closing the philosophical schools, including the Academy, by the Byzantine (East Roman) emperor Justinian in 529. Therefore, 529 has been considered by many as the mark of the ending of the European mathematical development in antiquity [32]. Hereafter, the Greek sciences were pursued in Near and Far Eastern countries for the next several centuries.

The Muslim empire

The Muslim empire[2] was initially established by nomads from the Arabian Peninsula in the 7th century. At its height, it spanned from the Atlantic Ocean in the west across North Africa and the Middle East to central Asia in the east [32]. This domination and conquest was a two-fold phenomenon; the spread of Arabic as the language and the

[2]The Muslim empire has been also commonly called the Arab empire. This is due to the fact that the official language within the Muslim empire was Arabic. Nevertheless, the empire was composed of various nations. Considering this, it is more appropriate to use the expression Muslim empire instead of Arab empire.

Islam as the religion on the one side, and an absorption of the old knowledge of the invaded civilisations, including Byzantines, Persians and Indians, by the Muslims on the other side [222]. This combination led to translation of the ancient works into Arabic and facilitated further development of this knowledge, especially in the branches of arithmetic, algebra, trigonometry and geometry. In particular, the contributions of Thabit ibn-Qurra (826 – 901) and Abu'l-Wefa (940 – 998) in translating the old Greek treatises, and Abu Rayhan al-Biruni (973 – 1048) in translating the Hindu mathematics played an important role in the survival of these old works, which were later handed over to the Latin world [32]. Apart from translations, the pioneering works of ibn-Qurra in the fields of geometry and number theory are also considered as the original inspirations of René Descartes in introducing the analytic geometry [54]. Moreover, al-Biruni, Abu'l-Wefa, and later Nasir Elddin al-Tusi (1201 – 1274) wrote original works on spherical triangles and trigonometry with application to astronomy. Their findings were further developed by Jamshid al-Kashi (1393 – 1449), who is known for his pioneering works in the introduction and the use of decimal fractions, the determination of the first sixteen decimals of π, and also the correct computation of trigonometrical tables [196].

Amongst other prominent medieval Islamic scientists, one may also name Mohammad ibn-Musa al-Khwarizmi (780 – 850), who, inspired by the works of the Hindu mathematicians, introduced the so-called Hindu-Arabic number system [207]. Furthermore, the word "algebra" is deduced from the title of his most important book "Al-jabr wa'l muqābalah". From this book, Europe later learned the branch of mathematics bearing this name [32, 207]. Apart from that, the Latin version of his own name introduced the word "algorithm", which is commonly used in computer sciences and mathematics [32, 34, 150]. The works of al-Khwarizmi on algebra were later followed by the mathematician and poet Umar al-Khayyam (1048 – 1123), who wrote a treatise on algebra that contained geometrical solutions of all types of cubic equations by means of parabolas, hyperbolas and circles [196].

The aspects mentioned above show only a very small portion of the contributions of Muslims in science. The interested reader is referred to [32, 34, 150, 196] for additional information. Nevertheless, the number of Muslim mathematicians who came after al-Kashi was so small, that his death can be considered as the end of the account of the Islamic mathematics [32]. The wane of dominance of the Islamic scientists was, however, simultaneous with the transition of Europe from the late Middle Ages into the early modern world.

Renaissance to the modern age

The Scientific Revolution in Europe took place roughly between 1550 and 1700. Before this period, the scholastic world view, a combination of Christianity with the ideas of Aristotle, was widespread in the European scientific centres [117]. This world view was, inter alia, based on the geocentric model of Ptolemy, which was assumed to be correct for about two millennia. The Ptolemy's model was seriously challenged for the first time by the heliocentric model of Nicolaus Copernicus (1473 – 1543). This model was later modified by Johannes Kepler (1571 – 1630), who replaced the circular Copernican orbits of the

Earth and other planets by elliptical motions. Furthermore, Galileo Galilei (1564 – 1642) proposed the mathematical formulation of the Copernicus' model. Believing that *the book of nature is written in mathematics* [159], Galileo used a combination of mathematics and experiment to begin the formulation of a new science of motion, that could successfully describe the motion of the Earth and explain familiar facts about dropped and thrown objects; what would become today's classical mechanics [117].

The ideas of Galileo Galilei were adopted by his contemporary René Descartes (1596 – 1650), who succeeded in developing the analytic geometry, proposed the Cartesian coordinates and also introduced the use of infinitesimal measures to calculate tangent lines [103]. The latter idea was later used by Isaac Newton and Gottfried Leibniz for the development of the infinitesimal calculus [123]. Furthermore, endeavoring to discover the laws of nature and believing that the universe could be understood in terms of the motion of "corpuscles" of matter, Descartes suggested the first formulation of the axiom of conservation of linear momentum [103]. In this regard, Descartes' method in explaining the motion of the corpuscles was in line with the theory of mechanisms, according to which the world is made up of tiny corpuscles of matter, which interact only by "local" physical contact [117]. Further development of this theory upon including the actions from the distance was mainly done later by Newton.

In 1687, Sir Isaac Newton (1642 – 1727) published his famous work "Philosophiae Naturalis Principia Mathematica"[3], usually referred to as "Principia". Therein, he presented, inter alia, his theory of gravitation and the laws of motion. Employing these, and by improving the theories of his "giant" predecessors[4], Newton proposed a unified mathematical treatment of motion, both on the Earth and in "the Heavens" [5]. However, the only motions Newton succeeded to reduce to mathematics are those of a "single point". Furthermore, according to Truesdell [266], he made no attempt to form his laws of motion in consistent mathematical expressions. In fact, it was Leonhard Euler (1707 – 1783) who completed Newton's principles and provided the momentum balance as we know it today. Nevertheless, Newton's innovative ideas, especially his method of calculus, played an inevitable role in later interpretation of the laws of nature in the form of differential equations in the four-dimensional spacetime; a process that eventually built the foundations of the theory of continuum mechanics.

3.2 The continuum-mechanical approach

Continuum mechanics is mainly concerned about the macroscopic description of the response of material bodies to external forces. In this regard, one proceeds from a continuous distribution of a body over its volume. Thus, a material body is considered as a

[3] In English "Mathematical Principles of Natural Philosophy".

[4] In a letter to Robert Hooke (1635 – 1703), dated 5th of February 1675, Newton writes: *"If I have seen further, it is by standing on the shoulder of giants"* [49].

[5] It is interesting to note that, the pre-Newton mechanics was mainly concerned about the motion of bodies in response to local forces. From this point of view, and considering the postulation of "non-local" forces (most importantly the gravity), Newton's physics has been taken by some as "post-mechanical" [117].

continuum, that is an isomorphism of the system of real numbers.

In this framework, the mathematical model of a physical phenomenon consists of some conservation principles, mostly expressed in the form of axiomatic balance laws. In their originial form, the balance relations are interpreted as partial differential equations (PDE) in space and time. Nevertheless, in certain circumstances, they may transform to differential algebraic equations (DAE). These equations, combined with thermodynamically consistent constitutive equations build a closed equation system. The closure is in the sense that the number of equations is exactly equal to the number of unknowns presented in the system. It guarantees the solvability and uniqueness of the solution of the system.

The early concepts of continuum mechanics were developed during the 17th, 18th and early years of the 19th centuries by luminaries like Jakob Bernoulli (1655 – 1705), Johann Bernoulli (1667 – 1748), Daniel Bernoulli (1700 – 1782), Leonhard Euler (1707 – 1783), Jean le Rond d'Alembert (1717 – 1783), Joseph-Louis Lagrange (1736 – 1813) and Siméon-Denis Poisson (1781 – 1840). In particular, Euler's contributions in obtaining the principles of linear and angular momentum, which are the basic axioms of mechanics, and the precise mathematical interpretation of these axioms were of vital importance to further developments in this field of science. A complete study and a comprehensive review of these developments is presented by Truesdell [265, 266]. In particular, according to Ehlers [83], Truesdell's publications with Toupin and Noll [267, 268] nearly contain the complete continuum-mechanical knowledge until the early 1960th. More recent contributions, presenting modern notations and applications, are also presented, for example, by Chadwick [47], Gurtin [124], Haupt [134] and Holzapfel [144].

In the following, selected aspects of modern continuum mechanics are briefly reviewed. We restrict ourselves to those topics, which are mostly related to the goals of this report. The presented material is based on the lecture notes of the course of Continuum Mechanics, offered by Professor Wolfgang Ehlers for the master program Computational Mechanics of Materials and Structures, at the University of Stuttgart in Germany, between 2000 and 2015. The notations are in accordance with the work of Ehlers [80], which is an extension of the fundamental textbook of de Boer [26].

3.2.1 Kinematics

Based on the fundamentals of continuum mechanics, a material body is defined as a three-dimensional (3-d) connected manifold of material points $\mathcal{P}$ embedded in the Euclidian point space $\mathbb{E}^3$ at time t, cf. Figure 3.1. The body is initially at rest. In this configuration, the spatial location of each material point $\mathcal{P}$ with respect to an arbitrary but fixed origin $\mathcal{O}$ is uniquely defined by a position vector $\mathbf{X}$. Thus, the initial positions of the material points at the initial time t^0 determine the reference configuration of the body $\mathcal{B}_0$, enclosed by the surface $\mathcal{S}_0$. The goal is to describe the motion of the body in response to some traction force $\mathbf{t}$ acting at a specific portion of the surface of the body, and some volume force $\mathbf{f}$ acting at every material point. In this regard, the motion of the material points is given by the placement function $\boldsymbol{\chi}$, uniquely determining the actual position $\mathbf{x}$ of the material points and, hence, the current configuration of the body $\mathcal{B}$ with the surface $\mathcal{S}$ at any time $t \geq t^0$, such that

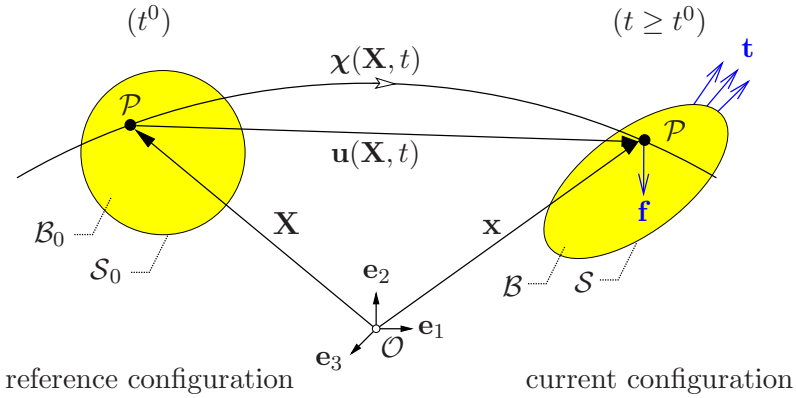

Figure 3.1: *Kinematics of a continuum body.*

$$\mathbf{x} = \boldsymbol{\chi}(\mathcal{P}\,, t) \quad \rightarrow \quad \mathbf{X} = \boldsymbol{\chi}(\mathcal{P}\,, t^0)\,. \tag{3.1}$$

The second relation approves the identification of each material point with its corresponding initial position vector. Thus, $(3.1)_1$ alternatively reads

$$\mathbf{x} = \boldsymbol{\chi}(\mathbf{X}\,, t)\,. \tag{3.2}$$

This is the so-called Lagrangean or the material representation of the motion of the body. Furthermore, the inverse motion of each material point is uniquely given by

$$\mathbf{X} = \boldsymbol{\chi}^{-1}(\mathbf{x}\,, t)\,, \tag{3.3}$$

where, $\boldsymbol{\chi}^{-1}$ denotes the Eulerian or the spatial inverse motion function. In the next step, one introduces the material deformation gradient $\mathbf{F}$, which is a tensor of second order defined as

$$\mathbf{F} := \frac{\partial \mathbf{x}}{\partial \mathbf{X}} = \operatorname{Grad} \mathbf{x} \quad \text{where} \quad \operatorname{Grad}(\,\cdot\,) := \frac{\partial(\,\cdot\,)}{\partial \mathbf{X}}\,. \tag{3.4}$$

Then, via introducing the displacement vector $\mathbf{u} = \mathbf{x} - \mathbf{X}$, the material deformation gradient alternatively reads

$$\mathbf{F} = \frac{\partial\,(\mathbf{u} + \mathbf{X})}{\partial \mathbf{X}} = \operatorname{Grad} \mathbf{u} + \mathbf{I}\,. \tag{3.5}$$

The existence of a uniquely invertible motion function requires the deformation gradient to be invertible too. In this regard, the inverse of $\mathbf{F}$ is denoted by $\mathbf{F}^{-1}$, and is calculated as follows:

$$\mathbf{F}^{-1} = (\det \mathbf{F})^{-1}\,(\operatorname{cof} \mathbf{F})^T\,. \tag{3.6}$$

Therein, $\det \mathbf{F}$ and $\operatorname{cof} \mathbf{F}$ represent the determinant and the cofactor of $\mathbf{F}$, respectively. Thus, $\mathbf{F}^{-1}$ exists only if the Jacobian $J := \det \mathbf{F} \neq 0$. Then, taking into account that $\mathbf{F}|_{t=t^0} = \mathbf{I}$, one concludes

$$J|_{t=t^0} = \det \mathbf{I} = 1 \quad \rightarrow \quad J > 0 \quad \forall t \geq t^0\,. \tag{3.7}$$

As the name suggests, the material deformation gradient provides a mathematically sound measure for the deformation of a body. This is considering that $\mathbf{F}$ functions as a linear

map, which transports a line element from the reference to the current configuration in a push-forward sense:

$$\mathrm{d}\mathbf{x} = \mathbf{F}\,\mathrm{d}\mathbf{X}\,. \tag{3.8}$$

Employing $\mathbf{F}^{-1}$, the existence of which is guaranteed by $(3.7)_2$, yields the reverse mechanism, which is a pull-back of a line element from the actual towards the reference frame:

$$\mathrm{d}\mathbf{X} = \mathbf{F}^{-1}\,\mathrm{d}\mathbf{x}\,. \tag{3.9}$$

Furthermore, the transformations of the oriented area elements[6] and the scalar-valued volume elements from the reference to the current configuration are regulated by the material deformation gradient. These transformation mechanisms read

$$\mathrm{d}\mathbf{a} = \operatorname{cof}\mathbf{F}\,\mathrm{d}\mathbf{A}\,, \quad \text{and} \quad \mathrm{d}v = \det\mathbf{F}\,\mathrm{d}V\,, \tag{3.10}$$

wherein

	reference configuration	current configuration
oriented area element	$\mathrm{d}\mathbf{A} = \mathrm{d}\mathbf{X}_1 \times \mathrm{d}\mathbf{X}_2$	$\mathrm{d}\mathbf{a} = \mathrm{d}\mathbf{x}_1 \times \mathrm{d}\mathbf{x}_2$
volume element	$\mathrm{d}V = (\mathrm{d}\mathbf{X}_1 \times \mathrm{d}\mathbf{X}_2)\cdot\mathrm{d}\mathbf{X}_3$	$\mathrm{d}v = (\mathrm{d}\mathbf{x}_1 \times \mathrm{d}\mathbf{x}_2)\cdot\mathrm{d}\mathbf{x}_3$

(3.11)

Apart from that, the velocity and the acceleration vectors are defined as the first and the second material time derivatives of the position vector $\mathbf{x}$, respectively. These quantities read in the Lagrangean frame

$$\dot{\mathbf{x}} := \frac{\mathrm{d}}{\mathrm{d}t}\boldsymbol{\chi}(\mathbf{X}\,,t) = \dot{\mathbf{x}}(\mathbf{X}\,,t)\,, \quad \ddot{\mathbf{x}} := \frac{\mathrm{d}^2}{\mathrm{d}t^2}\boldsymbol{\chi}(\mathbf{X}\,,t) = \ddot{\mathbf{x}}(\mathbf{X}\,,t)\,. \tag{3.12}$$

The Eulerian representations are consequently derived with the aid of the inverse motion function $\boldsymbol{\chi}^{-1}$ introduced in (3.3) as

$$\dot{\mathbf{x}}(\mathbf{X}\,,t) = \dot{\mathbf{x}}(\boldsymbol{\chi}^{-1}(\mathbf{x}\,,t)\,,t) = \dot{\mathbf{x}}(\mathbf{x}\,,t)\,, \quad \ddot{\mathbf{x}}(\mathbf{X}\,,t) = \ddot{\mathbf{x}}(\boldsymbol{\chi}^{-1}(\mathbf{x}\,,t)\,,t) = \ddot{\mathbf{x}}(\mathbf{x}\,,t)\,. \tag{3.13}$$

It is also worth mentioning that

$$\mathbf{u} = \mathbf{x} - \mathbf{X} \quad \Rightarrow \quad \dot{\mathbf{x}} = \dot{\mathbf{u}} \quad \text{and} \quad \ddot{\mathbf{x}} = \ddot{\mathbf{u}}\,. \tag{3.14}$$

3.2.2 Deformation and strain tensors

Various finite deformation and finite strain measures have been introduced by the experts over the years. Amongst others, the Cauchy-Green deformation tensors along with the Green-Lagrangean and the Almansian strain tensors are more related to our subjects of interest and, thus, are briefly introduced.

Considering the push-forward mechanism of the line elements given by (3.8), the square of the line element in the current configuration reads

$$\mathrm{d}\mathbf{x}\cdot\mathrm{d}\mathbf{x} = \mathbf{F}\,\mathrm{d}\mathbf{X}\cdot\mathbf{F}\,\mathrm{d}\mathbf{X} = \mathrm{d}\mathbf{X}\cdot(\mathbf{F}^T\,\mathbf{F})\,\mathrm{d}\mathbf{X} =: \mathrm{d}\mathbf{X}\cdot\mathbf{C}\,\mathrm{d}\mathbf{X}\,, \tag{3.15}$$

[6] See Section 3.2.3 for more elaboration on the concept of oriented area elements.

wherein the binary dot operator implies a scalar (inner) product between vectors, and $\mathbf{F}^T$ represents the transpose of $\mathbf{F}$. Moreover, use has been made of the following relation, holding for any two vectors $\mathbf{u}$ and $\mathbf{w}$, and a second-order tensor $\mathbf{T}$:

$$(\mathbf{T}\,\mathbf{w})\cdot\mathbf{u} = \mathbf{w}\cdot(\mathbf{T}^T\,\mathbf{u})\,. \tag{3.16}$$

The second-order tensor $\mathbf{C} := \mathbf{F}^T\,\mathbf{F}$ in (3.15) is then called the right Cauchy-Green deformation tensor, which is, obviously, a deformation measure existing in the reference configuration. Analogously, considering the pull-back mechanism of the line elements given in (3.9), the square of the line element in the reference configuration is given as

$$\mathrm{d}\mathbf{X}\cdot\mathrm{d}\mathbf{X} = \mathbf{F}^{-1}\,\mathrm{d}\mathbf{x}\cdot\mathbf{F}^{-1}\,\mathrm{d}\mathbf{x} = \mathrm{d}\mathbf{x}\cdot(\mathbf{F}\,\mathbf{F}^T)^{-1}\,\mathrm{d}\mathbf{x} =: \mathrm{d}\mathbf{x}\cdot\mathbf{B}^{-1}\,\mathrm{d}\mathbf{x}\,, \tag{3.17}$$

where $\mathbf{B} := \mathbf{F}\,\mathbf{F}^T$ is called left Cauchy-Green deformation tensor, which is, clearly, a deformation measure existing in the current configuration. Having these relations at hand, the Green-Lagrangean and the Almansian strain tensors, measuring the difference of squares of the line elements in the reference and in the current configurations, are introduced as follows:

$$\begin{aligned} \mathrm{d}\mathbf{x}\cdot\mathrm{d}\mathbf{x} - \mathrm{d}\mathbf{X}\cdot\mathrm{d}\mathbf{X} &= \mathrm{d}\mathbf{X}\cdot(\mathbf{C}-\mathbf{I})\,\mathrm{d}\mathbf{X} &&=: \mathrm{d}\mathbf{X}\cdot 2\,\mathbf{E}\,\mathrm{d}\mathbf{X}\,, \\ \mathrm{d}\mathbf{x}\cdot\mathrm{d}\mathbf{x} - \mathrm{d}\mathbf{X}\cdot\mathrm{d}\mathbf{X} &= \mathrm{d}\mathbf{x}\cdot(\mathbf{I}-\mathbf{B}^{-1})\,\mathrm{d}\mathbf{x} &&=: \mathrm{d}\mathbf{x}\cdot 2\,\mathbf{A}\,\mathrm{d}\mathbf{x}\,. \end{aligned} \tag{3.18}$$

Therein $\mathbf{E}$ and $\mathbf{A}$ respectively represent the Green-Lagrangean and the Almansian strain tensors, and read

$$\mathbf{E} = \tfrac{1}{2}\,(\mathbf{C}-\mathbf{I})\,, \quad \mathbf{A} = \tfrac{1}{2}\,(\mathbf{I}-\mathbf{B}^{-1})\,. \tag{3.19}$$

It should be noted that a linearisation of $\mathbf{E}$ and $\mathbf{A}$ around the undeformed reference configuration yields the same results. The quantity obtained through this linearisation is the infinitesimal strain tensor $\boldsymbol{\varepsilon}$ in the geometrically linear regime. It reads

$$\mathbf{E}_{\text{lin.}} \equiv \mathbf{A}_{\text{lin.}} =: \boldsymbol{\varepsilon} = \tfrac{1}{2}\,\big(\mathrm{Grad}\,\mathbf{u} + \mathrm{Grad}^T\,\mathbf{u}\big) = \mathrm{sym}\,(\mathrm{Grad}\,\mathbf{u})\,. \tag{3.20}$$

3.2.3 Stress tensors

In the most general case, the body $\mathcal{B}$ may be subjected to surface and also volume forces. The surface forces are naturally the contact forces (actions from the vicinity), acting only on the material points at the surface of the body. In contrast, the volume forces are due to some action from the distance and act on every material point. In this regard, an increment of the contact force $\mathrm{d}\mathbf{k}_{\mathcal{S}}$ applied to a surface element $\mathrm{d}a$ and an increment of the volume force $\mathrm{d}\mathbf{k}_V$ applied to a volume element $\mathrm{d}v$ are given as

$$\mathrm{d}\mathbf{k}_S = \mathbf{t}\,\mathrm{d}a \quad \text{and} \quad \mathrm{d}\mathbf{k}_V = \mathbf{f}\,\mathrm{d}v\,, \tag{3.21}$$

wherein, proceeding from a mass-specific gravitational force $\mathbf{b}$ as the action from a distance, $\mathbf{f} = \rho\,\mathbf{b}$, where ρ denotes the mass density of the material. Subsequent integration of the incremental forces and summing over the results then yields the total force $\mathbf{k}$ acting on the body:

$$\mathbf{k} = \mathbf{k}_S + \mathbf{k}_V = \int_{\mathcal{S}} \mathbf{t}\,\mathrm{d}a + \int_{\mathcal{B}} \rho\,\mathbf{b}\,\mathrm{d}v\,. \tag{3.22}$$

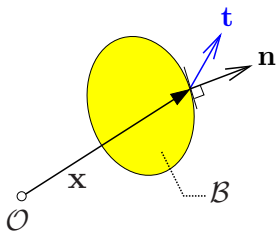

Figure 3.2: *Traction force* $\mathbf{t}$ *acting at the surface with the normal* $\mathbf{n}$.

In this context, it should be noted that, unlike the usual field functions, which are only functions of position $\mathbf{x}$ and time t, the surface traction force $\mathbf{t}$ depends also on the orientation of the surface element. This dependency is regulated via an outward-oriented unit vector $\mathbf{n}$, which is normal to the area element $\mathrm{d}a$ at the position $\mathbf{x}$, cf. Figure 3.2. Thus, $\mathbf{t} = \mathbf{t}(\mathbf{x}\,, \mathbf{n}\,, t)$. Using Cauchy's lemma and, subsequently, Cauchy's theorem is an appealing approach to replace this vector with a more convenient stress tensor $\mathbf{T} = \mathbf{T}(\mathbf{x}\,, t)$.

Cauchy's lemma and theorem are both introduced by Augustin-Louis Cauchy (1789–1857) in 1823. The lemma is derived considering the surface forces applied to a body, when it is considered as a whole, and when it is cut into two parts. Following that, by comparing these forces with each other and requesting their equivalence, one concludes

$$\mathbf{t}(\mathbf{x}\,, \mathbf{n}\,, t) = -\mathbf{t}(\mathbf{x}\,, -\mathbf{n}\,, t)\,. \tag{3.23}$$

Furthermore, Cauchy's theorem is based on the equilibrium of surface forces applied to a tetrahedral volume element, in which the volume terms are negligible compared to the area terms. Then, by considering the axiom of static equilibrium in conjunction with the above introduced lemma, one obtains

$$\mathbf{t}(\mathbf{x}\,, \mathbf{n}\,, t) = \mathbf{T}(\mathbf{x}, t)\,\mathbf{n}\,, \tag{3.24}$$

wherein, $\mathbf{T}$ depicts the Cauchy stress, also known as the true stress. The latter naming is due to the fact that $\mathbf{T}$ describes the surface force acting on the area element in the current configuration. Thus,

$$\mathrm{d}\mathbf{k}_S = \mathbf{t}\,\mathrm{d}a = \mathbf{T}\,\mathbf{n}\,\mathrm{d}a =: \mathbf{T}\,\mathrm{d}\mathbf{a}\,, \tag{3.25}$$

wherein $\mathrm{d}\mathbf{a} := \mathbf{n}\,\mathrm{d}a$ is the oriented area element in the current configuration. Furthermore, from $(3.10)_1$, one obtains

$$\mathrm{d}\mathbf{a} = \operatorname{cof}\mathbf{F}\;\mathrm{d}\mathbf{A} \quad \rightarrow \quad \mathrm{d}\mathbf{k}_S = \mathbf{T}\operatorname{cof}\mathbf{F}\;\mathrm{d}\mathbf{A} = \underbrace{\overbrace{\mathbf{T}\,(\det\mathbf{F})}^{\boldsymbol{\tau}}\,\mathbf{F}^{T-1}}_{\mathbf{P}}\;\mathrm{d}\mathbf{A}\,,$$

wherein, the Kirchhoff stress $\boldsymbol{\tau}$ and the first Piola-Kirchhoff stress $\mathbf{P}$ are introduced as

$$\boldsymbol{\tau} = (\det\mathbf{F})\;\mathbf{T}\,, \quad \mathbf{P} = \boldsymbol{\tau}\,\mathbf{F}^{T-1}\,. \tag{3.26}$$

Then, the second Piola-Kirchhoff stress tensor is found by a covariant pull-back[7] of the Kirchhoff stress, and reads

$$\mathbf{S} = \mathbf{F}^{-1}\,\boldsymbol{\tau}\,\mathbf{F}^{T-1}\,. \tag{3.27}$$

[7]The co- and contravariant push-forward and pull-back mechanisms are based on the representation of the vectorial and the tensorial objects in the natural (curvilinear) coordinate system. Comprehensive explanations are provided by de Boer [26], Karajan [155], Markert [187].

It should also be noted that, for the small strain approaches where Grad $\mathbf{u} \ll \mathbf{I}$, one defines

$$\boldsymbol{\sigma} :\approx \mathbf{S} \approx \mathbf{P} \approx \boldsymbol{\mathcal{T}} \approx \mathbf{T} \,. \tag{3.28}$$

Therein, $\boldsymbol{\sigma} = \boldsymbol{\sigma}(\mathbf{X}\,, t)$ represents the geometrically linear stress tensor.

3.2.4 Balance laws

The global representations of the master balance of continuum mechanics for a volume-specific scalar term Ψ and for a volume-specific vectorial term $\boldsymbol{\Psi}$ read

$$\begin{aligned} \frac{\mathrm{d}}{\mathrm{d}t}\int_{\mathcal{B}} \Psi \mathrm{d}v &= \int_{\mathcal{S}} (\boldsymbol{\phi}\cdot\mathbf{n})\,\mathrm{d}a + \int_{\mathcal{B}} \sigma\,\mathrm{d}v + \int_{\mathcal{B}} \hat{\Psi}\,\mathrm{d}v\,, \\ \frac{\mathrm{d}}{\mathrm{d}t}\int_{\mathcal{B}} \boldsymbol{\Psi} \mathrm{d}v &= \int_{\mathcal{S}} (\boldsymbol{\Phi}\,\mathbf{n})\,\mathrm{d}a + \int_{\mathcal{B}} \boldsymbol{\sigma}\,\mathrm{d}v + \int_{\mathcal{B}} \widehat{\boldsymbol{\Psi}}\,\mathrm{d}v\,. \end{aligned} \tag{3.29}$$

Therein, $\boldsymbol{\phi}\cdot\mathbf{n}$ and $\boldsymbol{\Phi}\,\mathbf{n}$ denote the efflux of the mechanical quantity through the surface $\mathcal{S}$ (action at the vicinity), σ and $\boldsymbol{\sigma}$ show the supply of the mechanical quantity (action from the distance), and $\hat{\Psi}$ and $\widehat{\boldsymbol{\Psi}}$ represent the production of the mechanical quantity.

The above master balances are valid for the overall body $\mathcal{B}$. The local version of these relations, valid for each material point $\mathcal{P}$, are obtained through two main steps: first, the material time derivation of the left-hand side is determined and, then, the Gaussian integration theorem is applied to the surface integrals on the right-hand side. Consequently, one obtains

$$\begin{aligned} \int_{\mathcal{B}} \left(\dot{\Psi} + \Psi\,\mathrm{div}\,\dot{\mathbf{x}}\right)\,\mathrm{d}v &= \int_{\mathcal{B}} \left(\mathrm{div}\,\boldsymbol{\phi} + \sigma + \hat{\Psi}\right)\,\mathrm{d}v\,, \\ \int_{\mathcal{B}} \left(\dot{\boldsymbol{\Psi}} + \boldsymbol{\Psi}\,\mathrm{div}\,\dot{\mathbf{x}}\right)\,\mathrm{d}v &= \int_{\mathcal{B}} \left(\mathrm{div}\,\boldsymbol{\Phi} + \boldsymbol{\sigma} + \widehat{\boldsymbol{\Psi}}\right)\,\mathrm{d}v\,. \end{aligned} \tag{3.30}$$

Thus, provided that the integrands are steady and sufficiently often steadily differentiable, the local form of the balance relations are given as

$$\dot{\Psi} + \Psi\,\mathrm{div}\,\dot{\mathbf{x}} = \mathrm{div}\,\boldsymbol{\phi} + \sigma + \hat{\Psi}\,, \quad \dot{\boldsymbol{\Psi}} + \boldsymbol{\Psi}\,\mathrm{div}\,\dot{\mathbf{x}} = \mathrm{div}\,\boldsymbol{\Phi} + \boldsymbol{\sigma} + \widehat{\boldsymbol{\Psi}}\,. \tag{3.31}$$

Replacing the parameters in the above relations by the quantities presented in Table 3.1 yields the conservation laws of continuum thermodynamics, i. e., the balances of mass, linear momentum, moment of momentum (m.o.m.), energy and entropy for a closed system [81], cf. Table 3.2 for interpretations of the symbols employed in Table 3.1.

In conclusion, the balance relations found after insertion of the respective quantities presented in Table (3.1) into $(3.31)_{1,2}$ read as follows:

- Balance of mass

$$\dot{\rho} + \rho\,\mathrm{div}\,\dot{\mathbf{x}} = 0\,. \tag{3.32}$$

- Balance of linear momentum

$$\rho\,\ddot{\mathbf{x}} = \mathrm{div}\,\mathbf{T} + \rho\,\mathbf{b}\,. \tag{3.33}$$

- Balance of angular momentum or moment of momentum

$$\mathbf{0} = \mathbf{I} \times \mathbf{T} \;\rightarrow\; \mathbf{T} = \mathbf{T}^T \,. \tag{3.34}$$

- Balance of energy

$$\rho\,\dot{\varepsilon} = \mathbf{T} \cdot \operatorname{grad} \dot{\mathbf{x}} - \operatorname{div} \mathbf{q} + \rho\, r \,. \tag{3.35}$$

- Balance of entropy

$$\rho\,\dot{\eta} \geq \operatorname{div} \phi_\eta + \sigma_\eta \,. \tag{3.36}$$

	$\Psi, \boldsymbol{\Psi}$	$\boldsymbol{\phi}, \boldsymbol{\Phi}$	$\sigma, \boldsymbol{\sigma}$	$\hat{\Psi}, \widehat{\boldsymbol{\Psi}}$
Mass	ρ	$\mathbf{0}$	0	0
Momentum	$\rho\,\dot{\mathbf{x}}$	$\mathbf{T}$	$\rho\,\mathbf{b}$	$\mathbf{0}$
M.o.m.	$\mathbf{x} \times (\rho\,\dot{\mathbf{x}})$	$\mathbf{x} \times \mathbf{T}$	$\mathbf{x} \times (\rho\,\mathbf{b})$	$\mathbf{0}$
Energy	$\rho\,\varepsilon + \frac{1}{2}\,\dot{\mathbf{x}} \cdot (\rho\,\dot{\mathbf{x}})$	$\mathbf{T}^T\,\dot{\mathbf{x}} - \mathbf{q}$	$\dot{\mathbf{x}} \cdot (\rho\,\mathbf{b}) + \rho\, r$	0
Entropy	$\rho\,\eta$	ϕ_η	σ_η	$\hat{\eta} \geq 0$

Table 3.1: *Physical quantities employed in the local balance relations (3.31).*

Parameter	Symbol	Parameter	Symbol
Mass density	ρ	Cauchy stress tensor	$\mathbf{T}$
Mass-specific body force vector	$\mathbf{b}$	Internal energy	ε
Heat influx vector	$\mathbf{q}$	External heat supply	r
Entropy	η	Efflux of entropy	$\phi_\eta := -\dfrac{\mathbf{q}}{\theta}$
External entropy supply	$\sigma_\eta := \dfrac{\rho\, r}{\theta}$	Absolute temperature	θ
Entropy production	$\hat{\eta}$		

Table 3.2: *Interpretation of the symbols presented in Table 3.1.*

3.2.5 Two representative examples

In what follows, the systems of governing equations for the problems of linear thermo-elastodynamics as well as incompressible and inviscid fluid flow are presented. The corresponding model problems will be utilised in the later parts of this contribution in order to discuss the coupling mechanisms and to present specific decoupling strategies.

Linear thermo-elastodynamics

As the name suggests, the problem of thermo-elastodynamics aims at describing the mutual changes in the temperature and deformation fields within an elastic solid. Thus, the balances of linear momentum and energy compose the system of governing equations for this problem. According to Armero & Simo [4], these equations in the geometrically linear regime read

$$\mathcal{X} \;:\; \begin{cases} \rho\,\ddot{\mathbf{u}} &= \operatorname{div}\boldsymbol{\sigma} + \rho\,\mathbf{b}\,, \\ c_v\,\dot{\vartheta} &= m\,\theta_0\operatorname{div}\dot{\mathbf{u}} - \operatorname{div}\mathbf{q} + r\,. \end{cases} \tag{3.37}$$

Therein, $\mathbf{u}$ shows the displacement vector and $\vartheta = \theta - \theta_0$ represents the relative temperature, determining the difference between the absolute temperature θ and a constant and homogeneous reference temperature θ_0. Moreover, ρ is the mass density, c_v is the volumetric heat capacity[8], $m = -(2\,\mu + 3\,\lambda)\,\alpha$ is the stress-temperature modulus that governs the coupling strength between the thermal and mechanical fields with α denoting the coefficient of thermal expansion and μ and λ being the Lamé constants. Furthermore, $\boldsymbol{\sigma}$ depicts the stress tensor in the geometrically linear regime, determined via the following constitutive relation:

$$\boldsymbol{\sigma} = \overset{4}{\mathbf{B}}_0\,\boldsymbol{\varepsilon} + m\,\vartheta\,\mathbf{I} \quad \text{with} \quad \overset{4}{\mathbf{B}}_0 := 2\,\mu\,(\mathbf{I}\otimes\mathbf{I})^{\overset{23}{T}} + \lambda\,(\mathbf{I}\otimes\mathbf{I})\,. \tag{3.38}$$

Therein, $\boldsymbol{\varepsilon}$ is the linear strain tensor as in (3.20) and $\overset{4}{\mathbf{B}}_0$ represents the 4^{th}-order elasticity tensor for infinitesimal deformations. In addition, $\mathbf{q}$ embodies the heat influx vector, governed by the Fourier's law of heat conduction:

$$\mathbf{q} = -k\,\operatorname{grad}\vartheta\,, \tag{3.39}$$

where $k > 0$ is the thermal conductivity. Inserting the constitutive relations (3.38) and (3.39) into (3.37) and assuming constant material parameters, one arrives at the following set of governing equations for the problem of linear thermo-elastodynamics

$$\mathcal{X} \;:\; \begin{cases} \rho\,\ddot{\mathbf{u}} &= \operatorname{div}(\overset{4}{\mathbf{B}}_0\,\boldsymbol{\varepsilon}) + m\,\operatorname{grad}\vartheta + \rho\,\mathbf{b}\,, \\ c_v\,\dot{\vartheta} &= m\,\theta_0\operatorname{div}\dot{\mathbf{u}} + k\operatorname{div}\operatorname{grad}\vartheta + r\,. \end{cases} \tag{3.40}$$

Incompressible and inviscid fluid flow

Describing the evolution of the pressure and velocity fields within a body of fluid, the set of governing equations for this problem is composed of the balances of linear momentum and mass, respectively shown by (3.33) and (3.32). Thus,

$$\mathcal{X} \;:\; \begin{cases} \rho\,\dot{\mathbf{v}} = \operatorname{div}\mathbf{T} + \rho\,\mathbf{b}\,, \\ \dot{\rho} + \rho\operatorname{div}\mathbf{v} = 0\,. \end{cases} \tag{3.41}$$

[8] Note that the volumetric heat capacity c_v with the SI unit $\frac{\mathrm{J}}{\mathrm{K\,m^3}}$ specifies the heat capacity per unit volume. It is not to be mistaken with the specific heat capacity at constant volume C_v with the SI unit $\frac{\mathrm{J}}{\mathrm{K\,kg}}$.

Note that $(3.41)_1$ represents the balance of linear momentum in a Lagrangean framework, that is, from the viewpoint of an observer who moves with the fluid particles. However, in the realm of fluid mechanics, it is more convenient to describe the motion of a fluid from the viewpoint of a stationary observer. This idea leads to the Eulerian version of $(3.41)_1$, which reads

$$\rho \left[\frac{\partial \mathbf{v}}{\partial t} + (\operatorname{grad} \mathbf{v})\, \mathbf{v} \right] = \operatorname{div} \mathbf{T} + \rho\, \mathbf{b}\,. \tag{3.42}$$

This relation, in conjunction with the balance of mass $(3.41)_2$ and considering the identity

$$\operatorname{div} (\mathbf{a} \otimes \mathbf{b}) = \mathbf{a} \operatorname{div} \mathbf{b} + (\operatorname{grad} \mathbf{a})\, \mathbf{b}\,, \quad \forall \{\mathbf{a}\,, \mathbf{b}\} \in \mathbb{R}^p\,, \tag{3.43}$$

alternatively reads

$$\frac{\partial (\rho\, \mathbf{v})}{\partial t} = \operatorname{div} (\mathbf{T} - \rho\, \mathbf{v} \otimes \mathbf{v}) + \rho\, \mathbf{b}\,. \tag{3.44}$$

Nevertheless, and as will be explained in more details in Section 7.3.1, an Eulerian description of the motion of a body of fluid within moving boundaries is usually avoided. In such a case, employing the so-called arbitrary Lagrangean-Eulerian (ALE) version of the equations, as described for example by Belytschko *et al.* [17] and Wall [275], or exploiting the idea of modified Eulerian description (MED) of the motion of fluid, as explained in the aforementioned section, proves to be more convenient.

It should further be noted that for an incompressible fluid, $\rho = \text{const.}$ and, thus, the balance of mass takes the following form, usually known as the continuity condition:

$$\operatorname{div} \mathbf{v} = 0\,. \tag{3.45}$$

Furthermore, having an incompressible and inviscid fluid, the stress tensor $\mathbf{T}$ is determined by the hydraulic pressure p, such that $\mathbf{T} = -p\, \mathbf{I}$. Considering these notes, the system of equations governing the motion of an incompressible and inviscid fluid in a Lagrangean frame takes the following form:

$$\mathcal{X} \;:\; \left\{ \begin{array}{ll} \rho\, \dot{\mathbf{v}} & = -\operatorname{grad} p + \rho\, \mathbf{b}\,, \\ 0 & = \operatorname{div} \mathbf{v}\,. \end{array} \right. \tag{3.46}$$

3.3 The Theory of Porous Media

The Theory of Porous Media (TPM) provides an excellent continuum-mechanical framework for the macroscopic description of the complex behaviour of mutliphasic material bodies. The roots of the TPM can be traced back to the original work of Truesdell [269] on the the Theory of Mixtures (TM) [83]. Enhancing the TM through inclusion of the concept of volume fractions by Bowen [30, 31] followed by the several treatises of de Boer & Ehlers [27] and Ehlers [77–79, 81, 82] has led to the development of the modern TPM, as we know it today. Complete presentation of the TPM can be found in the mentioned references. Furthermore, Ehlers [83] provides a historical account of the development of the TPM.

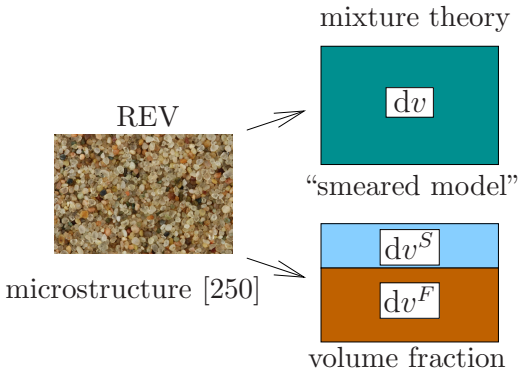

Figure 3.3: *REV with the granular microstructure of sand and the biphasic TPM macro model.*

Within this work, in Sections 6.2 and 7.3, we introduce a biphasic, fluid-saturated porous medium, composed of two immiscible constituents, namely one solid skeleton φ^S and one fluid pore content φ^F. For the macroscopic description of such a system in the framework of the TPM, a local representative elementary volume (REV) is defined and, subsequently, exploiting an averaging process, the real microstructure of the domain is smeared out over the REV. Consequently, the original microstructure is replaced by a homogeneous continuum $\varphi = \varphi^S \cup \varphi^F$, in which the constituents exist in the form of superimposed continua with internal interactions and individual states of motion, statistically distributed throughout the control space. The incorporated geometrical and physical fields are then understood as local averages of the corresponding microscopic quantities. Furthermore, the information about the microstructure of the model is captured by local volume fractions, specified by local ratios of the volume element of each constituent $\mathrm{d}v^\alpha$ to the volume element of the overall aggregate $\mathrm{d}v$ (cf. Figure 3.3):

$$n^\alpha := \frac{\mathrm{d}v^\alpha}{\mathrm{d}v}\,, \quad \alpha = \{S\,, F\}\,. \tag{3.47}$$

Following this, the saturation condition for the porous medium reads

$$\sum_\alpha n^\alpha = n^S + n^F = 1 \quad \text{with} \quad \left\{ \begin{array}{ll} n^S : & \text{solidity}\,, \\ n^F : & \text{porosity}\,. \end{array} \right. \tag{3.48}$$

Moreover, by relating the local mass $\mathrm{d}m^\alpha$ of each constituent φ^α to the volume element $\mathrm{d}v^\alpha$ of the very constituent, or to the volume element $\mathrm{d}v$ of the overall aggregate φ, one obtains two mass density functions, namely the material density $\rho^{\alpha R}$ and the partial density ρ^α, where

$$\mathrm{d}m^\alpha = \left\{ \begin{array}{c} \rho^{\alpha R}\,\mathrm{d}v^\alpha \\ \rho^\alpha\,\mathrm{d}v \end{array} \right\} \quad \rightarrow \quad \rho^\alpha = n^\alpha\,\rho^{\alpha R}\,. \tag{3.49}$$

3.3.1 Kinematical relations of mixtures

Following the idea of superimposed continua with internal interactions and individual motion functions, one proceeds from the assumption that every spatial point $\mathbf{x}$ of the

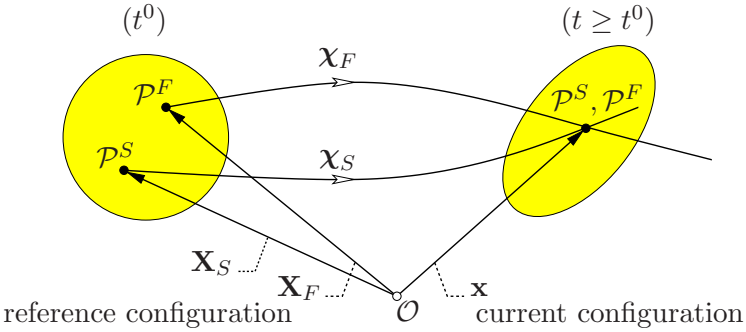

Figure 3.4: *Motion of a biphasic mixture.*

control space at any time t is simultaneously occupied by the material particles $\mathcal{P}^\alpha$ of all constituents φ^α, such that

$$\mathbf{x}_S = \mathbf{x}_F =: \mathbf{x}\,. \tag{3.50}$$

Nevertheless, each material particle $\mathcal{P}^\alpha$ follows an individual path defined by its unique and uniquely invertible motion function $\boldsymbol{\chi}_\alpha$:

$$\mathbf{x} = \boldsymbol{\chi}_\alpha(\mathbf{X}_\alpha\,, t) \quad \Longleftrightarrow \quad \mathbf{X}_\alpha = \boldsymbol{\chi}_\alpha^{-1}(\mathbf{x}\,, t)\,, \tag{3.51}$$

where $\mathbf{X}_\alpha$ represents the reference position of particle $\mathcal{P}^\alpha$ at the initial time t^0, cf. Figure 3.4. The motion function is further used to calculate the individual velocity and acceleration fields $\mathbf{v}_\alpha$ and $(\mathbf{v}_\alpha)'_\alpha$ of the constituent φ^α. In the Lagrangean setting, these fields are given by

$$\mathbf{v}_\alpha := \overset{\prime}{\mathbf{x}}_\alpha = \frac{\partial \boldsymbol{\chi}_\alpha(\mathbf{X}_\alpha\,, t)}{\partial t}\,, \quad (\mathbf{v}_\alpha)'_\alpha = \overset{\prime\prime}{\mathbf{x}}_\alpha = \frac{\partial^2 \boldsymbol{\chi}_\alpha(\mathbf{X}_\alpha\,, t)}{\partial t^2}\,, \tag{3.52}$$

wherein, $(\,\cdot\,)'_\alpha$ denotes the material time derivative with respect to the motion of the constituent φ^α, such that

$$(\,\cdot\,)'_\alpha := \frac{\mathrm{d}_\alpha(\,\cdot\,)}{\mathrm{d}t} = \frac{\partial(\,\cdot\,)}{\partial t} + \operatorname{grad}(\,\cdot\,)\,\mathbf{v}_\alpha \quad \text{with} \quad \operatorname{grad}(\,\cdot\,) = \frac{\partial(\,\cdot\,)}{\partial \mathbf{x}}\,. \tag{3.53}$$

Then, in order to describe the behaviour of the biphasic mixture, it is the common practice to proceed from a Lagrangean description of the solid matrix φ^S using the solid displacement $\mathbf{u}_S$ and the solid velocity $\mathbf{v}_S$ as the primary kinematic variables. However, the pore fluid φ^F could more conveniently be described in a modified Eulerian setting by use of the seepage velocity $\mathbf{w}_F$ describing the fluid motion with respect to the deforming solid skeleton. In this regard,

$$\mathbf{u}_S = \mathbf{x} - \mathbf{X}_S\,, \quad \mathbf{v}_S = (\mathbf{u}_S)'_S = \overset{\prime}{\mathbf{x}}_S \quad \text{and} \quad \mathbf{w}_F = \mathbf{v}_F - \mathbf{v}_S\,. \tag{3.54}$$

3.3.2 Mathematical model

Considering a fluid-saturated biphasic porous medium with intrinsically incompressible and inert constituents, namely one solid skeleton φ^S and one pore fluid φ^F, the system of governing equations comprises the solid-matrix linear-momentum balance, the pore-fluid

linear-momentum balance and the mixture volume balance [81]. In the absence of mass exchanges (inert φ^α), these relations read

$$\mathcal{X} \;:\; \left\{ \begin{array}{rcl} \rho^S \, (\mathbf{u}_S)'_S &=& \operatorname{div} \mathbf{T}^S + \rho^S \, \mathbf{b} + \hat{\mathbf{p}}^S \,, \\ \rho^F \, (\mathbf{v}_F)'_F &=& \operatorname{div} \mathbf{T}^F + \rho^F \, \mathbf{b} + \hat{\mathbf{p}}^F \,, \\ 0 &=& \operatorname{div} (\mathbf{v}_S + n^F \, \mathbf{w}_F) \,, \end{array} \right. \tag{3.55}$$

wherein, $(\,\cdot\,)''_\alpha := \mathrm{d}^2_\alpha / \mathrm{d}t^2$. Moreover, $n^F = 1 - n^S$, where the solidity n^S is uniquely defined through $\det \mathbf{F}_S$ by integration of the volume balance, and reads

$$n^S = n^S_{0S} \, (\det \mathbf{F}_S)^{-1} \,. \tag{3.56}$$

Therein, $n^S_{0S} = \text{const.}$ is the initial volume fraction of φ^S at time t^0. Furthermore, $\mathbf{T}^\alpha$ is the symmetric partial Cauchy stress tensor, and $\hat{\mathbf{p}}^\alpha$ denotes the direct momentum production which is, proceeding from a closed mixture, constrained, such that $\hat{\mathbf{p}}^S + \hat{\mathbf{p}}^F = \mathbf{0}$. The corresponding relations for these quantities read

$$\mathbf{T}^\alpha = \mathbf{T}^\alpha_E - n^\alpha \, p^F \, \mathbf{I} \,, \quad \hat{\mathbf{p}}^F = \hat{\mathbf{p}}^F_E + p^F \operatorname{grad} n^F \,. \tag{3.57}$$

Therein, p^F is the pore-fluid pressure, and $(\,\cdot\,)_E$ denotes the extra terms that should be determined via admissible constitutive equations. For instance, proceeding from an infinitesimal solid deformation, the extra stress tensor for the solid skeleton is determined by the Hookean elasticity law

$$\mathbf{T}^S_E \approx \boldsymbol{\sigma}^S_E = 2 \, \mu^S \, \boldsymbol{\varepsilon}_S + \lambda^S \, (\boldsymbol{\varepsilon}_S \cdot \mathbf{I}) \, \mathbf{I} \,, \tag{3.58}$$

where $\boldsymbol{\varepsilon}_S := \operatorname{sym}(\operatorname{grad} \mathbf{u}_S)$ is the linear solid strain tensor, and μ^S and λ^S are the Lamé constants of the porous solid matrix. Furthermore, Ehlers *et al.* [84] have shown via a dimensional analysis that in a macroscopic porous media approach, $\operatorname{div} \mathbf{T}^F_E \ll \hat{\mathbf{p}}^F_E$. Therefore, $\mathbf{T}^F_E$ is usually neglected and one assumes

$$\mathbf{T}^F = -n^F \, p^F \, \mathbf{I} \,. \tag{3.59}$$

Moreover, in the geometrically linear case with isotropic permeability, the constitutive equation for the extra momentum production term $\hat{\mathbf{p}}^F_E$ can be expressed as

$$\hat{\mathbf{p}}^F_E = - \frac{(n^F)^2 \, \gamma^{FR}}{k^F} \, \mathbf{w}_F \,, \tag{3.60}$$

wherein γ^{FR} is the effective weight of the pore fluid, and k^Frepresents the Darcy permeability (hydraulic conductivity).

It should also be noted that in the framework of the TPM, the motion of the pore fluid is commonly described in the modified Eulerian framework. Thus, the material time derivative with respect to the fluid motion in $(3.55)_2$ can be replaced by the following relation derived from $(3.53)_1$ and $(3.54)_3$:

$$(\,\cdot\,)'_F = (\,\cdot\,)'_S + \operatorname{grad}(\,\cdot\,) \, \mathbf{w}_F \,. \tag{3.61}$$

Thus, after inserting (3.57) and by including $(3.54)_2$ in order to reduce the order of temporal derivatives, the complete set of governing equations for the porous medium subsystem takes the form

$$\mathcal{X} \;:\; \begin{cases} (\mathbf{u}_S)'_S = \mathbf{v}_S \,, \\ \rho^S \, (\mathbf{v}_S)'_S = \operatorname{div} \mathbf{T}^S_E - n^S \operatorname{grad} p^F \; + \dfrac{(n^F)^2 \, \gamma^{FR}}{k^F} \, \mathbf{w}_F \,, \\ \rho^F \; [(\mathbf{v}_F)'_S + (\operatorname{grad} \mathbf{v}_F) \, \mathbf{w}_F] = -n^F \operatorname{grad} p^F - \dfrac{(n^F)^2 \, \gamma^{FR}}{k^F} \, \mathbf{w}_F \,, \\ 0 = \operatorname{div} (\mathbf{v}_S + n^F \, \mathbf{w}_F) \,. \end{cases} \tag{3.62}$$

3.4 Systems of coupled equations

As it was seen, the mathematical model of a physical phenomenon in the framework of continuum mechanics is composed of a set of partial differential equations. Thus, the mathematical model of a (transient) phenomenon, happening on some specific d-dimensional spatial domain $\Omega \subset \mathbb{R}^d$ and time interval $[t^0 \,, T] \subset \mathbb{R}$, may be written as[9]

$$\mathcal{X} \;:\; \boldsymbol{\mathcal{F}} \, (\mathfrak{u}(\mathbf{x} \,, t)) = \mathfrak{S} \, \mathfrak{u}(\mathbf{x} \,, t) - \mathfrak{f}(\mathbf{x} \,, t) = \mathbf{0} \,, \qquad \forall \, \mathbf{x} \in \Omega \quad \text{and} \quad t \in [t^0 \,, T] \,, \tag{3.63}$$

wherein $\mathfrak{u} : \mathbb{R}^d \times \mathbb{R} \to \mathbb{R}^p$ is the unknown state vector of the system, containing p time- and space-dependent field (state) variables, $\boldsymbol{\mathcal{F}} : \mathbb{R}^p \to \mathbb{R}^p$ is a vector containing the corresponding balance equations, $\mathfrak{f} : \mathbb{R}^d \times \mathbb{R} \to \mathbb{R}^p$ is the force vector, and $\mathfrak{S}$ embodies some differential operators in space and time. In particular, considering the balance relations of continuum mechanics, $\mathfrak{S}$ may be split into a pure temporal sub-operator $\mathfrak{S}_t$, and a mixed sub-operator $\overline{\mathfrak{S}}$, such that $\mathfrak{S} = \mathfrak{S}_t - \overline{\mathfrak{S}}$. Thus, (3.63) alternatively reads

$$\mathcal{X} \;:\; \mathfrak{S}_t \, \mathfrak{u}(\mathbf{x} \,, t) = \overline{\mathfrak{S}} \, \mathfrak{u}(\mathbf{x} \,, t) + \mathfrak{f}(\mathbf{x} \,, t) =: \boldsymbol{f}(\mathbf{x} \,, t) \,, \qquad \forall \, \mathbf{x} \in \Omega \quad \text{and} \quad t \in [t^0 \,, T] \,. \tag{3.64}$$

Proceeding from the mathematical model of a coupled multi-field phenomenon, the components of $\boldsymbol{\mathcal{F}}$ are coupled to each other. This coupling between the individual equations $\mathcal{F}_i = 0$ is such that at least some of them are expressed in terms of more than one field variable, and this interdependency cannot be eliminated on the equation level.

In what follows, the mechanism of coupling between the equations is firstly described. After that, the concepts of partial differential and differential algebraic equation systems are introduced. In particular, the computational issues caused by the algebraic constraints are addressed and, following that, exemplary methods for overcoming these difficulties are studied. At the end, the notion of stiff differential equations is introduced.

[9] To avoid unnecessary complexities in the notations, we proceed from an autonomous form of the differential equations. Note that, a non-autonomous system in form of $\overline{\boldsymbol{\mathcal{F}}} \, (\overline{\mathfrak{u}}(\mathbf{x} \,, t), t) = \mathbf{0}$ could always be brought to the autonomous form (3.63) by appending an auxiliary variable $\overline{\mathfrak{u}}_0$ to the vector of unknowns, such that $\mathfrak{u} := [\overline{\mathfrak{u}}_0 \,, \overline{\mathfrak{u}}]^T$ and by adding the equation $\overline{\mathcal{F}}_0 := \mathrm{d}\overline{\mathfrak{u}}_0 / \mathrm{d}t = 1$ to the set of equations, such that $\boldsymbol{\mathcal{F}} := [\overline{\mathcal{F}}_0 \,, \overline{\boldsymbol{\mathcal{F}}}]^T$.

3.4.1 PDE and DAE systems

To start off, consider the governing equations of the volume-coupled problem of thermo-elastodynamics (3.40). The 1-d counterpart of these equations read [4][10]

$$\mathcal{X} \;:\; \begin{cases} \mathcal{F}_u(u\,,\vartheta) &= \rho\,\dfrac{\mathrm{d}^2 u}{\mathrm{d}t^2} - E\,\dfrac{\partial^2 u}{\partial x^2} - m\,\dfrac{\partial \vartheta}{\partial x} - \rho\, b = 0\,, \\[2ex] \mathcal{F}_\vartheta(\vartheta\,,u) &= c_v\,\dfrac{\mathrm{d}\vartheta}{\mathrm{d}t} - k\,\dfrac{\partial^2 \vartheta}{\partial x^2} - \theta_0\, m\,\dfrac{\partial}{\partial x}\left(\dfrac{\mathrm{d}u}{\mathrm{d}t}\right) - r = 0\,, \end{cases} \tag{3.65}$$

where $E = \mu\,(3\,\lambda + 2\,\mu)/(\lambda + \mu)$ is the Young's modulus and other parameters are as described under (3.40). Comparing (3.63) to (3.65) yields the following identifications:

$$\boldsymbol{\mathcal{F}} = [\mathcal{F}_u\,,\mathcal{F}_\vartheta]^T\,, \quad \mathbf{u} = [u\,,\vartheta]^T\,, \quad \mathfrak{f} = [\rho\, b\,, r]^T\,,$$

$$\mathfrak{S} = \begin{bmatrix} \rho\,\dfrac{\mathrm{d}^2}{\mathrm{d}t^2} - E\,\dfrac{\partial^2}{\partial x^2} & -m\,\dfrac{\partial}{\partial x} \\[2ex] -\theta_0\, m\,\dfrac{\partial}{\partial x}\left(\dfrac{\mathrm{d}}{\mathrm{d}t}\right) & c_v\,\dfrac{\mathrm{d}}{\mathrm{d}t} - k\,\dfrac{\partial^2}{\partial x^2} \end{bmatrix}. \tag{3.66}$$

Studying $\mathfrak{S}$ reveals several important characteristics of the equation system at hand. First of all, it shows that (3.65) is a coupled system, wherein, the coupling between the field variables is governed by the (highlighted) off-diagonal members of the differential operator matrix. Thus, the bigger become the off-diagonal terms, the "stronger" gets the coupling between the state variables. Considering that, the strength of the coupling in this particular case is specified by the stress-temperature modulus, such that setting $m = 0$ yields an elimination of the off-diagonal terms, and uncouples the equation system. Moreover, the existence of the off-diagonal terms for the equations regarding both field variables shows that (3.65) is actually a two-way coupled problem. Furthermore, the presence of temporal derivatives in all diagonal terms of the operator matrix shows that for every field variable, i. e., u and ϑ, there exists an individual evolution equation, so that (3.65) can be recast in the form

$$\mathcal{X} \;:\; \begin{cases} \rho\,\dfrac{\mathrm{d}^2 u}{\mathrm{d}t^2} &= E\,\dfrac{\partial^2 u}{\partial x^2} + m\,\dfrac{\partial \vartheta}{\partial x} + \rho\, b\,, \\[2ex] c_v\,\dfrac{\mathrm{d}\vartheta}{\mathrm{d}t} &= k\,\dfrac{\partial^2 \vartheta}{\partial x^2} + \theta_0\, m\,\dfrac{\partial}{\partial x}\left(\dfrac{\mathrm{d}u}{\mathrm{d}t}\right) + r\,, \end{cases} \tag{3.67}$$

or in abstract form

$$\mathcal{X} \;:\; \mathfrak{S}_t\,\mathbf{u}(\mathbf{x}\,,t) = \overline{\mathfrak{S}}\,\mathbf{u}(\mathbf{x}\,,t) + \mathfrak{f}(\mathbf{x}\,,t) =: \boldsymbol{f}\,(\mathbf{x}\,,t) \tag{3.68}$$

[10] The 1-d version of the equations has been achieved considering a 1-d stress tensor $\boldsymbol{\sigma} = \sigma_{11}\,(\mathbf{e}_1 \otimes \mathbf{e}_1) = E\,\varepsilon_{11}\,(\mathbf{e}_1 \otimes \mathbf{e}_1)$ and assuming that $\{\frac{\partial \dot{u}_2}{\partial x_2}\,, \frac{\partial \dot{u}_3}{\partial x_3}\} \ll \frac{\partial \dot{u}_1}{\partial x_1}$, such that

$$\operatorname{div}\mathbf{v} = \frac{\partial \dot{u}_1}{\partial x_1} + \frac{\partial \dot{u}_2}{\partial x_2} + \frac{\partial \dot{u}_3}{\partial x_3} \approx \frac{\partial \dot{u}_1}{\partial x_1} =: \frac{\partial \dot{u}}{\partial x}\,.$$

with the following sub-operators:

$$\mathfrak{S}_t = \begin{bmatrix} \rho \dfrac{\mathrm{d}^2}{\mathrm{d}t^2} & 0 \\ 0 & c_v \dfrac{\mathrm{d}}{\mathrm{d}t} \end{bmatrix}, \qquad \overline{\mathfrak{S}} = \begin{bmatrix} E \dfrac{\partial^2}{\partial x^2} & m \dfrac{\partial}{\partial x} \\ \theta_0 \, m \dfrac{\partial}{\partial x} \left(\dfrac{\mathrm{d}}{\mathrm{d}t} \right) & k \dfrac{\partial^2}{\partial x^2} \end{bmatrix}. \tag{3.69}$$

Apparently, each state variable within (3.67) is accompanied by one evolution equation. In the literature, such equation sets are usually known as pure differential equation systems. Thus, recalling the coupling between the state variables, (3.67) represents a coupled *partial differential equations* (PDE) system [188]. A counterexample for this case can be seen by considering the governing equations (3.46) corresponding to the dynamics of an incompressible, inviscid fluid. These equations, in the 1-d space, i. e. for $\mathbf{v} = v(x\,,t)\,\mathbf{e}_1$ and $p = p(x\,,t)$ such that

$$\operatorname{grad} p = \frac{\partial p}{\partial x}\,\mathbf{e}_1\,, \tag{3.70}$$

and in absence of the body forces, read

$$\mathcal{X} \;:\; \begin{cases} \mathcal{F}_v(v\,,p) &= \rho \dfrac{\mathrm{d}v}{\mathrm{d}t} + \dfrac{\partial p}{\partial x} = 0\,, \\ \mathcal{F}_p(v) &= \dfrac{\partial v}{\partial x} = 0\,. \end{cases} \tag{3.71}$$

For this problem, v and p, respectively, represent the fluid velocity and the hydraulic pressure, and also define the set of state variables. Thus, $\mathfrak{u} = [v, p]^T$, $\mathfrak{f} = [0\,,0]^T$, and the operator matrices $\mathfrak{S}$, $\mathfrak{S}_t$ and $\overline{\mathfrak{S}}$ read

$$\mathfrak{S} = \begin{bmatrix} \rho \dfrac{\mathrm{d}}{\mathrm{d}t} & \dfrac{\partial}{\partial x} \\ \dfrac{\partial}{\partial x} & 0 \end{bmatrix}, \quad \mathfrak{S}_t = \begin{bmatrix} \rho \dfrac{\mathrm{d}}{\mathrm{d}t} & 0 \\ 0 & 0 \end{bmatrix}, \quad \overline{\mathfrak{S}} = \begin{bmatrix} 0 & -\dfrac{\partial}{\partial x} \\ -\dfrac{\partial}{\partial x} & 0 \end{bmatrix}. \tag{3.72}$$

Studying $\mathfrak{S}$ shows that (3.71), too, represents a two-way coupled problem. Nevertheless, and in contrast to the previous case, recasting (3.71) in the form of (3.68) shows that the vector $\mathfrak{S}_t\,\mathfrak{u}$ contains zero entries. As a result, $\mathcal{F}_p(v) = 0$ rather takes the role of an *algebraic* constraint, which determines the admissible space of the solution vector. Thus, (3.71) represents a coupled *differential algebraic equation* (DAE) system[11].

From the modelling point of view, the algebraic constraints may have different origins. For instance, in the above example, the algebraic constraint $(3.71)_2$ is a reformulated version of the mass balance, derived from an internal property of the system, i. e., the incompressibility of the fluid. A similar phenomenon has also been seen in modelling of the biphasic porous medium of the last section, wherein the incompressibility of the

[11] The notion of "algebraic equations" is originally used in relation with systems of ordinary differential equations, cf. Hairer & Wanner [132], p. 373. In the realm of PDE, an algebraic equation is one with merely spatial derivatives, which can be eliminated via spatial discretisation.

constituents had resulted in the transformation of the mass balances to the mixture volume balance $(3.62)_4$, which is also an algebraic constraint.

In other examples, the constraints may have roots in the external conditions applied to the system. This is particularly seen in multi-body dynamics, where different parts are supposed to move on specific paths, mathematically defined via algebraic equations. Consequently, these relations also constrain the admissible space of the solution vector, and transform the corresponding governing equations to a coupled DAE system. External constraints also arise in the modelling of surface-coupled problems, where satisfaction of the "interface constraints" assures the consistency of the solutions of the interacting subsystems on the common boundaries. This topic is investigated in more detail in Section 4.3.2.

The presence of the algebraic constraints causes difficulties in the numerical solution of the problems. In particular, using the finite-element method (FEM) for the spatial semi-discretisation, these constraints yield the singularity of the generalised mass and stiffness matrices. In this regard, the classification of the DAE systems is done based on the level of difficulty to solve them analytically or numerically. To this end, the notion of *index* serves as a measure for the level of difficulty. Nevertheless, different indices have been introduced in the literature, for instance, the differential index, the perturbation index, the strangeness index, the geometric index, the traceability index, and the structural index, cf. [164] the references therein. Amongst these, the *differential index* is more closely related to the subject of this work and, therefore, it is introduced in more detail in the following.

The differential index is determined by the minimum number of differentiations needed to be performed in order to achieve explicit evolution equations for every variable in the system [132, 164]. To make this point clear, one firstly has to distinguish between the primary variables with and without an evolution equation, i. e., the differential and the algebraic variables, respectively. Thus, one splits the vector of variables $\mathfrak{u}$ into a vector of the differential variables $\mathfrak{v}$, and a vector of the algebraic variables $\mathfrak{w}$, such that $\mathfrak{u} = [\mathfrak{v}\,,\mathfrak{w}]^T$. Furthermore, one splits the equations into a set of evolution equations $\boldsymbol{\mathcal{G}} = \mathbf{0}$ and a set of algebraic constraints $\boldsymbol{\mathcal{H}} = \mathbf{0}$, such that $\boldsymbol{\mathcal{F}} = [\boldsymbol{\mathcal{G}}\,,\boldsymbol{\mathcal{H}}]^T$. Hence, a coupled DAE system of *differential index 1* has the following form:

$$\mathcal{X} \;:\; \left\{ \begin{array}{rcccl} \boldsymbol{\mathcal{G}}\,(\mathfrak{v}\,,\mathfrak{w}) & = & \dot{\mathfrak{v}} - \boldsymbol{g}\,(\mathfrak{v}\,,\mathfrak{w}) & = & \mathbf{0}\,, \\ \boldsymbol{\mathcal{H}}\,(\mathfrak{w}\,,\mathfrak{v}) & = & \boldsymbol{h}\,(\mathfrak{w}\,,\mathfrak{v}) & = & \mathbf{0}\,, \end{array} \right. \qquad \forall\,\mathbf{x} \in \Omega \;\text{ and }\; t \in [t^0\,,T]\,, \tag{3.73}$$

wherein $(\,\cdot\,)\dot{} := \mathrm{d}(\,\cdot\,)/\mathrm{d}t$. Thus, (3.73) equivalently reads

$$\mathcal{X} \;:\; \left\{ \begin{array}{rcl} \dfrac{\mathrm{d}\mathfrak{v}}{\mathrm{d}t} & = & \boldsymbol{g}\,(\mathfrak{v}\,,\mathfrak{w})\,, \\ \mathbf{0} & = & \boldsymbol{h}\,(\mathfrak{w}\,,\mathfrak{v})\,, \end{array} \right. \qquad \forall\,\mathbf{x} \in \Omega \quad \text{and} \quad t \in [t^0\,,T]\,. \tag{3.74}$$

In order to show that the above relation represents an index-1 DAE system, one proceeds as follows: starting with the first material time derivative of $(3.74)_2$, one finds

$$\frac{\mathrm{d}\boldsymbol{h}}{\mathrm{d}t} = \frac{\partial \boldsymbol{h}}{\partial \mathfrak{w}}\,\frac{\mathrm{d}\mathfrak{w}}{\mathrm{d}t} + \frac{\partial \boldsymbol{h}}{\partial \mathfrak{v}}\,\frac{\mathrm{d}\mathfrak{v}}{\mathrm{d}t} = \mathbf{0} \;\rightarrow\; \frac{\mathrm{d}\mathfrak{w}}{\mathrm{d}t} = -\left(\frac{\partial \boldsymbol{h}}{\partial \mathfrak{w}}\right)^{-1} \frac{\partial \boldsymbol{h}}{\partial \mathfrak{v}}\,\frac{\mathrm{d}\mathfrak{v}}{\mathrm{d}t}\,, \tag{3.75}$$

which is possible only if $\partial \boldsymbol{h}/\partial \mathfrak{w}$ is invertible. Subsequent insertion of $(3.74)_1$ in $(3.75)_2$ yields

$$\frac{\mathrm{d}\mathfrak{w}}{\mathrm{d}t} = -\left(\frac{\partial \boldsymbol{h}}{\partial \mathfrak{w}}\right)^{-1} \frac{\partial \boldsymbol{h}}{\partial \mathfrak{v}}\, \boldsymbol{g}\,(\mathfrak{v}\,,\mathfrak{w})\,, \tag{3.76}$$

which is an explicit evolution equation for $\mathfrak{w}$. Thus, one material time derivation suffices to achieve explicit evolution equations for every primary variable in the equation system and, hence, (3.73) and, as well, (3.74) represent DAE systems of index 1.

Analogously, it could be shown that an equation system in the following form represents a DAE system of index 2:

$$\mathcal{X} \;:\; \left\{ \begin{array}{rcl} \dfrac{\mathrm{d}\mathfrak{v}}{\mathrm{d}t} & = & \boldsymbol{g}\,(\mathfrak{v}\,,\mathfrak{w})\,, \\ \mathbf{0} & = & \boldsymbol{h}\,(\mathfrak{v})\,, \end{array} \right. \qquad \forall\, \mathbf{x} \in \Omega \quad \text{and} \quad t \in [t^0\,,T]\,. \tag{3.77}$$

To this end, one starts with the first total time derivative of $(3.77)_2$. It yields

$$\widetilde{\boldsymbol{h}}(\mathfrak{w}\,,\mathfrak{v}) := \frac{\mathrm{d}\boldsymbol{h}}{\mathrm{d}t} = \frac{\partial \boldsymbol{h}}{\partial \mathfrak{v}}\,\frac{\mathrm{d}\mathfrak{v}}{\mathrm{d}t} = \frac{\partial \boldsymbol{h}}{\partial \mathfrak{v}}\,\boldsymbol{g}(\mathfrak{v}\,,\mathfrak{w}) = \mathbf{0}\,, \tag{3.78}$$

which is a hidden constraint for the problem [132]. Following that, by replacing $(3.77)_2$ by (3.78), one achieves the following index-reduced equation system:

$$\mathcal{X}_{red} \;:\; \left\{ \begin{array}{rcl} \dfrac{\mathrm{d}\mathfrak{v}}{\mathrm{d}t} & = & \boldsymbol{g}\,(\mathfrak{v}\,,\mathfrak{w})\,, \\ \mathbf{0} & = & \widetilde{\boldsymbol{h}}(\mathfrak{w}\,,\mathfrak{v})\,, \end{array} \right. \qquad \forall\, \mathbf{x} \in \Omega \quad \text{and} \quad t \in [t^0\,,T]\,, \tag{3.79}$$

which is in the form of (3.74). Thus, provided that $\det(\partial \widetilde{\boldsymbol{h}}/\partial \mathfrak{w}) \neq 0$, $\mathcal{X}_{red}$ represents a DAE system of index 1. Consequently, one further temporal derivative of $(3.79)_2$ yields an explicit evolution equation for the set of algebraic variables $\mathfrak{w}$ and, therefore, (3.77) is indeed of index 2. Furthermore, a comparison between (3.77) and (3.71) shows that the governing equations corresponding to the dynamics of inviscid, incompressible flow also belongs to the category of DAE systems of index 2.

An extension of this discussion naturally leads to the introduction of DAE systems with higher differential indices. Nevertheless, as the index increases, the numerical treatment of the DAE systems proves to get more difficult [132, 188]. In order to overcome this difficulty, it is common practice to apply special index reduction methods in order to reformulate the higher-index problem, ideally in the form of an index-1 DAE or even a pure differential problem. In this regard, among various index reduction methods on the market, the repeated differentiation of the algebraic constraint, as stated above to transform (3.77) into (3.79), is the most apparent one. Nevertheless, by successive differentiation, one basically replaces the original constraint by its derivative. Hence, the "exact" solution of the acquired equation system guarantees satisfaction of this newly found "hidden constraint", however, not the original constraint. From an analytical viewpoint, choosing consistent initial values for the problem is a plausible way to avoid this dilemma, and a possibility to obtain unique solutions for the original and the reduced equation systems. However, the situation is different for the numerical solution of the problem, because in

this case, the discretisation and round-off errors introduced to the system may be detrimental to the uniqueness of the solution [164]. Consequently, it might be that, in spite of having consistent initial values, a combination of a successive integration with a numerical scheme leads to violation of the original algebraic constraint, an effect known as the *drift-off phenomenon* [132]. To overcome this difficulty, different *projection methods*[12] have been introduced, which basically force the numerical solution of the reduced system to lie on the manifold defined by the original constraint as the steps are computed. Exploiting this idea to handle the algebraic incompressibility constraint in form of $(3.71)_2$ has particularly motivated the development of several solution strategies in the field of computational fluid dynamics [52, 120–122, 154, 183, 227, 229]. The projection method has also been used by Heider [137] and Markert *et al.* [190] to propose a numerical solution strategy for the DAE system, corresponding to dynamic saturated porous media with intrinsically incompressible constituents, cf. Section 6.2.

Employing the method of perturbed Lagrange multipliers [212], also known as the penalty method [139, 147, 261], is another possibility to replace the constrained equation systems with unconstrained ones. To elucidate the idea, recall the governing equations corresponding to an incompressible fluid (3.71)

$$\mathcal{X} \;:\; \left\{ \begin{array}{lcl} \mathcal{F}_v(v\,,p) & = & 0\,, \\ \mathcal{F}_p(v) & = & 0\,, \end{array} \right. \tag{3.80}$$

where $\mathcal{F}_v(v\,,p)$ embodies the differential equation, and $\mathcal{F}_p(v)$ is the algebraic constraint. Following the idea of the penalty-method formulation, one loosens the algebraic constraint by replacing it via

$$\mathcal{F}_p(v) = -\frac{1}{\Gamma}\,p\,, \tag{3.81}$$

where Γ is called the penalty parameter and, obviously, very large values of Γ result $\mathcal{F}_p(v) \approx 0$. This process yields a pseudo-constitutive relation for the pressure, which can be inserted directly into $(3.80)_1$ to make it solely dependent on the kinematic variable v:

$$p = -\Gamma\,\mathcal{F}_p(v) \quad \rightarrow \quad \mathcal{X} \;:\; \mathcal{F}_v(v\,,p(v)) = \mathcal{F}_v(v) = 0\,. \tag{3.82}$$

This procedure reduces the number of unknowns and transforms the problem to a smaller and unconstrained one, which only requires the calculation of the velocity. Note that, if desired, having the velocity calculated, the pressure can be recovered explicitly using a Poisson equation [139]. More details about the penalty method are presented in Section 7.3, where using this idea, a decoupled solution scheme for the surface-coupled problem of fluid-porous-media interaction is proposed.

Further categorisation of the coupled PDE or DAE systems into parabolic and hyperbolic types is much less significant. This is due to the fact that many problems are of mixed type or show varying characteristics in the course of time [188]. Instead, to study the property of stiffness of the coupled equations proves to be more relevant to the subject of this report. This is, especially, due to the stability issues caused by this class of problems.

[12] Belonging to the family of operator splitting methods, cf. Section 4.3.3.

3.4.2 Stiff problems

In the everyday life, an object is called "stiff" if it is "rigid", "not easily bent" or "stubborn". To define a stiff problem in a mathematical sense, however, proves to be more complicated. In fact, despite the considerable amount of work done on characterising these problems and on investigating their behaviour when solved numerically, the opinions of the experts on the definition of the stiff problems are far from standard[13]. Reviewing these opinions in order to find their "common denominator", one concludes that, the stiff problems can be introduced as follows:

Consider a problem that is composed of one or a set of ordinary differential equations and corresponding initial conditions. Assume that the solution of this problem possesses different parts with drastically different evolution rates, such that in the course of time, some parts of the solution fade away much faster than others. These parts act rather like a disturbance which is almost rapidly damped out and leaves the problem with a smooth solution. As a result, in certain time intervals, the problem would have a relatively smooth main solution accompanied by nearby rapidly changing solutions. In the literature, this attribute has been considered as the "essence of stiffness" [64], and in those intervals the problem is stiff.

To set up an example, consider the following evolution equation [132]:

$$\dot{u} = \lambda\,(u - \cos t)\,, \quad \text{with} \quad u|^{t=t^0} = u^0\,. \tag{3.83}$$

The analytical solution of this problem reads

$$u^a(t) = \frac{\lambda^2}{\lambda^2+1}\,\cos t - \frac{\lambda}{\lambda^2+1}\,\sin t + \left[u^0 - \frac{\lambda^2}{\lambda^2+1}\right] e^{\lambda\,t}\,. \tag{3.84}$$

This solution has two parts: a persistent trigonometric part, and an exponential part that, for $\Re(\lambda) < 0$, eventually fades away. The latter phenomenon is explained in more details in Section 5.3. Thus, in certain circumstances, i. e. for $t \gg 0$ or if $u^0 \approx (\lambda^2)/(\lambda^2+1)$, the exponential term in (3.84) becomes negligible compared to the trigonometric part, see Figure 3.5. In such circumstances, the problem becomes stiff.

Similar behaviour can also be seen in the field of multi-variable problems, if there exist some DOF in the system which reach their equilibrium state much faster than others [39, 189]. In this sense, stiff problems are observed in various scenarios. Famous applications include coupled diffusion-reaction processes in the gas mixtures [39, 132], combustion models, in which the explosion usually occurs much faster than the rest of the process [1], and the modelling of large engineering systems, such as nuclear reactors, where a subset of the components can have highly oscillatory movements [39]. The mathematical modelling of these phenomena generates coupled, stiff equation systems. In this regard, consider the following linear problem as an example:

$$\dot{\mathbf{u}} = \mathbf{Q}\,\mathbf{u} \quad \text{with} \quad \mathbf{u}|^{t=t^0} = \mathbf{u}^0\,. \tag{3.85}$$

[13]For instance, by the end of the *International Conference on Stiff Computation*, held in April 1982, in Utah, USA, the attendees were, inter alia, asked to propose an appropriate definition for the stiff problems. Reviewing the responses, summarised and presented by Aiken [1], reveals the amount of differences among the ideas of the specialists of the field.

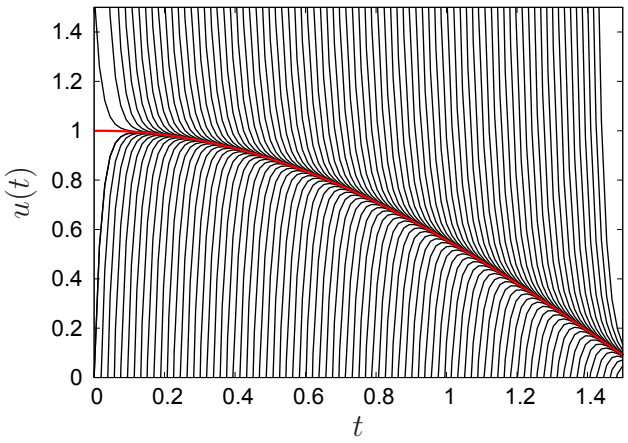

Figure 3.5: *Analytical solution of (3.83) for $\lambda = -50$, and various initial values u^0, where the red curve shows the smooth and persistent part of the solution, and the black curves represent the rapidly changing and transient nearby solutions.*

Therein, $\mathbf{u}$ contains p degrees of freedom of the problem, and $\mathbf{Q}$ depicts some $p \times p$ matrix of coefficients. This problem would be stiff in the above sense if there exist some eigenvalues of the matrix $\mathbf{Q}$ with $\Re(\lambda_j) \ll 0$ and there also exist eigenvalues of moderate magnitude [39].

The numerical treatment of stiff problems should be done with special care. In particular, to achieve stable results when integrated explicitly, one has to consider a critical time-step size[14] that is excessively small compared with the smoothness of the exact solution. Thus, one is basically limited to implicit schemes for numerical integration of very stiff problems. This will be discussed in more detail in Section 5.3 in conjunction with the concepts of A- and L-stability. Nevertheless, this observation leads to a more comprehensive definition for stiff problems proposed by Lambert [169]:

Definition of stiff problems

If in a certain time interval of integration, a numerical solution method is forced to use a time-step size which is excessively small in relation to the smoothness of the exact solution in that interval, then the problem is said to be *stiff* in that time interval. (3.86)

Operator splitting is another tool to overcome the difficulties in time integration of stiff problems. These kind of solution strategies along with other possibilities for numerical solutions of coupled problems are scrutinised in the next chapter.

[14]The critical time-step size $\Delta t_{crit.}$ is the biggest time-step size, for which the integrator may generate a stable result, cf. Chapter 5.

Chapter 4:
Numerical Solution Schemes

I thought that instead of the great number of precepts of which logic is composed, I would have enough with the following ones, provided that I made a firm and unalterable resolution not to violate them even in a single instance. The first rule was never to accept anything as true unless I recognized it to be certainly and evidently such [...] The second was to "divide" each of the difficulties which I encountered into as many parts as possible, and as might be required for an easier solution.

René Descartes (1596 – 1650) [221]

As mentioned earlier, analytical solution of continuous PDE may become very difficult. In particular, an analytical treatment of the intricate coupled systems of PDE may become even impossible. To cope with this difficulty, various numerical schemes have been developed, where the computational treatment of the dynamical system is done after spatial and temporal discretisation of the continuous governing equations. In some less commonly used solution schemes, e. g., in "direct grid approaches", spatial and temporal discretisations take place simultaneously [230]. Apart from such cases, the spatial discretisation and the temporal integration are usually performed in separate and consecutive steps.

Spatial discretisation of coupled PDE systems transforms them into semi-discrete systems of ODE in time. In this context, some of the most frequently used spatial discretisation schemes are the finite-element method (FEM) [33, 35], the finite-difference method (FDM) [200, 203] and the finite-volume method (FVM) [172, 273]. Subsequently, a numerical time-stepping method is used for the temporal integration of the generated ODE. Considering coupled ODE systems, this process of updating can be performed either monolithically or following a decoupled strategy.

In what comes next, the widely used families of Runge-Kutta (RK) methods and backward differentiation formulae (BDF) are firstly reviewed. These schemes play an important role in Section 5.3, where stability notions are introduced. After that, different monolithic and decoupled integration strategies are scrutinised.

4.1 Time-stepping procedures

Consider the following initial-value problem (IVP):

$$\dot{\mathbf{u}}(t) = \boldsymbol{f}(\mathbf{u}(t), t)\,, \quad t \in [0\,, T]\,, \quad \mathbf{u} \in \mathbb{R}^p\,, \quad \boldsymbol{f} \,:\, [0\,, T] \times \mathbb{R}^p \to \mathbb{R}^p\,, \quad \mathbf{u}(0) = \mathbf{u}^0\,. \tag{4.1}$$

It represents a set of ODE composed of p evolution equations for p variables collected in the vector $\mathbf{u}$. For numerical integration of (4.1), the time domain [0 ,T] is divided into a finite number of steps denoted by $0\,, \cdots, t^{n-1}\,, t^n\,, t^{n+1}\,, \cdots, T$. The time-step size is then given by $\Delta t^n := t^n - t^{n-1}$. Thus, proceeding from a constant time-step size Δt yields $t^n = n\,\Delta t$. The integration process then approximates the exact solution of the problem

at the time steps. In this conjunction, the approximated solution at time $t = t^n$ is shown by $\mathbf{u}^n$.

Temporal integration is performed in a step-by-step manner. To this end, one assumes that the solutions of the system up to a specific time, say $t = t^n$, is known. The task would be to use the available information in order to update the system, i. e. , to find $\mathbf{u}^{n+1}$ at the next time step $t = t^{n+1}$. This process, in the most general scenario, is done using k vectors of past information at times $t^{n-k+1}, \cdots, t^n$ and s additional intermediate solution vectors computed at the current step. Such a method is called a k-step, s-stage method [39]. Considering this, the so-called forward and backward Euler integration schemes (presented below) are examples of one-step, one-stage methods. Efforts for generalisation of these simple schemes have led to development of many multi-step, multi-stage time integrators, for example the RK and the BDF methods, as presented next.

Runge-Kutta methods

Named after Runge [238] and Kutta [165], the Runge-Kutta (RK) methods build a large group of multi-stage, one-step schemes. Applying a s-stage RK method for time integration of (4.1) yields [262]

$$\mathbf{u}^{n+1} = \mathbf{u}^n + \Delta t \sum_{i=1}^{s} b_i \, \mathbf{k}_i \,, \tag{4.2}$$

where

$$\mathbf{k}_i = \boldsymbol{f}(\mathbf{u}^n + \Delta t \sum_{j=1}^{s} a_{ij} \, \mathbf{k}_j \,, t^n + \Delta t \, c_i) \,. \tag{4.3}$$

Therein, a_{ij}, b_i and c_i are real parameters which define the method. These coefficients are best presented using the so-called Butcher tableau [41, 42]:

$$\begin{array}{c|ccc} c_1 & a_{11} & \cdots & a_{1s} \\ \vdots & \vdots & \ddots & \vdots \\ c_s & a_{s1} & \cdots & a_{ss} \\ \hline & b_1 & \cdots & b_s \end{array} \quad \equiv \quad \begin{array}{c|c} \mathbf{c} & \mathbf{A} \\ \hline & \mathbf{b}^T \end{array} \,. \tag{4.4}$$

Clearly, having a strictly lower triangular matrix $\mathbf{A}$, each vector $\mathbf{k}_i$ can be explicitly computed from $\mathbf{k}_1, \cdots \mathbf{k}_{i-1}$. In this case, the scheme is called an *explicit* Runge-Kutta (ERK) method. Otherwise, the scheme is called an *implicit* Runge-Kutta (IRK) method. The forward and the backward Euler schemes are the simplest explicit and implicit RK methods, respectively. For these procedures, the Butcher tableau reads

$$\begin{array}{c|c} 0 & 0 \\ \hline & 1 \end{array} \,, \qquad \begin{array}{c|c} 1 & 1 \\ \hline & 1 \end{array} \,. \tag{4.5}$$

Explicit forward Euler Implicit backward Euler

Backward differentiation formulae (BDF)

Also called "standard step-by-step methods" [199], the BDF methods were firstly introduced by Curtiss & Hirschfelder [59]. These stepping procedures have been successfully used by Gear [114] for numerical integration of stiff differential equations [131] and, therefore, they are sometimes called the Gear's methods [188]. The class of BDF schemes belongs to the family of implicit linear multi-step methods. The generic form of a k-step BDF method, when applied to the problem (4.1), reads

$$\sum_{i=0}^{k} \alpha_i \, \mathbf{u}^{n+i} = \Delta t \, \beta_k \, \boldsymbol{f}^{n+k} \,, \tag{4.6}$$

where the coefficients α_i and β_k are chosen such that a k-step BDF method becomes kth-order accurate. Then, a kth-order, k-step BDF method is commonly shown by BDFk. Nevertheless, all BDF methods with $k \geq 7$ are zero-unstable, cf. Hairer *et al.* [131], Chapter III. 3, Theorem 3.4. Furthermore, the BDF1 method is in fact the backward Euler scheme. Keeping this in mind, the BDF schemes for $2 \leq k \leq 6$ read [262]

$$\begin{aligned}
&\text{BDF2}: \quad 3\,\mathbf{u}^{n+2} - 4\,\mathbf{u}^{n+1} + \mathbf{u}^{n} = 2\,\Delta t\,\boldsymbol{f}^{n+2}\,,\\
&\text{BDF3}: \quad 11\,\mathbf{u}^{n+3} - 18\,\mathbf{u}^{n+2} + 9\,\mathbf{u}^{n+1} - 2\,\mathbf{u}^{n} = 6\,\Delta t\,\boldsymbol{f}^{n+3}\,,\\
&\text{BDF4}: \quad 25\,\mathbf{u}^{n+4} - 48\,\mathbf{u}^{n+3} + 36\,\mathbf{u}^{n+2} - 16\,\mathbf{u}^{n+1} + 3\,\mathbf{u}^{n} = 12\,\Delta t\,\boldsymbol{f}^{n+4}\,,\\
&\text{BDF5}: \quad 137\,\mathbf{u}^{n+5} - 300\,\mathbf{u}^{n+4} + 300\,\mathbf{u}^{n+3} - 200\,\mathbf{u}^{n+2} + 75\,\mathbf{u}^{n+1} - 12\,\mathbf{u}^{n} = 60\,\Delta t\,\boldsymbol{f}^{n+5}\,,\\
&\text{BDF6}: \quad 147\,\mathbf{u}^{n+6} - 360\,\mathbf{u}^{n+5} + 450\,\mathbf{u}^{n+4} - 400\,\mathbf{u}^{n+3} + 225\,\mathbf{u}^{n+2} - 72\,\mathbf{u}^{n+1} + 10\,\mathbf{u}^{n} =\\
&\qquad\qquad = 60\,\Delta t\,\boldsymbol{f}^{n+6}\,.
\end{aligned} \tag{4.7}$$

Discussions regarding the stability behaviour of numerical results produced by the RK and the BDF processes will be presented in Section 5.3.

4.2 Monolithic solution strategies

Temporal integration of time-dependent ODE systems can be executed in different manners. Many of the processes proposed to perform this task can be assigned either to the category of monolithic schemes, or to the family of decoupled solution strategies. These strategies are respectively introduced in the present and the next sections.

Following a monolithic time integration scheme, the problem is considered as a whole. Thus, the time advancement of every part of the model happens at once, employing the same integration method and time-step size. This treatment is especially advantageous when the coupled field interaction is highly nonlinear and, therefore, is best solved in a single solution using a coupled formulation. The reader is referred to [6, 85, 137, 189, 190, 190, 274] for some successful implementations of monolithic integrators for the solution of different coupled systems.

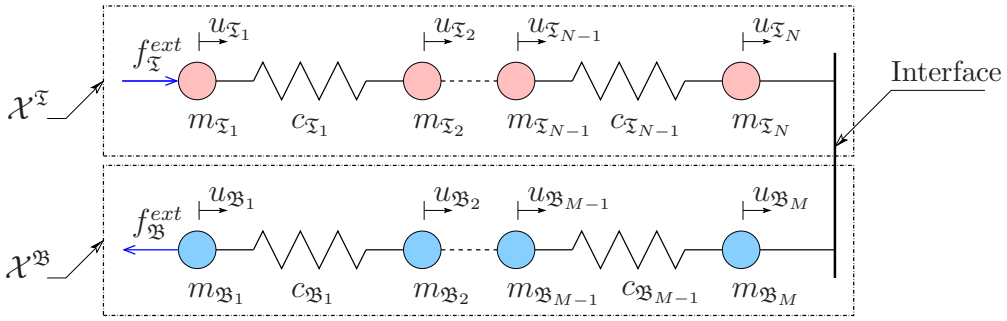

Figure 4.1: *Rheological model for a coupled problem.*

In order to introduce the method, consider the rheological model depicted in Figure 4.1 as a representative coupled system[1]. It embodies a surface interaction between subsystems $\mathcal{X}^{\mathfrak{T}}$ and $\mathcal{X}^{\mathfrak{B}}$. The degrees of freedom corresponding to the subsystem $\mathcal{X}^{\mathfrak{a}}$ with $\mathfrak{a} = \{\mathfrak{T}, \mathfrak{B}\}$ is depicted by $\mathbf{u}_{\mathfrak{a}} = [u_{\mathfrak{a}_i}]^T \in \mathbb{R}^{d_{\mathfrak{a}}}$, where $d_{\mathfrak{a}}$ represents the number of degrees of freedom of subsystem $\mathcal{X}^{\mathfrak{a}}$. Thus, $d_{\mathfrak{T}} = N$ and $d_{\mathfrak{B}} = M$. Note that in the problem at hand, $\mathbf{u}_{\mathfrak{a}}$ contains the displacements of the mass-points $m_{\mathfrak{a}_i}$, $i \in [1, \cdots, d_{\mathfrak{a}}]$. Furthermore, $c_{\mathfrak{a}_i}$ represents the stiffness of the i-th linear spring in the subsystem $\mathcal{X}^{\mathfrak{a}}$, and $\boldsymbol{f}_{\mathfrak{a}} = [f_{\mathfrak{a}_i}]^T \in \mathbb{R}^{d_{\mathfrak{a}}}$ embodies a priori known external forces applied to the system. Therefore,

$$\boldsymbol{f}^T_{\mathfrak{T}} = [f^{ext}_{\mathfrak{T}}, \cdots, 0]_{1\times N}, \quad \text{and} \quad \boldsymbol{f}^T_{\mathfrak{B}} = [-f^{ext}_{\mathfrak{B}}, \cdots, 0]_{1\times M}. \tag{4.8}$$

The coupling between the subsystems is such that the motion of the mass-points next to the interface are identical. Hence,

$$u_{\mathfrak{T}_N} = u_{\mathfrak{B}_M} =: u_{\mathfrak{I}}. \tag{4.9}$$

The set of governing equations of the system could be obtained in the sense of virtual work by investigating the stationary condition of the corresponding energy functional of the system. Note that the governing equations could also readily be written by means of the balance of linear momentum. The herein presented framework, however, has been chosen intentionally in order to prepare a consistent formulation that can be exploited for later presentation of decoupling techniques. The energy functional, which is composed of the sum of the energy functionals of the interacting subdomains, is given by

$$\Pi = \Pi_{\mathfrak{T}} + \Pi_{\mathfrak{B}}, \tag{4.10}$$

where $\Pi_{\mathfrak{a}}$ represents the energy functional of subsystem $\mathcal{X}^{\mathfrak{a}}$ and reads

$$\Pi_{\mathfrak{a}} = \mathbf{u}^T_{\mathfrak{a}} \left(\mathbf{M}_{\mathfrak{a}}\, \ddot{\mathbf{u}}_{\mathfrak{a}} + \frac{1}{2}\, \mathbf{K}_{\mathfrak{a}}\, \mathbf{u}_{\mathfrak{a}} - \boldsymbol{f}_{\mathfrak{a}}\right). \tag{4.11}$$

[1]The representative coupled system could have been presented in an abstract way. However, due to the fact that this thesis particularly addresses coupled phenomena arising in the engineering applications and, thus, will be especially interesting for specialists from application-oriented disciplines, the idea of employing an abstract equation system was avoided. It has been, however, intended to present the material such that the discussed subjects can be conveniently extended to more practical applications. To this end, state vectors and structural matrices are presented so that they resemble the objects obtained after the spatial discretisation of domains via the FEM.

Therein, $\mathbf{M}_{\mathfrak{a}}$ and $\mathbf{K}_{\mathfrak{a}}$ are the mass and the stiffness matrices of subsystem $\mathcal{X}^{\mathfrak{a}}$ given by

$$\begin{aligned} \mathbf{M}_{\mathfrak{a}} &= \operatorname{diag}\left[m_{\mathfrak{a}_i}\right], \quad \text{and} \\ \mathbf{K}_{\mathfrak{a}} &= \operatorname{tridiag}\left[-c_{\mathfrak{a}_{i-1}}, c_{\mathfrak{a}_{i-1}} + c_{\mathfrak{a}_i}, -c_{\mathfrak{a}_i}\right]. \end{aligned} \tag{4.12}$$

Next, recalling the coupling condition (4.9), each displacement vector $\mathbf{u}_{\mathfrak{a}}$ could be split in the following way

$$\mathbf{u}_{\mathfrak{a}} = [\mathbf{u}_{\mathfrak{a}}^{red}, \mathbf{u}_{\mathfrak{I}}]^T, \tag{4.13}$$

where $\mathbf{u}_{\mathfrak{I}} := [u_{\mathfrak{I}}]^T$, while the reduced vector $\mathbf{u}_{\mathfrak{a}}^{red} := [u_{\mathfrak{a}_1}, \cdots, u_{\mathfrak{a}_{d_{\mathfrak{a}}-1}}]^T$ contains the DOF of the mass-points within the subsystem $\mathcal{X}^{\mathfrak{a}}$. Consequently, one also distinguishes between external forces applied to the mass-points next to the interface and those applied to the internal masses, such that

$$\boldsymbol{f}_{\mathfrak{a}} = [\boldsymbol{f}_{\mathfrak{a}}^{red}, \boldsymbol{f}_{\mathfrak{I}}^{\mathfrak{a}}]^T \tag{4.14}$$

with $\boldsymbol{f}_{\mathfrak{a}}^{red} := [f_{\mathfrak{a}_1}, \cdots, f_{\mathfrak{a}_{d_{\mathfrak{a}}-1}}]^T$ and $\boldsymbol{f}_{\mathfrak{I}}^{\mathfrak{a}} := [f_{\mathfrak{a}_{d_{\mathfrak{a}}}}]^T$. Similarly, the mass and the stiffness matrices could be written in the following block forms

$$\mathbf{M}_{\mathfrak{a}} = \begin{bmatrix} \mathbf{M}_{\mathfrak{a}\mathfrak{a}} & \mathbf{0} \\ \mathbf{0} & \mathbf{M}_{\mathfrak{I}\mathfrak{I}}^{\mathfrak{a}} \end{bmatrix}, \quad \text{and} \quad \mathbf{K}_{\mathfrak{a}} = \begin{bmatrix} \mathbf{K}_{\mathfrak{a}\mathfrak{a}} & \mathbf{K}_{\mathfrak{a}\mathfrak{I}} \\ \mathbf{K}_{\mathfrak{I}\mathfrak{a}} & \mathbf{K}_{\mathfrak{I}\mathfrak{I}}^{\mathfrak{a}} \end{bmatrix}. \tag{4.15}$$

For the problem at hand, the blocks of the mass matrix read

$$\mathbf{M}_{\mathfrak{a}\mathfrak{a}} = \begin{bmatrix} m_{\mathfrak{a}_1} & \cdots & 0 \\ \vdots & \ddots & \vdots \\ 0 & \cdots & m_{\mathfrak{a}_{d_{\mathfrak{a}}-1}} \end{bmatrix}, \quad \mathbf{M}_{\mathfrak{I}\mathfrak{I}}^{\mathfrak{a}} = [m_{\mathfrak{a}_{d_{\mathfrak{a}}}}], \tag{4.16}$$

and the components of the stiffness matrix are given by

$$\mathbf{K}_{\mathfrak{I}\mathfrak{a}} = \mathbf{K}_{\mathfrak{a}\mathfrak{I}}^T = [0, \cdots, 0, -c_{\mathfrak{a}_{d_{\mathfrak{a}}-1}}], \quad \mathbf{K}_{\mathfrak{I}\mathfrak{I}}^{\mathfrak{a}} = [c_{\mathfrak{a}_{d_{\mathfrak{a}}-1}}],$$

$$\mathbf{K}_{\mathfrak{a}\mathfrak{a}} = \begin{bmatrix} c_{\mathfrak{a}_1} & -c_{\mathfrak{a}_1} & 0 & \cdots & 0 \\ -c_{\mathfrak{a}_1} & c_{\mathfrak{a}_1} + c_{\mathfrak{a}_2} & -c_{\mathfrak{a}_2} & & \vdots \\ 0 & \ddots & \ddots & \ddots & 0 \\ \vdots & & -c_{\mathfrak{a}_{d_{\mathfrak{a}}-3}} & c_{\mathfrak{a}_{d_{\mathfrak{a}}-3}} + c_{\mathfrak{a}_{d_{\mathfrak{a}}-2}} & -c_{\mathfrak{a}_{d_{\mathfrak{a}}-2}} \\ 0 & \cdots & 0 & -c_{\mathfrak{a}_{d_{\mathfrak{a}}-2}} & c_{\mathfrak{a}_{d_{\mathfrak{a}}-2}} + c_{\mathfrak{a}_{d_{\mathfrak{a}}-1}} \end{bmatrix}. \tag{4.17}$$

Thus, demanding the stationary condition for the energy functional yields

$$\delta\Pi(\mathbf{u}_{\mathfrak{T}}^{red}, \mathbf{u}_{\mathfrak{B}}^{red}, \mathbf{u}_{\mathfrak{I}}) = 0 \quad \rightarrow \quad \left\{ \frac{\partial \Pi}{\partial \mathbf{u}_{\mathfrak{T}}^{red}} = \mathbf{0}, \quad \frac{\partial \Pi}{\partial \mathbf{u}_{\mathfrak{B}}^{red}} = \mathbf{0}, \quad \frac{\partial \Pi}{\partial \mathbf{u}_{\mathfrak{I}}} = \mathbf{0} \right\}. \tag{4.18}$$

Building the above partial derivatives of the energy functional, one arrives at the following equation set

$$\mathcal{X} \ : \ \boldsymbol{\mathcal{F}} = \mathfrak{S}\,\mathfrak{u} - \mathfrak{f} = \mathbf{0}, \tag{4.19}$$

where $\mathfrak{u} := [\mathfrak{u}_{\mathfrak{T}}^{red}, \mathfrak{u}_{\mathfrak{B}}^{red}, \mathfrak{u}_{\mathfrak{J}}]^T$, $\mathfrak{f} := [\boldsymbol{f}_{\mathfrak{T}}^{red}, \boldsymbol{f}_{\mathfrak{B}}^{red}, \underbrace{\boldsymbol{f}_{\mathfrak{J}}^{\mathfrak{T}} + \boldsymbol{f}_{\mathfrak{J}}^{\mathfrak{B}}}_{=:\boldsymbol{f}_{\mathfrak{J}}}]^T$, and

$$\mathfrak{S} := \mathbf{M}\,\frac{\mathrm{d}^2}{\mathrm{d}t^2} + \mathbf{K} \tag{4.20}$$

with

$$\mathbf{M} := \begin{bmatrix} \mathbf{M}_{\mathfrak{T}\mathfrak{T}} & \mathbf{0} & \mathbf{0} \\ \mathbf{0} & \mathbf{M}_{\mathfrak{B}\mathfrak{B}} & \mathbf{0} \\ \mathbf{0} & \mathbf{0} & \underbrace{\mathbf{M}_{\mathfrak{J}\mathfrak{J}}^{\mathfrak{T}} + \mathbf{M}_{\mathfrak{J}\mathfrak{J}}^{\mathfrak{B}}}_{=:\mathbf{M}_{\mathfrak{J}\mathfrak{J}}} \end{bmatrix}, \quad \mathbf{K} := \begin{bmatrix} \mathbf{K}_{\mathfrak{T}\mathfrak{T}} & \mathbf{0} & \mathbf{K}_{\mathfrak{T}\mathfrak{J}} \\ \mathbf{0} & \mathbf{K}_{\mathfrak{B}\mathfrak{B}} & \mathbf{K}_{\mathfrak{B}\mathfrak{J}} \\ \mathbf{K}_{\mathfrak{T}\mathfrak{J}}^T & \mathbf{K}_{\mathfrak{B}\mathfrak{J}}^T & \underbrace{\mathbf{K}_{\mathfrak{J}\mathfrak{J}}^{\mathfrak{T}} + \mathbf{K}_{\mathfrak{J}\mathfrak{J}}^{\mathfrak{B}}}_{=:\mathbf{K}_{\mathfrak{J}\mathfrak{J}}} \end{bmatrix}. \tag{4.21}$$

Considering the interdependencies between the DOF caused by the off-diagonal terms in $\mathbf{K}$, relation (4.19) presents a coupled system of equations. Monolithic integration of this system is performed through simultaneous time advancement of the whole equation system, using the same time-marching method. Consider the mid-point rule

$$\dot{\mathfrak{u}}^{n+\frac{1}{2}} = \dot{\mathfrak{u}}^n + \frac{\Delta t}{2}\,\ddot{\mathfrak{u}}^{n+\frac{1}{2}}\,, \quad \mathfrak{u}^{n+\frac{1}{2}} = \mathfrak{u}^n + \frac{\Delta t}{2}\,\dot{\mathfrak{u}}^{n+\frac{1}{2}}\,, \quad \mathfrak{u}^{n+1} = 2\,\mathfrak{u}^{n+\frac{1}{2}} - \mathfrak{u}^n\,. \tag{4.22}$$

Employing this procedure, the monolithic integration of (4.19) is performed as follows:

$$\begin{aligned}
&\bullet \text{ from } (4.22)_1 \quad : \quad \mathbf{M}\,\dot{\mathfrak{u}}^{n+\frac{1}{2}} = \mathbf{M}\,\dot{\mathfrak{u}}^n + \frac{\Delta t}{2}\,\mathbf{M}\,\ddot{\mathfrak{u}}^{n+\frac{1}{2}}\,, \\
&\bullet \text{ from } (4.19) \quad : \quad \mathbf{M}\,\ddot{\mathfrak{u}}^{n+\frac{1}{2}} = \mathfrak{f}^{n+\frac{1}{2}} - \mathbf{K}\,\mathfrak{u}^{n+\frac{1}{2}}\,, \\
&\quad \text{hence} \quad : \quad \mathbf{M}\,\dot{\mathfrak{u}}^{n+\frac{1}{2}} = \mathbf{M}\,\dot{\mathfrak{u}}^n + \frac{\Delta t}{2}\,\left(\mathfrak{f}^{n+\frac{1}{2}} - \mathbf{K}\,\mathfrak{u}^{n+\frac{1}{2}}\right), \\
&\bullet \text{ from } (4.22)_2 \quad : \quad \mathbf{M}\,\mathfrak{u}^{n+\frac{1}{2}} = \mathbf{M}\,\mathfrak{u}^n + \frac{\Delta t}{2}\,\mathbf{M}\,\dot{\mathfrak{u}}^{n+\frac{1}{2}}\,, \\
&\quad \text{hence} \quad : \quad \mathbf{M}\,\mathfrak{u}^{n+\frac{1}{2}} = \mathbf{M}\,\mathfrak{u}^n + \frac{\Delta t}{2}\,\left[\mathbf{M}\,\dot{\mathfrak{u}}^n + \frac{\Delta t}{2}\,\left(\mathfrak{f}^{n+\frac{1}{2}} - \mathbf{K}\,\mathfrak{u}^{n+\frac{1}{2}}\right)\right].
\end{aligned} \tag{4.23}$$

The discrete version of (4.19) after execution of these steps reads

$$\mathfrak{S}_d\,\mathfrak{u}^{n+\frac{1}{2}} - \mathfrak{f}_d = \mathbf{0}\,, \tag{4.24}$$

where

$$\mathfrak{S}_d := \mathbf{M} + \left(\frac{\Delta t}{2}\right)^2 \mathbf{K}\,, \quad \text{and} \quad \mathfrak{f}_d := \mathbf{M}\,\mathfrak{u}^n + \frac{\Delta t}{2}\,\mathbf{M}\,\dot{\mathfrak{u}}^n + \left(\frac{\Delta t}{2}\right)^2 \mathfrak{f}^{n+\frac{1}{2}}\,. \tag{4.25}$$

From $(4.25)_2$, it is obvious that the vector $\mathfrak{f}_d$ is merely a function of prescribed external forces and known displacements at time t^n. Therefore, (4.24) can be employed to update the state of the system, such that

$$\mathfrak{u}^{n+\frac{1}{2}} = \mathfrak{S}_d^{-1}\,\mathfrak{f}_d\,. \tag{4.26}$$

Employing the monolithic strategies in conjunction with the implicit time-stepping procedures yields unconditionally stable numerical results (cf. Chapter 5). This is a superior advantage of this class of solvers over the rival decoupled solution methods, for, as will be explained, the latter may suffer from conditional stability of the results. This characteristic has motivated the development of specialised monolithic approaches. In this regard, several examples were mentioned at the beginning of this section and also within Section 1.2. In spite of this potential merit, a monolithic integration is not always recommended. This is mainly due to the following points:

1. Monolithic solvers prohibit different time-step sizes for various subsystems. This is the main drawback for problems, in which due to drastic difference in the speeds of the processes, or because of mesh refinement in specific parts of the domain, variables are preferably advanced with different time steps. An example for the former scenario is the very slow and gradual process of bone growth or degeneration (bone modelling and remodelling) that occurs as a response to the relatively high-frequency alteration of mechanical stresses. The latter case could be seen in problems, in which the complexity of specific parts of the domain requires local grid refinement and reduction of the time-step sizes.

2. They require a special solution algorithm for each individual coupled system. The monolithic approaches prohibit efficient re-using of solvers and require the development of a new solution algorithm for each new combination of previously studied systems. This is particularly disadvantageous where there already exist elaborated mathematical models and optimised solution schemes for each of the interacting components. Consequently, and considering the potential differences in the characteristics of the interacting components, the monolithic algorithms will be at most just semi-optimised.

3. They demand solution of large systems of equations. In particular, spatially discretised problems of practical size may comprise millions of coupled evolution equations. Using a monolithic solver to advance the problem in time, this large equation system should be solved holistically; a process that might be computationally too expensive.

Utilising decoupled solution algorithms, which are based on the partitioning of the problem or on the operator splitting, is a feasible alternative approach to overcome these disadvantages.

4.3 Decoupled solution strategies

Decoupled solution strategies are based on the idea of breakdown or decomposition of a "complex problem" into several "simpler communicating subproblems". The communication is in the sense of exchanging data among the subproblems, and has to be executed in such a way that the response of the decoupled system to some reasonable extent resembles the response of the original one. This process, if done appropriately, offers more flexibility in the solution of the problem. In this regard, the most significant features of the decoupled solution schemes are [92, 100, 101, 215]:

1. Independent modelling: employing a decoupled solver facilitates the possibility of using non-matching models. Following that, the subsystems could be integrated individually, in a parallel or a sequential manner.

2. Customisation: the numerical integration can be performed by exploiting tailored discretisation and solution algorithms and, consequently, suitable spatial and temporal grid sizes for the interacting fields.

3. Modularity: following a decoupled solution scheme, a general-purpose analyser for each subsystem can be developed and eventually "plugged in" as a modular component to any analyser corresponding to the rest of the system. Subsequently, and considering individual software tools as individual solution modules, this modularity implies the software reusability, as well.

Decoupling of equations is usually done via partitioning of the spatial domain, splitting of the differential operator, or a combination of both. Following that, the exchange of information between the generated subproblems can be done employing different strategies. Amongst these, the staggered time-marching algorithms are of great importance. This is especially due to the rather simple procedure behind, and the flexibility offered by these strategies.

In the following, some of the most common staggered time-marching algorithms and their variations are firstly introduced. Subsequently, the partitioning and the splitting methods are respectively presented in Sections 4.3.2 and 4.3.3.

4.3.1 Staggered time-marching algorithms

To explain the idea behind the staggered integration methods, consider the following system composed of coupled autonomous evolution equations for the exemplary unknown variables $\mathbf{u}_1(\mathbf{x}\,,t)$ and $\mathbf{u}_2(\mathbf{x}\,,t)$:

$$\mathcal{X} \;:\; \begin{cases} \mathcal{X}^1 \;:\; \dot{\mathbf{u}}_1 \;=\; \boldsymbol{f}_1(\mathbf{u}_1\,,\mathbf{u}_2)\,, \\ \\ \mathcal{X}^2 \;:\; \dot{\mathbf{u}}_2 \;=\; \boldsymbol{f}_2(\mathbf{u}_1\,,\mathbf{u}_2)\,. \end{cases} \tag{4.27}$$

Assume that $\mathbf{u}_1^n$ and $\mathbf{u}_2^n$ at time $t = t^n$ are known and the goal is to advance the system in time and find new values $\mathbf{u}_1^{n+1}$ and $\mathbf{u}_2^{n+1}$ at time $t^{n+1} = t^n + \Delta t$. Then, a staggered integration of (4.27) via the block-Gauss-Seidel (BGS) strategy [74, 152, 192, 193], also known as the conventional serial staggered (CSS) algorithm [91, 92, 223, 224] is executed through the following procedure (also see Figure 4.2):

The BGS time-marching strategy

(1) Choose $\mathbf{u}_2^p$ as a predictor for $\mathbf{u}_2^{n+1}$ and substitute it in $\mathcal{X}^1$.
(2) Advance $\mathcal{X}^1$ and find $\mathbf{u}_1^{n+1}$.
(3) Substitute $\mathbf{u}_1^{n+1}$ in $\mathcal{X}^2$.
(4) Advance $\mathcal{X}^2$ and find $\mathbf{u}_2^{n+1}$.

(4.28)

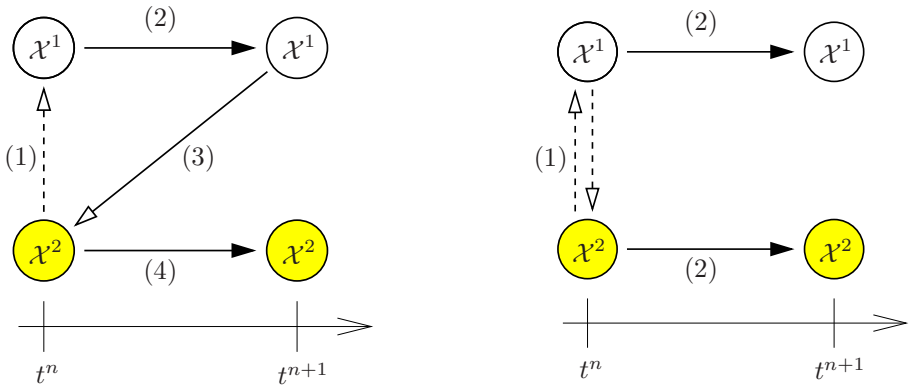

Figure 4.2: *The BGS method (left) and the BJ strategy (right) for data transfer between subsystems $\mathcal{X}^1$ and $\mathcal{X}^2$.*

The above procedure, which is also equivalent to the multiplicative Schwarz method [192, 193], represents a *serial (sequential)* and *collocated* staggered scheme; it is serial because the subsystems are advanced in time successively (not simultaneously), and collocated because it evaluates the subsystems at the same time-stations [223, 224].

Alternatively, a parallel and collocated staggered time integration is conceivable through the so-called block-Jacobi (BJ) strategy [192, 193], also known as the conventional parallel staggered (CPS) procedure [92, 276]. This scheme, which is equivalent to the additive Schwarz method [192, 193], reads (also see Figure 4.2):

The BJ time-marching strategy

(1) Choose $\mathbf{u}_1^p$ and $\mathbf{u}_2^p$ as predictors for $\mathbf{u}_1^{n+1}$ and $\mathbf{u}_2^{n+1}$ and, subsequently, substitute $\mathbf{u}_1^p$ in $\mathcal{X}^2$ and $\mathbf{u}_2^p$ in $\mathcal{X}^1$.
(2) Advance $\mathcal{X}^1$ and $\mathcal{X}^2$ in parallel, and find $\mathbf{u}_1^{n+1}$ and $\mathbf{u}_2^{n+1}$.

(4.29)

Employing any of the aforementioned staggered algorithms also allows for using different time-step sizes for time integration of the subsystems. To achieve this goal, the scheme can readily be equipped by an appropriate subcycling. Figure 4.3 depicts the flowchart of an exemplary multi-time stepping solution based on the CSS procedure. There, assuming an interaction between a faster subsystem $\mathcal{X}^1$ and a slower subsystem $\mathcal{X}^2$, the time stepping is performed in the following consecutive steps:

Multi-time stepping based on the CSS procedure

(1) Choose $\mathbf{u}_2^p$ as a predictor for the variables of the slower subsystem $\mathcal{X}^2$ at $t = t^{n+1}$, and substitute it in the faster subsystem $\mathcal{X}^1$.
(2) Advance the faster subsystem $\mathcal{X}^1$ and find $\mathbf{u}_1^{n+1}$. This is done using $\Delta t_1 = \Delta t_2/s$, within s steps.
(3) Substitute $\mathbf{u}_1^{n+1}$ in $\mathcal{X}^2$.
(4) Advance $\mathcal{X}^2$ using Δt_2 and find $\mathbf{u}_2^{n+1}$.

(4.30)

As it was mentioned, staggered time-marching processes are convenient tools for decoupled

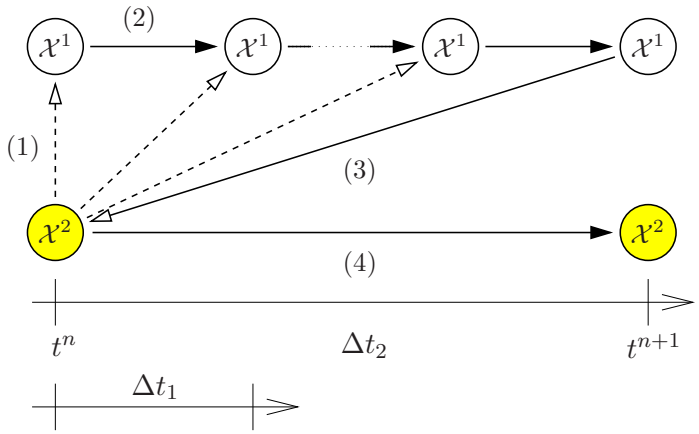

Figure 4.3: *Exemplary multi-time stepping method for interaction between a faster subsystem $\mathcal{X}^1$ and a slower subsystem $\mathcal{X}^2$.*

integration of coupled systems of equations. One, however, has to note that choosing the side to be predicted, the method used for building the predictor (for example considering an explicit or an implicit predictor), the integration schemes used within the subsystems and also the sequence of integration directly impact the stability and accuracy of the scheme, and, thus, play a crucial role in the success or the failure of the solution scheme. These issues are addressed in several publications, see for instance [86, 152, 192, 223, 224]. Also see Chapter 5 for discussions about the stability of the numerical time integration schemes, and Chapters 6 and 7 for applications and examples.

Knowing the basics about staggered integration schemes, two efficient techniques for decoupling of coupled PDE systems are presented in the next step. These are the space-partitioning methods and the operator-splitting schemes.

Remarks:

- Employing some type of a predictor-corrector iteration within each cycle of integration has been seen as a feasible way for compensating the time-lag between the integration of subsystems and, thus, for enhancing the accuracy and stability properties of staggered solution methods [92, 223, 244, 259].
- The predictors mentioned in the above staggered schemes are usually built upon the known variables from the last time step(s). From this point of view, the above procedures exhibit the properties of an explicit time integration method. Iterating between subsystems also provides an opportunity for a fully implicit staggered integration, known as the implicit-implicit, or the strong coupling solution method. See [192] for more details.

4.3.2 Partitioning in space

Geared by the terminology proposed by Felippa & Park [100], we refer to the process of *partitioning* as the decomposition of the spatial domain of a problem into several interacting non-overlapping *subdomains* or *partitions*. The interactions amongst the subdomains are then viewed as forcing effects, communicated between the individual components. To

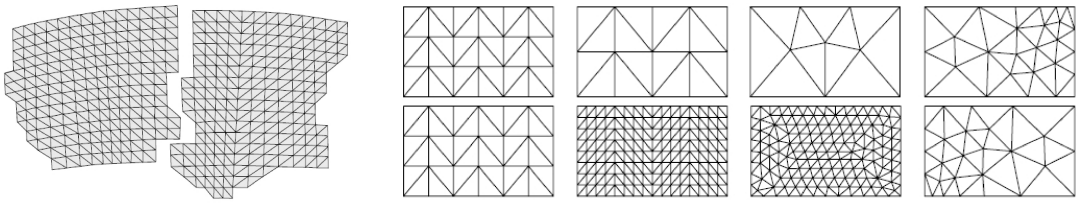

Figure 4.4: *Algebraic (left) and differential (right) partitioning [74, 101].*

study some of the techniques which are used in this context is the main concern of the present section.

Based on the priority of the spatial discretisation and the partitioning, one may end up with an *algebraic* or a *differential* partitioning. In the algebraic partitioning, the spatial discretisation of the complete coupled system takes place prior to the partitioning. This directly results in a matched mesh for different partitions. In contrast, in the differential partitioning, the decomposition of the system into subsystems is done first and, subsequently, each field is discretised separately. This may result in a matched or a non-matched mesh, see Figure 4.4.

In the context of surface interaction between physically or computationally heterogeneous bodies, partitioning results in separation of the interacting domains from each other. In this regard, various partitioned solution schemes have been developed which, based on their corresponding integration algorithm, can be categorised into two big groups, namely the Schur complement methods (SCM) and the staggered solution strategies. In what follows, the Schur complement methods and its variants, namely the primal and the dual Schur complement methods, are firstly introduced. Subsequently, and in conjunction with the idea of dual Schur complement methods, the concepts of global and localised Lagrange multipliers are explained. Finally, recognising the Lagrange multipliers as force-like vectors acting between the subdomains, an alternative formulation of the problem is proposed, and the procedure for staggered solution of the problem is studied.

To start the survey, recall the coupled system depicted in Figure 4.1, and its set of governing equations (4.19). Expansion yields the following relations, which are assigned to the subdomains $\mathcal{X}^{\mathfrak{T}}$ and $\mathcal{X}^{\mathfrak{B}}$, and to the interface $\mathcal{X}^{\mathfrak{I}}$:

$$\begin{aligned}
\mathcal{X}^{\mathfrak{T}} \quad &: \quad \mathbf{M}_{\mathfrak{TT}}\,\ddot{\mathbf{u}}^{red}_{\mathfrak{T}} + \mathbf{K}_{\mathfrak{TT}}\,\mathbf{u}^{red}_{\mathfrak{T}} + \mathbf{K}_{\mathfrak{TI}}\,\mathbf{u}_{\mathfrak{I}} = \boldsymbol{f}^{red}_{\mathfrak{T}}\,, \\
\mathcal{X}^{\mathfrak{B}} \quad &: \quad \mathbf{M}_{\mathfrak{BB}}\,\ddot{\mathbf{u}}^{red}_{\mathfrak{B}} + \mathbf{K}_{\mathfrak{BB}}\,\mathbf{u}^{red}_{\mathfrak{B}} + \mathbf{K}_{\mathfrak{BI}}\,\mathbf{u}_{\mathfrak{I}} = \boldsymbol{f}^{red}_{\mathfrak{B}}\,, \\
\mathcal{X}^{\mathfrak{I}} \quad &: \quad \mathbf{M}_{\mathfrak{II}}\,\ddot{\mathbf{u}}_{\mathfrak{I}} + \mathbf{K}^{T}_{\mathfrak{TI}}\,\mathbf{u}^{red}_{\mathfrak{T}} + \mathbf{K}^{T}_{\mathfrak{BI}}\,\mathbf{u}^{red}_{\mathfrak{B}} + \mathbf{K}_{\mathfrak{II}}\,\mathbf{u}_{\mathfrak{I}} = \boldsymbol{f}_{\mathfrak{I}}\,.
\end{aligned} \tag{4.31}$$

Adopting the idea of substructuring in the sense of Przemieniecki [228] provides a simple procedure for a partitioned solution of this equation system. To achieve this goal, one should firstly discretise the equations. However, in contrast to the monolithic integration of Section 4.2, discretisation of the equations can take place individually, e. g., employing the Newmark β-method [204, 205]:

$$\mathbf{u}^{n+1}_{\mathfrak{a}} = \mathbf{u}^{n}_{\mathfrak{a}} + \Delta t\,\dot{\mathbf{u}}^{n}_{\mathfrak{a}} + \tfrac{1}{2}\,\Delta t^2\,[2\,\beta_{\mathfrak{a}}\,\ddot{\mathbf{u}}^{n+1}_{\mathfrak{a}} + (1-2\,\beta_{\mathfrak{a}})\,\ddot{\mathbf{u}}^{n}_{\mathfrak{a}}]\,, \quad 0 \le \beta_{\mathfrak{a}} \le \tfrac{1}{2}\,, \quad \mathfrak{a} = \{\mathfrak{T}\,,\mathfrak{B}\,,\mathfrak{I}\}\,. \tag{4.32}$$

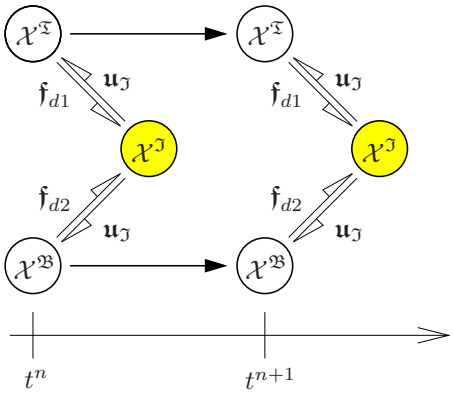

Figure 4.5: *Flowchart showing the partitioned solution following the primal Schur complement method.*

Consequently, the discrete version of (4.31) reads

$$\mathfrak{S}_d\,\mathfrak{u}^{n+1} - \mathfrak{f}_d = \mathbf{0}\,, \tag{4.33}$$

where $\mathfrak{u} := [\mathfrak{u}_{\mathfrak{T}}^{red}\,, \mathfrak{u}_{\mathfrak{B}}^{red}\,, \mathfrak{u}_{\mathfrak{J}}]^T$,

$$\mathfrak{S}_d := \mathbf{M} + \Delta t^2\,\boldsymbol{\beta}\,\mathbf{K} = \begin{bmatrix} \mathfrak{S}_{d11} & \mathbf{0} & \mathfrak{S}_{d13} \\ \mathbf{0} & \mathfrak{S}_{d22} & \mathfrak{S}_{d23} \\ \mathfrak{S}_{d31} & \mathfrak{S}_{d32} & \mathfrak{S}_{d33} \end{bmatrix}\,, \tag{4.34}$$

and

$$\mathfrak{f}_d := \mathbf{M}\,\mathfrak{u}^n + \Delta t\,\mathbf{M}\,\dot{\mathfrak{u}}^n + \frac{1}{2}\,\Delta t^2\,[2\,\boldsymbol{\beta}\,(\mathfrak{f}^{n+1} - \mathbf{M}\,\ddot{\mathfrak{u}}^n) + \mathbf{M}\,\ddot{\mathfrak{u}}^n] = [\mathfrak{f}_{d1}\,, \mathfrak{f}_{d2}\,, \mathfrak{f}_{d3}]^T\,. \tag{4.35}$$

Therein, $\boldsymbol{\beta} := \mathrm{diag}\,[\beta_{\mathfrak{a}}]$, $\mathfrak{f} := [\boldsymbol{f}_{\mathfrak{T}}^{red}\,, \boldsymbol{f}_{\mathfrak{B}}^{red}\,, \boldsymbol{f}_{\mathfrak{J}}]$, the mass matrix $\mathbf{M}$ and the stiffness matrix $\mathbf{K}$ are as in (4.21). Solving the first two rows of (4.33) for the displacement vectors corresponding to the mass-points within the subdomains gives

$$\begin{aligned} \mathcal{X}^{\mathfrak{T}} \quad &: \quad (\mathfrak{u}_{\mathfrak{T}}^{red})^{n+1} = \mathfrak{S}_{d11}^{-1}\,[\mathfrak{f}_{d1} - \mathfrak{S}_{d13}\,\mathfrak{u}_{\mathfrak{J}}^{n+1}]\,, \\ \mathcal{X}^{\mathfrak{B}} \quad &: \quad (\mathfrak{u}_{\mathfrak{B}}^{red})^{n+1} = \mathfrak{S}_{d22}^{-1}\,[\mathfrak{f}_{d2} - \mathfrak{S}_{d23}\,\mathfrak{u}_{\mathfrak{J}}^{n+1}]\,. \end{aligned} \tag{4.36}$$

Subsequent introduction of these results into the last row of (4.33) then yields

$$\mathcal{X}^{\mathfrak{J}} \;:\; \boldsymbol{\mathcal{S}}_{\mathfrak{S}_{d33}}\,\mathfrak{u}_{\mathfrak{J}}^{n+1} = \mathfrak{f}_{d3} - \mathfrak{S}_{d31}\,\mathfrak{S}_{d11}^{-1}\,\mathfrak{f}_{d1} - \mathfrak{S}_{d32}\,\mathfrak{S}_{d22}^{-1}\,\mathfrak{f}_{d2}\,, \tag{4.37}$$

where

$$\boldsymbol{\mathcal{S}}_{\mathfrak{S}_{d33}} := \mathfrak{S}_{d33} - \mathfrak{S}_{d31}\,\mathfrak{S}_{d11}^{-1}\,\mathfrak{S}_{d13} - \mathfrak{S}_{d32}\,\mathfrak{S}_{d22}^{-1}\,\mathfrak{S}_{d23} \tag{4.38}$$

represents the Schur complement matrix of the block $\mathfrak{S}_{d33}$. Then, the solution algorithm based on the primal Schur complement method can be described as follows (also see Figure

4.5):

The primal Schur complement method

(1) Using (4.37) with known external forces $\mathbf{f}_{d1}$ and $\mathbf{f}_{d2}$, calculate the new values of the interface displacement $\mathbf{u}_{\mathfrak{I}}^{n+1}$. This process can be done iteratively, employing the so-called balancing domain decomposition (BDD) methods [69, 141, 184, 185, 219].
(2) Insert the result into $(4.36)_{1,2}$ to obtain the new values of $(\mathbf{u}_{\mathfrak{T}}^{red})^{n+1}$ and $(\mathbf{u}_{\mathfrak{B}}^{red})^{n+1}$.

(4.39)

Remarks:

- The procedure as presented here is essentially identical to the original, physically motivated approach of Przemieniecki [228].
- Due to the fact that this formulation is based on explicit enforcement of consistency of boundary displacements (4.9), the Przemieniecki's substructuring is called a primal Schur complement method.

Implicit enforcement of consistency constraints through force-like Lagrange multipliers yields an alternative set of governing equations, which can be solved either in a staggered manner, or following the ideas of the dual Schur complement methods.

To prepare the partitioned equation system, recall that solving the mathematical model of a mechanical phenomenon is identical to finding a minimiser for the total energy functional of the system under prescribed boundary conditions. Thus, to solve the mathematical model of a surface-coupled system is actually a constrained optimisation problem, which can be treated using the method of Lagrange multipliers, consult any textbook about constrained optimisation problems, e. g., [22].

To elucidate the idea, consider the rheological model depicted in Figure 4.1, and its corresponding energy functional (4.10). An implicit enforcement of the interface constraint (4.9) is done through reformulating this relation as

$$u_{\mathfrak{T}_N} = u_{\mathfrak{B}_M} \quad \rightarrow \quad u_{\mathfrak{T}_N} - u_{\mathfrak{B}_M} = 0\,, \tag{4.40}$$

or equivalently

$$\mathcal{H}(\mathbf{u}_{\mathfrak{T}}\,,\mathbf{u}_{\mathfrak{B}}) := \mathbf{B}_{\mathfrak{T}}^T\,\mathbf{u}_{\mathfrak{T}} - \mathbf{B}_{\mathfrak{B}}^T\,\mathbf{u}_{\mathfrak{B}} = 0\,, \tag{4.41}$$

where $\mathbf{B}_{\mathfrak{a}}$, $\mathfrak{a} = \{\mathfrak{T}\,,\mathfrak{B}\}$, represents connection or consistency matrices, extracting and relating the boundary values of the degrees of freedom at the interface to each other. The connection matrices for this simple example read

$$\mathbf{B}_{\mathfrak{T}}^T = [0\,,\cdots,0\,,1]_{1\times N} \quad \text{and} \quad \mathbf{B}_{\mathfrak{B}}^T = [0\,,\cdots,0\,,1]_{1\times M}\,. \tag{4.42}$$

Thus, the interpretation of this problem in the context of a variational formulation takes the following form:

$$\min_{\mathbf{u}_{\mathfrak{T}}\,,\mathbf{u}_{\mathfrak{B}}} \Pi(\mathbf{u}_{\mathfrak{T}}\,,\mathbf{u}_{\mathfrak{B}}) \quad \text{subjected to} \quad \mathcal{H}(\mathbf{u}_{\mathfrak{T}}\,,\mathbf{u}_{\mathfrak{B}}) = 0\,. \tag{4.43}$$

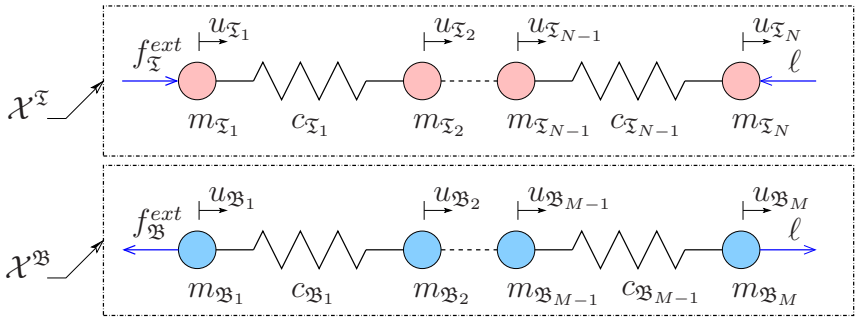

Figure 4.6: *Partitioning via the global Lagrange multiplier ℓ.*

Relation (4.43) embodies a constrained optimisation problem, which, via introducing a Lagrange multiplier ℓ, can be replaced by an augmented one given by

$$\min_{\mathbf{u}_{\mathfrak{T}},\mathbf{u}_{\mathfrak{B}},\ell} \mathfrak{L}(\mathbf{u}_{\mathfrak{T}}, \mathbf{u}_{\mathfrak{B}}, \ell) \quad \text{with} \quad \mathfrak{L} := \Pi(\mathbf{u}_{\mathfrak{T}}, \mathbf{u}_{\mathfrak{B}}) + \ell\, \mathcal{H}(\mathbf{u}_{\mathfrak{T}}, \mathbf{u}_{\mathfrak{B}}), \tag{4.44}$$

where $\mathfrak{L}$ is called the Lagrange functional. Nevertheless, replacement of the constrained problem (4.43) by an unconstrained one entails the additional cost of calculating the Lagrange multiplier as an extra unknown, which has to be determined along with the original vectors of unknown variables $\mathbf{u}_{\mathfrak{a}}$, via the solution of (4.44). To this end, one seeks for the stationary condition of the Lagrange functional, i. e.,

$$\delta\mathfrak{L}(\mathbf{u}_{\mathfrak{T}}, \mathbf{u}_{\mathfrak{B}}, \ell) = 0 \quad \rightarrow \quad \left\{ \frac{\partial \mathfrak{L}}{\partial \mathbf{u}_{\mathfrak{T}}} = \mathbf{0}, \quad \frac{\partial \mathfrak{L}}{\partial \mathbf{u}_{\mathfrak{B}}} = \mathbf{0}, \quad \frac{\partial \mathfrak{L}}{\partial \ell} = 0 \right\}. \tag{4.45}$$

Satisfaction of these conditions demands solution of the following set of governing equations

$$\mathfrak{S}\,\mathfrak{u} - \mathfrak{f} = \mathbf{0}, \tag{4.46}$$

where $\mathfrak{u} := [\mathbf{u}_{\mathfrak{T}}, \mathbf{u}_{\mathfrak{B}}, \ell]^T$, $\mathfrak{f} := [\boldsymbol{f}_{\mathfrak{T}}, \boldsymbol{f}_{\mathfrak{B}}, 0]^T$, and

$$\mathfrak{S} := \begin{bmatrix} \mathbf{M}_{\mathfrak{T}} \frac{\mathrm{d}^2}{\mathrm{d}t^2} + \mathbf{K}_{\mathfrak{T}} & \mathbf{0} & \mathbf{B}_{\mathfrak{T}} \\ \mathbf{0} & \mathbf{M}_{\mathfrak{B}} \frac{\mathrm{d}^2}{\mathrm{d}t^2} + \mathbf{K}_{\mathfrak{B}} & -\mathbf{B}_{\mathfrak{B}} \\ \mathbf{B}_{\mathfrak{T}}^T & -\mathbf{B}_{\mathfrak{B}}^T & 0 \end{bmatrix} \tag{4.47}$$

with the mass matrix $\mathbf{M}_{\mathfrak{a}}$ and the stiffness matrix $\mathbf{K}_{\mathfrak{a}}$ as introduced in (4.12).

Studying (4.46) reveals that it is, indeed, a partitioned set of equations, modelling a variation of the physical system as depicted in Figure 4.6. In particular, looking at the first two rows of this equation system shows that, in this example, the Lagrange multiplier has a direct physical meaning, such that it determines the internal reaction force $\boldsymbol{f}^{int}_{\mathfrak{a}}$ between the interacting subsystems, such that

$$\boldsymbol{f}^{int}_{\mathfrak{T}} = \mathbf{B}_{\mathfrak{T}}\,\ell, \quad \text{and} \quad \boldsymbol{f}^{int}_{\mathfrak{B}} = -\mathbf{B}_{\mathfrak{B}}\,\ell. \tag{4.48}$$

Time discretisation of (4.46) using the Newmark β-method (4.32) leads to

$$\mathfrak{S}_d\,\mathfrak{u}^{n+1} - \mathfrak{f}_d = \mathbf{0}, \tag{4.49}$$

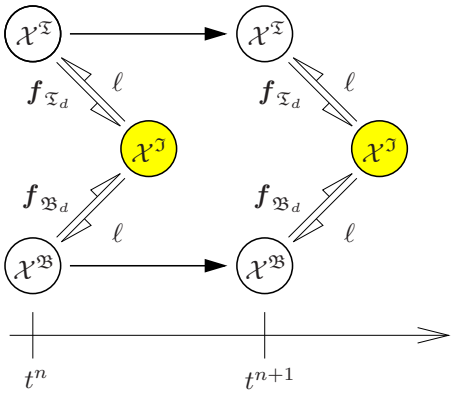

Figure 4.7: *Flowchart showing the partitioned solution following the dual Schur complement method.*

where

$$\mathfrak{S}_d := \begin{bmatrix} \overline{\mathbf{K}}_{\mathfrak{T}} & \mathbf{0} & \Delta t^2\,\beta_{\mathfrak{T}}\,\mathbf{B}_{\mathfrak{T}} \\ \mathbf{0} & \overline{\mathbf{K}}_{\mathfrak{B}} & \Delta t^2\,\beta_{\mathfrak{B}}\,\mathbf{B}_{\mathfrak{B}} \\ \mathbf{B}_{\mathfrak{T}}^T & -\mathbf{B}_{\mathfrak{B}}^T & 0 \end{bmatrix} \tag{4.50}$$

with

$$\overline{\mathbf{K}}_{\mathfrak{a}} = \mathbf{M}_{\mathfrak{a}} + \Delta t^2\,\beta_{\mathfrak{a}}\,\mathbf{K}_{\mathfrak{a}}\,, \quad \mathfrak{a} = \{\mathfrak{T}\,,\mathfrak{B}\}\,, \tag{4.51}$$

and $\mathfrak{f}_d := [\boldsymbol{f}_{\mathfrak{T}_d}\,,\boldsymbol{f}_{\mathfrak{B}_d}\,,0]^T$ with

$$\boldsymbol{f}_{\mathfrak{a}_d} := \mathbf{M}_{\mathfrak{a}}\,\mathbf{u}_{\mathfrak{a}}^n + \Delta t\,\mathbf{M}_{\mathfrak{a}}\,\dot{\mathbf{u}}_{\mathfrak{a}}^n + \frac{1}{2}\,\Delta t^2\,[2\,\beta_{\mathfrak{a}}\,(\boldsymbol{f}_{\mathfrak{a}}^{n+1} - \mathbf{M}_{\mathfrak{a}}\,\ddot{\mathbf{u}}_{\mathfrak{a}}^n) + \mathbf{M}_{\mathfrak{a}}\,\ddot{\mathbf{u}}_{\mathfrak{a}}^n]\,. \tag{4.52}$$

Next, employing the first two rows of (4.49), the displacement vectors of the subsystems at time $t = t^{n+1}$ can be presented in terms of the Lagrange multiplier, i. e.,

$$\begin{aligned} \mathcal{X}^{\mathfrak{T}} \quad &: \quad \mathbf{u}_{\mathfrak{T}}^{n+1} = \mathfrak{S}_{d11}^{-1}(\boldsymbol{f}_{\mathfrak{T}_d} - \mathfrak{S}_{d13}\,\ell^{n+1})\,, \\ \mathcal{X}^{\mathfrak{B}} \quad &: \quad \mathbf{u}_{\mathfrak{B}}^{n+1} = \mathfrak{S}_{d22}^{-1}(\boldsymbol{f}_{\mathfrak{B}_d} - \mathfrak{S}_{d23}\,\ell^{n+1})\,, \end{aligned} \tag{4.53}$$

wherein $\mathfrak{S}_{dij}$ is the block matrix on the i-th row and j-th column of the discrete coefficient matrix $\mathfrak{S}_d$ given by (4.50). Substituting these relations into the last row of (4.49) yields

$$\mathcal{X}^{\mathfrak{I}} \;:\; \boldsymbol{\mathcal{S}}_{\mathfrak{S}_{d33}}\,\ell^{n+1} = \mathfrak{S}_{d31}\,\mathfrak{S}_{d11}^{-1}\,\boldsymbol{f}_{\mathfrak{T}_d} + \mathfrak{S}_{d32}\,\mathfrak{S}_{d22}^{-1}\,\boldsymbol{f}_{\mathfrak{B}_d} \tag{4.54}$$

with

$$\boldsymbol{\mathcal{S}}_{\mathfrak{S}_{d33}} := \mathfrak{S}_{d31}\,\mathfrak{S}_{d11}^{-1}\,\mathfrak{S}_{d13} + \mathfrak{S}_{d32}\,\mathfrak{S}_{d22}^{-1}\,\mathfrak{S}_{d23}\,, \tag{4.55}$$

which is the Schur complement matrix of the block $\mathfrak{S}_{d33}$. Subsequently, a feasible partitioned solution of this problem is performed as follows (also see Figure 4.7):

The dual Schur complement method

(1) Using (4.54) and known external forces $\boldsymbol{f}_{\mathfrak{T}_d}$ and $\boldsymbol{f}_{\mathfrak{B}_d}$, calculate the new values of the Lagrange multiplier ℓ^{n+1}.
(2) Insert the result into $(4.53)_{1,2}$ to obtain $\mathbf{u}_{\mathfrak{T}}^{n+1}$ and $\mathbf{u}_{\mathfrak{B}}^{n+1}$.

(4.56)

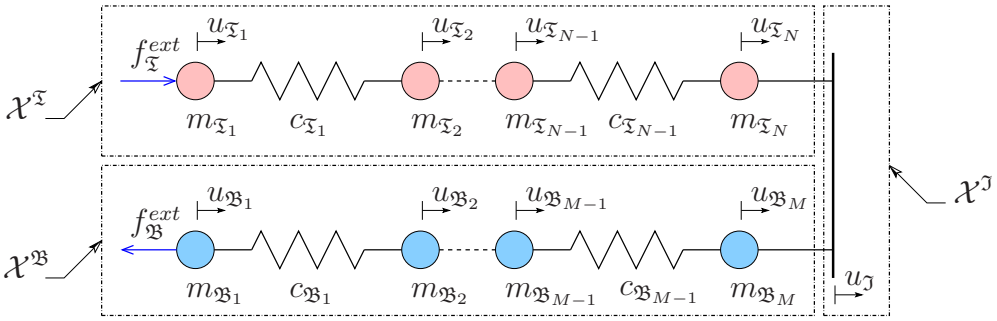

Figure 4.8: *Subsystems in the LLM method.*

Remarks:

- Considering the implicit enforcement of the interface consistency constraint via the force-like Lagrange multiplier, this scheme is called a dual Schur complement method.
- A preconditioned conjugate projected gradient algorithm for iterative solution of the problem has been introduced by Farhat & Roux [97], who called their method the finite-element tearing and interconnect (FETI), or the saddle-point domain-decomposition method [89]. See [90, 93–95, 98] for applications and more particulars.
- In spite of different formulations of the BDD and the FETI methods, it has been shown that at least some variants of these schemes are actually quite similar, or even identical. See [89, 106, 107, 160] for more information.
- As in the preceding there is only one common Lagrange multiplier acting between the partitioned subsystems, this scheme is sometimes called the *global* Lagrange-multipliers (GLM) method [235, 236], or the classical method of Lagrange multipliers [216].

Using global Lagrange multipliers yields physically motivated decoupled solution strategies which, in principle, allow for separate handling of the meeting subdomains by their respective tailored codes and solver. Nevertheless, this strategy implies a tight coupling between the subsystems that leads to a lack of modularity of solution schemes developed in this framework. In this regard, employing localised Lagrange-multipliers (LLM) method [214, 216, 235, 236], also called three-field domain decomposition method [36, 94] is a plausible way to overcome this flaw.

Following the idea of the LLM method, one loosens the coupling by considering the interface as an additional subsystem which acts like a medium or membrane that prohibits a direct interaction between the adjacent subsystems, cf. Figure 4.8. Thus, in this framework, the consistency of the degrees of freedom on the interface would be governed through the interface. Thus, the consistency constraint takes the following form:

$$\begin{cases} u_{\mathfrak{T}_N} = u_{\mathfrak{I}}\,, \\ u_{\mathfrak{B}_M} = u_{\mathfrak{I}}\,, \end{cases} \quad \rightarrow \quad \begin{cases} u_{\mathfrak{T}_N} - u_{\mathfrak{I}} = 0\,, \\ u_{\mathfrak{B}_M} - u_{\mathfrak{I}} = 0\,. \end{cases} \tag{4.57}$$

This relation in conjunction with the concept of a boundary extraction matrix $\mathbf{B}_{\mathfrak{a}}$ as

introduced in (4.42) then reads

$$\boldsymbol{\mathcal{H}}(\mathbf{u}_{\mathfrak{T}}\,,\mathbf{u}_{\mathfrak{B}}\,,u_{\mathfrak{J}}) := \left[\begin{array}{c} \mathbf{B}_{\mathfrak{T}}^{T}\,\mathbf{u}_{\mathfrak{T}} - u_{\mathfrak{J}} \\ \mathbf{B}_{\mathfrak{B}}^{T}\,\mathbf{u}_{\mathfrak{B}} - u_{\mathfrak{J}} \end{array}\right] = \mathbf{0}\,. \tag{4.58}$$

Consequently, after multiplying the constraint with a set of Lagrange multipliers, and adding the result to the total energy functional of the system Π as in (4.10), the augmented problem for this case takes the following form:

$$\min_{\mathbf{u}_{\mathfrak{T}}\,,\mathbf{u}_{\mathfrak{B}}\,,u_{\mathfrak{J}}\,,\ell^{\mathfrak{T}}\,,\ell^{\mathfrak{B}}} \mathfrak{L}(\mathbf{u}_{\mathfrak{T}}\,,\mathbf{u}_{\mathfrak{B}}\,,u_{\mathfrak{J}}\,,\ell^{\mathfrak{T}}\,,\ell^{\mathfrak{B}}) \quad \text{with} \quad \mathfrak{L} := \Pi(\mathbf{u}_{\mathfrak{T}}\,,\mathbf{u}_{\mathfrak{B}}) + \boldsymbol{\ell}^{T}\,\boldsymbol{\mathcal{H}}(\mathbf{u}_{\mathfrak{T}}\,,\mathbf{u}_{\mathfrak{B}}\,,u_{\mathfrak{J}})\,, \tag{4.59}$$

where the vector $\boldsymbol{\ell} := [\ell^{\mathfrak{T}}\,,\ell^{\mathfrak{B}}]^{T}$ contains the Lagrange multipliers. Considering this, the stationary condition for the Lagrange functional, i. e., $\delta\mathfrak{L} = 0$, demands the satisfaction of the following set of equations

$$\left\{\frac{\partial\mathfrak{L}}{\partial\mathbf{u}_{\mathfrak{T}}} = \mathbf{0}\,, \quad \frac{\partial\mathfrak{L}}{\partial\mathbf{u}_{\mathfrak{B}}} = \mathbf{0}\,, \quad \frac{\partial\mathfrak{L}}{\partial u_{\mathfrak{J}}} = 0\,, \quad \frac{\partial\mathfrak{L}}{\partial\ell^{\mathfrak{T}}} = 0\,, \quad \frac{\partial\mathfrak{L}}{\partial\ell^{\mathfrak{B}}} = 0\right\}. \tag{4.60}$$

Therefore, the set of governing equations of the problem is given as

$$\boldsymbol{\mathfrak{S}}\,\mathfrak{u} - \mathfrak{f} = \mathbf{0}\,, \tag{4.61}$$

where, $\mathfrak{u} := [\mathbf{u}_{\mathfrak{T}}\,,\mathbf{u}_{\mathfrak{B}}\,,u_{\mathfrak{J}}\,,\ell^{\mathfrak{T}}\,,\ell^{\mathfrak{B}}]^{T}$, $\mathfrak{f} := [\boldsymbol{f}_{\mathfrak{T}}\,,\boldsymbol{f}_{\mathfrak{B}}\,,0\,,0\,,0]^{T}$, and

$$\boldsymbol{\mathfrak{S}} := \left[\begin{array}{ccccc} \mathbf{M}_{\mathfrak{T}}\,\frac{\mathrm{d}^2}{\mathrm{d}t^2} + \mathbf{K}_{\mathfrak{T}} & \mathbf{0} & 0 & \mathbf{B}_{\mathfrak{T}} & 0 \\ \mathbf{0} & \mathbf{M}_{\mathfrak{B}}\,\frac{\mathrm{d}^2}{\mathrm{d}t^2} + \mathbf{K}_{\mathfrak{B}} & 0 & 0 & \mathbf{B}_{\mathfrak{B}} \\ \mathbf{0} & \mathbf{0} & 0 & 1 & 1 \\ \mathbf{B}_{\mathfrak{T}}^{T} & \mathbf{0} & -1 & 0 & 0 \\ \mathbf{0} & \mathbf{B}_{\mathfrak{B}}^{T} & -1 & 0 & 0 \end{array}\right]. \tag{4.62}$$

Looking at the first two rows of (4.61) reveals that, in the present case, one ends up with the following internal forces

$$\boldsymbol{f}_{\mathfrak{T}}^{int} = \mathbf{B}_{\mathfrak{T}}\,\ell^{\mathfrak{T}}\,, \quad \text{and} \quad \boldsymbol{f}_{\mathfrak{B}}^{int} = \mathbf{B}_{\mathfrak{B}}\,\ell^{\mathfrak{B}}\,, \tag{4.63}$$

which are localised forces, acting between the interface and each of the subdomains (cf. Figure 4.9) and, hence, this method is called the *localised* Lagrange-multipliers method. This procedure yields separation of the governing equations of the subsystems from each other and facilitates a complete partitioning of the problem. The partitioned problem generated in this way can conveniently be solved in a parallel manner, using optimised discretisation and solution methods for each subdomain. To elucidate the idea, consider an exemplary time discretisation of (4.61) via the Newmark β-method (4.32). This process yields

$$\boldsymbol{\mathfrak{S}}_{d}\,\mathfrak{u}^{n+1} - \mathfrak{f}_{d} = \mathbf{0}\,, \tag{4.64}$$

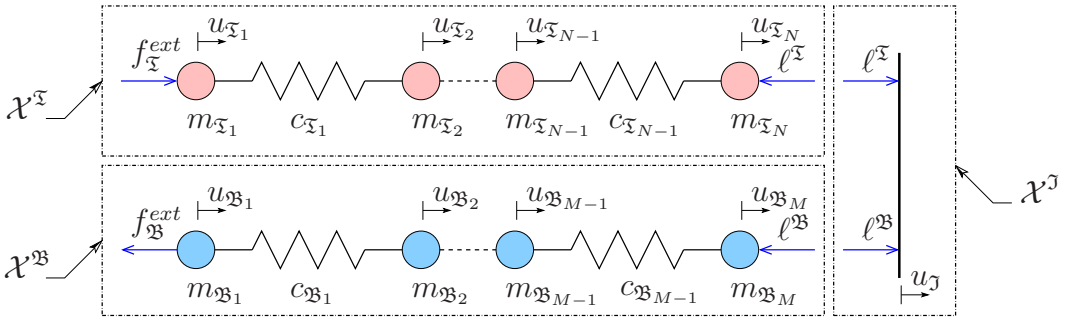

Figure 4.9: *Partitioning via localised Lagrange multipliers* $\ell^{\mathfrak{a}}\,,\mathfrak{a}=\{\mathfrak{T}\,,\mathfrak{B}\}$.

where,

$$\mathfrak{S}_d := \begin{bmatrix} \overline{\mathbf{K}}_{\mathfrak{T}} & \mathbf{0} & 0 & \Delta t^2\,\beta_{\mathfrak{T}}\,\mathbf{B}_{\mathfrak{T}} & 0 \\ \mathbf{0} & \overline{\mathbf{K}}_{\mathfrak{B}} & 0 & 0 & \Delta t^2\,\beta_{\mathfrak{B}}\,\mathbf{B}_{\mathfrak{B}} \\ \mathbf{0} & \mathbf{0} & 0 & 1 & 1 \\ \mathbf{B}_{\mathfrak{T}}^T & \mathbf{0} & -1 & 0 & 0 \\ \mathbf{0} & \mathbf{B}_{\mathfrak{B}}^T & -1 & 0 & 0 \end{bmatrix}, \tag{4.65}$$

and $\mathfrak{f}_d := [\boldsymbol{f}_{\mathfrak{T}_d}\,,\boldsymbol{f}_{\mathfrak{B}_d}\,,0\,,0\,,0]^T$. Therein, the matrix $\overline{\mathbf{K}}_{\mathfrak{a}}$ and the vector $\boldsymbol{f}_{\mathfrak{a}_d}$ are as defined by (4.51) and (4.52). Rearranging the first two rows of (4.64) yields

$$\begin{aligned} \mathcal{X}^{\mathfrak{T}} \;&:\; \mathbf{u}_{\mathfrak{T}}^{n+1} = \mathfrak{S}_{d11}^{-1}(\boldsymbol{f}_{\mathfrak{T}}^{n+1} - \mathfrak{S}_{d14}\,\ell_{\mathfrak{T}}^{n+1})\,, \\ \mathcal{X}^{\mathfrak{B}} \;&:\; \mathbf{u}_{\mathfrak{B}}^{n+1} = \mathfrak{S}_{d22}^{-1}(\boldsymbol{f}_{\mathfrak{B}}^{n+1} - \mathfrak{S}_{d25}\,\ell_{\mathfrak{B}}^{n+1})\,. \end{aligned} \tag{4.66}$$

Therein, $\mathfrak{S}_{dij}$ is the block matrix on the i-th row and j-th column of the discrete coefficient matrix $\mathfrak{S}_d$ given by (4.65). Inserting these relations into the last three rows of (4.64) yields the following equation system that has to be solved at the interface:

$$\mathcal{X}^{\mathfrak{I}} \;:\; \begin{bmatrix} \mathbf{F}_{\mathfrak{I}} & \mathbf{L} \\ \mathbf{L}^T & \mathbf{0} \end{bmatrix} \begin{bmatrix} \boldsymbol{\ell} \\ u_{\mathfrak{I}} \end{bmatrix}^{n+1} = \begin{bmatrix} \boldsymbol{f}_{\ell} \\ 0 \end{bmatrix}. \tag{4.67}$$

Therein, $\mathbf{L} := [1\,,1]^T$,

$$\mathbf{F}_{\mathfrak{I}} := \Delta t^2 \begin{bmatrix} \beta_{\mathfrak{T}}\,\mathbf{B}_{\mathfrak{T}}^T\,\overline{\mathbf{K}}_{\mathfrak{T}}^{-1}\,\mathbf{B}_{\mathfrak{T}} & \mathbf{0} \\ \mathbf{0} & \beta_{\mathfrak{B}}\,\mathbf{B}_{\mathfrak{B}}^T\,\overline{\mathbf{K}}_{\mathfrak{B}}^{-1}\,\mathbf{B}_{\mathfrak{B}} \end{bmatrix}, \tag{4.68}$$

and

$$\boldsymbol{f}_{\ell} := \left[\mathbf{B}_{\mathfrak{T}}^T\,\overline{\mathbf{K}}_{\mathfrak{T}}^{-1}\,\boldsymbol{f}_{\mathfrak{T}_d}\,,\; \mathbf{B}_{\mathfrak{B}}^T\,\overline{\mathbf{K}}_{\mathfrak{B}}^{-1}\,\boldsymbol{f}_{\mathfrak{B}_d}\right]^T. \tag{4.69}$$

Finally, partitioned solution of this problem is done as follows (also see Figure 4.10):

The localised Lagrange-multipliers method

(1) Insert the known external forces $\boldsymbol{f}_{\mathfrak{T}_d}$ and $\boldsymbol{f}_{\mathfrak{B}_d}$ into (4.67) and calculate the new values of the vector of Lagrange multipliers $\boldsymbol{\ell}^{n+1}$.
(2) Employ the results to update the displacement vectors via $(4.66)_{1,2}$.

(4.70)

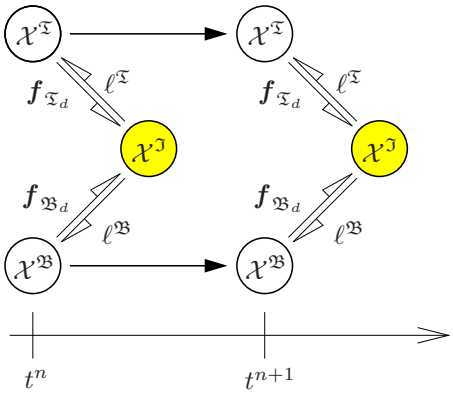

Figure 4.10: *Flowchart showing the partitioned solution following the LLM method.*

More details in this regard can be found in Section 7.3, where employing the idea of the LLM method, a partitioned solution scheme for the surface-coupled problem of fluid-porous-media interaction (FPMI) is presented.

As it can be seen from the presented flowcharts, the Schur complement methods allow for a parallel treatment of the problem. Moreover, employing the LLM method permits using non-matching spatial discretisation schemes and meshes in a convenient fashion. Nevertheless, using these partitioning methods demands the solution of an interface subproblem as in (4.37), (4.54) or (4.67). Execution of this step essentially entails additional development of an interface subroutine, which, on the one hand, needs to have access to the (finite-element) matrices of both subproblems and, on the other hand, includes some matrix inversion processes. These can be seen as the shortcomings of the mentioned solution strategies, because, firstly, the commercial finite-element solvers usually provide just limited or absolutely no information about the global mass and stiffness matrices. Secondly, inversion of the FE matrices when dealing with large problems with many DOF may become very expensive. In this regard, employing a staggered time-marching strategy provides another opportunity for the decoupled solution of the surface-coupled problems, without any need to solve an interface subproblem. To explain the procedure, consider the following alternative formulation of the problem containing the balances of momentum corresponding to the subsystems, and the kinematic constraint and the equilibrium of forces at the interface:

$$\begin{aligned}
\mathcal{X}^{\mathfrak{T}} \quad &: \quad \mathbf{M}_{\mathfrak{T}}\,\ddot{\mathbf{u}}_{\mathfrak{T}} + \mathbf{K}_{\mathfrak{T}}\mathbf{u}_{\mathfrak{T}} + \mathbf{B}_{\mathfrak{T}}\,\ell^{\mathfrak{T}} = \mathbf{f}_{\mathfrak{T}}\,, \\
\mathcal{X}^{\mathfrak{B}} \quad &: \quad \mathbf{M}_{\mathfrak{B}}\,\ddot{\mathbf{u}}_{\mathfrak{B}} + \mathbf{K}_{\mathfrak{B}}\mathbf{u}_{\mathfrak{B}} + \mathbf{B}_{\mathfrak{B}}\,\ell^{\mathfrak{B}} = \mathbf{f}_{\mathfrak{B}}\,, \\
\text{Kinematic constraint} \quad &: \quad \mathbf{B}_{\mathfrak{T}}^{T}\,\mathbf{u}_{\mathfrak{T}} = \mathbf{B}_{\mathfrak{B}}^{T}\,\mathbf{u}_{\mathfrak{B}}\,, \\
\text{Equilibrium of forces} \quad &: \quad \ell^{\mathfrak{T}} + \ell^{\mathfrak{B}} = 0\,.
\end{aligned} \tag{4.71}$$

A staggered solution of this system is feasible in the sense of the BGS strategy, cf. Section 4.3.1. To this end, one firstly needs to choose a subsystem, within which the coupling primary parameter, i. e., the interface displacement, is predicted. Considering $[\mathbf{B}_{\mathfrak{B}}^{T}\,\mathbf{u}_{\mathfrak{B}}]^{p} = u^{p}_{\mathfrak{B}_M}$ as a predictor for the displacement of the interface mass-point of the subsystem $\mathcal{X}^{\mathfrak{B}}$ at time t^{n+1}, a staggered time integration is executed through the following procedure

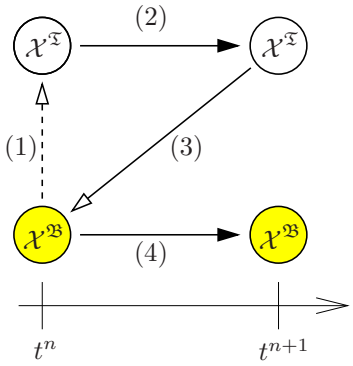

Figure 4.11: *Flowchart showing the partitioned solution following the BGS strategy.*

(also see Figure 4.11):

Partitioned solution following the BGS strategy

(1) Using $u^p_{\mathfrak{B}_M}$ and $(4.71)_3$, compute the interface displacement $u^{n+1}_{\mathfrak{T}_N}$.
(2) Considering $u^{n+1}_{\mathfrak{T}_N}$ as the BC, advance $\mathcal{X}^{\mathfrak{T}}$ to find $\mathbf{u}^{n+1}_{\mathfrak{T}}$ and $(\ell^{\mathfrak{T}})^{n+1}$.
(3) Using $(\ell^{\mathfrak{T}})^{n+1}$ and considering $(4.71)_4$, calculate $(\ell^{\mathfrak{B}})^{n+1}$.
(4) Considering $(\ell^{\mathfrak{B}})^{n+1}$ as the BC, solve $\mathcal{X}^{\mathfrak{B}}$ and update $\mathbf{u}^{n+1}_{\mathfrak{B}}$.

(4.72)

In Sections 7.1 and 7.2 of this monograph, two representative examples inspired by the surface-coupled problems of fluid-structure interaction (FSI) and structure-structure interaction (SSI) are presented and solved in a decoupled manner, using a staggered integration based on the block Gauss-Seidel (BGS) strategy. A graphical summary of the above-mentioned partitioned integration schemes is also presented in Figure 4.12.

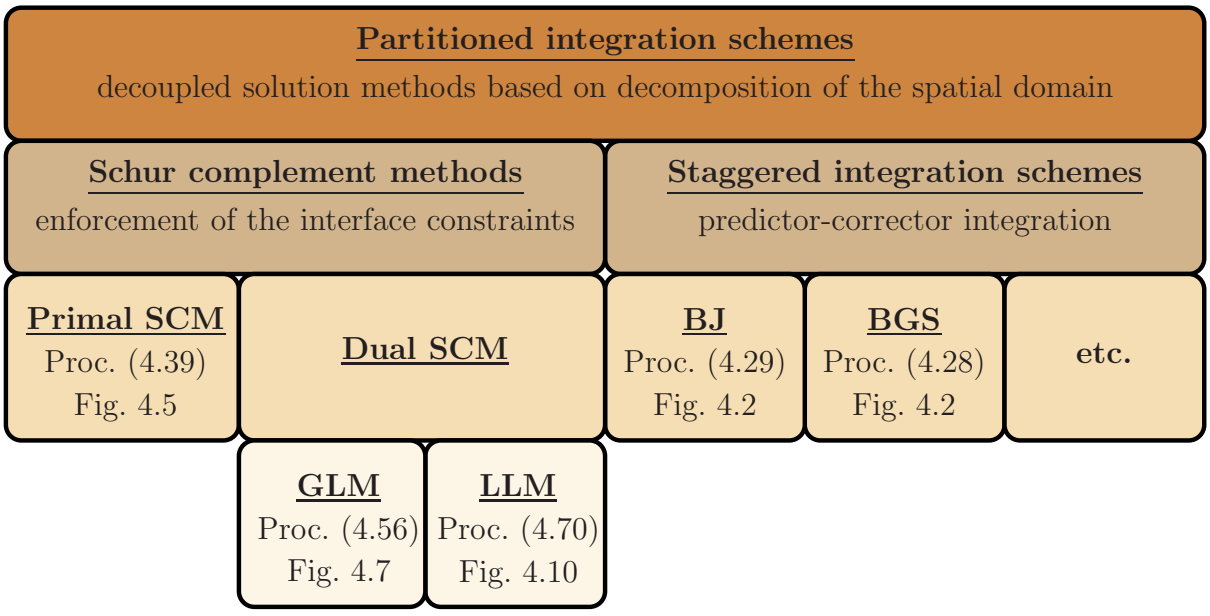

Figure 4.12: *Partitioned integration schemes.*

Remarks:

- Obviously, employing the idea of the block-Jacobi integration strategy, as explained in Section 4.3.1, provides another opportunity for staggered solution of the equation system (4.71) in a parallel manner. This is done through simultaneous prediction of the interface displacement from one subsystem, and the interface force from the other. Nevertheless, the inter-field parallelism achieved via this method is at the expense of amplified errors in the responses of the subsystems [225]. This is principally due to the fact that the BJ procedure does not implement any feedback between the subsystems within one coupled time step. Attempts to overcome this flaw in the field of fluid-structure interaction (FSI) have led to the development of the improved parallel staggered (IPS) procedure by Farhat & Lesoinne [92].
- It is worth mentioning that the primal Schur complement method, the dual Schur complement method and the BGS time integration strategy as introduced above are respectively equivalent to the Dirichlet-Dirichlet, Neumann-Neumann and Dirichlet-Neumann methods, commonly used for domain decomposition, cf., e. g., Lui [181].

4.3.3 Splitting in time

Employing an operator-splitting scheme (OSS) is another strategy for simplifying the task of solution of single as well as sets of partial differential equations. As the name suggests, the operator-splitting schemes, also known as the fractional step methods [101, 195, 234], result in splitting of complex differential operators into two or more parts that are each simpler to integrate than the original one[2]. The complexity of the operators may be, for example, in the sense of coexistence of stiff and non-stiff, or linear and non-linear operators. Subsequently, each resulting subproblem is advanced in time using individual time steps, in single or multiple (fractional) steps. Thus, in contrast to the partitioning that implies a decomposition of the spatial domain, the operator splitting is based on a decomposition of the time discretisation of the PDE within the time-step intervals.

Effectiveness of operator splitting has given rise to development of numerous solution strategies proposed for diverse coupled problems, cf. Section 1.2 for a list of selected relevant works. Concerning the numerical treatment of the sets of governing equations resulting from the continuum-mechanical modelling of physical phenomena, an explanation of the procedure of operator splitting is provided by McLachlan & Quispel [195]. A clear reinterpretation of this strategy is also given by Markert [188]. In what follows, an adaptation of this clarification in terms of the herein-used terminology is presented. To this end, recall the abstract system of evolution equations (3.68)

$$\mathcal{X} \;:\; \mathfrak{S}_t\,\mathbf{u}(\mathbf{x}\,,t) = \overline{\mathfrak{S}}\,\mathbf{u}(\mathbf{x}\,,t) + \mathfrak{f}(\mathbf{x}\,,t) =: \boldsymbol{f}\,(\mathbf{x}\,,t)\,. \tag{4.73}$$

Following the idea of operator-splitting, the time integration of this equation is performed

[2]This definition coincides with the "partitioning" methods of Hairer & Wanner [132].

based on the following procedure:

Operator splitting strategy

(1) Split RHS of the complex system $\mathcal{X}$ into simpler pieces, and build simpler subproblems $\{\mathcal{X}^{\mathfrak{a}} : \mathfrak{S}_t\,\mathfrak{u} = \boldsymbol{f}_{\mathfrak{a}}\}$, such that $\sum_{\mathfrak{a}} \boldsymbol{f}_{\mathfrak{a}} = \boldsymbol{f}$.
(2) Integrate each subproblem $\mathcal{X}^{\mathfrak{a}}$ individually.
(3) Combine the results to approximate the coupled solution.

(4.74)

It should be noted that the first step usually entails a splitting of the differential operator $\overline{\mathfrak{S}}$ into sub-operators $\overline{\mathfrak{S}}_{\mathfrak{a}}$, hence, the name operator splitting. Furthermore, following this method, the evolution of the variables is determined via successive integration of the resulting subproblems by means of individual integrators $\boldsymbol{\varphi}_{\mathfrak{a}}$. Thus, the updating of the system happens in fractional steps and, therefore, this group of solution strategies are also known as fractional-step methods.

To set up an example, consider the governing equations of the volume-coupled problem of linear thermoelasticity (3.67). In the absence of body forces and neglecting the radiation, these relations read

$$\mathcal{X} \;:\; \left\{ \begin{array}{rcl} \dfrac{\mathrm{d}^2 u}{\mathrm{d}t^2} & = & \dfrac{1}{\rho} \left[E\,\dfrac{\partial^2 u}{\partial x^2} + m\,\dfrac{\partial \vartheta}{\partial x} \right], \\ \dfrac{\mathrm{d}\vartheta}{\mathrm{d}t} & = & \dfrac{1}{c_v} \left[k\,\dfrac{\partial^2 \vartheta}{\partial x^2} + \theta_0\, m\,\dfrac{\partial}{\partial x}\left(\dfrac{\mathrm{d}u}{\mathrm{d}t}\right) \right]. \end{array} \right. \tag{4.75}$$

Following the arguments of Section 3.4, this is a coupled PDE system, governing the coupled evolution of the mechanical variable u and the thermal variable ϑ. Rearrangement of the equations and comparing to (4.73) yields the following identifications:

$$\underbrace{\begin{bmatrix} \dfrac{\mathrm{d}^2}{\mathrm{d}t^2} & 0 \\ 0 & \dfrac{\mathrm{d}}{\mathrm{d}t} \end{bmatrix}}_{\mathfrak{S}_t} \underbrace{\begin{bmatrix} u \\ \vartheta \end{bmatrix}}_{\mathfrak{u}} = \underbrace{\begin{bmatrix} \dfrac{1}{\rho} \left[E\,\dfrac{\partial^2 u}{\partial x^2} + m\,\dfrac{\partial \vartheta}{\partial x} \right] \\ \dfrac{1}{c_v} \left[k\,\dfrac{\partial^2 \vartheta}{\partial x^2} + \theta_0\, m\,\dfrac{\partial}{\partial x}\left(\dfrac{\mathrm{d}u}{\mathrm{d}t}\right) \right] \end{bmatrix}}_{\boldsymbol{f}}. \tag{4.76}$$

Thus, $\mathfrak{f} = [0\,,0]^T$, and the differential operator $\overline{\mathfrak{S}}$ for this problem reads

$$\overline{\mathfrak{S}} = \begin{bmatrix} \dfrac{E}{\rho}\,\dfrac{\partial^2}{\partial x^2} & \dfrac{m}{\rho}\,\dfrac{\partial}{\partial x} \\ \dfrac{\theta_0\, m}{c_v}\,\dfrac{\partial}{\partial x}\left(\dfrac{\mathrm{d}}{\mathrm{d}t}\right) & \dfrac{k}{c_v}\,\dfrac{\partial^2}{\partial x^2} \end{bmatrix}. \tag{4.77}$$

A splitting of this operator in the sense of the *isothermal operator-splitting method* of Armero & Simo [4] then yields

$$\overline{\mathfrak{S}} = \overline{\mathfrak{S}}_u + \overline{\mathfrak{S}}_\vartheta \tag{4.78}$$

with

$$\overline{\mathfrak{S}}_u = \begin{bmatrix} \dfrac{E}{\rho}\dfrac{\partial^2}{\partial x^2} & \dfrac{m}{\rho}\dfrac{\partial}{\partial x} \\ 0 & 0 \end{bmatrix}, \quad \overline{\mathfrak{S}}_\vartheta = \begin{bmatrix} 0 & 0 \\ \dfrac{\theta_0\, m}{c_v}\dfrac{\partial}{\partial x}\left(\dfrac{\mathrm{d}}{\mathrm{d}t}\right) & \dfrac{k}{c_v}\dfrac{\partial^2}{\partial x^2} \end{bmatrix}. \tag{4.79}$$

Employing these operators breaks down the coupled problem (4.75) into a mechanical subproblem $\mathcal{X}^u$ and a thermal subproblem $\mathcal{X}^\vartheta$, such that

$$\mathcal{X} \;:\; \begin{cases} \mathcal{X}^u \;:\; \mathfrak{S}_t\,\mathfrak{u} = \overline{\mathfrak{S}}_u\,\mathfrak{u} =: \boldsymbol{f}_u(u\,,\vartheta)\,, \\ \mathcal{X}^\vartheta \;:\; \mathfrak{S}_t\,\mathfrak{u} = \overline{\mathfrak{S}}_\vartheta\,\mathfrak{u} =: \boldsymbol{f}_\vartheta(\vartheta\,,u)\,, \end{cases} \quad \text{with} \quad \boldsymbol{f}_u + \boldsymbol{f}_\vartheta = \boldsymbol{f}\,. \tag{4.80}$$

Then, starting from a completely known state of the system $\mathfrak{u}^n = [u^n\,,\vartheta^n]^T$ at time t^n, the time integration is performed in fractional steps, using the time integrators $\boldsymbol{\varphi}_u$ and $\boldsymbol{\varphi}_\vartheta$. Doing so, the process of updating reads

$$\mathfrak{u}^n \xrightarrow{\boldsymbol{\varphi}_{u,\Delta t}} \mathfrak{u}^* \xrightarrow{\boldsymbol{\varphi}_{\vartheta,\Delta t}} \mathfrak{u}^{n+1}\,, \tag{4.81}$$

wherein, $\mathfrak{u}^* = [u^*\,,\vartheta^*]^T$ represents the intermediate state of the system. Further particulars about this solution scheme and, as well, the isentropic operator-splitting method of Armero & Simo [4], which is also proposed for the problem of thermoelasticity, are presented in Section 6.1. Furthermore, the OSS designed by Markert *et al.* [190] for the volume-coupled problem of dynamic porous media, and also an example for decoupled treatment of a multi-rate problem via operator splitting are respectively investigated in Sections 6.2 and 6.3.

As it was seen, the decoupled solution methods provide new opportunities for solution of the coupled PDE systems. These opportunities bring some advantages, which have already been mentioned in the previous parts of this monograph. Nevertheless, using a decoupled solver introduces additional errors to the system that may cause conditional stability of the numerical results produced by the scheme. Consequently, stability analysis and establishing the stability condition become pertinent steps in proposing new decoupled solution strategies. These issues are addressed in the next chapter.

Chapter 5:
Stability Analysis

In this chapter, the notions related to the stability analysis of numerical schemes and the significance of those notions are explained. Special attention has been paid to look at the material from an application-related viewpoint, and also to demonstrate several examples in order to prevent abstraction. At the end, it is endeavoured to propose a stability analysis algorithm that incorporates the salient features of the previous works done in this area. The focus is on presenting the procedure such that the algorithm can be employed to find the critical grid sizes in different scenarios with minimum difficulty and without any need to solve the whole problem.

5.1 Preliminaries

Numerical schemes can solve continuous PDE systems only approximately. Therefore, the obtained numerical results deviate from the exact response, which could have been achieved via analytical solution of the original equations. Special care must be taken in order to keep this deviation within a limited range and, consequently, to make the proposed solution strategy acceptable. In this context, the *truncation error* (also known as the *discretisation error* [46]) of a computational scheme is one quantitative measure that gives an estimation about the proximity of the numerical solution to the analytical one. In order to introduce this concept, recall the abstract form of the mathematical model of a transient physical phenomenon presented by (3.63)

$$\mathcal{X} \;:\; \boldsymbol{\mathcal{F}}\left(\mathbf{u}(\mathbf{x}\,,t)\right) = \boldsymbol{\mathfrak{S}}\,\mathbf{u}(\mathbf{x}\,,t) - \mathbf{f}(\mathbf{x}\,,t) = \mathbf{0}\,, \qquad \forall\,\mathbf{x} \in \Omega \subset \mathbb{R}^d \quad \text{and} \quad t \in [t^0\,,T]\,. \tag{5.1}$$

Assume that the analytical solution vector corresponding to this problem is shown by $\mathbf{u}^a = \mathbf{u}^a(\mathbf{x}\,,t)$. Thus, $\mathbf{u}^a$ perfectly satisfies the given set of differential equations. Proceeding from a numerical solution of this problem, all the derivatives are replaced by differential quotients. This process transforms (5.1) to a system of coupled algebraic finite-difference equations (FDE). In this regard, considering the standard 3-d physical space ($d=3$) and assuming a constant and uniform grid in space and time, for each grid point at time $t^n = n\,\Delta t$ and position $\mathbf{x}_{jkl} = [j\,\Delta x_1\,, k\,\Delta x_2\,, l\,\Delta x_3]^T$, the FDE system corresponding to (5.1) reads in the abstract form

$$\boldsymbol{\mathfrak{D}}\,\mathbf{u}^n_{jkl} = \mathbf{f}(\mathbf{x}_{jkl}, t^n)\,. \tag{5.2}$$

Therein, $\boldsymbol{\mathfrak{D}}$ represents some discrete finite-difference operator approximating the continuous differential operator $\boldsymbol{\mathfrak{S}}$, and $\mathbf{u}^n_{jkl}$ is an approximation of $\mathbf{u}^a(\mathbf{x}_{jkl}, t^n)$ that has to be calculated via numerical computation. Thus, the *local truncation error* is defined as

$$\mathbf{T}^n_{jkl} := \boldsymbol{\mathfrak{D}}\,\mathbf{u}^a(\mathbf{x}_{jkl}, t^n) - \mathbf{f}(\mathbf{x}_{jkl}, t^n)\,. \tag{5.3}$$

Based on this, a FDE is said to be *consistent* with the PDE, if its local truncation error vanishes for grid sizes going to zero [72, 260], i. e.,

$$\lim_{\substack{\Delta t \to 0 \\ \Delta \mathbf{x} \to \mathbf{0}}} \mathbf{T}^n_{jkl} = \mathbf{0}\,. \tag{5.4}$$

Moreover, the difference between the numerical and the exact solutions of the system at $t = t^n$ and $\mathbf{x} = \mathbf{x}_{jkl}$ is known as the *global truncation error* [46]

$$E^n_{jkl} := |\mathbf{u}^n_{jkl} - \mathbf{u}^a(\mathbf{x}_{jkl}, t^n)|\,, \tag{5.5}$$

wherein, $|(\,\cdot\,)|$ denotes some vector norm on $\mathbb{R}^p$. Following that, a finite-difference scheme is *convergent* if

$$\lim_{\substack{\Delta t \to 0 \\ \Delta \mathbf{x} \to \mathbf{0}}} E^n_{jkl} = 0\,. \tag{5.6}$$

It is worth mentioning that despite the close relation between consistency and convergence, they are generally not equivalent, i. e., consistency of a scheme is just the necessary (and not the sufficient) condition for the convergence of the scheme [260]. Another criterion for making a finite-difference scheme acceptable is its stability.

5.2 Stability, contractivity and monotonicity

The adjective "stable" commonly means resistant to changes. However, to be able to study the stability of the numerical solution schemes, this concept must be interpreted in a mathematically sound way. To start off, we introduce the stable equilibrium of a dynamic system according to Lyapunov [182]. In this regard, a specific state of the system is called *the stable equilibrium state* $\mathbf{u}^*$, if

$$\begin{gathered} \forall \varepsilon > 0\,, \quad \exists\,\{\delta_\varepsilon\,, \tau_\varepsilon\} > 0 \quad \text{such that} \\ \text{if} \quad |\mathbf{u}^0 - \mathbf{u}^*| < \delta_\varepsilon \quad \text{then} \quad |\mathbf{u}^r - \mathbf{u}^*| < \varepsilon \quad \text{for} \quad t > \tau_\varepsilon\,. \end{gathered} \tag{5.7}$$

Therein, $\mathbf{u}^r = \mathbf{u}^r(\mathbf{x}, t)$ is the "real" (or measured) state of the system at time t, and $\mathbf{u}^0(\mathbf{x}) := \mathbf{u}^r(\mathbf{x}, t^0)$ represents the initial state. Note that this definition is based on the measured response $\mathbf{u}^r(\mathbf{x}\,, t)$ of the systems, and not on the analytical solution $\mathbf{u}^a(\mathbf{x}\,, t)$, or on the numerical solution $\mathbf{u}^n_{jkl}$ of the mathematical model of the physical phenomenon. It is, however, assumed that an admissible mathematical model proposed for a physical system in some sense resembles the actual behaviour of the system. In particular, we assume that the analytical solution $\mathbf{u}^a(\mathbf{x}\,, t)$ of the mathematical model of a physical system is such that the stability properties of the real response are preserved. Thus,

$$\mathbf{u}^a(\mathbf{x}\,, t) \approx \mathbf{u}^r(\mathbf{x}\,, t) \quad \forall \mathbf{x} \in \Omega \quad \text{and} \quad t \in [t^0\,, T]\,, \tag{5.8}$$

and (5.7) can be rewritten as

$$\begin{gathered} \forall \varepsilon > 0\,, \quad \exists\,\{\delta_\varepsilon\,, \tau_\varepsilon\} > 0 \quad \text{such that} \\ \text{if} \quad |\mathbf{u}^0 - \mathbf{u}^*| < \delta_\varepsilon \quad \text{then} \quad |\mathbf{u}^a - \mathbf{u}^*| < \varepsilon \quad \text{for} \quad t > \tau_\varepsilon\,. \end{gathered} \tag{5.9}$$

Satisfaction of this relation ascertains that after a specific time τ_ε, the dynamic system stays within a neighbourhood ε of the equilibrium state $\mathfrak{u}^*$ provided that the initial perturbation $\mathfrak{u}^0$ remains in a suitable neighbourhood δ_ε of the equilibrium state $\mathfrak{u}^*$.

Existence of a stable equilibrium state is the necessary, however, not the sufficient condition for having a stable physical system. More precisely, a physical system, which possesses a stable equilibrium state $\mathfrak{u}^*$ is considered *stable* provided that after time $t > \tau_C$, the state vector $\mathfrak{u}^a$ remains in a finite neighbourhood $C > 0$ of the equilibrium state $\mathfrak{u}^*$, i. e.,

$$\exists\, \tau_C > 0 \quad \text{such that} \quad |\mathfrak{u}^a - \mathfrak{u}^*| < C \quad \text{for} \quad t > \tau_C\,. \tag{5.10}$$

Seeing this relation in the light of (5.9), it becomes clear that satisfaction of (5.10) is merely a matter of choosing a suitable bound δ_C for the initial perturbation. In this regard, one can introduce the following region associated with δ_C:

$$\boldsymbol{\mathcal{M}}^C := \{\boldsymbol{\zeta} \in \mathbb{R}^p \,:\, |\boldsymbol{\zeta} - \mathfrak{u}^*| < \delta_C\}\,. \tag{5.11}$$

Thus, $\mathfrak{u}^0 \in \boldsymbol{\mathcal{M}}^C$ becomes the necessary and sufficient condition for satisfaction of (5.10). Moreover, considering the boundedness of the initial perturbation due to (5.11), and the response due to (5.10), one concludes

$$\exists\, \kappa_0 > 0 \quad \text{such that} \quad |\mathfrak{u}^a - \mathfrak{u}^*| \leq \kappa_0\, |\mathfrak{u}^0 - \mathfrak{u}^*| \quad \text{for} \quad t > \tau_C\,. \tag{5.12}$$

Therefore, for any two time instances t_1 and t_2 such that $t_2 > t_1 > \tau_C$, one may write

$$\exists\, \kappa_1 > 0 \quad \text{such that} \quad |\mathfrak{u}^a(\mathbf{x}\,, t_1 + \Delta t) - \mathfrak{u}^*| \leq \kappa_1\, |\mathfrak{u}^a(\mathbf{x}\,, t_1) - \mathfrak{u}^*|\,, \tag{5.13}$$

wherein $\Delta t := t_2 - t_1$. Hence, in a stable system, the deviation of the response $\mathfrak{u}^a$ from the stable equilibrium state $\mathfrak{u}^*$ remains bounded as the time passes. Nevertheless, (5.13) does not provide any information about the evolution of the distance. In this regard, a stable system in which the distance from the stable equilibrium state does not increase over time is called a *monotone system*. Considering (5.13), it becomes clear that in this case one has

$$0 < \kappa_1 \leq 1\,. \tag{5.14}$$

Thus, the response of a monotone system is such that

$$|\mathfrak{u}^a(\mathbf{x}\,, t_1 + \Delta t) - \mathfrak{u}^*| \leq |\mathfrak{u}^a(\mathbf{x}\,, t_1) - \mathfrak{u}^*| \quad \text{for} \quad t_1 > \tau_C\,. \tag{5.15}$$

Defining the stability of the systems as presented above also implies that the response of a stable system depends Lipschitz continuously on the data, as explained next. To make this point clear, consider two distinct initial conditions $\{\mathfrak{u}^0\,, \mathfrak{v}^0\} \in \boldsymbol{\mathcal{M}}^C$, and the corresponding responses of the system $\mathfrak{u}^a(\mathbf{x}, t)$ and $\mathfrak{v}^a(\mathbf{x}, t)$. Then, from (5.11) it can be shown that[1]

$$|\mathfrak{u}^0 - \mathfrak{v}^0| < 2\,\delta_C\,, \tag{5.16}$$

[1] Using the inequality rule

$$|\mathbf{a} - \mathbf{b}| \leq |\mathbf{a}| + |\mathbf{b}|\,, \quad \text{where} \quad \{\mathbf{a}\,, \mathbf{b}\} \in \mathbb{R}^p\,.$$

and, considering (5.10), one has

$$|\mathfrak{u}^a - \mathfrak{v}^a| < 2\,C \quad \text{for} \quad t > \tau_C\,. \tag{5.17}$$

Hence,

$$\exists\,\kappa_2 > 0 \quad \text{such that} \quad |\mathfrak{u}^a - \mathfrak{v}^a| \leq \kappa_2\,|\mathfrak{u}^0 - \mathfrak{v}^0| \quad \text{for} \quad t > \tau_C\,, \tag{5.18}$$

wherein, κ_2 is called the Lipschitz constant. Expressed in words, (5.18) means that for a stable system, a finite change in the initial conditions does not cause an infinite change in the obtained solution. In such a circumstance, one says that the response depends *Lipschitz continuously* on the data [72, 151].

Relation (5.17) also guarantees that the difference between the response vectors $\mathfrak{u}^a$ and $\mathfrak{v}^a$ at any time $t > \tau_C$ is bounded. Thus, considering two distinct time instances t_1 and t_2, such that $t_2 > t_1 > \tau_C$ and $\Delta t := t_2 - t_1 > 0$, one concludes that for a stable system

$$\begin{gathered}\exists\,\kappa_3 > 0\,, \quad \text{such that} \\ |\mathfrak{u}^a(\mathbf{x}, t_1 + \Delta t) - \mathfrak{v}^a(\mathbf{x}, t_1 + \Delta t)| \leq \kappa_3\,|\mathfrak{u}^a(\mathbf{x}, t_1) - \mathfrak{v}^a(\mathbf{x}, t_1)|\,.\end{gathered} \tag{5.19}$$

Thus, the difference between any two responses of a stable system for the same step size Δt remains bounded. Nevertheless, (5.19) does not provide any further information about growth or shrinkage of the difference between the response functions in the course of time. In this regard, a stable system for which the difference between the responses does not increase, i. e., the response is *contractive*, is called a *dissipative system*. Obviously, a stable system is dissipative, if the coefficient κ_3 in (5.19) is such that $0 < \kappa_3 \leq 1$. Therefore, a physical system is dissipative if

$$|\mathfrak{u}^a(\mathbf{x}, t_1 + \Delta t) - \mathfrak{v}^a(\mathbf{x}, t_1 + \Delta t)| \leq |\mathfrak{u}^a(\mathbf{x}, t_1) - \mathfrak{v}^a(\mathbf{x}, t_1)| \quad \text{for} \quad t_1 > \tau_C\,. \tag{5.20}$$

Remarks:

- From a physical viewpoint, it is clear that

$$\text{if} \quad \mathfrak{u}^0 = \mathfrak{u}^* \quad \text{then} \quad \mathfrak{u}^r = \mathfrak{u}^* \quad \text{and} \quad \mathfrak{u}^a = \mathfrak{u}^* \quad \text{for} \quad t > t^0\,. \tag{5.21}$$

  Hence, in conjunction with (5.15) and (5.20) it becomes clear that for a physically stable system, contractivity of the response yields its monotonicity. The converse is, however, not true.
- For the ease of notation and sake of brevity, one can choose the stable equilibrium state as the reference state, and t^0 as the reference time, such that $\mathfrak{u}^* \equiv \mathbf{0}$ and $t^0 = 0$. Furthermore, in the following, we demand that the stability, contractivity and monotonicity hold for the entire course of the experiment, i. e., $\forall t \in (0\,, T]$. Considering this, we set $\tau_C \equiv t^0 = 0$.

In contrast to the analytical solution schemes, numerical treatment of the mathematical models is not necessarily stability preserving. In this regard and in analogy to (5.10), the numerical solution $\mathfrak{u}^n_{jkl}$ generated by a specific scheme as a response to an initial disturbance $\mathfrak{u}^0 \in \boldsymbol{\mathcal{M}}^C$ is called stable, if

$$\exists\,C > 0 \quad \text{such that} \quad |\mathfrak{u}^n_{jkl}| < C \quad \text{for} \quad t^n \in (0\,, T]\,. \tag{5.22}$$

Then, considering the boundness of the initial perturbation $\mathfrak{u}^0$ and the vector of numerical solution $\mathfrak{u}^n_{jkl}$, one concludes

$$\exists\, \kappa_0 > 0 \quad \text{such that} \quad |\mathfrak{u}^n_{jkl}| < \kappa_0\, |\mathfrak{u}^0_{jkl}| \quad \text{for} \quad t^n \in (0\,, T]\,, \tag{5.23}$$

wherein,

$$\mathfrak{u}^0_{jkl} := \mathfrak{u}^0(\mathbf{x}_{jkl})\,. \tag{5.24}$$

Therefore, for any two instances of time t^n and t^{n+1} it holds

$$\exists\, \kappa_1 > 0 \quad \text{such that} \quad |\mathfrak{u}^{n+1}_{jkl}| \leq \kappa_1\, |\mathfrak{u}^n_{jkl}| \quad \text{for} \quad \{t^{n+1}\,, t^n\} \in (0\,, T]\,. \tag{5.25}$$

This is another interpretation of the boundness of the solution vectors produced by a stable numerical scheme, without any particular information about their growth or shrinkage. Strictly demanding that the norm of the solution vector does not grow in the course of the experiment then yields

$$0 < \kappa_1 \leq 1 \quad \rightarrow \quad |\mathfrak{u}^{n+1}_{jkl}| \leq |\mathfrak{u}^n_{jkl}| \quad \text{for} \quad \{t^{n+1}\,, t^n\} \in (0\,, T]\,. \tag{5.26}$$

In this regard, a stable numerical scheme is called a *monotone scheme*, if the solution vectors obtained from that satisfy (5.26).

Furthermore, from (5.23), one concludes that for two distinct solutions $\mathfrak{u}^n_{jkl}$ and $\mathfrak{v}^n_{jkl}$ produced by a stable scheme for two distinct initial perturbations $\{\mathfrak{u}^0\,, \mathfrak{v}^0\} \in \boldsymbol{\mathcal{M}}^C$, it holds

$$\exists\, \kappa_2 > 0 \quad \text{such that} \quad |\mathfrak{u}^n_{jkl} - \mathfrak{v}^n_{jkl}| \leq \kappa_2\, |\mathfrak{u}^0_{jkl} - \mathfrak{v}^0_{jkl}| \quad \text{for} \quad t^n \in (0\,, T]\,. \tag{5.27}$$

Hence, the response calculated by a stable numerical scheme depends Lipschitz continuously on the data. Thus,

$$\exists\, \kappa_3 > 0 \quad \text{such that} \quad |\mathfrak{u}^{n+1}_{jkl} - \mathfrak{v}^{n+1}_{jkl}| \leq \kappa_3\, |\mathfrak{u}^n_{jkl} - \mathfrak{v}^n_{jkl}| \quad \text{for} \quad \{t^{n+1}\,, t^n\} \in (0\,, T]\,. \tag{5.28}$$

Restricting the attention to the cases where the distance between distinct solutions does not increase as time passes, one finds

$$|\mathfrak{u}^{n+1}_{jkl} - \mathfrak{v}^{n+1}_{jkl}| \leq |\mathfrak{u}^n_{jkl} - \mathfrak{v}^n_{jkl}| \quad \text{for} \quad \{t^{n+1}\,, t^n\} \in (0\,, T]\,. \tag{5.29}$$

Obviously, this relation can be obtained assuming $0 < \kappa_3 \leq 1$ in (5.28). Subsequently, a stable numerical scheme, the produced solution vectors of which satisfy (5.29) is called a *contractive scheme*.

Remark: Considering (5.26) and (5.29), it is trivially clear that for a scheme which accepts $\mathfrak{u}^n_{jkl} = \mathbf{0}$ as a solution vector, contractivity of the scheme induces its monotonicity.

5.3 Stability notions

In the last section, we got familiar with the concepts of monotonicity, contractivity and stability of the analytical and the numerical solutions of a problem. Following this, various stability measures in the context of the numerical integration procedures are studied in the present section. The focus is on the one-step Runge-Kutta methods and the multistep backward differentiation formulae introduced in Section 4.1. Explanations regarding more general schemes can be found by Dekker & Verwer [64], Hairer *et al.* [131], Hairer & Wanner [132] and Süli & Mayers [262].

5.3.1 Absolute, A- and $A(\alpha)$-stability

The concept of absolute stability was originally proposed in relation with a numerical method applied to a scalar, linear, autonomous equation [140, 168]:

$$\dot{\mathfrak{u}}(t) = \lambda\,\mathfrak{u}(t)\,, \quad \lambda \in \mathbb{C}\,, \quad t \geq 0\,, \quad \mathfrak{u}(0) = \mathfrak{u}^0\,. \tag{5.30}$$

This is the Dahlquist's test problem with the analytical solution

$$\mathfrak{u}^a(t) = \mathfrak{u}^0\, e^{\lambda\, t} = \mathfrak{u}^0\, e^{\Re(\lambda)\, t}\, \{\cos[\Im(\lambda)\, t] + I\, \sin[\Im(\lambda)\, t]\} \quad \text{with} \quad I := \sqrt{-1}\,. \tag{5.31}$$

Apparently, the real and imaginary parts of the coefficient λ play different roles in the evolution of the solution function $\mathfrak{u}^a(t)$. In particular, $\Im(\lambda)$ determines the phase and $\Re(\lambda)$ specifies the norm of the solution. More precisely, depending on $\Re(\lambda)$, the norm of the analytical solution $\mathfrak{u}^a$ may decrease, increase or remain constant, such that a non-increasing solution is achieved only if $\Re(\lambda) \leq 0$. This statement, in the light of the nomenclature introduced in the Section 5.2, means that for $\Re(\lambda) \leq 0$, the analytical solution of (5.30) becomes monotone, such that

$$|\mathfrak{u}^a(t + \Delta t)| \leq |\mathfrak{u}^a(t)|\,, \quad \text{for} \quad t > 0\,. \tag{5.32}$$

It should, however, be noted that for a homogeneous and linear problem in the form of (5.30), the concepts of monotonicity and contractivity of the analytical solution $\mathfrak{u}^a$ are identical. This is due to the fact that for such an equation, the difference of any two solutions is a solution, too.

By employing a numerical integration method, one naturally wishes that the resulted numerical solutions of (5.30) replicate the behaviour of the analytical one. In particular, having a monotone problem, i. e., $\Re(\lambda) \leq 0$, it is desired that the produced solutions be monotone too, such that

$$|\mathfrak{u}^{n+1}| \leq |\mathfrak{u}^n|\,. \tag{5.33}$$

To investigate this condition, the relation between the produced solutions in consecutive steps has to be established. In this regard, provided that there exists an *amplification function* $G(z)$ such that

$$\mathfrak{u}^{n+1} = G(z)\,\mathfrak{u}^n \quad \text{with} \qquad z := \Delta t\,\lambda\,, \tag{5.34}$$

one concludes

$$|\mathfrak{u}^{n+1}| \leq |\mathfrak{u}^n| \quad \text{if and only if} \quad |G(z)| \leq 1\,. \tag{5.35}$$

Thus, the question of contractivity of the results produced by a numerical method boils down to determine whether the corresponding amplification function satisfies $(5.35)_2$. Assuming that this is the case, the method is called absolutely stable:

Absolute stability
A method is called *absolutely stable* at $z \in \mathbb{C}$, if for this specific z, the amplification function $G(z)$ satisfies $(5.35)_2$.

(5.36)

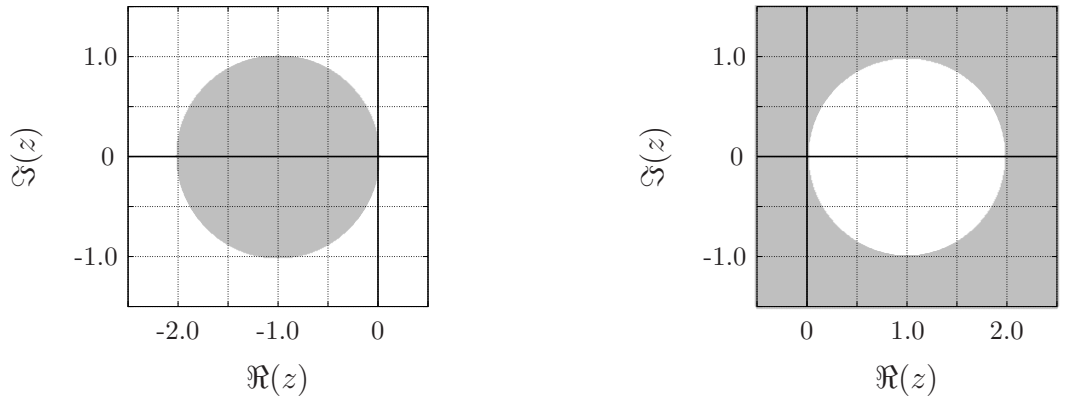

Figure 5.1: *Shaded areas show the stability regions* S *of the EEM (left) and the IEM (right).*

In this conjunction, one defines the *absolute stability region* S to be the location of all z, at which the method becomes absolutely stable, such that

$$\mathsf{S} := \{z \in \mathbb{C} \,:\, |G(z)| \leq 1\}\,. \tag{5.37}$$

It can be seen that determining the stability region of a scheme provides useful information about the behaviour of the produced numerical results. To this end, one has to build the amplification function and analyse its behaviour in response to different values of $z = \lambda\,\Delta t$. For example, applying the explicit (forward) Euler (EEM) method for discretisation of (5.30) yields

$$\frac{\mathfrak{u}^{n+1} - \mathfrak{u}^n}{\Delta t} = \lambda\,\mathfrak{u}^n \quad \rightarrow \quad \mathfrak{u}^{n+1} = (1 + \lambda\,\Delta t)\,\mathfrak{u}^n\,. \tag{5.38}$$

Thus, the amplification function $G(z)$ and the stability region S for this case are given as

$$G(z) := (1 + z) \quad \rightarrow \quad \mathsf{S} = \{z \in \mathbb{C} \,:\, [1 + \Re(z)]^2 + \Im(z)^2 \leq 1\}\,. \tag{5.39}$$

Therein, $\Re(z) := \Delta t\,\Re(\lambda)$ and $\Im(z) := \Delta t\,\Im(\lambda)$. Therefore, the stability region of the explicit Euler method is the interior of a circle of radius $r = 1$, and centred at $\Re(z) = -1$ and $\Im(z) = 0$, see Figure 5.1. Hence, one concludes that the scheme would generate contractive results as long as the coefficient λ and the time-step size Δt are such that $z \in \mathsf{S}$. It determines the particular conditions under which the method becomes absolutely stable. These conditions are usually known as the *stability condition* of the scheme.

The stability condition of a scheme is usually interpreted in the form of an inequality relation that specifies a limit for the presented discretisation parameter, here Δt. Considering this, and proceeding from the common assumption $\Delta t \in \mathbb{R}^+$, the stability condition for the explicit Euler method when applied on (5.30) can be found from $(5.39)_2$, and reads

$$\Delta t \leq -2\,\frac{\Re(\lambda)}{|\lambda|^2}\,. \tag{5.40}$$

From this relation, one immediately concludes that the EEM would generate contractive results only if the step size is such that (5.40) is satisfied. In this regard, a method with such a restricting stability condition is known as a *conditionally stable* method. It

should be noted that, in general, every explicit numerical methods is conditionally stable [39, 131].

Having the "conditionally stable" methods introduced, it makes perfect sense to proceed to the introduction of the so-called "unconditionally stable" integration schemes. In this regard, a method is called *unconditionally stable*, if, when applied to a dissipative problem, it always produces contractive results, independent of the size of the discretisation parameter, such that

$$\forall \lambda \in \mathbb{C} \quad \text{with} \quad \Re(\lambda) \leq 0 \quad \text{and} \quad \forall \Delta t \in \mathbb{R}^+ , \quad |G(z)| \leq 1 \, . \tag{5.41}$$

Relating the above discussion to the concept of a stability region, and keeping in mind that

$$\text{if} \quad \Delta t \in \mathbb{R}^+ \quad \text{then} \quad \Re(\lambda) \leq 0 \quad \leftrightarrow \quad \Re(z) \leq 0 \tag{5.42}$$

leads to the definition of A-stable schemes, firstly proposed by Dahlquist [60, 61]:

A-stability

An *A-stable scheme* is one with an absolute stability region S which covers the whole negative half-plane, such that

$$\mathsf{S} \supset \mathbb{C}^- := \{ z \in \mathbb{C} \, : \, \Re(z) \leq 0 \} \, . \tag{5.43}$$

Therefore, exploiting an A-stable method for numerical integration of a dissipative problem in the form of (5.30) always yields contractive numerical results, independent of the time-step size Δt. In this case, sometimes the amplification function $G(z)$ is also called A-stable or A-acceptable [75, 132].

The condition of A-stability is obviously a desirable property that is, for example, inherent to the family of implicit Runge-Kutta (IRK) methods [7, 75]. For instance, employing the implicit (backward) Euler method (IEM), which is an implicit one-stage RK method, for discretisation of (5.30) yields

$$\frac{\mathfrak{u}^{n+1} - \mathfrak{u}^n}{\Delta t} = \lambda \, \mathfrak{u}^{n+1} \quad \rightarrow \quad \mathfrak{u}^{n+1} = \frac{1}{1 - \lambda \, \Delta t} \, \mathfrak{u}^n \, . \tag{5.44}$$

From that, the amplification function apparently reads

$$G(z) = \frac{1}{1 - z} \, , \tag{5.45}$$

wherein, as before

$$z := \lambda \, \Delta t = \underbrace{\Delta t \, \Re(\lambda)}_{=: \Re(z)} + \underbrace{\Delta t \, \Im(\lambda)}_{=: \Im(z)} \, i \, . \tag{5.46}$$

Thus,

$$|G(z)| \leq 1 \quad \rightarrow \quad \mathsf{S} = \{ z \in \mathbb{C} \, : \, [1 - \Re(z)]^2 + \Im(z)^2 \geq 1 \} \, . \tag{5.47}$$

Hence, the stability region S for the implicit Euler method would be the exterior of a circle with radius $r = 1$, and centred at $\Re(z) = 1$ and $\Im(z) = 0$, see Figure 5.1. Therefore, $\mathsf{S} \supset \mathbb{C}^-$ and, hence, the implicit Euler method is A-stable.

Remark: The amplification function of an s-stage RK method (4.2) in the most general form reads [242, 257]

$$G(z) = \frac{\det(\mathbf{I} - z\,\mathbf{A} + z\,\mathbf{1}\,\mathbf{b}^T)}{\det(\mathbf{I} - z\,\mathbf{A})}\,. \tag{5.48}$$

Therein, $\mathbf{I}$ is the $s \times s$ identity matrix and $\mathbf{1} := [1\,, \cdots, 1]^T$.

The A-stability of the IRK schemes, however, comes at a price. In particular, employing these procedures for time integration of equation systems, proves to be very expensive. This is due to the fact that, for a system of m differential equations, an s-stage implicit Runge-Kutta method requires simultaneous solution of $s\,m$ equations. In this regard, using other variations of the IRK methods could somewhat reduce the computational effort. These are, for example, the diagonally implicit RK (DIRK) methods firstly introduced by Nørsett [206], the singly diagonal implicit RK (SDIRK) methods of Hairer *et al.* [131], and the singly implicit RK (SIRK) methods proposed by Burrage [38].

Using the so-called $A(\alpha)$-stable integration methods is another alternative for achieving contractive numerical solutions, when applied to dissipative problems with $\Re(\lambda) \leq 0$. In this regard, the $A(\alpha)$-stability is defined as follows:

$A(\alpha)$-stability

A method is said to be $A(\alpha)$-*stable* in the sense of Widlund [281], if its stability region S is such that

$$\mathsf{S} \supset \mathsf{S}_\alpha := \{z \in \mathbb{C} \,:\, |\arg(-z)| < \alpha\,, z \neq 0\}\,,$$

wherein, $\arg(\,\cdot\,) := \tan^{-1}\left(\Im(\,\cdot\,)/\Re(\,\cdot\,)\right)$. (5.49)

Thus, in contrast to the A-stable schemes, the stability region of an $A(\alpha)$-stable method covers only a sector of (and not the whole) left half-plane, see Figure 5.2. Nevertheless, and due to the fact that the stability region S includes the whole negative real axis, the numerical results produced by an $A(\alpha)$-stable scheme when applied to a dissipative problem would be contractive. Such a stability property can be seen, for example, in the backward differentiation formulae (BDF) introduced in Section 4.1. It is worth mentioning that, employing a BDF scheme for solution of a system of m differential equations requires the simultaneous solution of only m nonlinear equations per time step, that is a big advantage when compared to the IRK methods.

In order to find the region of absolute stability S of a BDF method (4.6), one firstly has to apply that method to the Dahlquist's test problem (5.30). It yields

$$\sum_{i=0}^{k} \alpha_i\,\mathfrak{u}^{n+i} = \beta_k\,\underbrace{\Delta t\,\lambda}_{=:z}\,\mathfrak{u}^{n+k}\,. \tag{5.50}$$

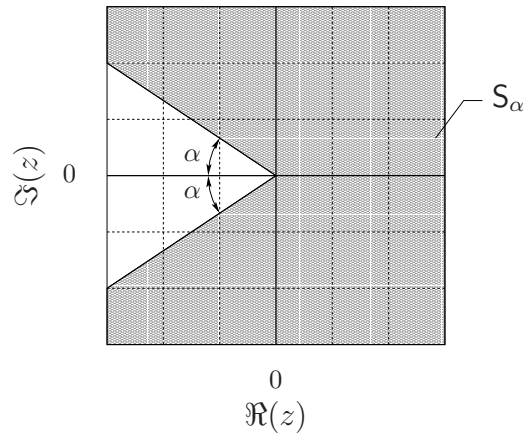

Figure 5.2: *Illustration of the region* S_α.

Bringing the RHS of the equation to the LHS, the above relation takes the form

$$\sum_{i=0}^{k-1} \alpha_i \, \mathfrak{u}^{n+i} + (\alpha_k - z\,\beta_k)\, \mathfrak{u}^{n+k} = 0\,. \tag{5.51}$$

This is a homogeneous, linear difference equation of order k, with solutions of the form

$$\mathfrak{u}^{(\bullet)} = \zeta^{(\bullet)}\,, \tag{5.52}$$

where $\zeta \in \mathbb{C}$ and $\zeta \neq 0$ (see [167], Theorem 2.4.1)[2]. Substituting (5.52) in (5.51) and dividing by ζ^n, one arrives at

$$\sum_{i=0}^{k-1} \alpha_i \, \zeta^i + (\alpha_k - z\,\beta_k)\, \zeta^k = 0\,. \tag{5.53}$$

This is called the *characteristic equation* of the difference equation (5.51). Apparently, the characteristic equation is a polynomial of order k with k roots $\zeta_j = \zeta_j(z)$. Following this, the absolute stability region S of a BDF method is defined as follows [132]:

$$\mathsf{S} = \left\{ z \in \mathbb{C} : \begin{array}{l} \text{all roots satisfy } |\zeta_j(z)| \leq 1, \\ \text{multiply roots satisfy } |\zeta_j(z)| < 1. \end{array} \right\}. \tag{5.54}$$

Going through the above procedure, the absolute stability regions of the BDF methods (4.7) appear to be as presented in Figure 5.3. It can be seen that for the BDF schemes of order 3 and higher, the region of absolute stability includes only a sector of the negative half-plane. However, it always certainly includes the negative real axis. Thus, those BDF schemes, the stability region of which includes only a sector of the negative half-plane, belong to the class of the $A(\alpha)$-stable integration methods.

[2]Note that in this context, $\mathfrak{u}^n$ represents the numerical solution at time $t = t^n$, whereas ζ^n denotes ζ to the power of n.

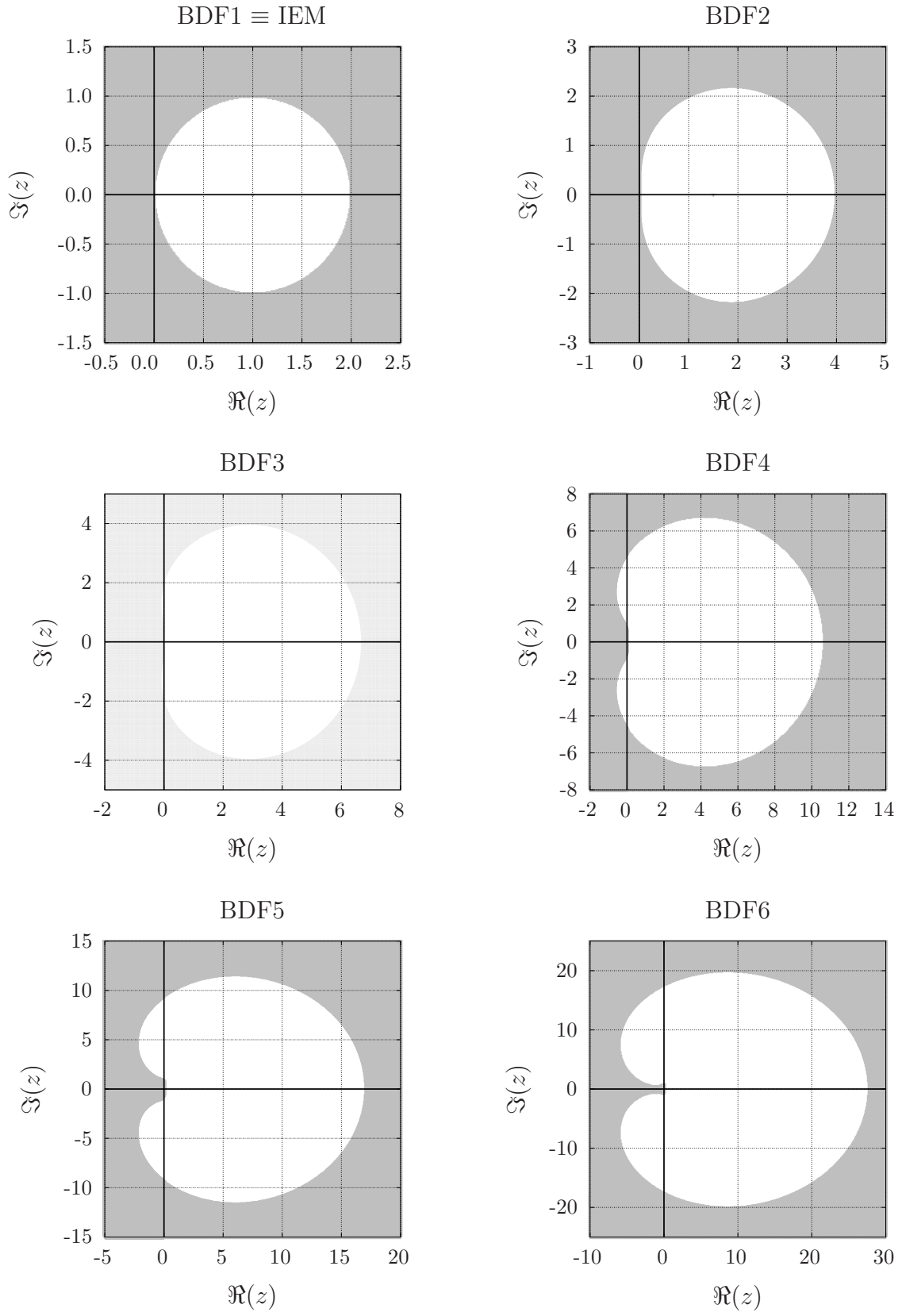

Figure 5.3: *Shaded areas show the stability regions of the BDFk methods,* $1 \leq k \leq 6$.

5.3.2 L-stability

As stated in the last section, explicit methods are only conditionally stable, such that these schemes generate stable results only if $z = \lambda\,\Delta t$ lies in a bounded neighbourhood of the imaginary axis. Hence, applying an explicit scheme to a stiff problem with $\Re(\lambda) \ll 0$ imposes a strong restriction to the time-step size Δt, which leads to inefficiency, cf. Section 3.4.2, where the notion of stiff problems is introduced. This is the main reason why using the explicit methods for time integration of the stiff problems is usually ruled out. Instead, employing an A-stable scheme, for instance a member of the family of the IRK methods, yields an amplification function $G(z)$, which always satisfies $|G(z)| \leq 1$ and, thus, generates stable results, independent of the degree of stiffness.

Obtaining stable results is, however, just a partial solution for time integration of the stiff problems. Apart from that, the behaviour of the amplification function must be such that increasing the stiffness causes the computed results to vanish faster. In particular, applying the method to an "infinitely" stiff problem, one expects that the numerical result vanishes after "one" step of time integration. This idea leads to the definition of the L-stable schemes, firstly proposed by Ehle [76]:

L-stability

A method is called *L-stable* (left-stable) if it is A-stable and if in addition

$$\lim_{z\to-\infty} G(z) = 0\,. \tag{5.55}$$

Employing a method that is A-, but not L-stable, for time integration of stiff problems leads to undesired behaviour of the numerical results. To demonstrate this phenomenon, consider the trapezoidal rule (TR), which is an IRK method. Applying to (5.30), one obtains

$$\mathfrak{u}^{n+1} = \mathfrak{u}^n + \frac{\Delta t}{2}\,(\lambda\,\mathfrak{u}^n + \lambda\,\mathfrak{u}^{n+1}) \quad \rightarrow \quad \mathfrak{u}^{n+1} = \frac{1+\Delta t\,\lambda/2}{1-\Delta t\,\lambda/2}\,\mathfrak{u}^n =: \frac{1+z/2}{1-z/2}\,\mathfrak{u}^n\,. \tag{5.56}$$

Thus, the amplification function for the TR reads

$$G(z) = \frac{1+z/2}{1-z/2}\,. \tag{5.57}$$

Plotting the region of absolute stability S for this scheme proves that $\mathsf{S} \supset \mathbb{C}^-$ and, hence, the TR is A-stable, see Figure 5.4. Nevertheless, examining the behaviour of the $G(z)$ for $z \to -\infty$, one obtains

$$\lim_{z\to-\infty} G(z) = -1\,. \tag{5.58}$$

Hence, the TR is A-, but not L-stable. In particular, this relation shows that, for very stiff problems, i. e., for extreme values of z, the amplification function approaches -1. Consequently, using the TR for temporal integration in such a circumstance primarily yields a change of sign but very small changes in the modulus from $\mathfrak{u}^n$ to $\mathfrak{u}^{n+1}$ and, thus,

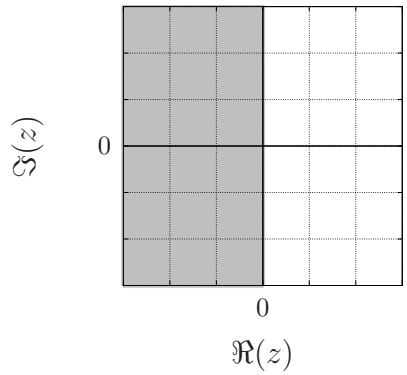

Figure 5.4: *Shaded area shows the region of absolute stability* S *for the TR.*

oscillations around the exact solution. In contrast, recalling the amplification function of the implicit Euler (IE) method (5.46), one concludes that this procedure is L-stable.

Remark: From the Dahlquist's second barrier [60], it follows that no linear multistep method of order greater than 2 is A-stable. Thus, the BDF methods of order 3 and higher cannot be A-stable, nor strictly speaking L-stable. However, the BDF2 method is L-stable [9].

5.3.3 Further stability measures

The above-mentioned stability notions were introduced in conjunction with a "linear" and "autonomous" test problem (5.30). For the sake of completeness, more general forms of evolution equations (nonlinear, nonautonomous) and their corresponding stability measures will be introduced, and the relation between these types of stabilities will be briefly presented. A detailed scrutinisation of these concepts is beyond the scope of this work. Comprehensive discussions can be found in [39, 64, 132] and the references therein.

AN-stability

The concept of AN-stability has been firstly introduced by Burrage & Butcher [40], in conjunction with the following problem:

$$\dot{\mathfrak{u}}(t) = \lambda(t)\,\mathfrak{u}(t)\,, \quad \lambda(t) \in \mathbb{C}\,, \quad t \geq 0\,, \quad \mathfrak{u}(0) = \mathfrak{u}^0\,. \tag{5.59}$$

It is the "nonautonomous" version of the test problem (5.30), which for $\Re(\lambda(t)) \leq 0$ becomes dissipative and, thus, the analytical solution of this problem becomes contractive and monotone, cf. the explanations beneath (5.32). Then, the property of AN-stability reads:

AN-stability
A RK method is *AN-stable* if, when applied to the nonautonomous, linear problem (5.59), it generates monotone results in the sense of (5.33).

(5.60)

Note that, for any RK method, AN-stability of the scheme invokes its A-stability [64].

B-stability

To introduce this property, consider the following equation:

$$\dot{\mathbf{u}}(t) = \boldsymbol{f}(\mathbf{u}(t))\,, \quad t \geq 0\,, \quad \mathbf{u}(0) = \mathbf{u}^0\,. \tag{5.61}$$

This relation represents an "autonomous" system of evolution equations which, depending on the structure of $\boldsymbol{f} : \mathbb{R}^p \to \mathbb{R}^p$, can be linear or nonlinear. Such a system is dissipative if [43]

$$< \boldsymbol{f}(\boldsymbol{\zeta}_1) - \boldsymbol{f}(\boldsymbol{\zeta}_2)\,, \boldsymbol{\zeta}_1 - \boldsymbol{\zeta}_2 > \leq 0\,, \quad \forall\, \boldsymbol{\zeta}_1\,, \boldsymbol{\zeta}_2 \in \mathbb{R}^p\,, \tag{5.62}$$

wherein, $< (\cdot)\,, (\cdot) >$ represents an inner product on $\mathbb{R}^p$ with $|(\cdot)|$ the corresponding vector norm, such that $|(\cdot)|^2 =< (\cdot)\,, (\cdot) >$. In this case, the exact solutions of the system are contractive in the sense of (5.20). Inspired by this class of problems, Butcher [43] introduced the concept of B-stability for the RK methods:

B-stability

A RK method is *B-stable* if, for all autonomous and dissipative problems, the scheme produces contractive results, such that

$$|\mathbf{u}^{n+1} - \mathbf{v}^{n+1}| \leq |\mathbf{u}^n - \mathbf{v}^n| \qquad \text{for} \quad 0 < t^n < t^{n+1}\,.$$

Therein, $\mathbf{u}^n$ and $\mathbf{v}^n$ are the numerical results produced by the scheme at time $t = t^n$ in response to the initial perturbations $\mathbf{u}^0$ and $\mathbf{v}^0$, respectively. (5.63)

Note that B-stability of a RK method implies both A- and AN-stability [132].

BN-stability

The above discussion has been later extended by Burrage & Butcher [40] to the general, "nonautonomous" problems in form of

$$\dot{\mathbf{u}}(t) = \boldsymbol{f}(\mathbf{u}(t), t)\,, \quad t \geq 0\,, \quad \mathbf{u}(0) = \mathbf{u}^0\,. \tag{5.64}$$

In this case, the problem would be dissipative if [40, 64]

$$< \boldsymbol{f}(\boldsymbol{\zeta}_1\,, t) - \boldsymbol{f}(\boldsymbol{\zeta}_2\,, t)\,, \boldsymbol{\zeta}_1 - \boldsymbol{\zeta}_2 > \leq 0\,, \quad \forall\, \boldsymbol{\zeta}_1\,, \boldsymbol{\zeta}_2 \in \mathbb{R}^p \quad \text{and} \quad t \geq 0\,. \tag{5.65}$$

This extension leads to the definition of the BN-stable RK methods [40]:

BN-stability

A RK method is *BN-stable* if, for all nonautonomous and dissipative problems, the scheme produces contractive results in the sense of (5.63). (5.66)

It should be noted that the property of BN-stability induces B-stability [64].

Algebraic stability

In an attempt to find a simpler alternative for the somewhat complex criteria needed for obtaining B-stability, Burrage & Butcher [40] and Crouzeix [58] introduced the concept of algebraic stability, as follows:

Algebraic stability

A RK method is *algebraically stable*, if its corresponding matrices

$$\mathbf{B} := \mathrm{diag}(b_1\,,\cdots,b_s) \quad \text{and} \quad \mathbf{M} := \mathbf{B}\,\mathbf{A} + \mathbf{A}^T\,\mathbf{B} - \mathbf{b}\,\mathbf{b}^T \tag{5.67}$$

are both non-negative definite.

Satisfaction of this *algebraic* condition is sufficient for a method to become not only B-, but also BN- and AN-stable, hence the name of this property.

Possessing the above-mentioned stability properties by a time integrator guarantees unconditional contractivity of the numerical solutions, when applied to a dissipative problem. There exist, however, circumstances, where to achieve unconditional stability is not trivial. For instance, using an explicit time integrator, as was already said, always leads to conditional stability. Furthermore, decoupling of the equations may also destroy the dissipativity of the problem and, consequently, cause conditional stability. Thus, the design of new decoupled solution algorithms must always be accompanied by an exhaustive stability analysis. Considering the coupled PDE systems, the stability analysis could readily be performed using the method of von Neumann, as explained in detail in the next section.

Remarks:

- In conclusion, for every RK method it holds
  Algebraic stability $\rightarrow$ BN-stability $\rightarrow$ B-stability $\rightarrow$ AN-stability $\rightarrow$ A-stability.
- A RK process (4.2) is nonconfluent if $c_1\,,c_2\,,\cdots,c_s$ are distinct. For nonconfluent RK methods the concepts of AN-, BN- and algebraic stability become equivalent ([64], Theorem 4.3.8).

5.4 von Neumann stability analysis

Recalling (5.23), the results obtained from the numerical solution of a PDE system is stable if

$$\exists\,\kappa_0 > 0 \quad \text{such that} \quad |\mathfrak{u}^n_{jkl}| < \kappa_0\,|\mathfrak{u}^0_{jkl}| \quad \text{for} \quad t^n \in (0\,,T]\,, \tag{5.68}$$

wherein,

$$\mathfrak{u}^0_{jkl} := \mathfrak{u}^0(\mathbf{x}_{jkl})\,. \tag{5.69}$$

To establish the condition under which this relation holds, i. e., the stability condition, is the central point of interest in the stability analysis of numerical solution methods, and now turns to the primary concern in what follows.

5.4.1 The stability criterion

Considering the Parseval's identity [260, 263], an equivalent form of (5.68) reads

$$\exists\, \kappa_0 > 0 \quad \text{such that} \quad |\hat{\mathbf{u}}^n| < \kappa_0\, |\hat{\mathbf{u}}^0| \quad \text{for} \quad t^n \in (0\,, T]\,, \tag{5.70}$$

where $\hat{\mathbf{u}}^n$ and $\hat{\mathbf{u}}^0$ are the Fourier transforms of $\mathbf{u}^n_{jkl}$ and $\mathbf{u}^0_{jkl}$, respectively. Moreover, from the inverse Fourier transform, one has

$$\mathbf{u}^n_{jkl} = \frac{1}{\sqrt{2\pi}} \int_{-\pi/\Delta x_1}^{\pi/\Delta x_1} \int_{-\pi/\Delta x_2}^{\pi/\Delta x_2} \int_{-\pi/\Delta x_3}^{\pi/\Delta x_3} e^{I\,(j+k+l)\Theta}\, \hat{\mathbf{u}}^n\,(\xi_1, \xi_2, \xi_3)\, \mathrm{d}\xi_3\, \mathrm{d}\xi_2\, \mathrm{d}\xi_1 \tag{5.71}$$

with $I := \sqrt{-1}$, $\Theta \in [-\pi, \pi]$ and $\xi_a := \Theta/\Delta x_a$ for $a = \{1, 2, 3\}$. Then, for a linear homogeneous problem, following the procedure proposed by Charney *et al.* [48] and replacing (5.71) in (5.2), one obtains

$$\hat{\mathbf{u}}^{n+1} = \mathbf{G}(\Delta t, \Delta \mathbf{x})\, \hat{\mathbf{u}}^n \quad \rightarrow \quad \hat{\mathbf{u}}^n = [\mathbf{G}(\Delta t, \Delta \mathbf{x})]^n\, \hat{\mathbf{u}}^0, \quad \text{where} \quad 0 \leq n \leq \frac{T}{\Delta t}\,. \tag{5.72}$$

Therein, $\mathbf{G}(\Delta t, \Delta \mathbf{x}) \in \mathbb{C}^{p \times p}$ is called the *amplification matrix*. Comparing (5.72) and (5.70), the stability requirement is obviously related to the boundness of $[\mathbf{G}(\Delta t, \Delta \mathbf{x})]^n$. It means, the numerical scheme is stable if and only if

$$\exists\ \kappa_8 > 0 \quad \text{such that} \quad \| \, [\mathbf{G}(\Delta t, \Delta \mathbf{x})]^n \, \| \leq \kappa_8 \quad \text{for} \quad 0 \leq n \leq \frac{T}{\Delta t}\,. \tag{5.73}$$

Therein, $\|(\,\cdot\,)\|$ represents the *natural* or *induced matrix norm*, which for an exemplary matrix $\mathbf{A} \in \mathbb{C}^{m \times m}$ is defined as

$$\|\mathbf{A}\| := \sup_{|\mathbf{v}|=1} |\mathbf{A}\,\mathbf{v}|\,, \qquad \text{where} \quad \mathbf{v} \in \mathbb{R}^m \quad \text{and} \quad |\mathbf{v}| := \left(\sum_{i=1}^{m} v_i^2 \right)^{1/2}. \tag{5.74}$$

The spectral radius $\varrho := \varrho(\mathbf{G})$ of the amplification matrix is defined as $\max|\gamma_i|$, where γ_i are the eigenvalues of the amplification matrix $\mathbf{G}$. Then, it can be shown that [230]

$$\varrho^n \leq \| \, [\mathbf{G}(\Delta t, \Delta \mathbf{x})]^n \, \|\,. \tag{5.75}$$

Comparing (5.73) and (5.75), it is obvious that a necessary condition for the boundness of $\mathbf{G}^n$ is to have a real constant $\kappa_9 \in \mathbb{R}$ such that $\varrho^n \leq \kappa_9$. Then, assuming $\kappa_9 \geq 1$, one concludes

$$\varrho \leq \kappa_9^{1/n} \quad \xrightarrow{\forall\, n \in [0, T/\Delta t]} \quad \varrho \overset{!}{\leq} \kappa_9^{\Delta t/T} \approx 1 + \mathcal{O}(\Delta t)\,, \tag{5.76}$$

which is known as the von Neumann stability criterion [230]. Accordingly, $\varrho < 1$ is a sufficient condition to satisfy $(5.76)_2$ and to guarantee the boundness of the spectral radius.

Remark: It is shown by Varga [272] that $\varrho < 1$ yields

$$\lim_{n \to \infty} \|\mathbf{G}^n\| = 0 \quad \rightarrow \quad \lim_{n \to \infty} |\hat{\mathbf{u}}^n| = 0 \quad \rightarrow \quad \lim_{n \to \infty} |\mathbf{u}^n_{jkl}| = 0\,. \tag{5.77}$$

Considering the assumption $\mathbf{u}^* \equiv \mathbf{0}$, the above implies asymptotic stability of the numerical results [15].

Having a normal amplification matrix, i. e., if $\mathbf{G}$ commutes with its Hermitian conjugate, one has [64]

$$\|\mathbf{G}(\Delta t\,, \Delta \mathbf{x})\| = \varrho\,. \tag{5.78}$$

Thus,

$$\varrho < 1 \quad \rightarrow \quad \|\mathbf{G}(\Delta t\,, \Delta \mathbf{x})\| < 1 \quad \rightarrow \quad |\hat{\mathbf{u}}^{n+1}| < |\hat{\mathbf{u}}^{n}| \quad \rightarrow \quad |\mathbf{u}^{n+1}_{jkl}| < |\mathbf{u}^{n}_{jkl}|\,, \tag{5.79}$$

which guarantees the monotonicity of the numerical solution. Moreover, from (5.78) one concludes

$$\|\mathbf{G}(\Delta t\,, \Delta \mathbf{x})\|^n = \varrho^n\,. \tag{5.80}$$

Hence, having a normal amplification matrix, satisfaction of the von Neumann stability criterion becomes a necessary and sufficient stability condition in the sense of (5.68). This is always the case for problems with just one state variable, but for more general cases with several state variables, the amplification matrix is usually not normal, yielding only a necessary but not sufficient stability condition [230].

5.4.2 A pragmatic algorithm for stability analysis

The eigenvalues of a matrix can be found via determining the roots of the matrix's characteristic equation. Considering the amplification matrix $\mathbf{G}$, we call its characteristic equation the *amplification polynomial* $G_A(\gamma)$ and the eigenvalues can be found via solving the following equation

$$G_A(\gamma) := \det\left(\mathbf{G} - \gamma\,\mathbf{I}\right) = \alpha_0 + \alpha_1\,\gamma + \cdots + \alpha_{n-1}\,\gamma^{n-1} + \alpha_n\,\gamma^n = 0. \tag{5.81}$$

Therein, $\mathbf{I}$ is the $p \times p$ identity matrix and $\alpha_i \in \mathbb{C}$. Thus, an equivalent interpretation for the von Neumann stability criterion (5.76) reads

$$|\gamma_i| \overset{!}{\leq} 1 \quad \text{with} \quad \gamma_i : \; i\text{-th root of } G_A(\gamma) = 0\,. \tag{5.82}$$

Our aim is to determine the conditions under which (5.82) is satisfied without explicit computation of the roots. In this regard, we firstly introduce the following definitions:

Inners of a matrix (5.83)

The *inners* of a square matrix are the matrix itself and all the matrices obtained by omitting successively the first and last rows and the first and last columns [87].

Positive innerwise matrix (5.84)

A matrix is called *positive innerwise* if the determinants of all of its inners are positive [153].

Schur-Cohn matrix

Having the amplification polynomial $G_A(\gamma)$ as an algebraic polynomial of order $n \geq 1$ with $\alpha_i \in \mathbb{C}$, *the Schur-Cohn matrix* $\mathbf{D}$ reads

$$\mathbf{D} := \begin{bmatrix} \alpha_n & \alpha_{n-1} & \cdots & \alpha_2 & \alpha_1 & 0 & 0 & \cdots & & \alpha_0 \\ 0 & \ddots & & & \vdots & & & & & \vdots \\ \vdots & & \alpha_n & \alpha_{n-1} & \alpha_{n-2} & 0 & 0 & \alpha_0 & & \cdot \\ \cdot & & 0 & \alpha_n & \alpha_{n-1} & 0 & \alpha_0 & \alpha_1 & & \cdot \\ \cdot & & 0 & 0 & \alpha_n & \alpha_0 & \alpha_1 & \alpha_2 & & \cdot \\ \cdot & & 0 & 0 & \bar{\alpha}_0 & \bar{\alpha}_n & \bar{\alpha}_{n-1} & \bar{\alpha}_{n-2} & & \cdot \\ \cdot & & 0 & \bar{\alpha}_0 & \bar{\alpha}_1 & 0 & \bar{\alpha}_n & \bar{\alpha}_{n-1} & & \cdot \\ \vdots & & \bar{\alpha}_0 & \bar{\alpha}_1 & \bar{\alpha}_2 & 0 & 0 & \bar{\alpha}_n & & \cdot \\ 0 & & & & \vdots & & & & \ddots & \vdots \\ \bar{\alpha}_0 & \bar{\alpha}_1 & \cdots & \bar{\alpha}_{n-2} & \bar{\alpha}_{n-1} & 0 & 0 & \cdots & 0 & \bar{\alpha}_n \end{bmatrix}, \tag{5.85}$$

where $(\bar{\cdot})$ indicates the complex conjugate of $(\cdot)$.

Following that, the Schur-Cohn criterion (SCC) is given as below:

SCC: All the roots of the polynomial $G_A(\gamma)$ lie on or inside the unit circle on the complex plane if and only if the Schur-Cohn matrix $\mathbf{D}$ is positive innerwise [153, 247].

However, to directly establish the conditions under which $\mathbf{D}$ is positive innerwise can be computationally very expensive. Instead, one transforms $G_A(\gamma)$ to a Hurwitz polynomial to alleviate this problem [100]. This transformation is done after a modification of the amplification polynomial and changing the variable from γ to s using the following map:

$$\gamma = \frac{1+s}{1-s} \quad \rightarrow \quad G_A(\gamma) = G_A(\frac{1+s}{1-s}) =: \frac{G_H(s)}{D_H(s)}\,. \tag{5.86}$$

Doing so and suppressing all common factors in the fraction $G_H(s)/D_H(s)$, satisfaction of the von Neumann stability criterion becomes equivalent to having negative real parts for all the roots of the newly found polynomial $G_H(s)$, i. e.,

$$|\gamma_i| \overset{!}{\leq} 1 \iff \Re(s_i) \overset{!}{\leq} 0\,, \tag{5.87}$$

where s_i represents all roots of $G_H(s) = 0$. This condition can be checked via an algorithm provided by Routh [237]. Utilising this algorithm, one can find the number of roots of a polynomial with positive real part without explicitly solving for the roots. Letting this number be equal to zero, one can actually find the number of roots on the left half-plane. Later, Hurwitz [149] independently proposed a method to find the conditions under which all roots of a polynomial lie in the negative half-plane. Nevertheless, both of these methods are essentially identical and yield the same results [50]. Therefore, the criterion for having

all the roots of a polynomial on the left half-plane is introduced as the Routh-Hurwitz criterion. Before presenting this criterion, consider that the Hurwitz determinant is given as follows:

Hurwitz determinant

Having the polynomial $G_H(s) = \sum_{i=0}^{n} \beta_i \, s^i$ as an algebraic polynomial of order $n \geq 1$ with β_i real and $\beta_0 \geq 0$, *the Hurwitz determinant* Δ_i is defined as

$$\Delta_i := \begin{vmatrix} \beta_1 & \beta_3 & \beta_5 & \cdots & \beta_{2\,i-1} \\ \beta_0 & \beta_2 & \beta_4 & \cdots & \beta_{2\,i-2} \\ 0 & \beta_1 & \beta_3 & \cdots & \beta_{2\,i-3} \\ 0 & \beta_0 & \beta_2 & \cdots & \beta_{2\,i-4} \\ \cdot & \cdot & \cdot & \cdots & \cdot \\ \cdot & \cdot & \cdot & \cdots & \beta_i \end{vmatrix} . \tag{5.88}$$

Remark: Obviously, if $\beta_0 < 0$, the whole polynomial must be multiplied by -1.

Following this, the Routh-Hurwitz criterion (RHC) reads:

RHC: The necessary stability condition given by (5.87) is satisfied if and only if all of the Hurwitz determinants corresponding to $G_H(s)$ are positive [149].

Although the RHC is easier to handle than the SCC, the evaluation of all Hurwitz determinants Δ_i still proves difficult. However, Fujiwara [108] has verified that the results obtained from these two criteria can also be achieved by an easier-to-handle method proposed by Liénard & Chipart [176]. The so-called Liénard-Chipart stability criterion (LCC) is given as follows:

LCC: Having a polynomial of order $n \geq 1$ in the form of $G_H(s) = \sum_{i=0}^{n} \beta_i \, s^i$ with β_i real and $\beta_0 \geq 0$, $(5.87)_1$ and consequently $(5.87)_2$ holds if and only if the corresponding parameters presented in Table 5.1 are all positive, where Δ_i is as defined in (5.88) [176].

In conclusion, the algorithm (5.89) or the flowchart provided in Figure 5.5 can be used to obtain the necessary stability condition for general numerical solution schemes applied to coupled PDE systems.

Remarks:

- The success of using the Liénard-Chipart criterion in establishing an analytical (parametric) necessary stability condition for specific solution schemes directly depends on the complexity of the coefficients β_i of the Hurwitz polynomial $G_H(s)$ and the Hurwitz determinants Δ_i. To this end, one usually has to make some effort in rearranging the expressions in order to find out if the corresponding terms are always positive and, if not, whether there are particular circumstances under which they stay positive. However, and in the worst case, where an analytical necessary stability condition cannot be found, one can undergo a numerical study to find the

Order	Expression
1	β_0, β_1
2	$\beta_0, \beta_1, \beta_2$
3	$\beta_0, \beta_1, \Delta_2, \beta_3$
4	$\beta_0, \beta_1, \Delta_3, \beta_3, \beta_4$
5	$\beta_0, \beta_1, \Delta_2, \beta_3, \Delta_4, \beta_5$
6	$\beta_0, \beta_1, \Delta_3, \beta_3, \Delta_5, \beta_5, \beta_6$

Table 5.1: *Liénard-Chipart stability criterion for* $n \leq 6$.

critical grid sizes for specific scenarios. By doing this, only the numerical values of constitutive model parameters need to be inserted in the expressions obtained for β_i and Δ_i. Doing so, these parameter become solely functions of spatial and temporal grid sizes. Subsequently, the changes in their values as the grid sizes change can be monitored and the region in which all of them stay positive can be found. Of particular note in this connection is that this procedure does not require the numerical solution of the whole problem.

- Note that stability and accuracy are different concepts, such that it is quite possible for a method to be stable and highly inaccurate [102].
- The linear stability analysis presented here reveals a necessary stability condition for stability of nonlinear systems too. In this regard, the stability analysis has to be done after linearisation of the equations.

Algorithm for finding the necessary stability condition (NSC).

(1) Build the amplification matrix **G**
(2) Find the amplification polynomial $G_A(\gamma)$
(3) **IF** the SCC is applicable **THEN**
NSC: **D** being positive innerwise
ELSE
(4) Replace $\gamma = (1+s)/(1-s)$ and
(5) Compose the Hurwitz polynomial $G_H(s)$
(6) **IF** the RHC is applicable **THEN**
NSC: Δ_i being positive
ELSE
(7) The LCC should be used
NSC: all expressions of Table 5.1 being positive

(5.89)

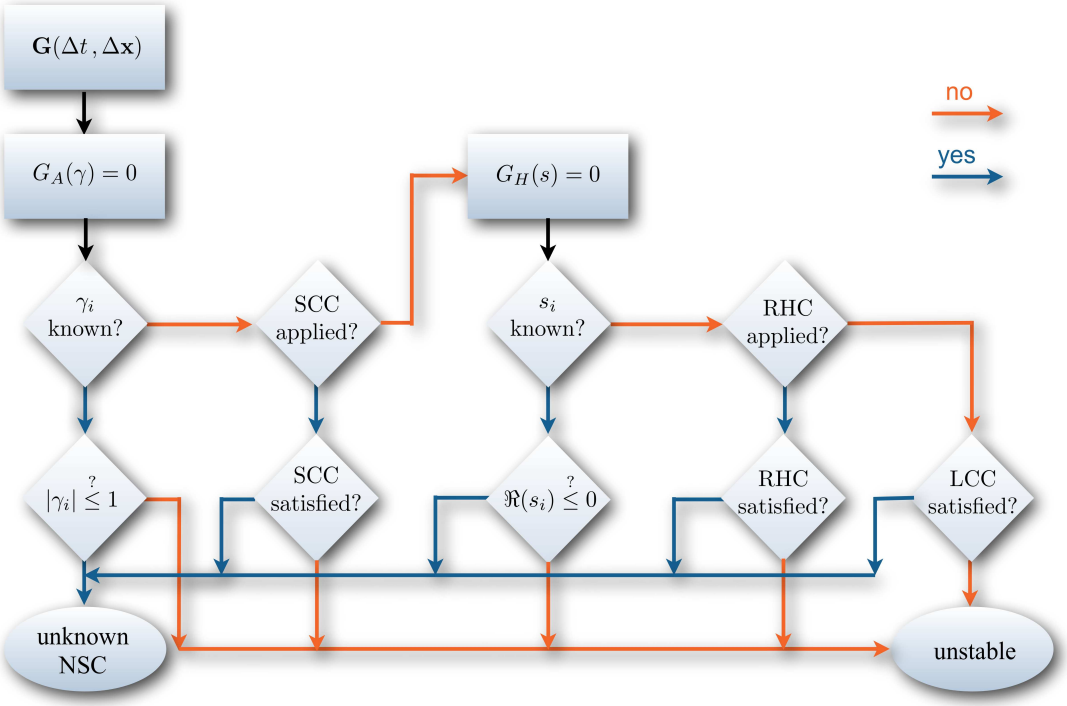

Figure 5.5: *Stability analysis flowchart related to the algorithm (5.89).*

Chapter 6:
Applications: Part I – Volume-Coupled Problems

The coupled problems, along with various strategies for numerical treatment of them, as well as the issues regarding the stability of these numerical schemes are studied in the preceding chapters of this contribution. The focus is now turned to put the knowledge acquired in those parts into practice. To this end, various examples are presented in what follows. The examples are grouped into the classes of volume- and surface-coupled problems, which are, respectively, studied in the present and next chapters. Each example is put in a section composed of four main subsections: (i) the model problem, presenting the mathematical model of the case at hand, (ii) selected decoupled solution strategies, (iii) stability analysis, and (iv) benchmark numerical examples.

6.1 Thermo-elastodynamics (TED)

As the first application, the coupled problem of linear thermo-elastodynamics is considered. Two decoupled solution schemes are discussed and the stability of both strategies is investigated. Solving numerical examples, the applicability of the solution schemes and the validity of the results obtained from the stability analysis are inspected.

6.1.1 Model problem

To present the corresponding operator-splitting strategies, consider (3.65). This is the 1-d version of the system of governing equations for the volume-coupled problem of thermo-elastodynamics. Neglecting the body forces and the radiation, these equations read

$$\mathcal{X} \;:\; \left\{ \begin{array}{rcl} \dot{u} &=& v\,, \\ \dot{v} &=& \dfrac{1}{\rho}\,\left[E\,u_{,xx} + m\,\vartheta_{,x}\right]\,, \\ \dot{\vartheta} &=& \dfrac{1}{c_v}\,\left[k\,\vartheta_{,xx} + \theta_0\,m\,v_{,x}\right]\,, \end{array} \right. \tag{6.1}$$

wherein the parameters are as defined under (3.40) and (3.65). Furthermore, $a_{,b} := \partial a/\partial b$ and $a_{,bb} := \partial^2 a/\partial b^2$. Choosing deformation, velocity and temperature as the state variables, i. e., $\mathbf{u} = [u, v, \vartheta]^T$, (6.1) can be rewritten in compact matrix form as

$$\mathcal{X} \;:\; \dot{\mathbf{u}}(x,t) = \overline{\mathfrak{S}}\,\mathbf{u}(x\,,t) =: \boldsymbol{f}\,(\mathbf{u}(x,t)) \tag{6.2}$$

with the differential operator $\overline{\mathfrak{S}}$ given as

$$\overline{\mathfrak{S}} := \begin{bmatrix} 0 & 1 & 0 \\ \dfrac{E}{\rho}\dfrac{\partial^2}{\partial x^2} & 0 & \dfrac{m}{\rho}\dfrac{\partial}{\partial x} \\ 0 & \dfrac{\theta_0\, m}{c_v}\dfrac{\partial}{\partial x} & \dfrac{k}{c_v}\dfrac{\partial^2}{\partial x^2} \end{bmatrix} . \tag{6.3}$$

6.1.2 Decoupled solution schemes

Two operator-splitting schemes for decoupled solution of (6.2) have been proposed by Armero & Simo [4]. For the reasons explained later, these OSS are called the *isothermal* and the *isentropic* operator-splitting methods. These procedures split the differential operator $\overline{\mathfrak{S}}$ into a displacement sub-operator $\overline{\mathfrak{S}}_u$ and a temperature sub-operator $\overline{\mathfrak{S}}_\vartheta$, which read as follows:

The isothermal operator splitting:

$$\overline{\mathfrak{S}}_u := \begin{bmatrix} 0 & 1 & 0 \\ \dfrac{E}{\rho}\dfrac{\partial^2}{\partial x^2} & 0 & \dfrac{m}{\rho}\dfrac{\partial}{\partial x} \\ 0 & 0 & 0 \end{bmatrix} , \quad \overline{\mathfrak{S}}_\vartheta := \begin{bmatrix} 0 & 0 & 0 \\ 0 & 0 & 0 \\ 0 & \dfrac{\theta_0\, m}{c_v}\dfrac{\partial}{\partial x} & \dfrac{k}{c_v}\dfrac{\partial^2}{\partial x^2} \end{bmatrix} . \tag{6.4}$$

The isentropic operator splitting:

$$\overline{\mathfrak{S}}_u := \begin{bmatrix} 0 & 1 & 0 \\ \dfrac{E}{\rho}\dfrac{\partial^2}{\partial x^2} & 0 & \dfrac{m}{\rho}\dfrac{\partial}{\partial x} \\ 0 & \dfrac{\theta_0\, m}{c_v}\dfrac{\partial}{\partial x} & 0 \end{bmatrix} , \quad \overline{\mathfrak{S}}_\vartheta := \begin{bmatrix} 0 & 0 & 0 \\ 0 & 0 & 0 \\ 0 & 0 & \dfrac{k}{c_v}\dfrac{\partial^2}{\partial x^2} \end{bmatrix} . \tag{6.5}$$

Using these sub-operators breaks down the problem into a mechanical subproblem $\mathcal{X}^u$ and a thermal subproblem $\mathcal{X}^\vartheta$, such that

$$\mathcal{X} \;:\; \begin{cases} \mathcal{X}^u \;:\; \dot{\mathfrak{u}} = \overline{\mathfrak{S}}_u\, \mathfrak{u} =: \boldsymbol{f}_u(\mathfrak{u}) \,, \\ \\ \mathcal{X}^\vartheta \;:\; \dot{\mathfrak{u}} = \overline{\mathfrak{S}}_\vartheta\, \mathfrak{u} =: \boldsymbol{f}_\vartheta(\mathfrak{u}) \,, \end{cases} \quad \text{with} \quad \boldsymbol{f}_u + \boldsymbol{f}_\vartheta = \boldsymbol{f} \,. \tag{6.6}$$

Subsequently, the numerical time integration is performed in the sense of the fractional-step method via successive integration of the mechanical and the thermal subproblems. In this regard, considering $\boldsymbol{\varphi}_u$ and $\boldsymbol{\varphi}_\vartheta$ as the integration processes for $\mathcal{X}^u$ and $\mathcal{X}^\vartheta$, the time marching process reads

$$\mathfrak{u}^n \xrightarrow{\boldsymbol{\varphi}_{u,\Delta t}} \mathfrak{u}^* \xrightarrow{\boldsymbol{\varphi}_{\vartheta,\Delta t}} \mathfrak{u}^{n+1} \,, \tag{6.7}$$

wherein $\mathbf{u}^n$ denotes a completely known state of the system at time t^n, $\mathbf{u}^*$ includes the intermediate variables, and $\mathbf{u}^{n+1}$ represents the updated state of the system at time t^{n+1}.

It should be noted that the difference between the sub-operators yields different values for the intermediate temperatures ϑ^*: the "isothermal" splitting method proceeds from an "isothermal" mechanical subproblem, such that $\vartheta^* = \vartheta^n$, whereas in the "isentropic" splitting method, ϑ^* is found assuming an "isentropic" mechanical subproblem, yielding

$$\vartheta^* = \vartheta^n - \frac{\theta_0}{c_v}\, m\, [(u^{n+1})_{,x} - (u^n)_{,x}]\,. \tag{6.8}$$

Nonetheless, in both schemes, the mechanical variables u and v are updated in a similar manner, such that the whole change in these variables takes place within the mechanical subproblem. Therefore, $u^* = u^{n+1}$ and $v^* = v^{n+1}$. Considering theses notes, the time integration is executed according to the following procedure:

Time marching following the isothermal and the isentropic OSS

(1) Choose ϑ^* as a predictor for ϑ^{n+1} and substitute it in $\mathcal{X}^u$.
(2) Integrate $\mathcal{X}^u$ and find $u^* = u^{n+1}$ and $v^* = v^{n+1}$.
(3) Substitute u^{n+1} and v^{n+1} in $\mathcal{X}^\vartheta$.
(4) Integrate $\mathcal{X}^\vartheta$ and find ϑ^{n+1}.

(6.9)

6.1.3 Stability analysis

The finite-difference (FD) stencil corresponding to (6.2) can be achieved by discretising the continuous PDE using the central difference (CD) scheme for the spatial and the trapezoidal rule (TR) for the temporal discretisation. Considering the isothermal splitting method, the FD stencil reads

$$\mathcal{X}^u \;:\; \begin{cases} \dfrac{u_j^{n+1} - u_j^n}{\Delta t} &= v_j^{n+1/2}\,, \\ \dfrac{v_j^{n+1} - v_j^n}{\Delta t} &= \dfrac{1}{\rho}\left[\dfrac{E}{\Delta x^2}\,(u_{j+1}^{n+1/2} - 2\,u_j^{n+1/2} + u_{j-1}^{n+1/2}) + \dfrac{m}{2\,\Delta x}\,(\vartheta_{j+1}^n - \vartheta_{j-1}^n)\right], \end{cases}$$

$$\mathcal{X}^\vartheta \;:\; \left\{ \frac{\vartheta_j^{n+1} - \vartheta_j^n}{\Delta t} = \frac{1}{c_v}\left[\frac{k}{\Delta x^2}\,(\vartheta_{j+1}^{n+1/2} - 2\,\vartheta_j^{n+1/2} + \vartheta_{j-1}^{n+1/2}) + \frac{\theta_0\, m}{2\,\Delta x}\,(v_{j+1}^{n+1} - v_{j-1}^{n+1})\right], \right. \tag{6.10}$$

where $(\,\cdot\,)^{n+1/2} := \frac{1}{2}\,[(\,\cdot\,)^{n+1} + (\,\cdot\,)^n]$. Then, following the procedure explained in Section 5.4, the amplification polynomial reads

$$G_A(\gamma) =$$

$$= \begin{vmatrix} (1-\frac{1}{\gamma}) & -\frac{\Delta t}{2}\,(\frac{1}{\gamma}+1) & 0 \\ \frac{E\,\Delta t}{\Delta x^2}\,(\frac{1}{\gamma}+1)\,(1-\cos\Theta) & \rho\,(1-\frac{1}{\gamma}) & -\frac{m\,\Delta t}{\gamma\,\Delta x}\,i\sin\Theta \\ 0 & -\frac{m\,\Delta t}{\Delta x}\,i\sin\Theta & \frac{c_v}{\theta_0}\,(1-\frac{1}{\gamma}) + \frac{k\,\Delta t}{\theta_0\,\Delta x^2}\,(\frac{1}{\gamma}+1)\,(1-\cos\Theta) \end{vmatrix} . \tag{6.11}$$

Replacing γ as proposed in (5.86) yields a 3rd-order Hurwitz polynomial $G_H(s)$, and consequently, by help of Table 5.1 and as shown in detail in Appendix A, the LCC is satisfied if and only if

$$\{\beta_0,\,\beta_1,\,\Delta_2,\,\beta_3\} \geq 0 \quad \rightarrow \quad \frac{\Delta t}{\Delta x} \overset{!}{\leq} \frac{2\,\sqrt{\rho\,c_v/\theta_0}}{|m|}\,. \tag{6.12}$$

Inequality $(6.12)_2$, which has also been presented by Armero & Simo [4], is the necessary stability condition for the isothermal splitting scheme and reveals the conditional stability of this solution method. This is due to the fact that the subproblems generated by this method are non-dissipative [4].

Next, considering the isentropic splitting scheme and using ϑ^* as given in (6.8) yields

$$\mathbf{A}\,\hat{\mathbf{u}}^{n+1} + \mathbf{B}\,\hat{\mathbf{u}}^{n} = \mathbf{0} \quad \rightarrow \quad \hat{\mathbf{u}}^{n+1} = -\mathbf{A}^{-1}\,\mathbf{B}\hat{\mathbf{u}}^{n} := \mathbf{G}\,\hat{\mathbf{u}}^{n}\,, \tag{6.13}$$

where $\hat{\mathbf{u}}^n$ is the Fourier transform of $\mathbf{u}_j^n$, cf. (5.71), and

$$\mathbf{A} := \begin{bmatrix} \frac{1}{\Delta t} & -\frac{1}{2} & 0 \\ a_{21} & \frac{\rho}{\Delta t} & 0 \\ 0 & -\frac{1}{2}\,\frac{m}{\Delta x}\,i\,\sin\Theta & a_{33} \end{bmatrix}, \qquad \mathbf{B} := \begin{bmatrix} -\frac{1}{\Delta t} & -\frac{1}{2} & 0 \\ b_{21} & -\frac{\rho}{\Delta t} & -\frac{m}{\Delta x}\,i\,\sin\Theta \\ 0 & -\frac{1}{2}\,\frac{m}{\Delta x}\,i\,\sin\Theta & b_{33} \end{bmatrix} \tag{6.14}$$

with

$$a_{12} = \frac{1}{2\,\Delta x^2}\,\left[(1-\cos^2\Theta)\,m^2 + 2\,(1-\cos\Theta)\,E\,c_v\right], \quad a_{33} = \frac{c_v}{\Delta t} + \frac{k}{\Delta x^2}\,(1-\cos\Theta)\,,$$

$$b_{12} = -\frac{1}{2\,\Delta x^2}\,\left[(\cos^2\Theta-1)\,m^2 + 2\,(1-\cos\Theta)\,E\right], \quad b_{33} = -\frac{c_v}{\Delta t} + \frac{k}{\Delta x^2}\,(1-\cos\Theta)\,. \tag{6.15}$$

Assembling $\mathbf{G}$ and accordingly $G_A(\gamma)$ and $G_H(s)$, which are 3rd-order polynomials, it can be shown that the LCC is always satisfied and, therefore, this method is unconditionally stable. In fact, splitting of the problem with the isentropic method produces dissipative subproblems and, thus, applying any B-stable integrator leads to unconditional stability.

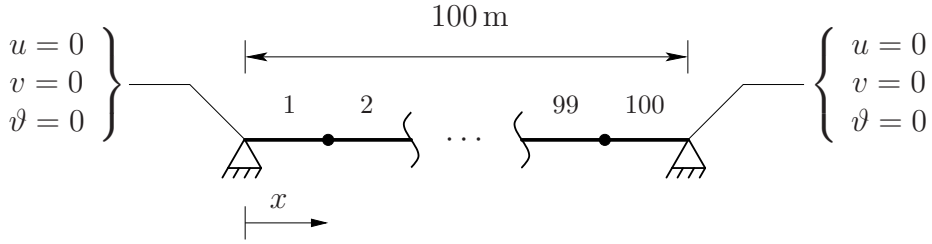

Figure 6.1: *Geometry and boundary conditions of the 1-d thermoelastic vibration [4].*

Stability in higher dimensions

Applying the isothermal operator-splitting scheme to the governing equations (3.37), one ends up with a Hurwitz polynomial of order 5 for the 2-d, and of order 6 for the 3-d problem. Consequently, and based on the LCC, the positivity of the following expressions must be inspected:

$$\text{2-d: } \{\beta_0\,,\beta_1\,,\Delta_2\,,\beta_3\,,\Delta_4\,,\beta_5\} \quad \text{and} \quad \text{3-d: } \{\beta_0\,,\beta_1\,,\Delta_3\,,\beta_3\,,\Delta_5\,,\beta_5\,,\beta_6\}\,. \tag{6.16}$$

A careful investigation has shown that for a d-dimensional problem, $d = \{2,3\}$, the necessary condition to satisfy the LCC and, hence, the necessary stability condition reads

$$\sqrt{\sum_{i=1}^{d}\left(\frac{\Delta t}{\Delta x_i}\right)^2} \overset{!}{\leq} \frac{2\sqrt{\rho\, c_v/\theta_0}}{|m|}\,. \tag{6.17}$$

Nevertheless, applying the isentropic operator-splitting method to the general from of the problem (3.37) leads to unconditional stability.

6.1.4 Numerical example I

In what follows, a 1-d thermoelastic vibration problem adopted from [4] is employed in order to verify the results of the stability analysis. The problem is composed of a homogeneous bar with geometry and material parameters as presented in Figure 6.1 and Table 6.1, where both ends of the bar are thermally and mechanically fixed. A perturbation in the form of a sinusoidal initial velocity along the length moves the system away from its stable equilibrium state and causes a horizontal vibration, hence, $\mathbf{u}^0(x) = [0,\, \sin(\pi\, x/100), 0]^T$. Consequently, and assuming a fairly strong thermomechanical coupling, this mechanical stimulation will entail a variation in the temperature. Following that, the critical time-step size, i. e., the biggest Δt which satisfies the necessary stability condition for the isothermal operator-splitting scheme, can be found from $(6.12)_2$ and reads

$$\Delta t^{isot.}_{crit.} = 2\,\Delta x \quad \xrightarrow{\Delta x = 1\,\mathrm{m}} \quad \Delta t^{isot.}_{crit.} = 2\,\mathrm{s}\,. \tag{6.18}$$

Thus, all the roots of the amplification polynomial lie inside the unit circle on the complex plane, and the absolute value of the roots and, consequently, the spectral radius associated with the amplification matrix are less than unity as long as $\Delta t < 2$ s, see Figure 6.2.

Parameter	Symbol	Value	SI unit
Mass density	ρ	1	$\mathrm{kg/m^3}$
1st Lamé constant	μ	3/8	Pa
2nd Lamé constant	λ	6/8	Pa
Stress-temperature modulus	m	-1	Pa/K
Volumetric specific heat	c_v	1	$\mathrm{J/(K\,m^3)}$
Thermal conductivity	k	1	$\mathrm{W/(K\,m)}$

Table 6.1: *Material parameters for the 1-d thermoelastic vibration example problem.*

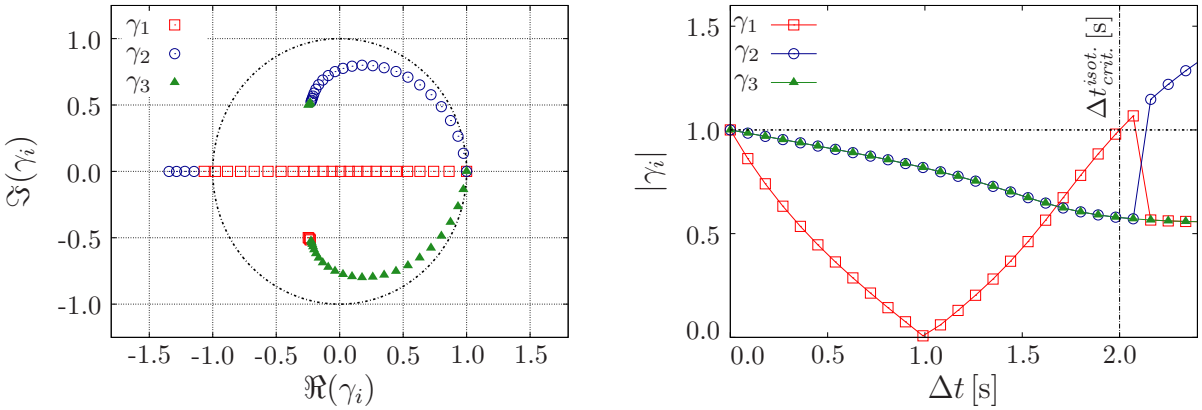

Figure 6.2: *Location of roots of the amplification polynomial for the isothermal decoupled solution scheme for* $\Delta t \in [0, 2.5]$ *s.*

Moreover, $(6.18)_2$ predicts that $\Delta t = 2$ s is theoretically the biggest time-step size for which the isothermal OSS might yield a stable solution.

Depicting the roots of the amplification polynomial for the isentropic operator-splitting scheme reveals that all the roots always lie inside the unit circle on the complex plane. Moreover, the absolute value of the roots and, hence, the spectral radius remain smaller than unity. It approves the unconditional stability of this scheme, see Figure 6.3. It is worth mentioning that these results have been obtained without a direct solution of the IBVP and regardless of specific boundary and initial conditions. However, to verify these conclusions, also the numerical solution of the IBVP via the monolithic and also the herein discussed decoupled schemes has been carried out. This has been done by a FE code developed in *Scilab*[1] and for $0 \leq t \leq 300$ s. Two different time-step sizes have been considered, namely $\Delta t_1 = 1\,\mathrm{s} < \Delta\, t^{isot.}_{crit.}$ and $\Delta t_2 = 3\,\mathrm{s} > \Delta\, t^{isot.}_{crit.}$. The time integration of the monolithic approach is done applying the Crank-Nicholson scheme, whereas, following [4], for both decoupled solution schemes the Crank-Nicholson time-integration scheme for the mechanical and the implicit Euler time integration scheme for the thermal subproblem are used.

Figure 6.4 shows the calculated evolution of the temperature for an exemplary point at $x =$

[1] Scientific free software package for numerical computations, cf. `www.scilab.org`.

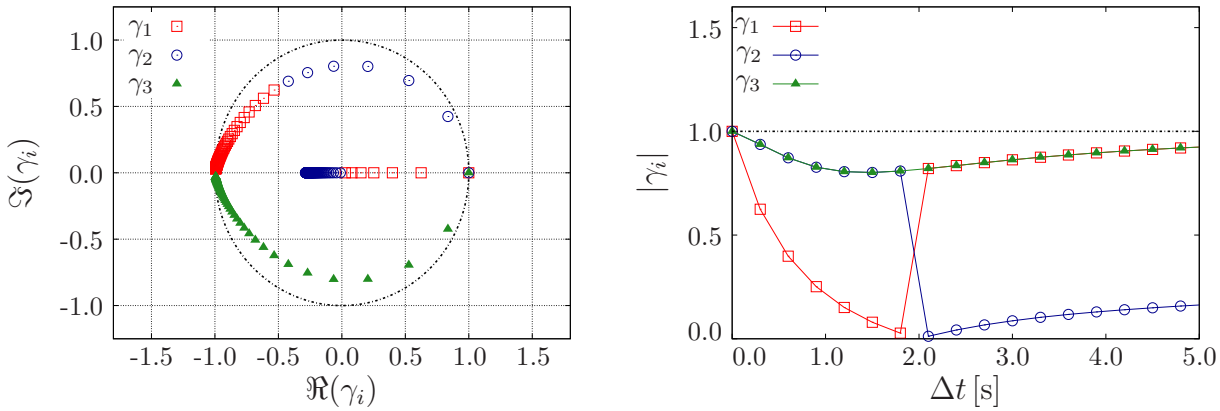

Figure 6.3: *Location of roots of the amplification polynomial for the isentropic decoupled solution scheme for* $\Delta t \in [0, 5]\, s$.

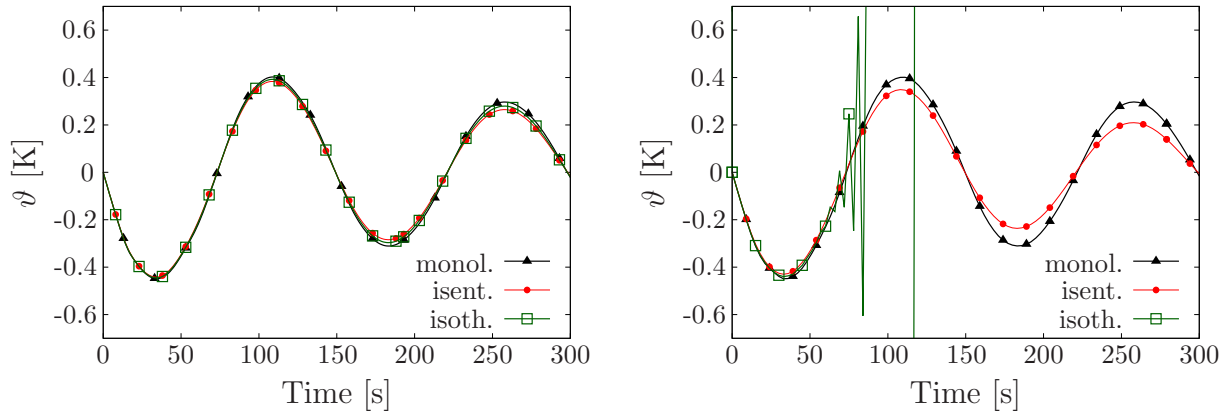

Figure 6.4: *Temperature evolution at* $x = 25\ m$ *and for* $\Delta t_1 = 1\ s$ *(left) and* $\Delta t_2 = 3\ s$ *(right).*

25 m. It is observed that, as predicted, the isothermal splitting scheme shows a conditional stability and, despite considering implicit time integrators for both subproblems, one obtains an unstable solution for a time-step size bigger than $\Delta\, t^{isot.}_{crit.}$. Nevertheless, this is not the case for the implicit monolithic and the isentropic splitting schemes, because they are unconditionally stable.

6.1.5 Numerical example II

In the next step, in order to inspect the strength of the proposed stability analysis algorithm in predicting the necessary stability condition of a 2-d problem, a beam with the geometry presented in Figure 6.5 has been considered. Assuming a homogeneous mesh with $\Delta x_1 = \Delta x_2 = 1\,\mathrm{m}$ and considering the material parameters as presented in Table 6.1, the critical time-step size for this problem, when solved via the isothermal splitting scheme, is calculated from (6.17) and reads

$$\Delta t^{isot.}_{crit.} = 1.15\,\mathrm{s}\,. \tag{6.19}$$

Thus, $\Delta t = \Delta t^{isot.}_{crit.}$ is the biggest time-step size for which the absolute values of the roots of the amplification polynomial and, hence, the spectral radius of the amplification matrix remain smaller than unity, cf. Figure 6.6.

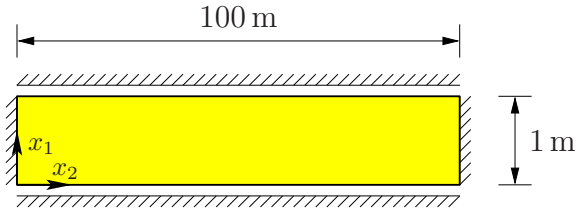

$$\text{BC}_\vartheta: \quad \vartheta = 0\,\text{K} \quad \text{at} \quad x_2 = 0\,\text{m} \quad \text{and} \quad x_2 = 100\,\text{m}\,,$$
$$q_{x_1} = 0\,\frac{\text{W}}{\text{m}^2} \quad \text{at} \quad x_1 = 0\,\text{m} \quad \text{and} \quad x_1 = 1\,\text{m}\,.$$

Figure 6.5: *Geometry and boundary conditions of the 2-d thermoelastic vibration.*

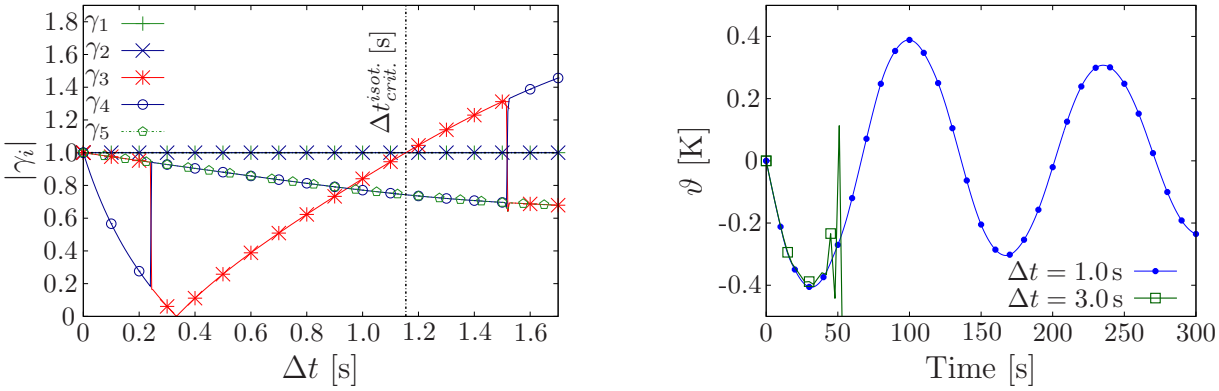

Figure 6.6: *Roots of the amplification polynomial for the 2-d beam (left) and the temperature evolution calculated at* $\mathbf{x} = (1\,, 25)$ *m (right).*

Furthermore, (6.19) predicts that using $\Delta t > \Delta t^{isot.}_{crit.}$ for temporal discretisation of the problem leads to instability. In order to evaluate this statement, the a. m. *Scialb* code has been further developed and employed for numerical solution of the problem. Considering an initial horizontal velocity $v_{x_2}(\mathbf{x}\,, 0) = \sin(\pi\, x_2/100)\,\text{m}$, in conjunction with the boundary conditions depicted in Figure 6.5, the evolution of the temperature for $0 \leq t \leq 300\,\text{s}$ has been monitored. It has been obtained that using a time-step size bigger than $\Delta t^{isot.}_{crit.}$ destroys the stability of the numerical results, cf. Figure 6.6.

6.1.6 Numerical example III

Subsequently, a simple 3-d beam as presented in Figure 6.7 has been considered. Using the material parameters from Table 6.1 in conjunction with a homogeneous mesh with $\Delta x_1 = \Delta x_2 = \Delta x_3 = 0.25\,\text{m}$, the critical time-step size for a decoupled solution of the problem using the isothermal splitting method is determined by (6.17) and reads

$$\Delta t^{isot.}_{crit.} = 0.3\,\text{s}\,. \tag{6.20}$$

To inspect the result of the stability analysis, the *Scilab* FE-solver was further developed. This development was such that it enabled the code to handle 3-d examples, where the geometry and the mesh were generated by the FE-package *Abaqus*[2]. Considering an initial horizontal velocity $v_{x_2}(\mathbf{x}\,, 0) = \sin(\pi\, x_2/10)$ m, the developed solution package was

[2]Software package for finite element analysis and computer-aided engineering, cf. `www.simluia.com`.

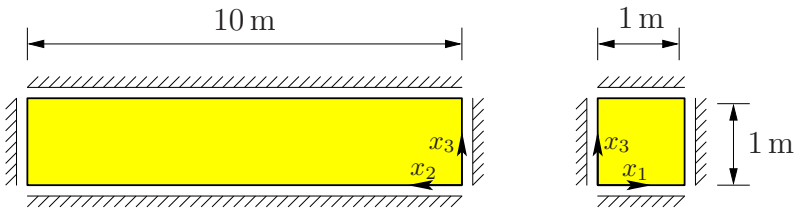

$$\text{BC}_\vartheta\text{: } \mathbf{q} = \mathbf{0}\,\frac{\text{W}}{\text{m}^2} \text{ on all boundaries.}$$

Figure 6.7: *Geometry and boundary conditions of the 3-d thermoelastic vibration.*

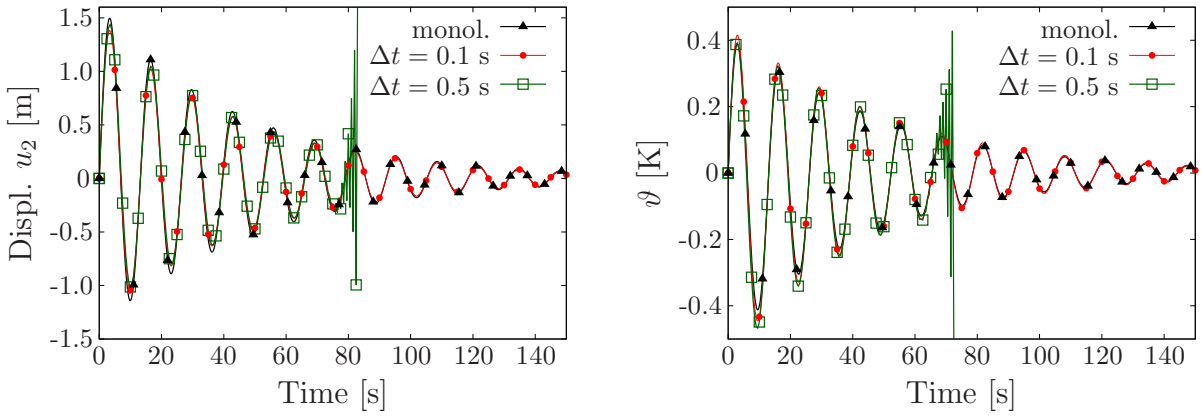

Figure 6.8: *The displacement evolution (left) and the temperature evolution (right) in the 3-d beam, calculated at* $\mathbf{x} = (1.0\,, 7.5\,, 1.0)$ *m.*

employed for solution of the IBVP. Employing different time-step sizes, it was seen that for $\Delta t > \Delta t^{isot.}_{crit.}$ the problem becomes unstable. This is shown in Figure 6.8 depicting the evolution of the temperature and the displacement in the course of time. Furthermore, the selected snapshots depicted in Figure 6.9 show the coupled behaviour of the displacement and the temperature fields, when the problem is solved via the isothermal splitting method, using a step size $\Delta t = 0.1$ s.

6.1.7 Numerical example IV

The developed FE-solver was further employed for solution of a more complex IBVP defined by the geometry and the boundary conditions presented in Figure 6.10, and the material parameters given in Table 6.2.

In order to solve the problem, the geometry was firstly created and, subsequently, discretised in the *Abaqus* environment. Following that, employing the corresponding material parameters and considering the grid sizes $\Delta x_1 = 20$ mm, $\Delta x_2 = 8$ mm and $\Delta x_3 = 12$ mm, the critical time-step size was determined via (6.17). It reads

$$\Delta t^{isot.}_{crit.} = 0.03\,\text{s}\,. \tag{6.21}$$

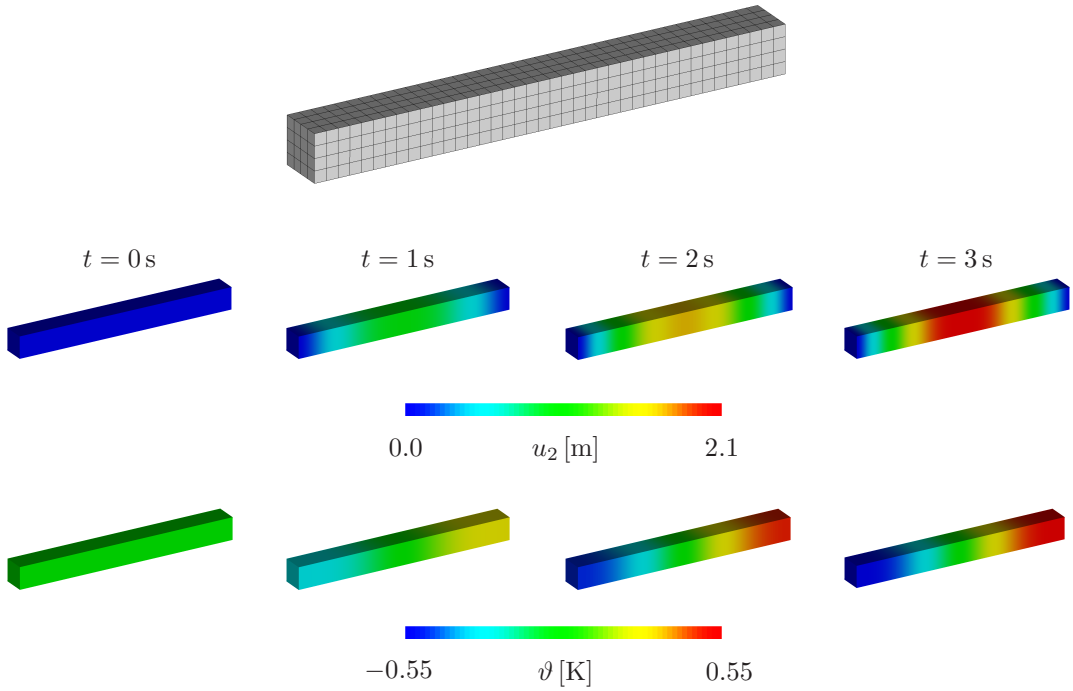

Figure 6.9: *Snapshots showing the coupled evolution of horizontal displacement u_2 (top) and temperature ϑ (bottom) within the first 3 seconds.*

Subsequently, the IBVP was solved monolithically as well as employing the isothermal operator-splitting method, where the decoupled solution was performed using two exemplary time-step sizes, one smaller than and one bigger than the critical step size.

Monitoring the results obtained at a sampling point at $\mathbf{x} = (0.1\,, 0.1\,, 0.083)\,\mathrm{m}$, it was seen that for $\Delta t > \Delta t_{crit.}^{isot.}$ the scheme becomes unstable, cf. Figure 6.11. Moreover, Figure 6.12 depicts selected snapshots corresponding to the contours of displacement and temperature, when the problem is solved via the isothermal splitting method, using $\Delta t = 0.01$ ms.

Parameter	Symbol	Value	SI unit
Mass density	ρ	7850	$\mathrm{kg/m^3}$
1st Lamé constant	μ	77.9	GPa
2nd Lamé constant	λ	115.3	GPa
Stress-temperature modulus	m	-6	MPa/K
Volumetric specific heat	c_v	434	$\mathrm{J/(K\,m^3)}$
Thermal conductivity	k	60.5	$\mathrm{W/(K\,m)}$

Table 6.2: *Material parameters for the 3-d example in Figure 6.10.*

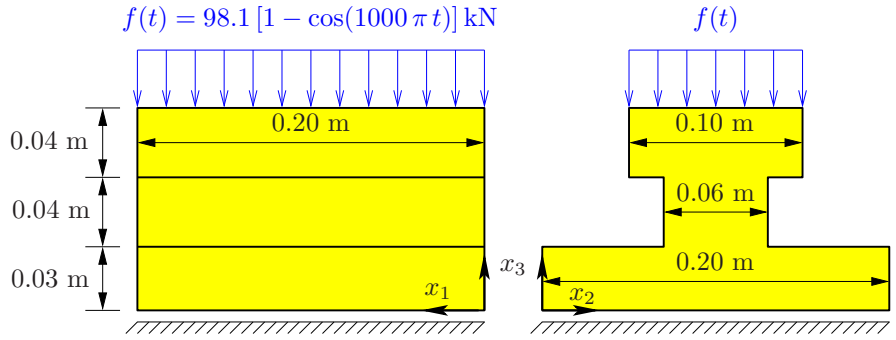

BC_ϑ: $\mathbf{q} = \mathbf{0}\,\frac{\mathrm{W}}{\mathrm{m}^2}$ on all boundaries.

Figure 6.10: *Geometry and boundary conditions for the example IV.*

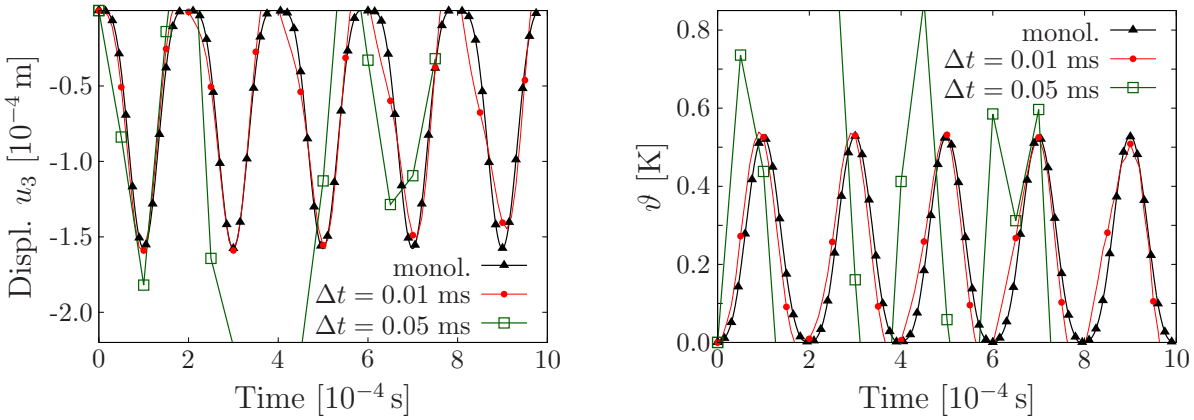

Figure 6.11: *The evolution of the displacement (left) and the temperature (right) in the 3-d example in Figure 6.10, calculated at* $\mathbf{x} = (0.1\,, 0.1\,, 0.083)$ *m.*

6.2 Porous-media dynamics (PMD)

A detailed discussion of dynamic porous media problems and a careful comparison between the corresponding monolithic and partitioned solution schemes has been presented by Heider [137] and Markert *et al.* [190]. In this section, proceeding from the corresponding 1-d system of governing equations (3.62), a semi-explicit-implicit splitting scheme is studied and its stability characteristics are investigated

6.2.1 Model problem

In the framework of the Theory of Porous Media (TPM) and proceeding from intrinsically incompressible constituents, i. e., $\rho^{\alpha R} = \text{const.}$, where $\rho^{\alpha R}$ is the effective or intrinsic density of the constituent φ^α ($\alpha = S$: solid skeleton; $\alpha = F$: pore fluid), the set of governing equations for the dynamic biphasic model is composed of the solid momentum balance, the fluid momentum balance and the mixture volume balance, cf. (3.62). The 1-d version of these equations, obtained under the assumption of confined compression and geometrically-linear deformations is given as

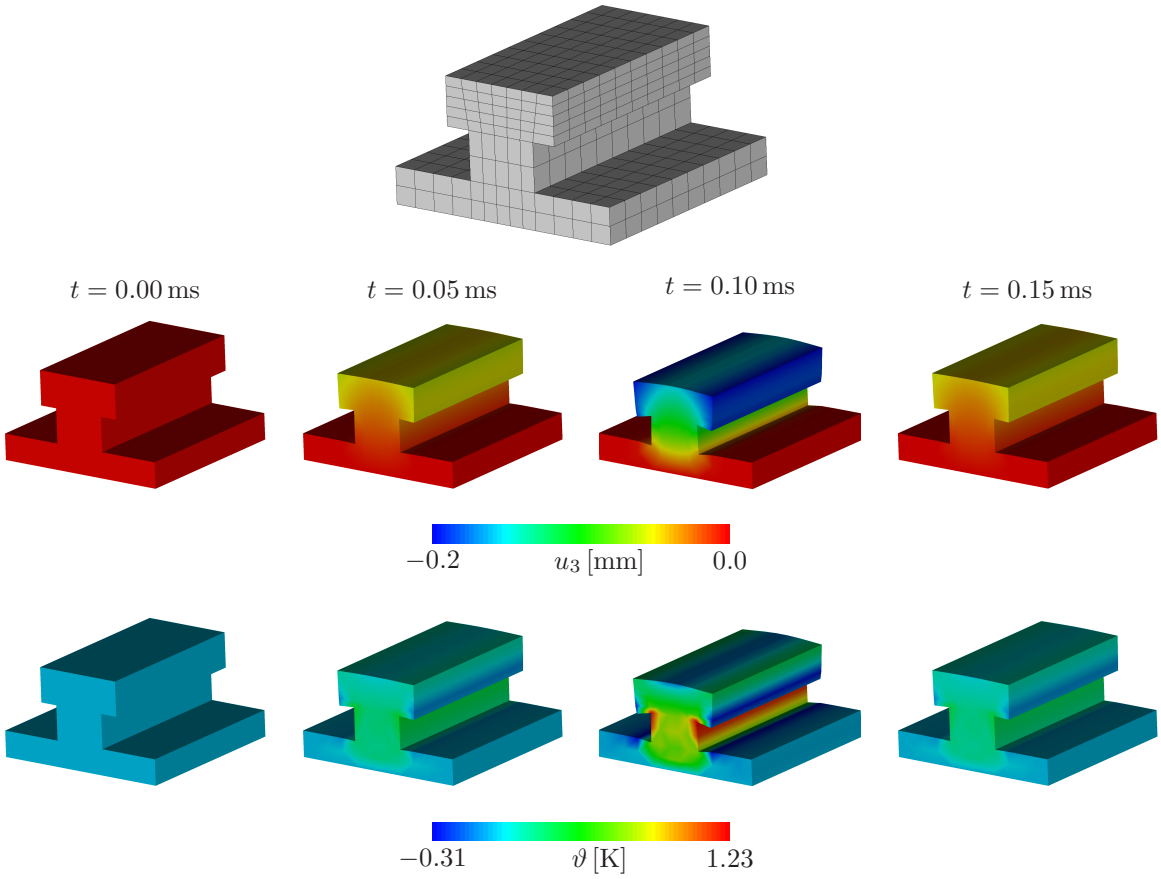

Figure 6.12: *Snapshots showing the coupled evolution of the vertical displacement u_3 (top) and the temperature ϑ (bottom) within one cycle of loading and unloading.*

$$\mathcal{X}\ :\ \begin{cases} \dot{u}_S &= v_S\,, \\ \dot{v}_S &= \dfrac{1}{\rho^S}\left[\left(2\,\mu^S+\lambda^S\right)(u_S)_{,xx} - n^S\,p_{,x} + \dfrac{(n^F)^2\,\gamma^{FR}}{k^F}\,(v_F-v_S)\right], \\ \dot{v}_F &= \dfrac{1}{\rho^F}\left[-n^F\,p_{,x} - \dfrac{(n^F)^2\,\gamma^{FR}}{k^F}\,(v_F-v_S)\right], \\ 0 &= n^S\,(v_S)_{,x} + n^F\,(v_F)_{,x}\ , \end{cases} \tag{6.22}$$

wherein, following the notations used in Section 3.3, $\rho^\alpha = n^\alpha\,\rho^{\alpha R}$ is the partial density with $n^\alpha := \mathrm{d}v^\alpha/\mathrm{d}v$ being the volume fraction of φ^α, μ^S and λ^S are the Lamé constants of the porous solid matrix, γ^{FR} is the effective fluid weight and k^F represents the Darcy permeability. Consequently, the solid deformation u_S, the solid velocity v_S, the fluid velocity v_F and the pore-fluid pressure p define an appropriate set of state variables for this problem, i. e., $\mathbf{u} := [u_S, v_S, v_F, p]^T$. It should be noted that the mixture volume balance $(6.22)_4$ has been obtained as a direct result of the mass balance by assuming intrinsically incompressible constituents. However, this algebraic constraint does not provide an

evolution equation for the pore pressure. Therefore, (6.22) is a DAE system of index 2 (cf. Section 3.4), which reads in the compact form

$$\mathcal{X} \;:\; \mathfrak{S}_t \mathbf{u}(x\,,t) = \overline{\mathfrak{S}}\,\mathbf{u}(x,t) =: \boldsymbol{f}(\mathbf{u}(x\,,t))\,. \tag{6.23}$$

Therein, the differential operators $\mathfrak{S}_t$ and $\overline{\mathfrak{S}}$ are given as

$$\mathfrak{S}_t = \begin{bmatrix} \frac{\mathrm{d}}{\mathrm{d}t} & 0 & 0 & 0 \\ 0 & \frac{\mathrm{d}}{\mathrm{d}t} & 0 & 0 \\ 0 & 0 & \frac{\mathrm{d}}{\mathrm{d}t} & 0 \\ 0 & 0 & 0 & 0 \end{bmatrix}, \quad \text{and} \quad \overline{\mathfrak{S}} = \begin{bmatrix} 0 & 1 & 0 & 0 \\ \overline{\mathfrak{S}}_{21} & \overline{\mathfrak{S}}_{22} & \overline{\mathfrak{S}}_{23} & \overline{\mathfrak{S}}_{24} \\ 0 & \overline{\mathfrak{S}}_{32} & \overline{\mathfrak{S}}_{33} & \overline{\mathfrak{S}}_{34} \\ 0 & \overline{\mathfrak{S}}_{42} & \overline{\mathfrak{S}}_{43} & 0 \end{bmatrix}. \tag{6.24}$$

with

$$\begin{aligned} &\overline{\mathfrak{S}}_{21} = \frac{2\,\mu^S + \lambda^S}{\rho^S}\,\frac{\partial^2}{\partial x^2}\,, \quad \overline{\mathfrak{S}}_{22} = -\frac{(n^F)^2\,\gamma^{FR}}{\rho^S\,k^F}\,, \quad \overline{\mathfrak{S}}_{23} = \frac{(n^F)^2\,\gamma^{FR}}{\rho^S\,k^F}\,, \quad \overline{\mathfrak{S}}_{24} = -\frac{n^S}{\rho^S}\,\frac{\partial}{\partial x}\,, \\ &\overline{\mathfrak{S}}_{32} = \frac{(n^F)^2\,\gamma^{FR}}{\rho^F\,k^F}\,, \qquad \overline{\mathfrak{S}}_{33} = -\frac{(n^F)^2\,\gamma^{FR}}{\rho^F\,k^F}\,, \quad \overline{\mathfrak{S}}_{34} = -\frac{n^F}{\rho^F}\,\frac{\partial}{\partial x}\,, \\ &\overline{\mathfrak{S}}_{42} = n^S\,\frac{\partial}{\partial x}\,, \qquad \overline{\mathfrak{S}}_{43} = n^F\,\frac{\partial}{\partial x}\,. \end{aligned} \tag{6.25}$$

6.2.2 Decoupled solution scheme

Equation system (6.22) is often used in geomechanics in order to find the response of soil to external dynamic stimulations, e. g. seismic loads. To this end, proceeding from a numerical solution algorithm and using small time steps for temporal discretisation is a common practice. This is in order to capture the variations of the naturally high-frequency seismic loads. Employing smaller time-step sizes, however, increases the number of time steps and, thus, the computational costs. Using an explicit time-stepping process is a plausible way to compensate this cost increase. Nevertheless, proceeding from a FE-based solution scheme, the presence of the algebraic constraint renders the corresponding mass matrix singular and, thus, prohibits the application of explicit monolithic treatment of the dynamic problem (6.22). Implementing the operator-splitting method presented by Markert *et al.* [190], one can separate the momentum balances from the algebraic constraint and, consequently, overcome this dilemma. The proposed method leads to a separation of the displacement and velocity fields from the pore-fluid pressure. Nevertheless, and unlike the isothermal and isentropic schemes discussed above, the processes of operator splitting and temporal discretisation for this problem are interwoven. To elucidate the idea, consider the following sub-operators resulting from splitting of the differential operator $\overline{\mathfrak{S}}$:

$$\overline{\mathfrak{S}}_v = \begin{bmatrix} 0 & 0 & 0 & 0 \\ \overline{\mathfrak{S}}_{21} & \overline{\mathfrak{S}}_{22} & \overline{\mathfrak{S}}_{23} & 0 \\ 0 & \overline{\mathfrak{S}}_{32} & \overline{\mathfrak{S}}_{33} & 0 \\ 0 & 0 & 0 & 0 \end{bmatrix}, \quad \overline{\mathfrak{S}}_p = \begin{bmatrix} 0 & 1 & 0 & 0 \\ 0 & 0 & 0 & \overline{\mathfrak{S}}_{24} \\ 0 & 0 & 0 & \overline{\mathfrak{S}}_{34} \\ 0 & \overline{\mathfrak{S}}_{42} & \overline{\mathfrak{S}}_{43} & 0 \end{bmatrix}. \tag{6.26}$$

Employing these sub-operators yields a decoupled system of equations, which reads

$$\mathcal{X} \;:\; \begin{cases} \mathcal{X}^v \;:\; \mathfrak{S}_t\,\mathfrak{u} = \overline{\mathfrak{S}}_v\,\mathfrak{u} =: \boldsymbol{f}_v(\mathfrak{u})\,, \\ \\ \mathcal{X}^p \;:\; \mathfrak{S}_t\,\mathfrak{u} = \overline{\mathfrak{S}}_p\,\mathfrak{u} =: \boldsymbol{f}_p(\mathfrak{u})\,, \end{cases} \quad \text{with} \quad \boldsymbol{f}_v + \boldsymbol{f}_p = \boldsymbol{f}\,. \tag{6.27}$$

Thus, the evolution of the vector of state variables $\mathfrak{u}$ can be computed from successive numerical integration of the velocity subproblem $\mathcal{X}^v$ and the pressure subproblem $\mathcal{X}^p$, such that

$$\mathfrak{u}^n \xrightarrow{\boldsymbol{\varphi}_{v,\Delta t}} \mathfrak{u}^* \xrightarrow{\boldsymbol{\varphi}_{p,\Delta t}} \mathfrak{u}^{n+1}\,. \tag{6.28}$$

Therein, $\mathfrak{u}^* = [u_S^*\,, v_S^*\,, v_F^*\,, p^*]^T$ denotes the intermediate state of the system. Nevertheless, from the structure of the velocity sub-operator $\overline{\mathfrak{S}}_v$ it is clear that integrating the velocity subproblem $\mathcal{X}^v$ does not alter the values of the solid displacement u_S and the pore pressure p, such that $u_S^* = u_S^n$ and $p^* = p^n$. Thus, $\mathfrak{u}^* = [u_S^n\,, v_S^*\,, v_F^*\,, p^n]^T$, where v_S^* and v_F^* denote the intermediate velocities, predicted via neglecting the algebraic constraint (the mixture volume balance) and in the absence of the pressure gradient $\nabla p := p_{,x}$. Subsequent integration of $\mathcal{X}^p$ projects these predicted values into the solenoidal space and also updates the pore-pressure and the solid-displacement fields.

The above procedure presents a decoupled solution algorithm, similar to the projection scheme of Chorin [52], which is commonly applied to the incompressible fluid models. In an attempt to increase the accuracy and inspired by the scheme of van Kan [154], Markert *et al.* [190] proceed from an implicit pressure gradient ∇p^{n+1} in $(6.22)_{2,3}$. Subsequently, an additive split of this pressure gradient is considered:

$$\nabla p^{n+1} := \nabla q + \nabla \widetilde{p}, \quad \text{with} \quad \nabla q := \nabla p^n \quad \text{and} \quad \nabla \widetilde{p} = \nabla p^{n+1} - \nabla p^n\,. \tag{6.29}$$

Following that, the terms ∇q and $\nabla \widetilde{p}$, respectively, determine the pressure gradients in the velocity and the pressure subproblems, such that the enhanced subproblems read

$$\begin{aligned} \mathcal{X}^v \;:\; \begin{bmatrix} \dot{u}_S \\ \dot{v}_S \\ \dot{v}_F \\ 0 \end{bmatrix} &= \begin{bmatrix} 0 & 0 & 0 \\ \overline{\mathfrak{S}}_{21} & \overline{\mathfrak{S}}_{22} & \overline{\mathfrak{S}}_{23} \\ 0 & \overline{\mathfrak{S}}_{32} & \overline{\mathfrak{S}}_{33} \\ 0 & 0 & 0 \end{bmatrix} \begin{bmatrix} u_S \\ \\ v_S \\ \\ v_F \end{bmatrix} + \begin{bmatrix} 0 \\ -\frac{n^S}{\rho^S}\,\nabla q \\ -\frac{n^F}{\rho^F}\,\nabla q \\ 0 \end{bmatrix}, \\ \\ \mathcal{X}^p \;:\; \begin{bmatrix} \dot{u}_S \\ \dot{v}_S \\ \dot{v}_F \\ 0 \end{bmatrix} &= \begin{bmatrix} 0 & 1 & 0 \\ 0 & 0 & 0 \\ 0 & 0 & 0 \\ 0 & \overline{\mathfrak{S}}_{42} & \overline{\mathfrak{S}}_{43} \end{bmatrix} \begin{bmatrix} u_S \\ \\ v_S \\ \\ v_F \end{bmatrix} + \begin{bmatrix} 0 \\ -\frac{n^S}{\rho^S}\,\nabla \widetilde{p} \\ -\frac{n^F}{\rho^F}\,\nabla \widetilde{p} \\ 0 \end{bmatrix}. \end{aligned} \tag{6.30}$$

Thus, the temporal discretisation of subproblems yields

$$\mathcal{X}^v \;:\; \begin{cases} \dfrac{(v_S^* - v_S^n)}{\Delta t} &= \dfrac{1}{\rho^S}\left[(2\,\mu^S + \lambda^S)\,(u_S^n)_{,xx} - n^S\,p_{,x}^n + \dfrac{(n^F)^2\,\gamma^{FR}}{k^F}\,(v_F^* - v_S^*)\right], \\ \dfrac{(v_F^* - v_F^n)}{\Delta t} &= \dfrac{1}{\rho^F}\left[-n^F\,p_{,x}^n - \dfrac{(n^F)^2\,\gamma^{FR}}{k^F}\,(v_F^* - v_S^*)\right]. \end{cases}$$

$$\mathcal{X}^p \;:\; \begin{cases} \dfrac{(u_S^{n+1} - u_S^n)}{\Delta t} &= \frac{1}{2}\,(v_S^{n+1} + v_S^n)\,, \\ \dfrac{(v_S^{n+1} - v_S^*)}{\Delta t} &= -\frac{n^S}{\rho^S}\,(p_{,x}^{n+1} - p_{,x}^n)\,, \\ \dfrac{(v_F^{n+1} - v_F^*)}{\Delta t} &= -\frac{n^F}{\rho^F}\,(p_{,x}^{n+1} - p_{,x}^n)\,, \\ 0 &= n^S\,(v_S^{n+1})_{,x} + n^F\,(v_F^{n+1})_{,x}\,. \end{cases} \tag{6.31}$$

Subsequently, the decoupled solution is executed as per the following procedure:

Decoupled solution of PMD [190]

(6.32)

(1) Compute intermediate velocities by simultaneous solution of $(6.31)_2$ and $(6.31)_3$.
(2) Find v_S^{n+1} and v_F^{n+1} from $(6.31)_4$ and $(6.31)_5$.
(3) Replace the intermediate velocities calculated in Step 1 in the results of Step 2.
(4) Replace v_S^{n+1} and v_F^{n+1} found in Step 3 in $(6.31)_6$.
(5) Solve $(6.31)_6$ and update the pore-fluid pressure.
(6) Use this value to compute new values for the velocities and the solid displacement from $(6.31)_3$, $(6.31)_4$ and $(6.31)_5$.

6.2.3 Stability analysis

Using the central difference (CD) scheme for the spatial discretisation of (6.31) and following the algorithm explained in Section 5.4.2, one ends up with a 3rd-order Hurwitz polynomial $G_H(s)$, the stability of which can be investigated via the LCC. Referring to Table 5.1, one concludes that all the roots of a 3rd-order Hurwitz polynomial have a negative real part if and only if

$$\{\beta_0,\, \beta_1,\, \Delta_2,\, \beta_3\} \geq 0\,. \tag{6.33}$$

Examining these expressions shows that β_0 and β_3 are always positive. However, positiveness of β_1 can be acquired if

$$\frac{\rho^{SR}}{\rho^{FR}} \geq 1\,, \tag{6.34}$$

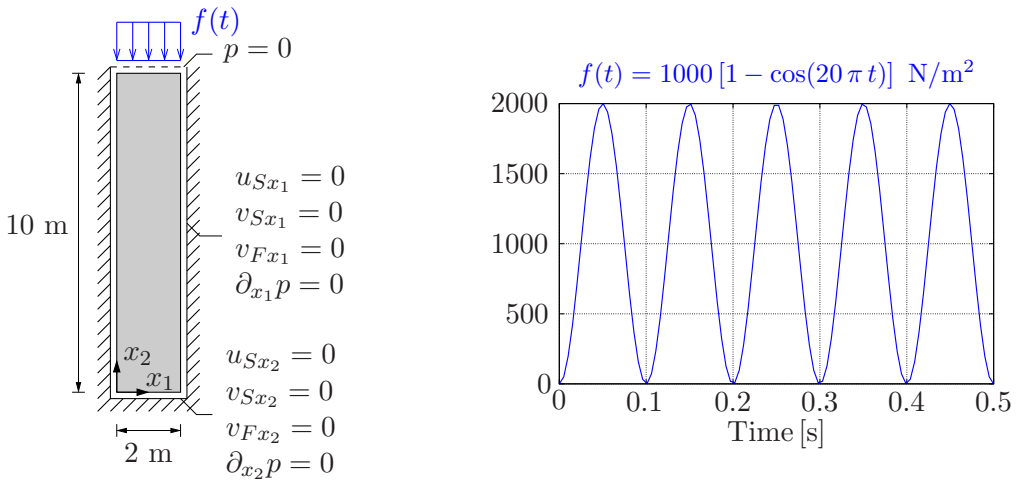

Figure 6.13: *Geometry and boundary conditions (left) and loading path (right) of the dynamic confined compression of a saturated poroelastic column.*

which is usually physically satisfied. Otherwise,

$$\left(\frac{\Delta t}{\Delta x}\right)^2 \overset{!}{\leq} \frac{1}{2\,(2\,\mu^S + \lambda^S)\,n^F} \left[\frac{n^S}{\rho^S} - \frac{n^F}{\rho^F}\right]^{-1} . \tag{6.35}$$

Due to the complexity of the resulting Δ_2, it is not easy to check its positiveness for the general case. Instead, one can perform a case study for a canonical IBVP.

6.2.4 Numerical example

As the benchmark example, consider a saturated poroelastic column under a harmonic loading. Proceeding from homogeneous and isotropic conditions, the column is surrounded by impermeable, frictionless and rigid boundaries except for the loaded top side, which is perfectly drained. The column is periodically loaded on its top and the responding variations in the solid displacement, the fluid velocity and the pore-fluid pressure are calculated. The problem and the loading path are as illustrated in Figure 6.13. The other relevant data is adopted from [66], see Table 6.3. Note that in the geometrically linear regime, $n^\alpha \approx n^\alpha_{0S} = \text{const.}$ with n^α_{0S} being the initial volume fraction of φ^α at time t^0. A (semi-)analytical solution of the problem via Laplace transform can be found in [28]. Moreover, in [66] a numerical solution of the problem obtained via a monolithic solution scheme is presented. However, the focus here is on the decoupled solution scheme and the goal is to examine the stability behaviour of the solution as a response to changes in the time-step size. Moreover, the independence of the critical time-step size from the permeability factor is investigated.

Considering the data given in Table 6.3, it is clear that (6.34) is per se satisfied and, therefore, there is no need to check (6.35). Hence, evaluating the von Neumann stability criterion boils down to examining the positiveness of Δ_2. Inserting the numerical values for $\Delta x = 1$ m, it is observed that this condition is satisfied for $\Delta t \leq 11 \cdot 10^{-3}$ s, and hence, $\Delta t_{crit.} = 11 \cdot 10^{-3}$ s. Consequently, all the roots of the amplification polynomial must lie on or inside the unit circle in the complex plane and, therefore, the absolute values of the

Parameter	Symbol	Value	SI unit
1st Lamé constant of solid skeleton	μ^S	$5.583 \cdot 10^6$	Pa
2st Lamé constant of solid skeleton	λ^S	$8.375 \cdot 10^6$	Pa
Volume fraction of solid	n^S_{0S}	0.67	–
Volume fraction of fluid	n^F_{0S}	0.33	–
Material density of dense solid	ρ^{SR}	2000	kg/m^3
Material density of pore fluid	ρ^{FR}	1000	kg/m^3
Effective fluid weight	γ^{FR}	9800	N/m^3
Darcy permeability	k^F	10^{-2}	m/s

Table 6.3: *Material parameters for the porous media dynamics example problem [66].*

roots remain smaller than unity as long as $\Delta t \leq \Delta t_{crit.}$, see Figure 6.14. Furthermore, and regardless of specific initial and boundary conditions, the stability analysis predicts that $\Delta t_{crit.} = 11 \cdot 10^{-3}$ s is theoretically the biggest time-step size for which the solution may be stable.

These conclusions are verified by a numerical solution of the problem for $0 \leq t \leq 0.5$ s, which is accomplished by a FE code developed in *Scilab*. Doing so, one observes that the solution starts to diverge even for $\Delta t = 0.007$ s, which is obviously smaller than the predicted $\Delta t_{crit.}$, see Figure 6.15. However, it is not surprising, because the von Neumann stability analysis, as already mentioned, provides a necessary but not sufficient condition for the stability of the numerical scheme.

Moreover, the spectral radii for distinct values for the permeability factor k^F and spatial grid size Δx are plotted in Figure 6.16. It can be seen that drastic changes in the value of the permeability factor have only little influence on the critical time-step size. This result, which is obtained without solving the whole IBVP, proves the independence of the stability condition of the solution scheme from the permeability factor. This is totally in

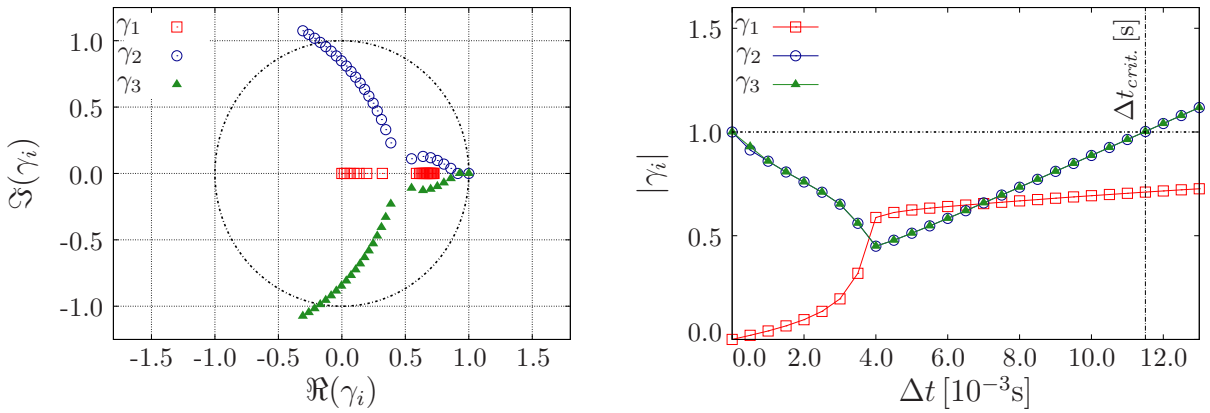

Figure 6.14: *Location of roots of the amplification polynomial for $k^F = 10^{-2}$ m/s, $\Delta x = 1$ m and $\Delta t \in [0, 0.013]$ s.*

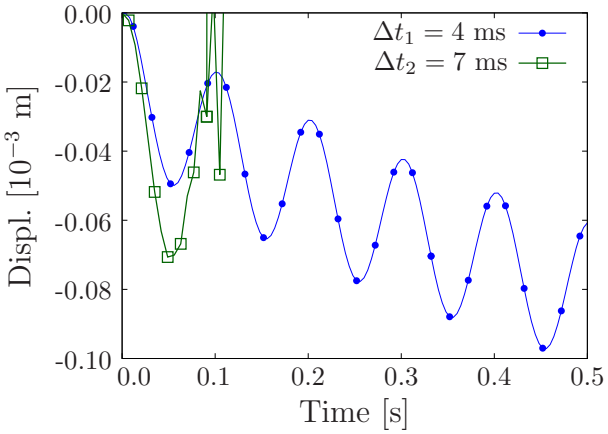

Figure 6.15: *Top displacement of the PMD example depicated in Figure 6.13, calculated at* $\Delta x = 1\,m$. *Parameters taken from Table 6.3.*

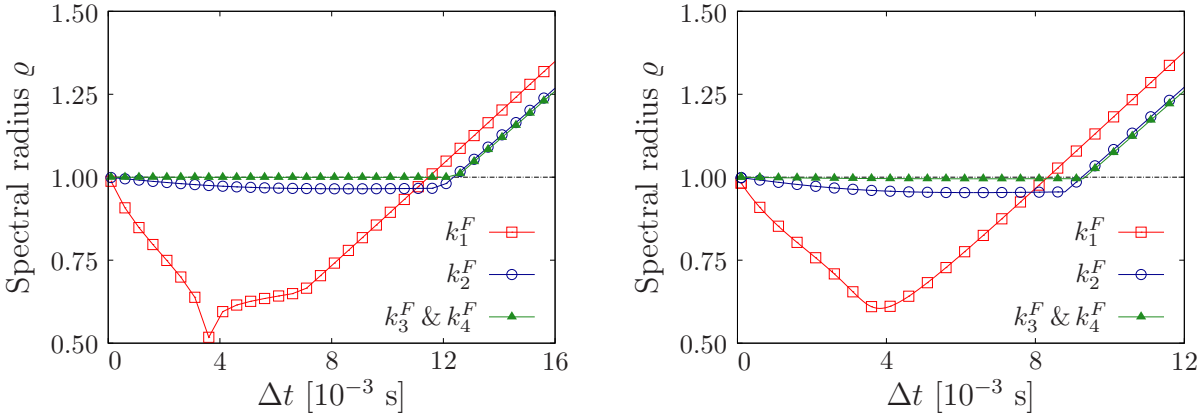

Figure 6.16: *The spectral radii for* $\Delta x = 1\,m$ *(left) and* $\Delta x = 0.75\,m$ *(right) with* $k_1^F = 10^{-2}\,m/s$, $k_2^F = 10^{-3}\,m/s$, $k_3^F = 10^{-5}\,m/s$ *and* $k_4^F = 10^{-10}\,m/s$. *Other parameters taken from Table 6.3.*

line with the conclusions presented in [190], where the critical time-step sizes for different cases have been found via a numerical computation of the whole problem.

Remark: Equation system (6.22) represents a dissipative problem. This is due to the fact that the constitutive equation (3.60) introduced for the extra momentum production yields an increase of the entropy within the system and, thus, renders the problem irreversible, cf. Ehlers [82]. Considering this and following the discussions of Section 5.2, one infers that the instability of the presented OSS indicates the absence of dissipativity of the generated subproblems. In this regard, employing a contractive scheme, for example an implicit monolithic strategy, would have yielded unconditionally stable numerical results. Furthermore, modifying the splitting strategy, such that it produces dissipative subproblems, is another plausible option for obtaining an unconditionally stable solution method.

6.3 A multi-rate example

6.3.1 Model problem

In order to set up a multi-rate problem, consider the rheological model depicted in Figure 6.17. It is a simple coupled system, wherein the motion of the masses m_1 and m_2 are governed by the following set of equations:

$$\mathcal{X} \; : \; \begin{cases} \dot{u}_1 &= v_1 \,, \\ \dot{v}_1 &= \dfrac{1}{m_1} \left[c_2 \, u_2 - (c_1 + c_2) \, u_1 - d \, v_1 \right] \,, \\ \dot{u}_2 &= v_2 \,, \\ \dot{v}_2 &= \dfrac{1}{m_2} \left[c_2 \, (u_1 - u_2) - f^{ext} \right] \,. \end{cases} \tag{6.36}$$

Therein, u_i and v_i, $i = \{1\,,2\}$, represent the displacement and the velocity of the mass m_i, respectively, c_i denotes the stiffness of the springs and d is the damper constant. Furthermore, f^{ext} represents an external load acting on the mass m_2.

Introducing $\mathbf{u} = [u_1\,, v_1\,, u_2\,, v_2]^T$ as the vector of unknowns for this problem, (6.36) reads in the compact form

$$\mathcal{X} \; : \; \dot{\mathbf{u}}(t) = \overline{\mathfrak{S}}\, \mathbf{u}(t) + \mathfrak{f}(t) =: \boldsymbol{f}(\mathbf{u}(t), t) \,, \tag{6.37}$$

wherein, $\mathfrak{f} := [0\,, 0\,, 0\,, -f^{ext}]^T$ and, furthermore,

$$\overline{\mathfrak{S}} := \begin{bmatrix} 0 & 1 & 0 & 0 \\ -\dfrac{c_1 + c_2}{m_1} & -\dfrac{d}{m_1} & \dfrac{c_2}{m_1} & 0 \\ 0 & 0 & 0 & 1 \\ \dfrac{c_2}{m_2} & 0 & -\dfrac{c_2}{m_2} & 0 \end{bmatrix} . \tag{6.38}$$

6.3.2 Decoupled solution scheme

Depending on the material parameters of the problem, the masses m_1 and m_2 may oscillate with considerably different frequencies. This scenario motivates a decoupled solution

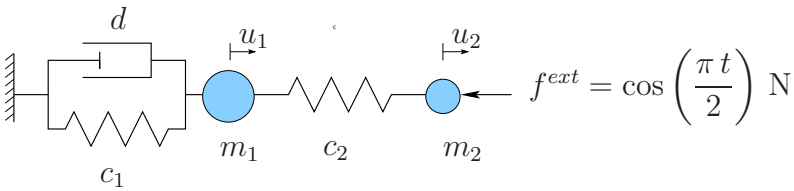

Figure 6.17: *The rheological model for the multi-rate problem.*

of the problem, using different time-step sizes for the temporal discretisation of the corresponding equations of motions. It can be done by splitting the operator $\overline{\mathfrak{S}}$ in such a way that it generates two subproblems, each of which describing the motion of merely one of the point masses. In this regard, a feasible split of $\overline{\mathfrak{S}}$ reads

$$\overline{\mathfrak{S}}_1 := \begin{bmatrix} 0 & 1 & 0 & 0 \\ -\dfrac{c_1+c_2}{m_1} & -\dfrac{d}{m_1} & \dfrac{c_2}{m_1} & 0 \\ 0 & 0 & 0 & 0 \\ 0 & 0 & 0 & 0 \end{bmatrix}, \quad \overline{\mathfrak{S}}_2 := \begin{bmatrix} 0 & 0 & 0 & 0 \\ 0 & 0 & 0 & 0 \\ 0 & 0 & 0 & 1 \\ \dfrac{c_2}{m_2} & 0 & -\dfrac{c_2}{m_2} & 0 \end{bmatrix}. \tag{6.39}$$

Following that, the decoupled system generated by the above sub-operators reads

$$\mathcal{X} \;:\; \begin{cases} \mathcal{X}^1 \;:\; \dot{\mathfrak{u}} = \overline{\mathfrak{S}}_1\,\mathfrak{u} =: \boldsymbol{f}_1(\mathfrak{u})\,, \\ \\ \mathcal{X}^2 \;:\; \dot{\mathfrak{u}} = \overline{\mathfrak{S}}_2\,\mathfrak{u} + \mathfrak{f}(t) =: \boldsymbol{f}_2(\mathfrak{u})\,, \end{cases} \quad \text{with} \quad \boldsymbol{f}_1 + \boldsymbol{f}_2 = \boldsymbol{f}\,. \tag{6.40}$$

Successive integration of the subproblems reveals the response of the system to the external stimuli. To elucidate this procedure for a multi-rate problem, assume that the states of m_2 alter with a much higher frequency compared with the alterations in the states of m_1. In this case, the time-step size Δt_2 used for integration of the faster subproblem $\mathcal{X}^2$ shall be smaller than the step size Δt_1 employed for integration of the slower subproblem $\mathcal{X}^1$. Considering this, and assuming that $\Delta t_1 = s\,\Delta t_2$, $s \in \mathbb{N}$, the time marching may be executed according procedure (4.30) introduced in Section 4.3.1, and reads as follows (cf. Figure 6.18):

Multi-rate time integration based on the CSS

(1) Predict the variables of the slower subsystem $\mathcal{X}^1$, and replace them in the faster subsystem $\mathcal{X}^2$.
(2) Using $\Delta t_2 = \Delta t_1/s$, integrate the faster subsystem $\mathcal{X}^2$. This step shall be repeated s times.
(3) Substitute the output of the last step in $\mathcal{X}^1$.
(4) Advance $\mathcal{X}^1$ using the time-step size $\Delta t_1 = s\,\Delta t_2$.

(6.41)

6.3.3 Stability analysis

Utilising the trapezoidal rule (TR) for temporal discretisation, the FD stencil corresponding to the fast subproblem $\mathcal{X}^2$ reads

$$\mathcal{X}^2 \;:\; \begin{cases} \dfrac{u_2^{n+(k+1)} - u_2^{n+(k)}}{\Delta t_2} &= v_2^{(k)+1/2}\,, \\ \\ \dfrac{v_2^{n+(k+1)} - v_2^{n+(k)}}{\Delta t_2} &= \dfrac{1}{m_2}\left[c_2\,(u_1^n - u_2^{(k)+1/2}) - (f^{ext})^{(k)+1/2}\right], \end{cases} \tag{6.42}$$

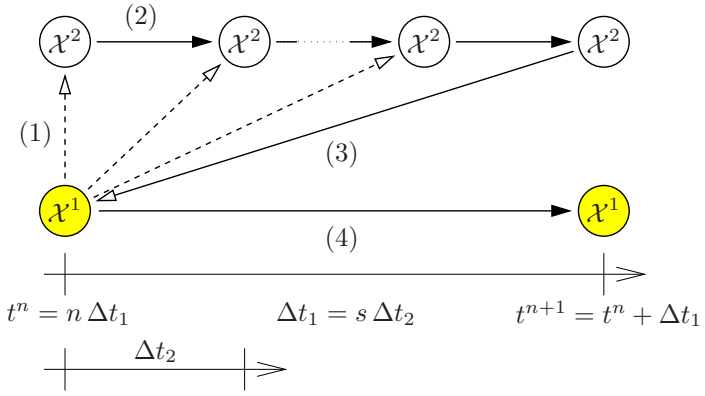

Figure 6.18: *Multi-time integration scheme proposed for (6.36).*

wherein $k \in [0\,,\,s] \subset \mathbb{N}$ is the counter for the sub-cycles, $(\,\bullet\,)^{n+(k)}$ represents the calculated variable at time $t = n\,\Delta t_1 + k\,\Delta t_2$, and $(\,\bullet\,)^{(k)+1/2} := \frac{1}{2}\,[(\,\bullet\,)^{n+(k+1)} + (\,\bullet\,)^{n+(k)}]$. Performing the above integration for s cycles eventually reveals the values of u_2^{n+1} and v_2^{n+1} at time $t = \underbrace{n\,\Delta t_1}_{t^n} + \underbrace{s\,\Delta t_2}_{\Delta t_1} =: t^{n+1}$. These values are then replaced in the slower subproblem and, thus, the FD stencil corresponding to $\mathcal{X}^1$ reads

$$\mathcal{X}^1 \;:\; \begin{cases} \dfrac{u_1^{n+1} - u_1^n}{\Delta t_1} &=& v_1^{n+1/2}\,, \\[2ex] \dfrac{v_1^{n+1} - v_1^n}{\Delta t_1} &=& \dfrac{1}{m_1}\left[c_2\,u_2^{n+1} - (c_1 + c_2)\,u_1^{n+1/2} - d\,v_1^{n+1/2}\right]\,. \end{cases} \tag{6.43}$$

Exploiting (6.42) and (6.43) to assemble the amplification matrix $\mathbf{G}$ and subsequently the Hurwitz polynomial G_H shows that the latter is a polynomial of order 4. Investigating the coefficients of the Hurwitz polynomial in the light of the LCC reveals that the corresponding parameters, namely β_0, β_1, Δ_3, β_3 and β_4, are all positive and, thus, the proposed solution method is unconditionally stable. This is in line with the results obtained by Smolinski *et al.* [254] for a similar solution algorithm.

6.3.4 Numerical example

In order to investigate the validity of the results obtained from the stability analysis and also to examine the applicability of the proposed solution method, a numerical benchmark example with the material parameters presented in Table 6.4 has been considered.

It has been observed that for these parameters, the norms of roots of the amplification polynomial remain always smaller than unity, cf. Figure 6.19. It approves the unconditional stability of the scheme. Next, the problem has been solved monolithically and also following the herein-presented decoupled solution strategy. The monolithic time integration has been performed using a constant time-step size $\Delta t_{monol.} = 0.1\,\mathrm{s}$, whereas the integration for the decoupled scheme has been executed employing $\Delta t_1 = 10\,\Delta t_2 =: 10\,\Delta t_{monol.}$. The results are also presented in Figure 6.19 and show, firstly, the stability of scheme and, secondly, the good agreement between results obtained from the decoupled scheme with those of the monolithic solver.

Parameter	Symbol	Value	SI unit
Mass no. 1	m_1	20	kg
Mass no. 2	m_2	5	kg
Stiffness of spring no. 1	c_1	1	N/m
Stiffness of spring no. 2	c_2	1	N/m
Damper constant	d	10	N s/m

Table 6.4: *Material parameters for the multi-rate example*

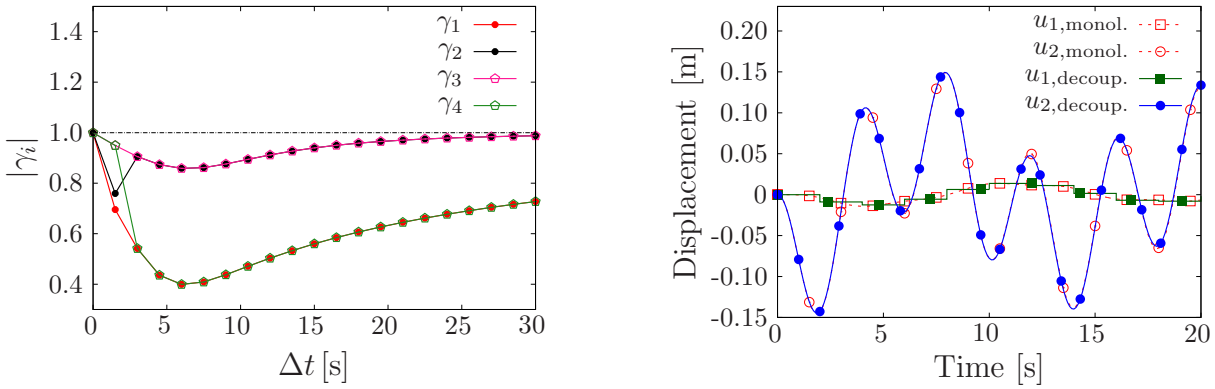

Figure 6.19: *Evolution of the roots of the amplification polynomial in response to alteration of the time-step size (left) and the calculated displacements obtained from monolithic and decoupled treatment of (6.36) (right).*

Chapter 7:
Applications: Part II – Surface-Coupled Problems

Examples for the volume-coupled problems were presented in the preceding chapter. In what follows, three examples belonging to the class of surface-coupled problems will be presented. Analogous to the procedure of the last chapter, each example is put in a section, comprising four subsections: (i) the model problem, presenting the mathematical model of the case at hand, (ii) selected decoupled solution strategies, (iii) stability analysis, and (iv) benchmark numerical examples.

7.1 Fluid-structure interaction (FSI)

Consider a 1-d rheological model as shown in Figure 7.1. Therein, one distinguishes between a linear elastic solid subsystem $\mathcal{X}^S$ and a compressible, viscous fluid subsystem $\mathcal{X}^F$, which are interacting via an interface membrane. The system of governing equations for this model reads

$$\mathcal{X}^F : \begin{cases} \dot{u}_F &= v_F \,, \\ \dot{v}_F &= \dfrac{1}{m_F} \left(f_F^{int} - f_{vis} \right) , \end{cases} \qquad \mathcal{X}^S : \begin{cases} \dot{u}_S &= v_S \,, \\ \dot{v}_S &= \dfrac{1}{m_S} \left(f_S^{int} - c_S \, u_S \right) , \end{cases} \tag{7.1}$$

where $m_{\mathfrak{a}}$ with $\mathfrak{a} = \{F \,, S\}$ is the mass, $u_{\mathfrak{a}}$ and $v_{\mathfrak{a}}$ are the displacement and velocity of $m_{\mathfrak{a}}$, $f_{\mathfrak{a}}^{int}$ is the force that is exerted by the interface on $m_{\mathfrak{a}}$, $c_{\mathfrak{a}}$ is the spring constant, d_F denotes the damper constant and f_{vis} represents the internal force in $\mathcal{X}^F$, such that

$$\dot{f}_{vis} = c_F \, v_F - \frac{c_F}{d_F} \, f_{vis} \,. \tag{7.2}$$

Moreover, the kinematic consistency at the interface and equilibrium of the interface traction forces yield

$$u_S = u_F \quad \text{and} \quad f_S^{int} + f_F^{int} = 0 \,. \tag{7.3}$$

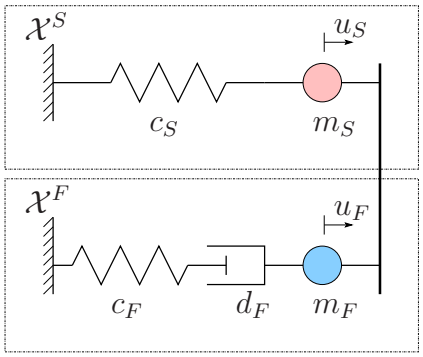

Figure 7.1: *The rheological model for the FSI.*

7.1.1 Decoupled solution schemes

The block-Gauss-Seidel staggered integration strategy (cf. Section 4.3.1) provides a suitable framework for the decoupled solution of the problem at hand. In this regard, considering $\mathbf{u}_\mathfrak{a} = [u_\mathfrak{a}\,, v_\mathfrak{a}]^T$ as the vector of unknowns in the subproblem $\mathcal{X}^\mathfrak{a}$ and based on choosing $\mathbf{u}_\mathfrak{a}^p$ as a predictor for $\mathbf{u}_\mathfrak{a}^{n+1}$, one comes up with two different solution algorithms. In the first one, hereafter called the *FS* scheme, one proceeds from a predictor $\mathbf{u}_S^p$ for the solid subsystem, and the time integration is performed as per the following sequence:

The *FS* scheme

(1) **Kinematic constraint:** insert $\mathbf{u}_F^p = \mathbf{u}_S^p$ in $\mathcal{X}^F$.
(2) **Fluid integration:** using the predictor $\mathbf{u}_F^{n+1} = \mathbf{u}_F^p$, advance $\mathcal{X}^F$ and compute f_F^{n+1}.
(3) **Balance of forces:** insert $f_S^{n+1} = -f_F^{n+1}$ in $\mathcal{X}^S$.
(4) **Solid integration:** employing f_S^{n+1}, advance $\mathcal{X}^S$ and find $\mathbf{u}_S^{n+1}$.

(7.4)

In the second solution algorithm, hereafter called the *SF* scheme, one proceeds from a predictor for the fluid degrees of freedom $\mathbf{u}_F^p$, and the time integration is performed in a reverse sequence:

The *SF* scheme

(1) **Kinematic constraint:** insert $\mathbf{u}_S^p = \mathbf{u}_F^p$ in $\mathcal{X}^S$.
(2) **Solid integration:** using the predictor $\mathbf{u}_S^{n+1} = \mathbf{u}_S^p$, advance $\mathcal{X}^S$ and compute f_S^{n+1}.
(3) **Balance of forces:** insert $f_F^{n+1} = -f_S^{n+1}$ in $\mathcal{X}^F$.
(4) **Fluid integration:** employing f_F^{n+1}, advance $\mathcal{X}^F$ and find $\mathbf{u}_F^{n+1}$.

(7.5)

7.1.2 Stability analysis

Using the TR for temporal discretisation of the equations and following the stability analysis procedure of Section 5.4.2, one ends up for both cases with a 3rd-order Hurwitz polynomial and, consequently, by help of Table 5.1, the LCC is satisfied if and only if

$$\{\beta_0,\, \beta_1,\, \Delta_2,\, \beta_3\} \geq 0\,. \tag{7.6}$$

Considering $G_H^{FS}(s)$ and $G_H^{SF}(s)$, it can be shown that (7.6) is satisfied as long as Δt remains smaller than or equal to the following critical time-step sizes:

$$\Delta t_{crit.}^{FS} = \frac{2\, m_S\, c_F}{d_F\,(c_F + c_S)} \quad \text{and} \quad \Delta t_{crit.}^{SF} = \frac{2}{c_S}\sqrt{c_S\, m_F}\,. \tag{7.7}$$

From these results, it is obvious that both decoupled solution schemes are only conditionally stable. Moreover, it can be seen that the sequence of integration has a direct influence

Parameter	Symbol	Value	SI unit
Mass in $\mathcal{X}^S$	m_S	20	kg
Mass in $\mathcal{X}^F$	m_F	10	kg
Spring constant in $\mathcal{X}^S$	c_S	80	N/m
Spring constant in $\mathcal{X}^F$	c_F	40	N/m
Damper constant	d_F	10	N s/m

Table 7.1: *Material parameters for the FSI example problem.*

on $\Delta t_{crit.}$ and, hence, must be chosen carefully according to corresponding fluid and solid material parameters. It supports the fact that, in general, the sequence of integration of the subsystems is crucial to determine the efficiency or even the success or failure of a method, which is based on the Gauss-Seidel procedure [152]. Furthermore, both of the amplification matrices, $\mathbf{G}^{FS}$ and $\mathbf{G}^{SF}$, are normal and, therefore, (7.7) represents the necessary and sufficient stability condition for the *FS* and *SF* decoupled solution schemes.

7.1.3 Numerical example

Consider the material parameters given in Table 7.1. Accordingly, from (7.7), one finds

$$\Delta t^{FS}_{crit.} = \frac{4}{3} \approx 1.3\,\mathrm{s} \quad \text{and} \quad \Delta t^{SF}_{crit.} = \frac{\sqrt{2}}{2} \approx 0.7\,\mathrm{s}\,. \tag{7.8}$$

Therefore, (5.82) is satisfied as long as Δt is smaller than the corresponding $\Delta t_{crit.}$ given by (7.8), see Figures 7.2 and 7.3. It is interesting to note that for this specific case, $\Delta t^{FS}_{crit.}$ is almost twice as big as $\Delta t^{SF}_{crit.}$. That means, the *FS* solver has the potential to integrate a specific time interval with only half as much steps as the *SF* algorithm. It demonstrates the importance of performing the stability analysis and accordingly decide on the sequence of integration prior solving the problem. To verify this result, an initial perturbation in form of $u^0_S = u^0_F = 1\,\mathrm{m}$ is considered. Then, the *FS* and the *SF* solvers

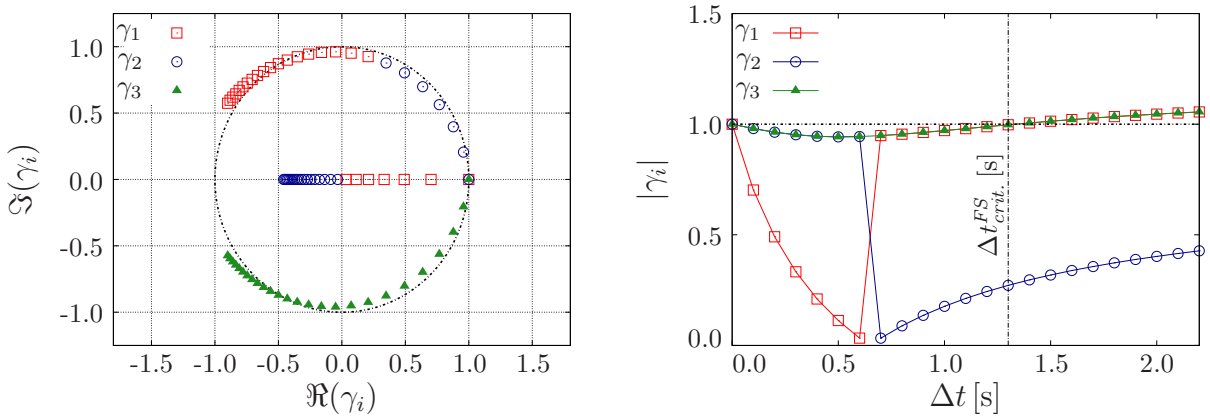

Figure 7.2: *Location of roots of the amplification polynomial for the FS decoupled solution scheme for* $\Delta t \in [0, 2.2]$ *s.*

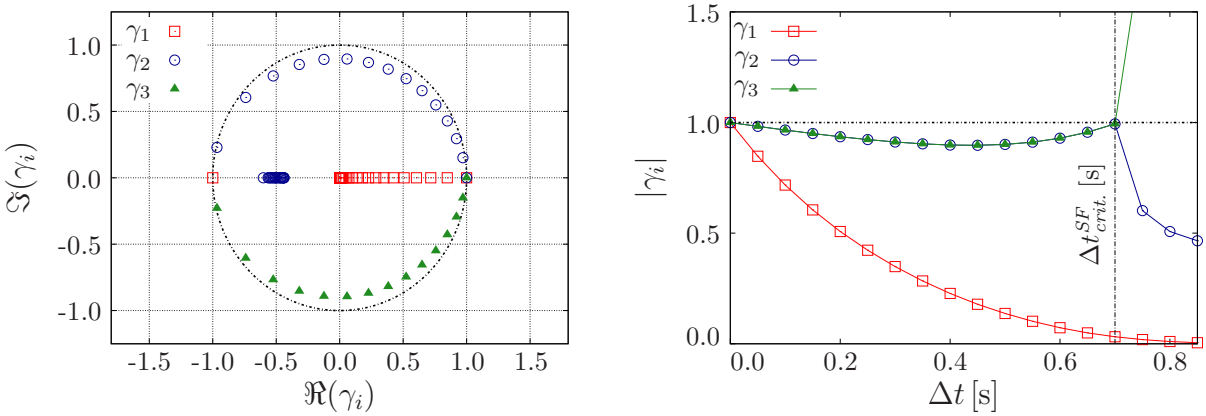

Figure 7.3: *Location of roots of the amplification polynomial for the SF decoupled solution scheme for* $\Delta t \in [0, 0.85]$ *s.*

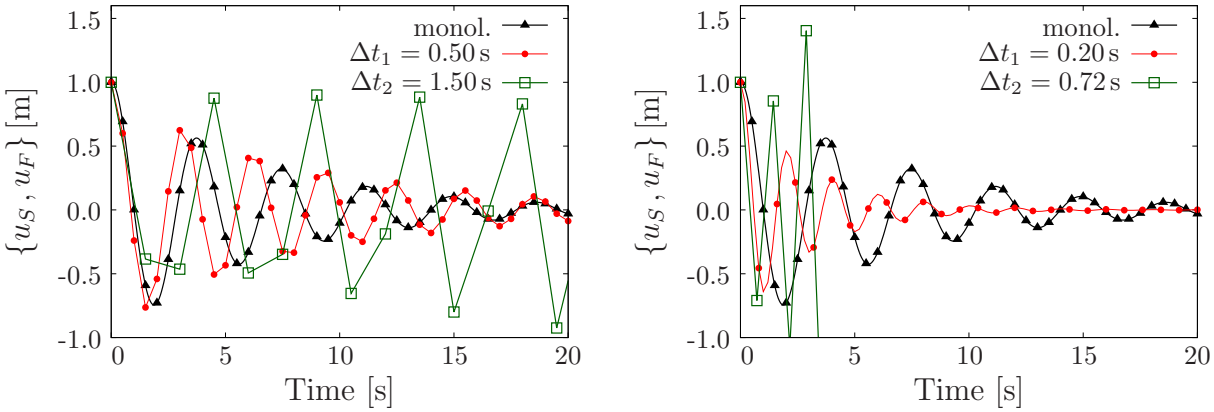

Figure 7.4: *Evolution of the interface displacement for FS (left) and SF (right) decoupled solution schemes.*

are used to compute the evolution of the interface displacement as time elapses and the results for exemplary time-step sizes are depicted in Figure 7.4. It is apparent that for each case the solution is stable as long as $\Delta t \leq \Delta t_{crit.}$. Furthermore, it is seen that the stable results calculated via the *SF* method have a low accuracy. This, however, does not contradict the stability of the scheme, cf. the remarks at the end of Chapter 5.

7.2 Structure-structure interaction (SSI)

Consider the rheological model in Figure 7.5 adopted from [152]. Therein, $\mathcal{X}^{S_e}$ represents an elastic solid subsystem with the following governing equations system:

$$\mathcal{X}^{S_e} \; : \; \begin{cases} \dot{u}^1_{S_e} &= v^1_{S_e}\,, \\ \dot{u}^2_{S_e} &= v^2_{S_e}\,, \\ \dot{v}^1_{S_e} &= \dfrac{1}{m^1_{S_e}} \left[c^2_{S_e} \left(u^2_{S_e} - u^1_{S_e} \right) - c^1_{S_e}\, u^1_{S_e} \right], \\ \dot{v}^2_{S_e} &= \dfrac{1}{m^2_{S_e}} \left[f^{int}_{S_e} + c^2_{S_e} \left(u^1_{S_e} - u^2_{S_e} \right) \right]. \end{cases} \tag{7.9}$$

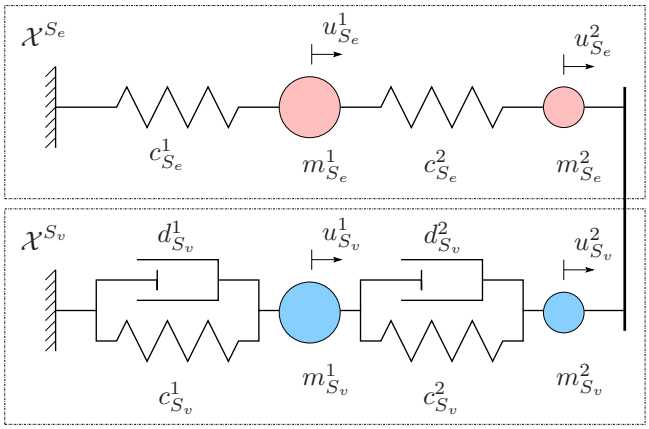

Figure 7.5: *The rheological model for the SSI [152].*

Furthermore, $\mathcal{X}^{S_v}$ represents a viscoelastic solid subsystem governed by the following relations:

$$\mathcal{X}^{S_v} \; : \; \begin{cases} \dot{u}^1_{S_v} &= v^1_{S_v}\,, \\ \dot{u}^2_{S_v} &= v^2_{S_v}\,, \\ \dot{v}^1_{S_v} &= \dfrac{1}{m^1_{S_v}} \left[c^2_{S_v}\,(u^2_{S_v} - u^1_{S_v}) + d^2_{S_v}\,(v^2_{S_v} - v^1_{S_v}) - c^1_{S_v}\,u^1_{S_v} - d^1_{S_v}\,v^1_{S_v} \right], \\ \dot{v}^2_{S_v} &= \dfrac{1}{m^2_{S_v}} \left[f^{int}_{S_v} + c^2_{S_v}\,(u^1_{S_v} - u^2_{S_v}) + d^2_{S_v}\,(v^1_{S_v} - v^2_{S_v}) \right]. \end{cases} \tag{7.10}$$

In the above relations, $m^i_{\mathfrak{a}}$ represents the i-th mass in the subsystem $\mathcal{X}^{\mathfrak{a}}$ with $\mathfrak{a} = \{S_e\,, S_v\}$, and $u^i_{\mathfrak{a}}$ and $v^i_{\mathfrak{a}}$ are the displacement and velocity of $m^i_{\mathfrak{a}}$. Moreover, $f_{\mathfrak{a}}$ is the force that is exerted by the interface on $m^2_{\mathfrak{a}}$, $c^i_{\mathfrak{a}}$ is the spring constant and $d^i_{S_v}$ denotes the damper constant. For simplicity, it is also assumed that $c^1_{\mathfrak{a}} = c^2_{\mathfrak{a}}$, $d^1_{S_v} = d^2_{S_v}$, $m^1_{S_e} = 2\,m^2_{S_e}$ and $m^1_{S_v} = 2\,m^2_{S_v}$. Furthermore, the kinematic consistency at the interface in contribution with the equilibrium of the interface traction forces yield

$$u^2_{S_e} = u^2_{S_v} \quad \text{and} \quad f^{int}_{S_e} + f^{int}_{S_v} = 0\,. \tag{7.11}$$

7.2.1 Decoupled solution schemes

Introducing $\mathfrak{u}_{\mathfrak{a}}$ as the state vector for $\mathcal{X}^{\mathfrak{a}}$, and $\mathfrak{u}^p_{\mathfrak{a}}$ as the vector of predicted values, one ends up with the following staggered solution methods, (cf. procedures (7.4) and (7.5)):

The *SvSe* scheme

(1) **Kinematic constraint:** insert $\mathfrak{u}^p_{S_v} = \mathfrak{u}^p_{S_e}$ in $\mathcal{X}^{S_v}$.
(2) **Integrate $\mathcal{X}^{S_v}$:** advance $\mathcal{X}^{S_v}$ and compute $f^{n+1}_{S_v}$.
(3) **Balance of forces:** insert $f^{n+1}_{S_e} = -f^{n+1}_{S_v}$ in $\mathcal{X}^{S_e}$.
(4) **Integration $\mathcal{X}^{S_e}$:** advance $\mathcal{X}^{S_e}$ and find $\mathfrak{u}^{n+1}_{S_e}$.

(7.12)

The *SeSv* scheme

(1) **Kinematic constraint:** insert $\mathbf{u}^p_{S_e} = \mathbf{u}^p_{S_v}$ in $\mathcal{X}^{S_e}$.
(2) **Integrate $\mathcal{X}^{S_e}$:** advance $\mathcal{X}^{S_e}$ and compute $f^{n+1}_{S_e}$.
(3) **Balance of forces:** insert $f^{n+1}_{S_v} = -f^{n+1}_{S_e}$ in $\mathcal{X}^{S_v}$.
(4) **Integration $\mathcal{X}^{S_v}$:** advance $\mathcal{X}^{S_v}$ and find $\mathbf{u}^{n+1}_{S_v}$.

(7.13)

7.2.2 Stability analysis

Discretising the equations using the TR and, subsequently, assembling the amplification matrices and the amplification polynomials, one ends up with a 6th-order Hurwitz polynomial for both cases. Therefore, following the LCC and Table 5.1, the necessary stability condition reads

$$\{\beta_0, \beta_1, \beta_3, \beta_5, \beta_6, \Delta_3, \Delta_5\} \geq 0 \ . \tag{7.14}$$

Investigating the conditions under which the coefficients of $G_H^{SeSv}(s)$ and $G_H^{SvSe}(s)$ are positive yields

$$\Delta t^{SvSe}_{crit.} = \frac{1}{c_{S_v}} \left(\sqrt{(d_{S_v})^2 + 2\, m^1_{S_e}\, c_{S_v}} - d_{S_v} \right) \quad \text{and} \quad \Delta t^{SeSv}_{crit.} = \frac{1}{c_{S_e}} \sqrt{2\, c_{S_e}\, m^1_{S_v}} \, . \tag{7.15}$$

However, the expressions obtained for the Hurwitz determinants Δ_3 and Δ_5 are too complicated and, hence, the condition under which they remain positive must be checked numerically as is done in the next section. Nevertheless, it is already obvious that both schemes are only conditionally stable.

7.2.3 Numerical example

Consider the material properties in Table 7.2. Insertion of these values in the expressions presented in (7.14) yields

$$\Delta t^{SvSe}_{crit.} \approx 1.4\,\mathrm{s} \quad \text{and} \quad \Delta t^{SeSv}_{crit.} \approx 0.7\,\mathrm{s} \, . \tag{7.16}$$

Looking at Figures 7.6 and 7.7 shows that for both cases the von Neumann stability condition is satisfied as long as the corresponding critical time-step sizes given by (7.16) are not violated. Furthermore, the considerable difference between $\Delta t^{SvSe}_{crit.}$ and $\Delta t^{SeSv}_{crit.}$ shows the potential difference in efficiencies of the schemes, in response to reverting the sequence of integration of the subsystems.

To verify these results, an initial perturbation in the form of $u^1_{S_e}|_{t=0} = u^1_{S_v}|_{t=0} = 1\,\mathrm{m}$ is applied to the system and the response is numerically computed, see Figure 7.8. One can see that in each case the solution is stable only if $\Delta t < \Delta t_{crit.}$. It is worth mentioning that the low accuracy of the stable results obtained via the *SeSv* method does not disagree with the stability of the scheme, as mentioned before.

Parameter	Symbol	Value	SI unit
Mass no. 1 in $\mathcal{X}^{S_e}$	$m^1_{S_e}$	20	kg
Mass no. 2 in $\mathcal{X}^{S_e}$	$m^2_{S_e}$	40	kg
Mass no. 1 in $\mathcal{X}^{S_v}$	$m^1_{S_v}$	10	kg
Mass no. 2 in $\mathcal{X}^{S_v}$	$m^2_{S_v}$	20	kg
Spring constant in $\mathcal{X}^{S_e}$	c_{S_e}	80	N/m
Spring constant in $\mathcal{X}^{S_v}$	c_{S_v}	40	N/m
Damper constant	d_{S_v}	0.05	N s/m

Table 7.2: *Material parameters for the SSI example problem*

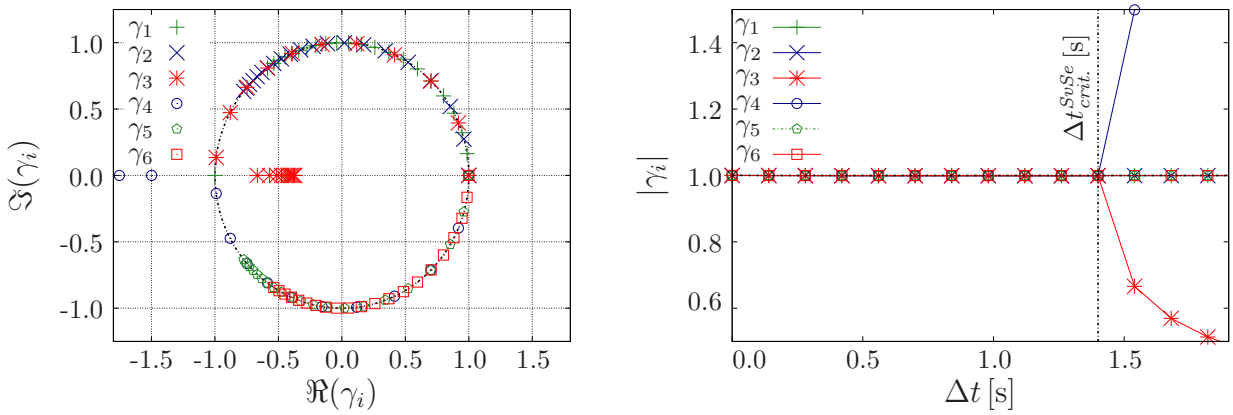

Figure 7.6: *Location of roots of the amplification polynomial for the SvSe decoupled solution scheme for* $\Delta t \in [0, 1.9]\,s$.

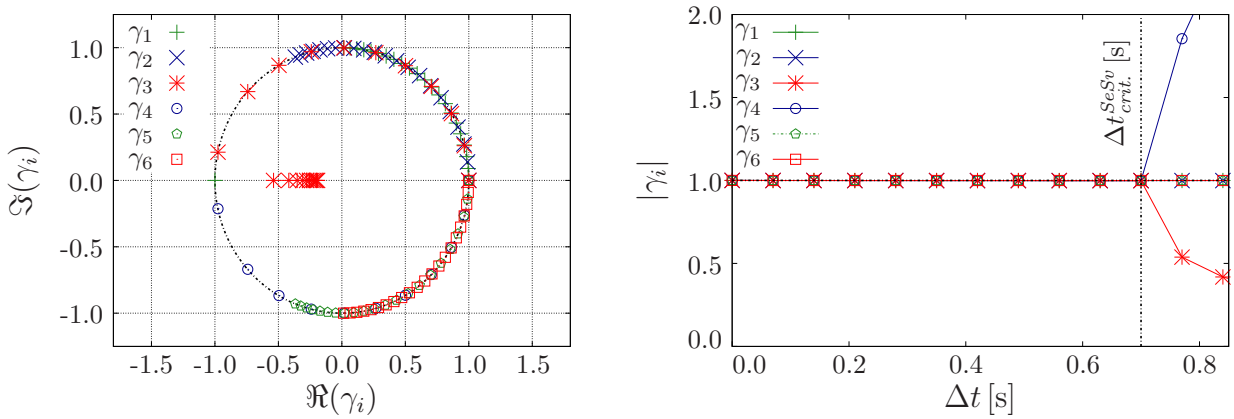

Figure 7.7: *Location of roots of the amplification polynomial for the SeSv decoupled solution scheme for* $\Delta t \in [0, 0.85]\,s$.

7.3 Fluid-porous-medium interaction (FPMI)

The fluid-porous-media interaction (FPMI) refers to a surface interaction among several non-overlapping subsystems, composed of either a bulk fluid or a porous medium. This could be the interaction of blood with a blood vessel wall, a body of water with an

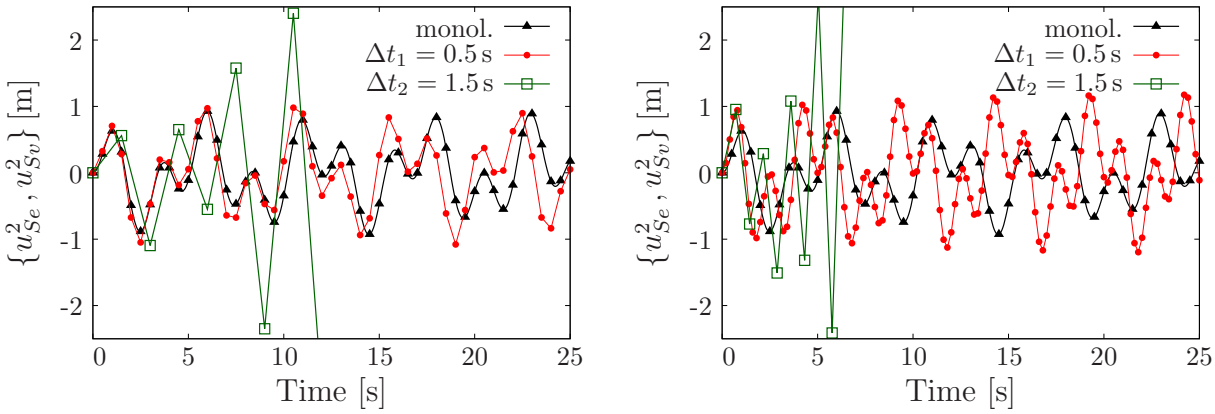

Figure 7.8: *Evolution of the interface displacement for SvSe (left) and SeSv (right) decoupled solution schemes.*

earth-dam structure, or acoustic waves with acoustic panels used in soundproofing, etc.

In this section, a partitioned scheme for the numerical simulation of the surface-coupled problem of FPMI is proposed by adopting the method of localised Lagrange multipliers (cf. Section 4.3.2), which facilitates an automatic spatial partitioning of the problem and a parallel treatment of the interacting components. Moreover, proceeding from the interaction between an incompressible bulk fluid with a saturated biphasic porous medium composed of intrinsically incompressible and inert constituents, the characteristics of the governing equations are scrutinised, and the various constraints within the subsystems are identified. Following this, the method of perturbed Lagrange multipliers (cf. Section 3.4.1) is used to replace the constrained equation systems within each subdomain by unconstrained ones. Furthermore, considering the 1-d version of the equations, a stability analysis of the proposed solution method is performed, and the unconditional stability of the partitioned solution scheme is shown. Solving 1-d and 2-d numerical benchmark examples, the applicability of the proposed scheme is demonstrated.

7.3.1 Model problem

Consider an incompressible and inviscid fluid φ^L interacting with one biphasic, fluid-saturated porous medium φ^P, composed of intrinsically incompressible and inert constituents, namely one elastic solid skeleton φ^S and one inviscid pore fluid φ^F. Furthermore, and following the idea of the localised Lagrange-multipliers (LLM) method, consider

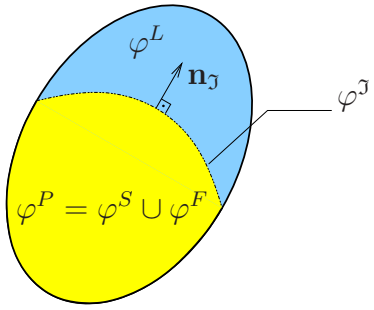

Figure 7.9: *Constituents and domains in FPMI.*

the interface $\varphi^{\mathfrak{I}}$ as an immaterial surface, which acts as an additional subsystem between the interacting subdomains, see Figure 7.9.

For this set up, the set of governing equations comprises the balance relations for the porous medium $\mathcal{X}^P$, plus the ones belonging to the bulk fluid $\mathcal{X}^L$, subjected to specific consistency constraints at the interface $\mathcal{X}^{\mathfrak{I}}$. The governing equations corresponding to the porous medium subdomain can be presented in the framework of the Theory of Porous Media (TPM) and reads (cf. (3.62)):

$$\mathcal{X}^P \; : \; \begin{cases} (\mathbf{u}_S)'_S = \mathbf{v}_S \,, \\ \\ \rho^S \, (\mathbf{v}_S)'_S = \operatorname{div} \mathbf{T}^S_E - n^S \operatorname{grad} p^F \; + \dfrac{(n^F)^2 \, \gamma^{FR}}{k^F} \, \mathbf{w}_F \,, \\ \\ \rho^F \; [(\mathbf{v}_F)'_S + (\operatorname{grad} \mathbf{v}_F) \, \mathbf{w}_F] = -n^F \operatorname{grad} p^F - \dfrac{(n^F)^2 \, \gamma^{FR}}{k^F} \, \mathbf{w}_F \,, \\ \\ 0 = \operatorname{div} (\mathbf{v}_S + n^F \, \mathbf{w}_F) \,. \end{cases} \tag{7.17}$$

Furthermore, the set of governing equations for an incompressible and inviscid fluid is composed of the fluid linear-momentum balance and the continuity condition, cf. Section 3.2.5. Using the notion of material time derivative introduced by (3.53), these equations read

$$\mathcal{X}^L \; : \; \begin{cases} \rho^L \, (\mathbf{v}_L)'_L \;\; = \;\; -\operatorname{grad} p^L \,, \\ \\ \qquad 0 \qquad = \;\; \operatorname{div} \mathbf{v}_L \,. \end{cases} \tag{7.18}$$

Therein, ρ^L is the density, $\mathbf{v}_L$ represents the velocity, and p^L is the hydraulic pressure of the bulk fluid.

Notes on the bulk fluid momentum balance

Equation $(7.18)_1$ represents the Lagrangean version of the bulk fluid linear momentum balance (cf. Section 3.2.1 for discussions about the Lagrangean and the Eulerian representations). It describes the motion of the fluid from the viewpoint of an observer, who moves with the fluid particles. An Eulerian counterpart of this relation could be found by replacing the material time derivative by means of $(3.53)_1$. It yields the description of the motion of the fluid from the viewpoint of a "stationary observer", and reads

$$\rho^L \left[\frac{\partial \mathbf{v}_L}{\partial t} + (\operatorname{grad} \mathbf{v}_L) \, \mathbf{v}_L \right] = -\operatorname{grad} p^L \,. \tag{7.19}$$

From a numerical viewpoint, however, one proceeds from discretised domains, such that "stationary nodes" replace the concept of "stationary observer". As a result, one ends up with a "stationary mesh", in which the first term on the LHS of (7.19) determines the local changes of velocity at each node, and the second term the convection (or advection) with respect to the stationary cells.

Although widely used in computational fluid dynamics, exploiting an Eulerian stationary mesh for the discretisation of fluid bodies with moving boundaries, where the mesh is

supposed to follow the motion of the material at the boundaries, proves to be ineffective. This has motivated the development of the so-called arbitrary Lagrangean-Eulerian (ALE) methods, where the motion of the fluid is described by an observer (a mesh) with "arbitrary motion", see [17, 275] for more details. Alternatively, using the concept of the modified Eulerian description (MED) yields a similar, yet not identical, formulation to the ALE method.

Extensively used in the framework of the TPM, the MED conventionally aims at describing the motion of the pore fluid from the viewpoint of an observer (a mesh), whose motion is identical to that of the porous solid skeleton. A reinterpretation of this idea, in the way explained below, leads to a more general framework for description of the motion of a material by means of a mesh with an "arbitrary motion". The arbitrariness of the motion is in the sense that the mesh may be stationary (Eulerian mesh), may move with the material (Lagrangean mesh), or neither of both. In this regard, considering an exemplary constituent φ^β as the material whose motion should be described, one firstly introduces the mesh as an additional constituent-like φ^M to the domain. Thus, assuming φ^β to be a continuum occupying the whole domain, one can assign a material particle $\mathcal{P}^\beta$ with the actual position vector $\mathbf{x}_\beta$ to each mesh-point $\mathcal{P}^M$ with the actual position vector $\mathbf{x}_M$, such that

$$\mathbf{x}_\beta = \mathbf{x}_M =: \mathbf{x}\,. \tag{7.20}$$

Furthermore, proceeding from individual unique and uniquely invertible motion functions $\boldsymbol{\chi}_\beta$ and $\boldsymbol{\chi}_M$ yields

$$\begin{aligned} \mathbf{x} = \boldsymbol{\chi}_\beta(\mathbf{X}_\beta\,,t) \quad &\Longleftrightarrow \quad \mathbf{X}_\beta = \boldsymbol{\chi}_\beta^{-1}(\mathbf{x}\,,t)\,, \\ \mathbf{x} = \boldsymbol{\chi}_M(\mathbf{X}_M\,,t) \quad &\Longleftrightarrow \quad \mathbf{X}_M = \boldsymbol{\chi}_M^{-1}(\mathbf{x}\,,t)\,, \end{aligned} \tag{7.21}$$

where $\mathbf{X}_\beta$ and $\mathbf{X}_M$, respectively, represent the positions of the material particle $\mathcal{P}^\beta$ and the mesh-point $\mathcal{P}^M$ in the reference configuration at initial time t^0, see Figure 7.10. Subsequently, the velocity fields $\mathbf{v}_\beta$ and $\mathbf{v}_M$ are given by (cf. $(3.52)_1$)

$$\mathbf{v}_\beta := \overset{\prime}{\mathbf{x}}_\beta = \frac{\partial \boldsymbol{\chi}_\beta(\mathbf{X}_\beta\,,t)}{\partial t} \quad \text{and} \quad \mathbf{v}_M := \overset{\prime}{\mathbf{x}}_M = \frac{\partial \boldsymbol{\chi}_M(\mathbf{X}_M\,,t)}{\partial t}\,, \tag{7.22}$$

and the material time derivatives with respect to the motion of the constituent φ^β and

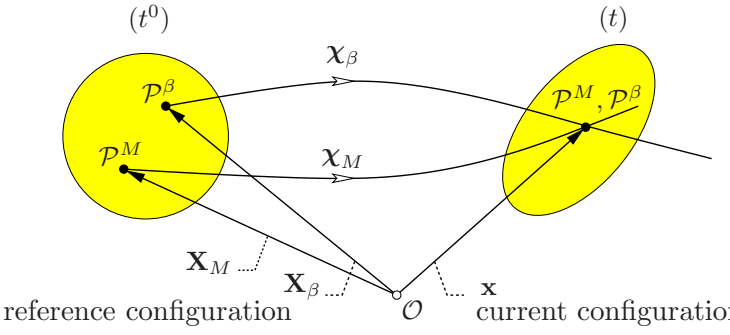

Figure 7.10: *Motion of an exemplary constituent φ^β and the constituent-like mesh φ^M.*

the mesh φ^M, respectively, read (cf. (3.53))

$$(\,\cdot\,)'_\beta := \frac{\mathrm{d}_\beta(\,\cdot\,)}{\mathrm{d}t} = \frac{\partial(\,\cdot\,)}{\partial t} + \operatorname{grad}(\,\cdot\,)\,\mathbf{v}_\beta\,, \quad \text{and} \quad (\,\cdot\,)'_M := \frac{\mathrm{d}_M(\,\cdot\,)}{\mathrm{d}t} = \frac{\partial(\,\cdot\,)}{\partial t} + \operatorname{grad}(\,\cdot\,)\,\mathbf{v}_M\,. \tag{7.23}$$

Thus, the material time derivative of the mechanical quantities in the framework of MED is given by

$$(\,\cdot\,)'_\beta = (\,\cdot\,)'_M + \operatorname{grad}(\,\cdot\,)\,(\mathbf{v}_\beta - \mathbf{v}_M)\,. \tag{7.24}$$

Employing this result allows for a general representation of the thermomechanical balance relations. The generality is such that the Lagrangean and the Eulerian representations of the relations become special cases, which could automatically be achieved by an appropriate choice of the mesh velocity. To demonstrate this, consider the linear momentum balance of the bulk fluid φ^L as given by $(7.18)_1$. Replacing $(\mathbf{v}_L)'_L$ by means of (7.24) yields

$$\rho^L\,[(\mathbf{v}_L)'_M + (\operatorname{grad}\mathbf{v}_L)\,\mathbf{w}_L] = -\operatorname{grad} p^L\,, \tag{7.25}$$

wherein $\mathbf{w}_L := \mathbf{v}_L - \mathbf{v}_M$. Thus,

$$\begin{cases} \mathbf{v}_M \equiv \mathbf{v}_L \;\; \rightarrow \;\; \rho^L\,(\mathbf{v}_L)'_M \equiv \rho^L\,(\mathbf{v}_L)'_L = -\operatorname{grad} p^L\,, & : \text{ Lagrangean rep. } (7.18)_1\,, \\[2ex] \mathbf{v}_M \equiv \mathbf{0} \;\; \rightarrow \;\; \rho^L\left[\dfrac{\partial \mathbf{v}_L}{\partial t} + (\operatorname{grad}\mathbf{v}_L)\,\mathbf{v}_L\right] = -\operatorname{grad} p^L\,, & : \text{ Eulerian rep. } (7.19)\,. \end{cases} \tag{7.26}$$

Equation (7.25) can as well be employed for the description of the motion of a fluid body with moving boundaries. To this end, one can use a mesh which is attached to the boundaries and follows its motion. Nevertheless, the motion of the mesh within the domain can be different than that of the fluid, such that $\mathbf{v}_M$ becomes an additional unknown that shall be determined. It can be done by considering φ^M as a pseudo-material with unit density, the motion of which is governed by

$$\mathcal{X}^M \;:\; \begin{cases} (\mathbf{u}_M)'_M = \mathbf{v}_M\,, \\[2ex] (\mathbf{v}_M)'_M = \operatorname{div}\mathbf{T}^M\,, \end{cases} \tag{7.27}$$

where the second equation is a pseudo-momentum balance for the mesh and the first equation has been added to reduce the order of the time derivative. Next, one needs to select a constitutive relation for the stress tensor $\mathbf{T}^M$. For example, assuming the mesh to behave as an elastic body, the stress tensor $\mathbf{T}^M$ in the geometrically linear regime reads

$$\mathbf{T}^M \approx \boldsymbol{\sigma}^M = 2\,\mu^M\,\boldsymbol{\varepsilon}_M + \lambda^M\,(\boldsymbol{\varepsilon}_M \cdot \mathbf{I})\,\mathbf{I}\,, \tag{7.28}$$

where $\boldsymbol{\varepsilon}_M := \operatorname{sym}(\operatorname{grad}\mathbf{u}_M)$, and λ^M and μ^M should be chosen appropriately. One should, however, note that φ^M plays the role of a fictitious material, which neither interacts with the bulk fluid nor can carry any applied boundary load. Hence, (7.27) can be solved separately from and prior to (7.25) and only in conjunction with a Dirichlet boundary condition, see Section 7.3.2.

Penalty method formulation

Equations (7.17) and (7.18) are systems of DAE, which have to be solved such that the corresponding algebraic constraints, namely the continuity equation in $\mathcal{X}^L$ and the mixture volume balance in $\mathcal{X}^P$, are not violated. Nevertheless, as it was discussed in Section 3.4.1, absence of the pressure variable in the constraints increases the differential index of the equation system and yields difficulties in the numerical solution of the problems. Using the penalty method of Section 3.4.1 one can replace the constrained equation systems with unconstrained ones and, hence, overcome this problem. To this end, consider the following generic coupled DAE system representing (7.17) and, as well, (7.18):

$$\mathcal{X} \;:\; \begin{cases} \boldsymbol{\mathcal{G}}(\boldsymbol{y}, p) = \mathbf{0}\,, \\ \\ \mathcal{H}(\boldsymbol{y}) = 0\,. \end{cases} \tag{7.29}$$

Therein, $\boldsymbol{y}$ depicts the respective kinematic variables, $\boldsymbol{\mathcal{G}}(\boldsymbol{y}\,, p)$ embodies the set of differential equations, and $\mathcal{H}(\boldsymbol{y})$ represents the algebraic constraint. Employing the idea of the penalty-method formulation and introducing Γ as the penalty parameter, one obtains

$$\mathcal{H}(\boldsymbol{y}) = -\frac{1}{\Gamma}\, p \quad \rightarrow \quad p = -\Gamma\, \mathcal{H}(\boldsymbol{y}) \quad \rightarrow \quad \mathcal{X} \;:\; \boldsymbol{\mathcal{G}}(\boldsymbol{y}) = \mathbf{0}\,. \tag{7.30}$$

Applying this model to the equation systems (7.17) and (7.18), the pseudo-constitutive relations for the fluid pressure in $\mathcal{X}^L$ and the pore-fluid pressure in $\mathcal{X}^P$ read

$$p^L = -\Gamma^L \operatorname{div} \mathbf{v}_L\,, \qquad p^F = -\Gamma^P \operatorname{div} (\mathbf{v}_S + n^F\, \mathbf{w}_F)\,. \tag{7.31}$$

Inserting these results in $(7.17)_{2,3}$ and (7.25) yields

$$\mathcal{X}^P \;:\; \begin{cases} (\mathbf{u}_S)'_S = \mathbf{v}_S\,, \\ \\ \rho^S\, (\mathbf{v}_S)'_S = \operatorname{div} \mathbf{T}^S_E + n^S\, \Gamma^P \operatorname{grad} \operatorname{div} (\mathbf{v}_S + n^F\, \mathbf{w}_F) + \dfrac{(n^F)^2\, \gamma^{FR}}{k^F}\, \mathbf{w}_F\,, \\ \\ \rho^F\, [(\mathbf{v}_F)'_S + (\operatorname{grad} \mathbf{v}_F)\, \mathbf{w}_F] = n^F\, \Gamma^P \operatorname{grad} \operatorname{div} (\mathbf{v}_S + n^F\, \mathbf{w}_F) - \dfrac{(n^F)^2\, \gamma^{FR}}{k^F}\, \mathbf{w}_F\,, \end{cases} \tag{7.32}$$

and

$$\mathcal{X}^L \;:\; \rho^L\, [(\mathbf{v}_L)'_M + (\operatorname{grad} \mathbf{v}_L)\, \mathbf{w}_L] = \Gamma^L \operatorname{grad} \operatorname{div} \mathbf{v}_L\,. \tag{7.33}$$

Consequently, the governing equations of both subdomains become merely functions of kinematic variables, such that, after bringing every term on the RHS of the equations (7.32) and (7.33) to the LHS, these can be written in the following compact form:

$$\mathcal{X}^P : \boldsymbol{\mathcal{G}}_P(\boldsymbol{y}_P) = \mathbf{0}\,, \quad \text{and} \quad \mathcal{X}^L : \boldsymbol{\mathcal{G}}_L(\boldsymbol{y}_L) = \mathbf{0}\,, \tag{7.34}$$

wherein $\boldsymbol{y}_P := [\mathbf{u}_S\,, \mathbf{v}_S\,, \mathbf{v}_F]^T$ and $\boldsymbol{y}_L := [\mathbf{v}_L]$.

Remarks:

- The one-way coupling between (7.27) and (7.33) allows for the determination of the mesh motion decoupled from the solution of the bulk-fluid equation of motion. Therefore, $\boldsymbol{y}_M := [\mathbf{u}_M\,,\mathbf{v}_M]^T$ is not included in the set of unknown variables in $(7.34)_2$.
- In principle, the penalty parameter is an arbitrary large number [261] which, provided that the range of the material parameters does not vary too much, is problem-independent [139]. Moreover, numerical experiences with fluids as well as biphasic problems have shown that the influence of alterations of the penalty parameter on the response of the system is negligible [139, 147, 255, 261]. Therefore, a precise estimation of this parameter is generally not necessary. However, the relation proposed by Suh *et al.* [261] provides an approximation for the order of magnitude:

$$\Gamma^P = c\,\tau_0\,\frac{2\,\mu^S + \lambda^S}{n^S}\,, \tag{7.35}$$

  where $c = 10^6$ and τ_0 is a reference time, see [255, 261] and references therein for more details. Here, this value is also exploited for the penalty parameter in the liquid subsystem, i. e., $\Gamma^L = \Gamma^P$.
- The penalty method can be seen as an approximation to the method of Lagrange multipliers, wherein, instead of assuming unknown Lagrange multipliers (here pressures), one proceeds from a constitutive relation for the multipliers as in $(7.30)_2$, and ends up with a modified form of the constraint as in $(7.30)_1$.

The interface

To establish a consistent mathematical model, additional constraints at the interface have to be taken into account. Assuming an interface with a normal motion determined by the normal motion of the solid skeleton, the first constraint reads

$$\mathbf{w}_{S\mathfrak{J}} \cdot \mathbf{n}_{\mathfrak{J}} = 0\,, \tag{7.36}$$

where $\mathbf{w}_{S\mathfrak{J}} := \mathbf{v}_S^{int} - \mathbf{v}_{\mathfrak{J}}$ determines the difference between the solid skeleton velocity $\mathbf{v}_S^{int}$ at the interface and the interface velocity $\mathbf{v}_{\mathfrak{J}}$, and $\mathbf{n}_{\mathfrak{J}}$ is a unit normal vector at the interface pointing from the porous subdomain to the bulk-fluid subdomain, cf. Figure 7.9. Moreover, in order to ensure the conservation of fluid mass and the balance of forces at the interface, the following relations shall be satisfied [191]:

$$\begin{aligned} &\left[\rho^{FR}\,(n^S\,\mathbf{v}_S^{int} + n^F\,\mathbf{v}_F^{int}) - \rho^L\,\mathbf{v}_L^{int}\right]\cdot\mathbf{n}_{\mathfrak{J}} = 0\,,\\ &(\mathbf{T}^S + \mathbf{T}^F - \mathbf{T}^L)\,\mathbf{n}_{\mathfrak{J}} = (\rho^F\mathbf{v}_F^{int}\otimes\mathbf{w}_{F\mathfrak{J}} - \rho^L\,\mathbf{v}_L^{int}\otimes\mathbf{w}_{L\mathfrak{J}})\,\mathbf{n}_{\mathfrak{J}}\,. \end{aligned} \tag{7.37}$$

Therein, $\mathbf{v}_\beta^{int}$ represents the velocity of the constituents at the interface, and $\mathbf{w}_{\beta\mathfrak{J}} := \mathbf{v}_\beta^{int} - \mathbf{v}_{\mathfrak{J}}$ with $\beta = \{L\,,F\,,S\}$. Moreover, assuming an undrained interface, such that no fluid mass exchange between the subsystems takes place, is not only a sufficient condition for satisfaction of the kinematic constraints, but also yields significant simplification of

the equations and, consequently, transparency of the herein-presented solution procedure. In this case, the normal velocity of the bulk fluid at the interface would be identical to the normal velocity of the interface, such that

$$\mathbf{v}_L^{int} \cdot \mathbf{n}_\mathfrak{I} = \mathbf{v}_\mathfrak{I} \cdot \mathbf{n}_\mathfrak{I} \quad \rightarrow \quad \mathbf{w}_{L\mathfrak{I}} \cdot \mathbf{n}_\mathfrak{I} = 0\,. \tag{7.38}$$

Then, having similar fluids in both subsystems such that $\rho^{FR} = \rho^L$ and recalling (7.36), $(7.37)_1$ in conjunction with the saturation condition (3.48) reads

$$(n^S\,\mathbf{v}_\mathfrak{I} + n^F\,\mathbf{v}_F^{int} - \mathbf{v}_\mathfrak{I}) \cdot \mathbf{n}_\mathfrak{I} = 0 \quad \rightarrow \quad \mathbf{v}_F^{int} \cdot \mathbf{n}_\mathfrak{I} = \mathbf{v}_\mathfrak{I} \cdot \mathbf{n}_\mathfrak{I} \quad \rightarrow \quad \mathbf{w}_{F\mathfrak{I}} \cdot \mathbf{n}_\mathfrak{I} = 0\,. \tag{7.39}$$

Consequently, after insertion of $(7.38)_2$ and $(7.39)_3$, $(7.37)_2$ reads

$$\bar{\mathbf{t}}_{int}^S + \bar{\mathbf{t}}_{int}^F + \bar{\mathbf{t}}_{int}^L = \mathbf{0}\,, \tag{7.40}$$

where $\bar{\mathbf{t}}_{int}^\alpha := \mathbf{T}^\alpha\,\mathbf{n}_\mathfrak{I}$, $\alpha = \{F\,, S\}$, and $\bar{\mathbf{t}}_{int}^L := -\mathbf{T}^L\,\mathbf{n}_\mathfrak{I}$ determine the traction forces applied to φ^α and φ^L at the interface. Note that the negative sign in the second equation is due to the fact that $\mathbf{n}_\mathfrak{I}$ is inward oriented with respect to the bulk-fluid subdomain. Nevertheless, using the method of Lagrange multipliers, the multipliers play the role of the interface forces. In particular, as was already discussed in Section 4.3.2, using the LLM method yields automatic satisfaction of balance of forces at the interface, such that there is no need for explicit inclusion of the linear-momentum balance in the interface equation system. Following this, the interface subsystem comprising the kinematic constraints at the interface reads

$$\mathcal{X}^\mathfrak{I} \;:\; \left\{ \begin{array}{l} (\mathbf{v}_S^{int} - \mathbf{v}_\mathfrak{I}) \cdot \mathbf{n}_\mathfrak{I} = 0\,, \\ \\ (\mathbf{v}_F^{int} - \mathbf{v}_\mathfrak{I}) \cdot \mathbf{n}_\mathfrak{I} = 0\,, \\ \\ (\mathbf{v}_L^{int} - \mathbf{v}_\mathfrak{I}) \cdot \mathbf{n}_\mathfrak{I} = 0\,, \end{array} \right. \quad \rightarrow \quad \mathcal{X}^\mathfrak{I} : \boldsymbol{\mathcal{H}}_\mathfrak{I}(\boldsymbol{y}_P\,, \boldsymbol{y}_L\,, \boldsymbol{y}_\mathfrak{I}) = \mathbf{0}\,, \tag{7.41}$$

wherein $\boldsymbol{y}_P := [\mathbf{u}_S\,, \mathbf{v}_S\,, \mathbf{v}_F]^T$, $\boldsymbol{y}_L := [\mathbf{v}_L]$, and $\boldsymbol{y}_\mathfrak{I} := [\mathbf{v}_\mathfrak{I}]$.

Localised Lagrange multipliers

The balance relations $(7.34)_1$ and $(7.34)_2$ together with the constraint $(7.41)_2$ build a problem, the solution of which reveals the response of the system to specific initial and boundary conditions. Following the discussions of Section 4.3.2, the variational version of this problem reads

$$\min_{\boldsymbol{y}} \Pi(\boldsymbol{y}) \quad \text{subjected to } \boldsymbol{\mathcal{H}}_\mathfrak{I} = \mathbf{0}\,, \tag{7.42}$$

where $\boldsymbol{y} := [\boldsymbol{y}_P\,, \boldsymbol{y}_L\,, \boldsymbol{y}_\mathfrak{I}]^T$, and $\Pi := \Pi_P + \Pi_L$ represents the sum of the space-time functionals for the isolated porous medium and the bulk fluid subsystems:

$$\Pi_P = \sum_{i=1}^{3} \int_{V^P} \int_{(\boldsymbol{y}_P)_i} (\boldsymbol{\mathcal{G}}_P)_i \cdot \mathrm{d}(\boldsymbol{y}_P)_i \,\mathrm{d}v\,, \quad \Pi_L = \int_{V^L} \int_{\boldsymbol{y}_L} \boldsymbol{\mathcal{G}}_L \cdot \mathrm{d}\boldsymbol{y}_L \,\mathrm{d}v\,, \tag{7.43}$$

where the binary dot operator implies a scalar (inner) product between vectors, and $V^{\mathfrak{a}}$ with $\mathfrak{a} = \{P\,, L\}$ represents the corresponding volumes of the subdomains as depicted in Figure 7.11. Therein, the spatial domains V^L and V^P are enclosed by the respective boundaries S^L and S^P. Each boundary is further split into two non-overlapping portions, namely an interface boundary $S^{\mathfrak{a}}_{int}$, and an exterior boundary $S^{\mathfrak{a}}_{ext}$, such that $S_{int} := S^{\mathfrak{a}}_{int} = S^L \cap S^P$ and $S^{\mathfrak{a}}_{ext} := S^{\mathfrak{a}} \backslash S_{int}$. Then, following the method of Lagrange multipliers, the constrained problem (7.42) is replaced by an augmented one given by

$$\min_{\boldsymbol{y}\,,\boldsymbol{\ell}} \mathfrak{L}(\boldsymbol{y}\,,\boldsymbol{\ell}) \quad \text{with} \quad \mathfrak{L} := \Pi(\boldsymbol{y}) + \int_{S_{int}} \boldsymbol{\ell}^T \boldsymbol{\mathcal{H}}_{\mathfrak{I}}\, \mathrm{d}a \tag{7.44}$$

with $\mathfrak{L}$ as the Lagrange functional and $\boldsymbol{\ell} := [\ell^S\,, \ell^F\,, \ell^L]^T$ as the vector of localised Lagrange multipliers, which are additional unknowns supposed to be determined via solution of (7.44). To this end, one has to seek for the stationary condition of the Lagrange functional, i. e., $\delta\mathfrak{L}(\boldsymbol{y}\,,\boldsymbol{\ell}) = 0$. This yields the following set of field equations, which describe the behaviour of the system

$$\begin{aligned}
&\int_{V^P} (\boldsymbol{\mathcal{G}}_P)_1 \cdot \delta\mathbf{u}_S\, \mathrm{d}v = 0\,, && \int_{S_{int}} (\ell^S + \ell^F + \ell^L)\, \mathbf{n}_{\mathfrak{I}} \cdot \delta\mathbf{v}_{\mathfrak{I}}\, \mathrm{d}a = 0\,,\\
&\int_{V^P} (\boldsymbol{\mathcal{G}}_P)_2 \cdot \delta\mathbf{v}_S\, \mathrm{d}v + \int_{S_{int}} \ell^S\, \mathbf{n}_{\mathfrak{I}} \cdot \delta\mathbf{v}_S\, \mathrm{d}a = 0\,, && \int_{S_{int}} (\mathcal{H}_{\mathfrak{I}})_1\, \delta\ell^S\, \mathrm{d}a = 0\,,\\
&\int_{V^P} (\boldsymbol{\mathcal{G}}_P)_3 \cdot \delta\mathbf{v}_F\, \mathrm{d}v + \int_{S_{int}} \ell^F\, \mathbf{n}_{\mathfrak{I}} \cdot \delta\mathbf{v}_F\, \mathrm{d}a = 0\,, && \int_{S_{int}} (\mathcal{H}_{\mathfrak{I}})_2\, \delta\ell^F\, \mathrm{d}a = 0\,,\\
&\int_{V^L} \boldsymbol{\mathcal{G}}_L \cdot \delta\mathbf{v}_L\, \mathrm{d}v \quad + \int_{S_{int}} \ell^L\, \mathbf{n}_{\mathfrak{I}} \cdot \delta\mathbf{v}_L\, \mathrm{d}a \;= 0\,, && \int_{S_{int}} (\mathcal{H}_{\mathfrak{I}})_3\, \delta\ell^L\, \mathrm{d}a = 0\,.
\end{aligned} \tag{7.45}$$

Reviewing $(7.45)_2 - (7.45)_4$, it becomes obvious that, therein, the Lagrange multipliers possess an explicit physical meaning, representing the local normal forces acting between the interface and each of the subdomains, cf. Figure 7.11.

7.3.2 Decoupled solution scheme

Spatial discretisation

Following the idea of the FEM, the spatial domains are split into a finite number of elements yielding an approximation of each continuous subdomain $V^{\mathfrak{a}}$ by a discrete one $(V^{\mathfrak{a}})^h$ enclosed by a discrete boundary $(S^{\mathfrak{a}})^h = (S^{\mathfrak{a}}_{int})^h \cup (S^{\mathfrak{a}}_{ext})^h$. It is worth mentioning that the choice of the element types and grid sizes for each subdomain could be done individually, based on the characteristics of that domain, such that in general $(S^L_{int})^h \neq (S^P_{int})^h$. The spatial discretisation of each subdomain then yields a finite-element mesh, including $\mathcal{N}^{\mathfrak{a}}$ nodes and $\mathcal{E}^{\mathfrak{a}}$ elements. Introducing $\overline{\mathcal{N}}^{\mathfrak{a}}$ as the set of boundary nodes, one distinguishes between $\overline{\mathcal{N}}^{\mathfrak{a}}_{int}$ and $\overline{\mathcal{N}}^{\mathfrak{a}}_{ext}$, where the former is the set of boundary nodes belonging to $(S^{\mathfrak{a}}_{int})^h$ and the latter is the set of the nodes existing on $(S^{\mathfrak{a}}_{ext})^h$, and $\overline{\mathcal{N}}^{\mathfrak{a}} = \overline{\mathcal{N}}^{\mathfrak{a}}_{int} \cup \overline{\mathcal{N}}^{\mathfrak{a}}_{ext}$. Moreover, the following trial functions are defined:

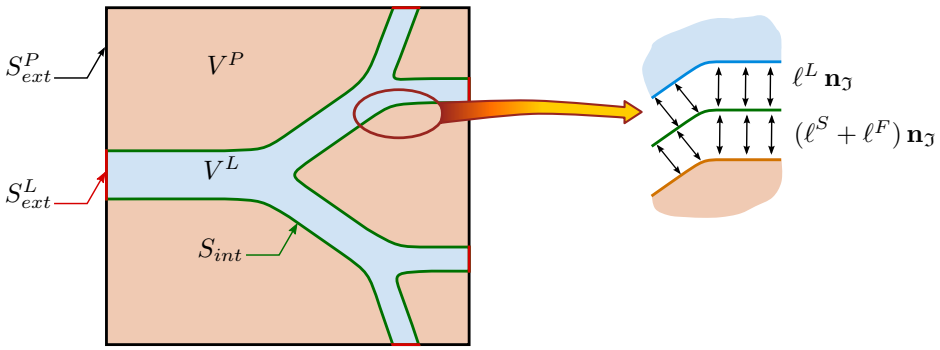

Figure 7.11: *Domains, boundaries and localised Lagrange multipliers.*

$$\begin{aligned}
&\mathbf{u}_S \approx \mathbf{u}_S^h = \mathbf{U}_S\,\mathbf{u}_S^{nd}\,, \quad && \mathbf{v}_S \approx \mathbf{v}_S^h = \mathbf{V}_S\,\mathbf{v}_S^{nd}\,, && \mathbf{v}_F \approx \mathbf{v}_F^h = \mathbf{V}_F\,\mathbf{v}_F^{nd}\,,\\
&\mathbf{u}_M \approx \mathbf{u}_M^h = \mathbf{U}_M\,\mathbf{u}_M^{nd}\,, && \mathbf{v}_M \approx \mathbf{v}_M^h = \mathbf{V}_M\,\mathbf{v}_M^{nd}\,, && \mathbf{v}_L \approx \mathbf{v}_L^h = \mathbf{V}_L\,\mathbf{v}_L^{nd}\,,\\
&\mathbf{v}_\mathfrak{J} \approx \mathbf{v}_\mathfrak{J}^h = \mathbf{V}_\mathfrak{J}\,\mathbf{v}_\mathfrak{J}^{nd}\,, && \ell^\beta \approx (\ell^\beta)^h = \boldsymbol{\mathscr{L}}_\beta\,(\boldsymbol{\ell}^\beta)^{nd} && \text{with} \quad \beta = \{S\,,F\,,L\}\,.
\end{aligned} \tag{7.46}$$

Therein, $\mathbf{U}_S$, $\mathbf{V}_S$, $\mathbf{V}_F$, $\mathbf{U}_M$, $\mathbf{V}_M$, $\mathbf{V}_L$, $\mathbf{V}_\mathfrak{J}$ and $\boldsymbol{\mathscr{L}}_\beta$ contain the interpolation functions corresponding to the nodal unknowns $\mathbf{u}_S^{nd}\,,\mathbf{v}_S^{nd}\,,\mathbf{v}_F^{nd}\,,\mathbf{u}_M^{nd}\,,\mathbf{v}_M^{nd}\,,\mathbf{v}_L^{nd}\,,\mathbf{v}_\mathfrak{J}^{nd}$ and $(\boldsymbol{\ell}^\beta)^{nd}$ of the FE mesh. To keep the notation simple in what comes next, the superscript nd is dropped.

Spatial discretisation of the subdomains could be done following standard FE procedures, using linear or higher-order interpolation functions. Special care, however, shall be taken in the selection of the interpolation function for the multipliers. In this regard, as mentioned by Park *et al.* [217] and Ross *et al.* [235], using Dirac delta functions for interpolation of the multipliers not only offers a complete separation of the subdomains, but also yields significant ease in the numerical computations of the finite-element operators, as will be discussed later. Following that, discretisation of the multipliers ℓ^β reads

$$(\ell^\beta)^h = \boldsymbol{\mathscr{L}}_\beta\,\boldsymbol{\ell}^\beta = \sum_{i=1}^{\overline{N}^\beta_{int}} (\mathscr{L}_\beta)_i\,\ell^\beta_i \quad \text{with} \quad (\mathscr{L}_\beta)_i = \begin{cases} 1 & \text{if } \mathbf{x} = \mathbf{x}_i\,,\\ 0 & \text{else}\,. \end{cases} \tag{7.47}$$

Therein, $(\mathscr{L}_\beta)_i$ and ℓ^β_i, respectively, represent the shape function and nodal value of the multiplier corresponding to the i-th boundary node of the constituent β, positioned at $\mathbf{x} = \mathbf{x}_i$. Moreover, the location of the interface nodes could be determined via the zero-moment rule, as explained in detail by Park *et al.* [217] and Ross *et al.* [235].

Then, considering the same interpolation functions for discretisation of the variational terms, i. e. $\delta(\,\cdot\,)$ in (7.45), and also for assembling the weak form of (7.27), and applying the product rule and the Gaussian integral theorem, one obtains the weak form of the governing equations as

$$\mathfrak{S}\,\mathfrak{u} - \mathfrak{f} = \mathbf{0}\,. \tag{7.48}$$

Therein,

$$\mathfrak{u} := [\boldsymbol{y}_P\,,\boldsymbol{y}_L^{MED}\,,\boldsymbol{y}_\mathfrak{J}\,,\boldsymbol{\ell}^P\,,\boldsymbol{\ell}^L]^T\,, \quad \boldsymbol{y}_L^{MED} := [\boldsymbol{y}_M\,,\boldsymbol{y}_L]^T\,, \quad \boldsymbol{\ell}^P := [\boldsymbol{\ell}^S\,,\boldsymbol{\ell}^F]^T\,. \tag{7.49}$$

Furthermore,

$$\mathfrak{f} := [\boldsymbol{f}_P\,,\boldsymbol{f}_L^{MED}\,,\mathbf{0}\,,\mathbf{0}\,,\mathbf{0}]^T\,, \tag{7.50}$$

where

$$\boldsymbol{f}_L^{MED} := [\mathbf{0}\,, \boldsymbol{f}_{L2}\,, \boldsymbol{f}_{L3}]^T\,, \quad \boldsymbol{f}_P := [\mathbf{0}\,, \boldsymbol{f}_{P2}\,, \boldsymbol{f}_{P3}]^T \tag{7.51}$$

embody the known force vector on the exterior boundary nodes $\overline{\mathcal{N}}^{\mathfrak{a}}_{ext}$ such that

$$\begin{aligned} \boldsymbol{f}_{L2} &= \int_{S^L_{ext}} \delta\mathbf{u}_M \cdot \bar{\mathbf{t}}^M \,\mathrm{d}a\,, \quad \boldsymbol{f}_{L3} = \int_{S^L_{ext}} \delta\mathbf{v}_L \cdot \bar{\mathbf{t}}^L \,\mathrm{d}a\,, \\ \boldsymbol{f}_{P2} &= \int_{S^P_{ext}} \delta\mathbf{u}_S \cdot \bar{\mathbf{t}}^S \,\mathrm{d}a\,, \quad \boldsymbol{f}_{P3} = \int_{S^P_{ext}} \delta\mathbf{v}_F \cdot \bar{\mathbf{t}}^F \,\mathrm{d}a \end{aligned} \tag{7.52}$$

with $\bar{\mathbf{t}}^{(\bullet)} = \mathbf{T}^{(\bullet)}\,\mathbf{n}$, where $\mathbf{n}$ is the outward-oriented unit vector at the boundary. Moreover,

$$\mathfrak{S} := \begin{bmatrix} \mathbf{M}_P \frac{\mathrm{d}_S}{\mathrm{d}t} + \mathbf{K}_P & \mathbf{0} & \mathbf{0} & \mathbf{B}_P & \mathbf{0} \\ \mathbf{0} & \mathbf{M}_L \frac{\mathrm{d}_M}{\mathrm{d}t} + \mathbf{K}_L & \mathbf{0} & \mathbf{0} & \mathbf{B}_L \\ \mathbf{0} & \mathbf{0} & \mathbf{0} & \mathbf{L}_P^T & \mathbf{L}_L^T \\ \mathbf{B}_P^T & \mathbf{0} & -\mathbf{L}_P & \mathbf{0} & \mathbf{0} \\ \mathbf{0} & \mathbf{B}_L^T & -\mathbf{L}_L & \mathbf{0} & \mathbf{0} \end{bmatrix} \tag{7.53}$$

with $\mathbf{M}_{\mathfrak{a}}$ and $\mathbf{K}_{\mathfrak{a}}$, $\mathfrak{a} = \{P\,, L\}$, representing the mass and stiffness matrices belonging to the subsystems $\mathcal{X}^P$ and $\mathcal{X}^L$, and they read

$$\mathbf{M}_{\mathfrak{a}} := \begin{bmatrix} \mathbf{I} & \mathbf{0} & \mathbf{0} \\ \mathbf{0} & \mathbf{M}_{\mathfrak{a}22} & \mathbf{0} \\ \mathbf{0} & \mathbf{0} & \mathbf{M}_{\mathfrak{a}33} \end{bmatrix}\,, \quad \mathbf{K}_{\mathfrak{a}} := \begin{bmatrix} \mathbf{0} & -\mathbf{I} & \mathbf{0} \\ \mathbf{K}_{\mathfrak{a}21} & \mathbf{K}_{\mathfrak{a}22} & \mathbf{K}_{\mathfrak{a}23} \\ \mathbf{0} & \mathbf{K}_{\mathfrak{a}32} & \mathbf{K}_{\mathfrak{a}33} \end{bmatrix} \tag{7.54}$$

with

$$\begin{aligned} \mathbf{M}_{L22} &= \int_{V^L} \mathbf{V}_M^T\,\mathbf{V}_M \,\mathrm{d}v\,, \quad \mathbf{M}_{L33} := \int_{V^L} \mathbf{V}_L^T\,\rho^L\,\mathbf{V}_L \mathrm{d}v\,, \\ \mathbf{K}_{L21} &= -\int_{V^L} \nabla\mathbf{V}_M^T\,\boldsymbol{\mathcal{D}}_e^M\,\nabla\mathbf{V}_M \,\mathrm{d}v\,, \quad \mathbf{K}_{L22} = \mathbf{0}\,, \quad \mathbf{K}_{L23} = \mathbf{0}\,, \\ \mathbf{K}_{L32} &:= -\int_{V^L} \mathbf{V}_L^T\,\nabla\mathbf{V}_L\,\mathbf{v}_L\,\mathbf{V}_M \,\mathrm{d}v\,, \\ \mathbf{K}_{L33} &:= \Gamma^L \int_{V^L} \nabla\mathbf{V}_L^T\,\rho^L\nabla\mathbf{V}_L \mathrm{d}v + \int_{V^L} \mathbf{V}_L^T\,\nabla\mathbf{V}_L\,\mathbf{v}_L\,\mathbf{V}_L \,\mathrm{d}v \end{aligned} \tag{7.55}$$

and

$$
\begin{aligned}
\mathbf{M}_{P22} = & \int_{V^P} \mathbf{V}_S^T \, \rho^S \, \mathbf{V}_S \, \mathrm{d}v \,, \quad \mathbf{M}_{P33} = \int_{V^P} \mathbf{V}_F^T \, \rho^F \, \mathbf{V}_F \, \mathrm{d}v \,, \\
\mathbf{K}_{P21} = & - \int_{V^P} \nabla \mathbf{V}_S^T \, \boldsymbol{\mathcal{D}}_e^S \, \nabla \mathbf{V}_S \, \mathrm{d}v \,, \\
\mathbf{K}_{P22} = & \int_{V^P} \mathbf{V}_S^T \, \frac{(n^F)^2 \, \gamma^{FR}}{k^F} \, \mathbf{V}_S \, \mathrm{d}v - \Gamma^P \int_{V^P} \nabla \mathbf{V}_S^T \, (n^S)^2 \, \nabla \mathbf{V}_S \, \mathrm{d}v \,, \\
\mathbf{K}_{P23} = & - \int_{V^P} \mathbf{V}_S^T \, \frac{(n^F)^2 \, \gamma^{FR}}{k^F} \, \mathbf{V}_F \, \mathrm{d}v - \Gamma^P \int_{V^P} \nabla \mathbf{V}_S^T \, n^S \, n^F \, \nabla \mathbf{V}_F \, \mathrm{d}v \,, \\
\mathbf{K}_{P32} = & - \int_{V^P} \mathbf{V}_F^T \, \frac{(n^F)^2 \, \gamma^{FR}}{k^F} \, \mathbf{V}_S \, \mathrm{d}v - \Gamma^P \int_{V^P} \nabla \mathbf{V}_F^T \, n^F \, n^S \, \nabla \mathbf{V}_S \, \mathrm{d}v - \\
& - \int_{V^P} \mathbf{V}_F^T \, \nabla \mathbf{V}_F \, \mathbf{v}_F \, \mathbf{V}_S \, \mathrm{d}v \,, \\
\mathbf{K}_{P33} = & \int_{V^P} \mathbf{V}_F^T \, \frac{(n^F)^2 \, \gamma^{FR}}{k^F} \, \mathbf{V}_F \, \mathrm{d}v + \Gamma^P \int_{V^P} \nabla \mathbf{V}_F^T \, (n^F)^2 \, \nabla \mathbf{V}_F \, \mathrm{d}v + \\
& + \int_{V^P} \mathbf{V}_F^T \, \nabla \mathbf{V}_F \, \mathbf{v}_F \, \mathbf{V}_F \, \mathrm{d}v \,.
\end{aligned}
\tag{7.56}
$$

Herein, $\boldsymbol{\mathcal{D}}_e^S = \boldsymbol{\mathcal{D}}_e^S(\mu^S \,, \lambda^S)$ and $\boldsymbol{\mathcal{D}}_e^M = \boldsymbol{\mathcal{D}}_e^M(\mu^M \,, \lambda^M)$ represent elasticity matrices for the linear elastic treatment. Furthermore,

$$
\mathbf{B}_P = \begin{bmatrix} \mathbf{0} & \mathbf{0} \\ \mathbf{B}_{P21} & \mathbf{0} \\ \mathbf{0} & \mathbf{B}_{P32} \end{bmatrix} \,, \quad \mathbf{B}_L = \begin{bmatrix} \mathbf{0} \\ \mathbf{0} \\ \mathbf{B}_{L3} \end{bmatrix}
\tag{7.57}
$$

with

$$
\begin{aligned}
\mathbf{B}_{P21} := & \int_{S_{int}} \mathbf{V}_S^T \, \mathbf{n}_\mathfrak{I} \, \boldsymbol{\mathscr{L}}_S \, \mathrm{d}a \,, \quad \mathbf{B}_{P32} := \int_{S_{int}} \mathbf{V}_F^T \, \mathbf{n}_\mathfrak{I} \, \boldsymbol{\mathscr{L}}_F \, \mathrm{d}a \,, \\
\mathbf{B}_{L3} := & \int_{S_{int}} \mathbf{V}_L^T \, \mathbf{n}_\mathfrak{I} \, \boldsymbol{\mathscr{L}}_L \, \mathrm{d}a \,.
\end{aligned}
\tag{7.58}
$$

Exploiting the Dirac delta function for interpolation of the multipliers renders these operators to sparse Boolean matrices that extract the boundary values of the velocity vectors normal to the interface:

$$
\mathbf{B} := \begin{bmatrix} \mathbf{B}_P & \mathbf{0} \\ \\ \mathbf{0} & \mathbf{B}_L \end{bmatrix} \quad \rightarrow \quad \mathbf{B}^T \begin{bmatrix} \boldsymbol{y}_P \\ \\ \boldsymbol{y}_M \\ \\ \boldsymbol{y}_L \end{bmatrix} = \begin{bmatrix} \mathbf{B}_S^T \, \mathbf{v}_S \\ \\ \mathbf{B}_F^T \, \mathbf{v}_F \\ \\ \mathbf{B}_L^T \, \mathbf{v}_L \end{bmatrix} = \begin{bmatrix} \bar{\mathbf{v}}_S^{int} \\ \\ \bar{\mathbf{v}}_F^{int} \\ \\ \bar{\mathbf{v}}_L^{int} \end{bmatrix}
\tag{7.59}
$$

with $\bar{\mathbf{v}}_\beta^{int}$ containing the nodal values, depicting the component of $\mathbf{v}_\beta^{int}$ along $\mathbf{n}^\mathfrak{I}$, where $\mathbf{v}_\beta^{int} = \mathbf{v}_\beta(\mathcal{N}^\mathfrak{a})|_{\mathcal{N}^\mathfrak{a} \in \overline{\mathcal{N}}_{int}^\mathfrak{a}}$. Furthermore, $\mathbf{L}_P = [\mathbf{L}_S \,, \mathbf{L}_F]^T$ and $\mathbf{L}_L$ are finite element assembly operators, which relate the force-like multipliers on both sides of the interface:

$$\mathbf{L}_\beta := \int_{S_{int}} \boldsymbol{\mathscr{L}}_\beta^T \, \mathbf{n}_\mathfrak{J}^T \, \mathbf{V}_\mathfrak{J} \, \mathrm{d}a \,. \tag{7.60}$$

Provided having matched meshes at the interface, that means for $(S_{int}^L)^h = (S_{int}^P)^h$, $\mathbf{L}_\beta$ transforms to Boolean matrices. This operator also relates the interface displacements to the displacement of the subsystems at the interface.

Remarks:

- The presence of large penalty parameters within the equations yields an unrealistically stiff behaviour of the finite elements. This problem can be alleviated using selective reduced integration, where the numerical integration of the terms including the penalty parameter is done on fewer integration points compared with the other terms [146].
- Note that $\mathbf{B}_\mathfrak{a} \, \boldsymbol{\ell}^\mathfrak{a} =: \boldsymbol{f}_\mathfrak{a}^{int}$ represents the discretised forces applied to the nodes at the interface surface of each subsystem.
- Multiplying the third line of the above matrix with the vector of unknowns yields $\mathbf{L}_P^T \, \boldsymbol{\ell}^P + \mathbf{L}_L^T \, \boldsymbol{\ell}^L = \mathbf{0}$. Satisfaction of this relation guarantees the balance of forces between the subsystems.

Temporal discretisation

An implicit time integration by means of the mid-point rule as presented in (4.22) is used for the temporal discretisation of (7.48). Then, the time discretisation of (7.48) yields

$$\mathfrak{S}_d \, \mathfrak{u}^{n+\frac{1}{2}} - \mathfrak{f}_d = \mathbf{0} \,, \tag{7.61}$$

where $\mathfrak{f}_d := [\boldsymbol{f}_{P_d} \,, \boldsymbol{f}_{L_d} \,, \mathbf{0} \,, \mathbf{0} \,, \mathbf{0}]^T$ with

$$\boldsymbol{f}_{\mathfrak{a}_d} := \mathbf{M}_\mathfrak{a} \, \boldsymbol{y}_\mathfrak{a}^n + \frac{\Delta t}{2} \boldsymbol{f}_\mathfrak{a}^{n+\frac{1}{2}} \,, \quad \mathfrak{a} = \{P \,, L\} \,, \tag{7.62}$$

and

$$\mathfrak{S}_d := \begin{bmatrix} \overline{\mathbf{K}}_P & \mathbf{0} & \mathbf{0} & \frac{\Delta t}{2} \mathbf{B}_P & \mathbf{0} \\ \mathbf{0} & \overline{\mathbf{K}}_L & \mathbf{0} & \mathbf{0} & \frac{\Delta t}{2} \mathbf{B}_L \\ \mathbf{0} & \mathbf{0} & \mathbf{0} & \mathbf{L}_P^T & \mathbf{L}_L^T \\ \mathbf{B}_P^T & \mathbf{0} & -\mathbf{L}_P & \mathbf{0} & \mathbf{0} \\ \mathbf{0} & \mathbf{B}_L^T & -\mathbf{L}_L & \mathbf{0} & \mathbf{0} \end{bmatrix} \quad \text{with} \quad \overline{\mathbf{K}}_\mathfrak{a} := \mathbf{M}_\mathfrak{a} + \frac{\Delta t}{2} \mathbf{K}_\mathfrak{a} \,. \tag{7.63}$$

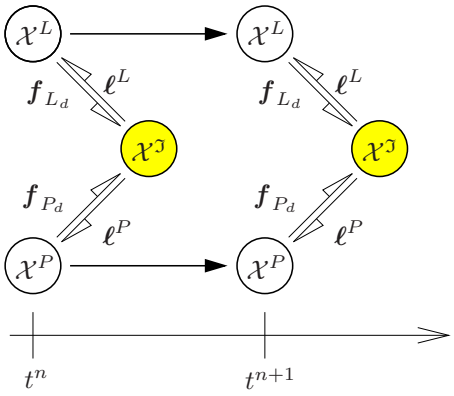

Figure 7.12: *Flowchart showing the partitioned solution following the LLM method.*

Solution algorithm

Solving the first two rows of (7.61) for the kinematic variables of the subsystems, these can be written in terms of the Lagrange multipliers, i. e., $\boldsymbol{y}_\mathfrak{a}^{n+\frac{1}{2}} = \boldsymbol{y}_\mathfrak{a}^{n+\frac{1}{2}}(\boldsymbol{\ell}^{n+\frac{1}{2}}, \cdots)$. Substituting these relations into the last three rows of (7.61) yields the following equation system that has to be solved at the interface:

$$\begin{bmatrix} \mathbf{F}_\mathfrak{I} & \mathbf{L} \\ \mathbf{L}^T & \mathbf{0} \end{bmatrix} \begin{bmatrix} \boldsymbol{\ell} \\ \boldsymbol{y}_\mathfrak{I} \end{bmatrix}^{n+\frac{1}{2}} = \begin{bmatrix} \boldsymbol{f}_\ell \\ \mathbf{0} \end{bmatrix} . \tag{7.64}$$

Therein,

$$\mathbf{L} := [\mathbf{L}_P \,, \mathbf{L}_L]^T \,, \quad \boldsymbol{f}_\ell := \left[\mathbf{B}_P^T \overline{\mathbf{K}}_P^{-1} \boldsymbol{f}_{P_d} \,,\; \mathbf{B}_L^T \overline{\mathbf{K}}_L^{-1} \boldsymbol{f}_{L_d}\right]^T \,, \tag{7.65}$$

and

$$\mathbf{F}_\mathfrak{I} := \frac{\Delta t}{2} \begin{bmatrix} \mathbf{B}_P^T \overline{\mathbf{K}}_P^{-1} \mathbf{B}_P & \mathbf{0} \\ \mathbf{0} & \mathbf{B}_L^T \overline{\mathbf{K}}_L^{-1} \mathbf{B}_L \end{bmatrix} . \tag{7.66}$$

Insertion of (7.62) in $(7.65)_2$ reveals that $\boldsymbol{f}_\ell$ is a function of the prescribed boundary conditions on the external surface and of the known displacements and velocities at time t^n. Therefore, the right-hand side of (7.64) is completely known. Solution of this equation yields the new values for the frame velocity and also the multipliers at time t^{n+1}. Having these values at hand, the frame velocity is then used as the Dirichlet boundary condition for calculation of the mesh motion in the bulk fluid subsystem. Moreover, the multipliers (interface forces) are substituted in the interacting subsystems and, subsequently, the subdomains are updated as per the flowchart depicted in Figure 7.12.

7.3.3 Stability analysis

Employing the algorithm of Section 5.4.2, a linear stability analysis of the proposed solution scheme is executed. It should be noted that the stability analysis can be done for the general 3-d version of the governing equations. However, this makes the relations too

lengthy and unclear. Hence, in order to study the effects of the decoupling of the problem on the linear stability, we consider a linearised 1-d test problem. In this regard, the 1-d counterpart of the governing equations (7.32), (7.33) and (7.41) after linearisation read[1]

$$
\begin{aligned}
\mathcal{X}^P: \quad & \left\{ \begin{array}{l} (u_S)'_S = v_S\,, \\ \\ \rho^S\,(v_S)'_S = H_A^S\,(u_S)_{,xx} + \dfrac{(n^F)^2\,\gamma^{FR}}{k^F}\,w_F + n^S\,\Gamma^P\,[n^S\,(v_S)_{,xx} + n^F (v_F)_{,xx}]\,, \\ \\ \rho^F\,(v_F)'_S = -\dfrac{(n^F)^2\,\gamma^{FR}}{k^F}\,w_F + n^F\,\Gamma^P\,[n^S\,(v_S)_{,xx} + n^F (v_F)_{,xx}]\,, \end{array} \right. \\
\mathcal{X}^L: \quad & \rho^L\,(v_L)'_M = \Gamma^L\,(v_L)_{,xx}\,, \\
\mathcal{X}^\mathfrak{I}: \quad & \left\{ \begin{array}{l} v_S^{int} - v_\mathfrak{I} = 0\,, \\ \\ v_F^{int} - v_\mathfrak{I} = 0\,, \\ \\ v_L^{int} - v_\mathfrak{I} = 0\,, \end{array} \right.
\end{aligned}
\tag{7.67}
$$

wherein $(\,\cdot\,)_{,xx} := \partial^2(\,\cdot\,)/\partial x^2$. Moreover, $H_A^S := 2\,\mu^S + \lambda^S$ represents the aggregate modulus of the solid skeleton. In the next step, these equations should be temporally and spatially discretised. The temporal discretisation is done via the mid-point rule (4.22). The spatial discretisation is done using the central difference (CD) scheme, such that, assuming a uniform grid for an exemplary variable at time $t^n = n\,\Delta t$ and position $(x_\beta)_h = h\,\Delta x_\beta$, the spatial discretisation reads

$$
\frac{\partial^2}{\partial x^2}\,(\,\cdot\,)_h^n = \frac{(\,\cdot\,)_{h+1}^n - 2\,(\,\cdot\,)_h^n + (\,\cdot\,)_{h-1}^n}{(\Delta x_\beta)^2}
\tag{7.68}
$$

with $\beta = \{L\,, F\,, S\}$ and typically, $\Delta x_S = \Delta x_F =: \Delta x_P$. Then, following the stability analysis algorithm of Section 5.4, and as it is presented in detail in Appendix B for the present case, one ends up with a Hurwitz polynomial of order 3 with the following LCC parameters:

$$
\begin{aligned}
\beta_0 &= 1 - \cos\,\Theta\,, \\
\beta_1 &= (1 - \cos\,\Theta)\,(\Gamma^L + \Gamma^P)\,, \\
\beta_2 &= 16\,(\rho^S + \rho^F + \rho^L)\,.
\end{aligned}
\tag{7.69}
$$

It is obvious that

$$
\{\beta_0,\,\beta_1,\,\beta_2\} \geq 0 \quad \forall\,\Theta \in [-\pi, \pi] \quad \text{and} \quad \forall\,\Delta t\,, \Delta x_\mathfrak{a} > 0
\tag{7.70}
$$

and, hence, the partitioned solution scheme applied to the equation system (7.67) is unconditionally stable.

[1] Note that considering a linearised model, the nonlinear convective term $(\operatorname{grad}\mathbf{v}_F)\,\mathbf{w}_F$ can be omitted, cf. Heider [137]. Furthermore, following Markert *et al.* [190], in the geometrically linear regime one has $n^\alpha(\mathbf{u}_S) \approx n_{0\alpha}^\alpha$=const. with $\alpha = \{F\,, S\}$.

Parameter	Symbol	Value	SI unit
Aggregate modulus of the solid skeleton	H_A^S	$20 \cdot 10^6$	Pa
Volume fraction of solid (solidity)	n_{0S}^S	0.67	–
Volume fraction of fluid (porosity)	n_{0S}^F	0.33	–
Effective density of dense solid	ρ^{SR}	2000	$\mathrm{kg/m^3}$
Effective density of pore fluid	ρ^{FR}	1000	$\mathrm{kg/m^3}$
Effective fluid weight	γ^{FR}	9800	$\mathrm{N/m^3}$
Darcy permeability	k^F	10^{-3}	m/s

Table 7.3: *Material parameters for the FPMI examples [66].*

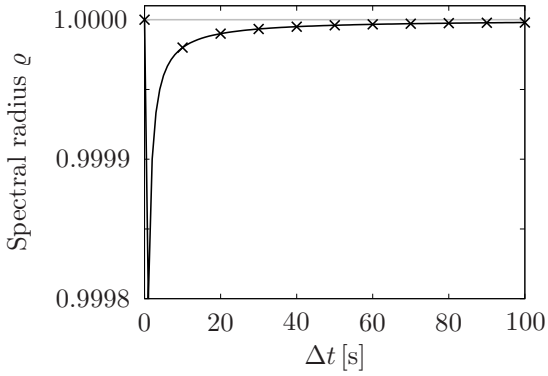

Figure 7.13: *Spectral radius of the amplification matrix of the FPMI problem ($\Delta x = 1\,\mathrm{m}$).*

7.3.4 Numerical example I

To set up the examples, the numerical values as presented in Table 7.3 have been chosen[2]. At first, a numerical stability analysis has been performed. In this regard, using the material parameters, the amplification matrix and, subsequently, the amplification polynomial have been assembled. Following this, the roots of the amplification polynomial for an exemplary uniform spatial grid size $\Delta x := \Delta x_{\mathfrak{a}} = 1\,\mathrm{m}$, and considering different values of Δt have been calculated. It has been seen that for values of Δt up to 100 s, all of the roots of the amplification polynomial and, hence, the spectral radii remain always smaller than unity, see Figure 7.13. It shows satisfaction of the necessary stability condition for the proposed partitioned solution method for very big time-step sizes, as it was predicted by the analytical stability analysis of the last section. To verify this conclusion, a 1-d benchmark example as depicted in Figure 7.14 with the following initial conditions has

[2]Note that to consider a relatively big permeability factor has been by purpose, in order to reduce the stiffness of the problem and, consequently, to prevent numerical difficulties in the porous medium as addressed by Markert *et al.* [190] and references therein. Nevertheless, and as it is shown later, even using extremely small values for k^F would not jeopardise the applicability and stability of the solution algorithm.

been considered:

$$u_L^0 := 1\ \mathrm{m}\,, \quad v_\beta(x,0) = 0\ \mathrm{m/s} \quad \text{with} \quad \beta = \{L\,, F\,, S\}\,. \tag{7.71}$$

Using the above partitioned solution algorithm and employing a finite-element code developed in *Scilab*, the governing system of equations (7.67) has been solved and the evolution of the Lagrange multipliers as well as the motion of the solid at the interface for $0 \leq t \leq 1400\,\mathrm{s}$ and $5 \leq \Delta t \leq 40\,\mathrm{s}$ have been calculated. It has been obtained that even drastic changes in the time-step size do not influence the stability of the solution, as it has been also predicted by the analytical and numerical stability analyses, see Figure 7.15.

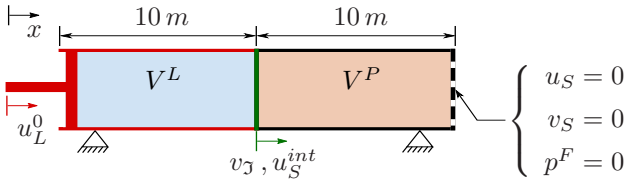

Figure 7.14: *Geometry and boundary conditions of 1-d FPMI.*

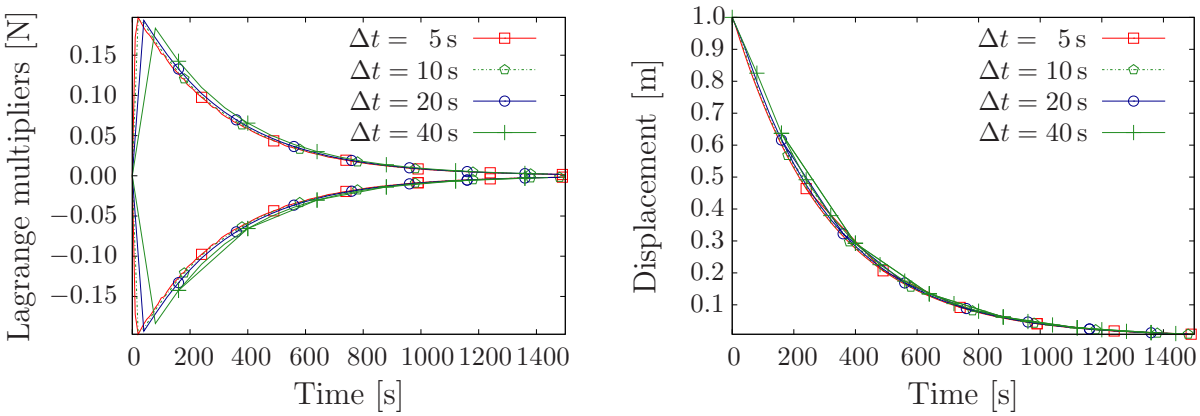

Figure 7.15: *Evolution of the Lagrange multipliers (left) and the solid displacement (right) at the interface ($k^F = 10^{-3}\,\mathrm{m/s}$).*

To further inspect the influence of the changes in the permeability factor on the solution, the problem has also been solved for various values of k^F. To this end, the motion of the solid has been calculated at the interface for $10^{-10} \leq k^F \leq 10^{-2}\,\mathrm{m/s}$, $0 \leq t \leq 1400\,\mathrm{s}$ and $\Delta t = 5\,\mathrm{s}$, see Figure 7.16. It has been seen that, as expected, decreasing the value of the hydraulic conductivity causes an increase in the viscous drag in the fluid momentum production, which in turn yields a slower response of the system. Moreover, it has been shown that for all cases the scheme leads to a stable solution.

7.3.5 Numerical example II

For further inspection of the capability of the solution method, a 2-d example under plane-stain conditions has been set up. It describes the interaction between two rectangular subdomains as depicted in Figure 7.17. The material parameters have been obtained from Table 7.3.

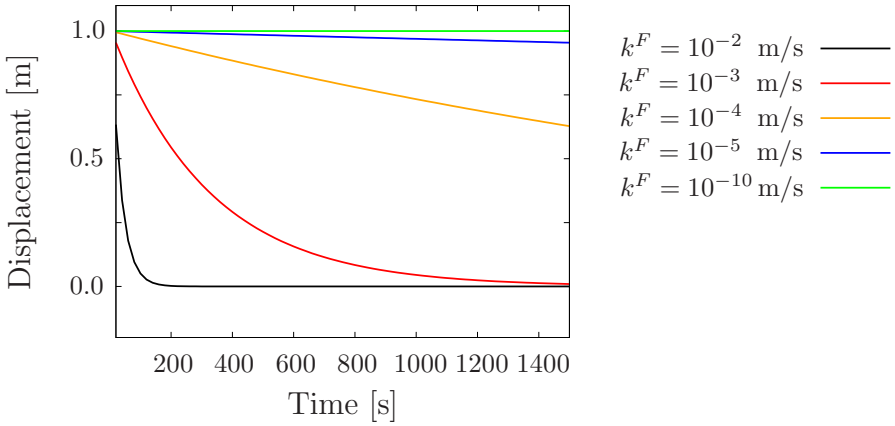

Figure 7.16: *Solid displacement u_S^{int} at the interface for different values of the permeability.*

Considering the applied boundary conditions, one expects the problem to proceed as follows: at the beginning, the porous medium V^P is still "unloaded". Therefore, no interaction force acts between the subdomains at the interface. Hence, the loads $\bar{t}_2^L$ applied to the bulk fluid φ^L at the boundaries II and VI cause an influx of the bulk fluid on these boundaries. This influx of the "incompressible" bulk fluid yields expansion of V^L and, consequently, downward motion of the interface. This motion is naturally accompanied by deformation of the solid skeleton in V^P, and an efflux of the pore fluid from the boundaries IX and XI. From this perspective, the phenomenon happening within the porous medium is standard consolidation, where the reaction forces at the interface (the Lagrange multipliers), which determine the resistance of the porous medium against downward motion of the interface, are proportional to the deformation of the solid skeleton and the velocity of the pore fluid at the vicinity of the interface. Thus, further expansion of the bulk-fluid subdomain causes further deformation of the solid skeleton and, hence, higher resistance of the porous medium against deformation. This resistance alters the bulk-fluid flow and, as the time elapses, it eventually gets big enough to prohibit any further expansion of the bulk-fluid subdomain. After that, in the porous-medium subdomain V^P, the solid skeleton φ^S does not deform any more and the pore fluid φ^F becomes stationary. Furthermore, in the bulk-fluid subdomain V^L, the bulk fluid φ^L experiences an accelerating flow, where it only enters the subdomain on the boundary VI and exits on the boundary II. The mathematical model of the above problem is composed of the governing equations of the porous medium and the bulk fluid subdomains, subjected to the set of kinematic constraints. The strong form of these relations is presented by (7.32), (7.33) and (7.41), respectively. Employing the finite-element method for spatial discretisation yields the weak form of the equations as presented in (7.48). The numerical treatment of this system can be performed in a decoupled manner, following the solution algorithm presented in Section 7.3.2. To this end, separated solvers for the bulk-fluid and the porous-medium subproblems have been developed. This has been done in the FE package PANDAS[3]. Furthermore, an `interface` module for the treatment of the equation system (7.64) has been

[3]Porous media Adaptive Nonlinear finite element solver based on Differential Algebraic Systems, see `http://www.get-pandas.com`.

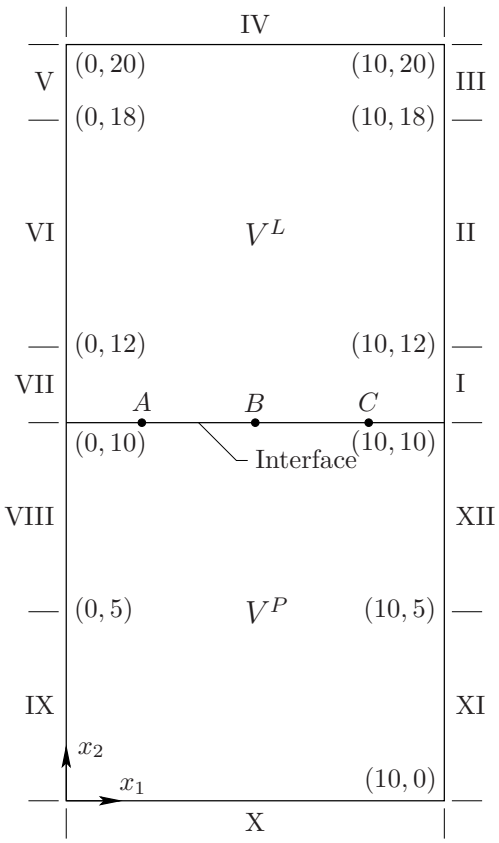

BC for the bulk fluid:

I, III, V, VII :
$v_{M1} = 0\,, \quad v_{L1} = 0$

II :
$v_{M1} = 0\,, \quad v_{M2} = 0\,, \quad \bar{t}_2^L = -10.00$ [kN/m]

IV :
$v_{M2} = 0\,, \quad v_{L2} = 0$

VI :
$v_{M1} = 0\,, \quad v_{M2} = 0\,, \quad \bar{t}_2^L = 10.05$ [kN/m]

BC for the porous medium:

VIII, XII :
$v_{S1} = 0\,, \quad v_{F1} = 0$

IX, XI :
$v_{S1} = 0\,, \quad \bar{t}_1^F = 0$

X :
$v_{S2} = 0\,, \quad v_{F2} = 0$

Position of the sampling points:

$A\,(2, 10), \quad B\,(5, 10), \quad C\,(8, 10)$

Figure 7.17: *Geometry and boundary conditions of the 2-d FPMI. Coordinates are in meter.*

developed in *Python*[4]. Subsequently, another *Python* script, namely a `manager`, has been written for regulating the flow of information between the modules, and for controlling their sequence of performance, in particular, parallel execution of the bulk fluid and the porous medium subroutines.

The package has then been exploited for solution of the initial boundary-value problem. To this end, a uniform mesh with the element size $\Delta x_{1\mathfrak{a}} = \Delta x_{2\mathfrak{a}} = 0.5\,\mathrm{m}$ has been used for the spatial discretisation of both subdomains. Subsequently, the time integration has been executed with a time-step size $\Delta t = 0.01\,\mathrm{s}$ for $0 \leq t \leq 2\,\mathrm{s}$. The time-step size and the duration of calculation are chosen such that the above-described changes in the fluid-flow regime can be well captured. Figure 7.18 shows selected snapshots obtained at representative times, i. e., at $t = 0.02\,\mathrm{s}$ that is the first instance after the subsystems are coupled to each other (this will be explained in more details below), at $t = 0.50\,\mathrm{s}$ as an exemplary transient state, and at $t = 1.00\,\mathrm{s}$, where the interface velocities of the constituents become very small in comparison to the bulk-fluid velocity on the inlet VI and the outlet II. Furthermore, the upper row depicts the results for the bulk-fluid and the lower row represents the response of the porous-medium subdomain. Considering this, the arrows demonstrate the directions of the bulk-fluid velocity $\mathbf{v}_L$ and the pore-fluid velocity

[4]Programming language, see `www.python.org`

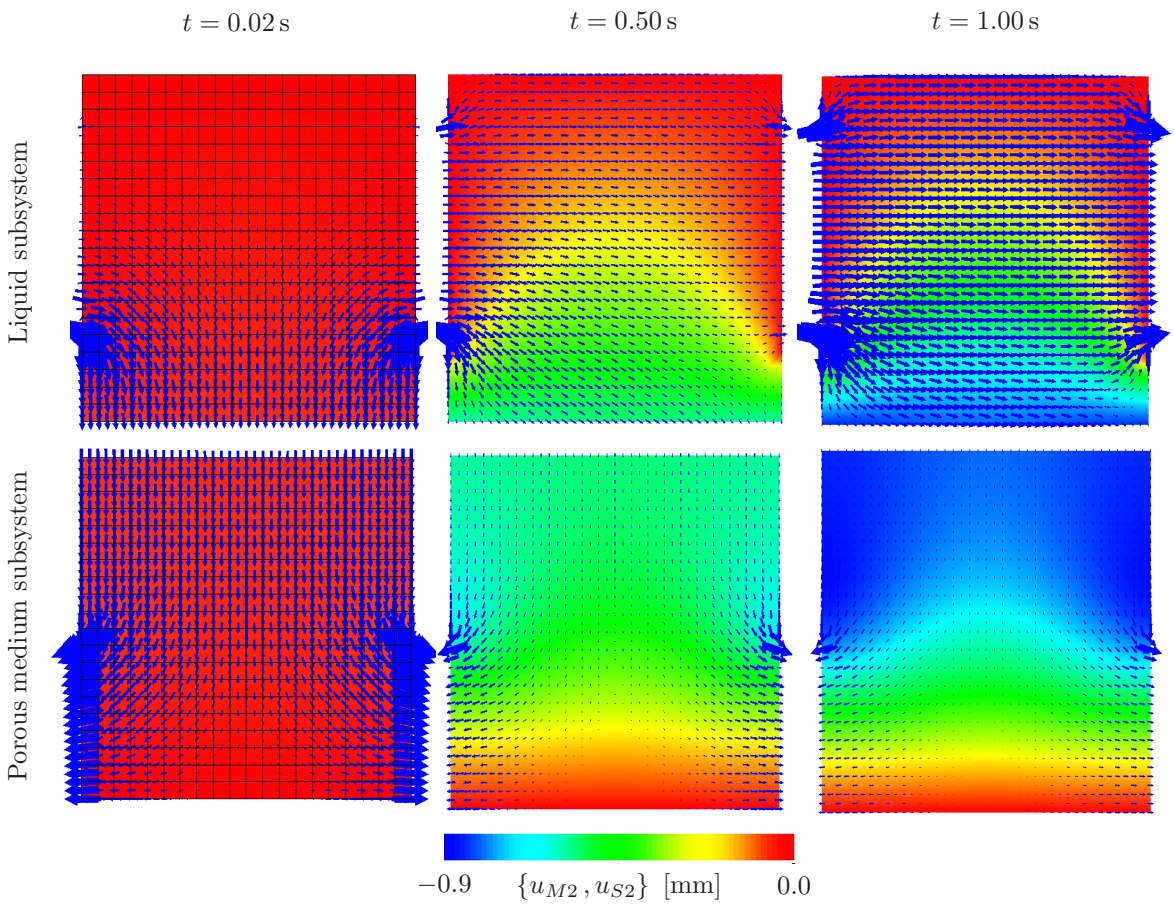

Figure 7.18: *Snapshots showing the responses of the subsystems at selected times. The arrows represent the bulk-fluid velocity* $\mathbf{v}_L$ *and the pore-fluid velocity* $\mathbf{v}_F$ *within the subsystems.*

$\mathbf{v}_F$ within the subdomains. Apart from that, the contours of the vertical mesh deformation u_{M2} and solid skeleton deformation u_{S2} are shown. Studying these results reveals an agreement between the response calculated by the code and the predicted behaviour of the system as presented at the beginning of this section. Moreover, the conformity between the fluid mesh motion and that of the solid skeleton can be well seen. Figure 7.19 demonstrates a better representation of this conformity. For a more precise investigation, the calculated variables at sample interface positions A (at $x_1 = 2\,\mathrm{m}\,, x_2 = 10\,\mathrm{m}$), B (at $x_1 = 5\,\mathrm{m}\,, x_2 = 10\,\mathrm{m}$) and C (at $x_1 = 8\,\mathrm{m}\,, x_2 = 10\,\mathrm{m}$) have been extracted. Subsequently, the evolution of the interaction forces (the Lagrange multipliers), as well as that of the interface velocities of the bulk fluid $\mathbf{v}_L^{int}$, of the pore fluid $\mathbf{v}_F^{int}$ and of the solid skeleton $\mathbf{v}_S^{int}$ along the normal vector $\mathbf{n}^\Im$ have been monitored. The results are shown in Figures 7.20 and 7.21, respectively. Looking at these diagrams shows that at time $t = 0.01\,\mathrm{s}$, the interface forces are equal to zero, see Figure 7.20. This is due to the fact that at this time, the bulk-fluid and the porous-medium subroutines update the corresponding subsystems for the first time and, thus, the interaction forces at the interface are still zero. This situation causes an "artificial" downward flow of the bulk fluid at the interface, whereas the porous-medium subsystem is still stationary. It yields a mismatch between the velocities of the constituents calculated at time $t = 0.01\,\mathrm{s}$, see Figure 7.21. These non-matching velocities are then sent to the `interface` subroutine, where the new interface

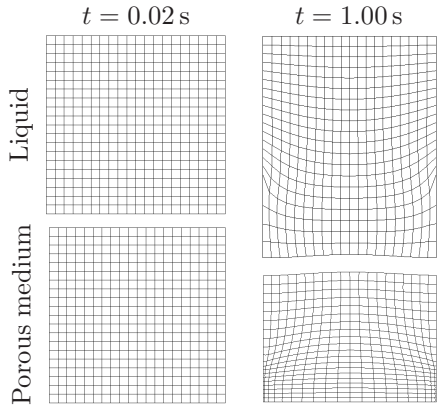

Figure 7.19: *Mesh and solid skeleton configurations at $t = 0.02\,\mathrm{s}$ and $t = 1.00\,\mathrm{s}$. For the sake of visualisation, the displacements have been scaled by a factor of 1000.*

loads at time $t = 0.02\,\mathrm{s}$ are calculated such that, on the one side, the balance of forces at the interface is satisfied, and, on the other side, applying the interface loads as Neumann boundary conditions to the subsystems yields matching velocities of the constituents at the interface. Referring back to Figure 7.20 shows that the interface loads calculated at time $t = 0.02\,\mathrm{s}$ (and the steps thereafter), indeed, satisfy the balance of forces. Furthermore, from Figure 7.21, it is clear that employing these forces for updating the subsystems yields matching velocities of the constituents at the interface in the next steps. It is also worth mentioning that the "overshoot" seen in the loads calculated at time $t = 0.02\,\mathrm{s}$ is in principle due to the considerable mismatch between the velocities of the constituents in the previous step.

Further investigation of the diagrams shows that for $t > 0.02\,\mathrm{s}$, the interface forces show only minor alterations (compared to the initial overshoot) and the velocities asymptotically approach $0\,\mathrm{m/s}$, while the balance of forces and the kinematic constraint at the interface are always well satisfied. Furthermore, the changes in the displacements of the bulk-fluid dynamic mesh $\mathbf{u}_M^{int}$ and that of the solid skeleton $\mathbf{u}_S^{int}$ along the normal vector $\mathbf{n}^{\mathfrak{I}}$ at the same sample points have been monitored. Figure 7.22 depicts the development of these quantities in the course of time, and reveals the consistency between the deformation of the bulk-fluid subdomain and that of the porous medium.

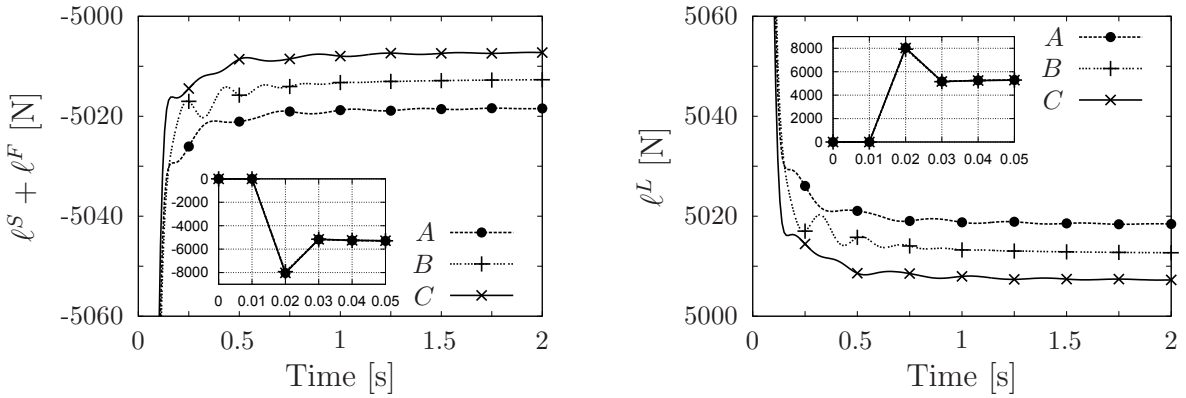

Figure 7.20: *Evolution of the Lagrange multipliers ℓ^β, $\beta = \{S\,, F\,, L\}$, at sampling points A, B and C.*

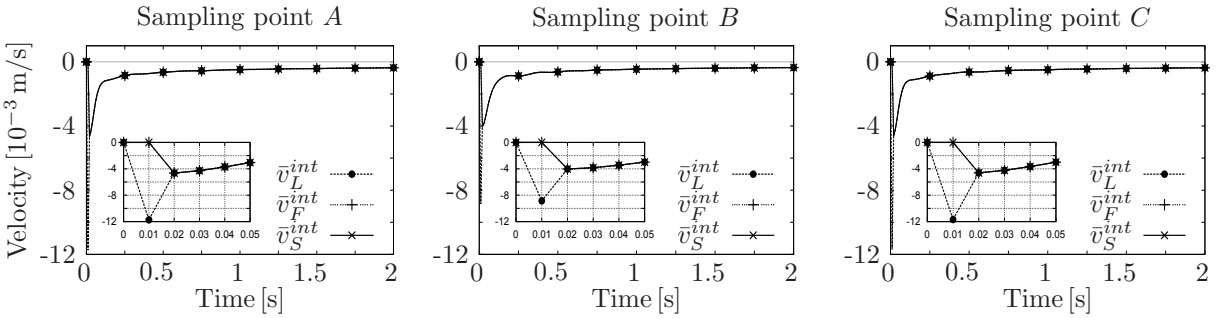

Figure 7.21: *Normal interface velocities $\bar{v}_\beta^{int}$ at the sampling points A, B and C, calculated by the bulk fluid and the porous medium subroutines.*

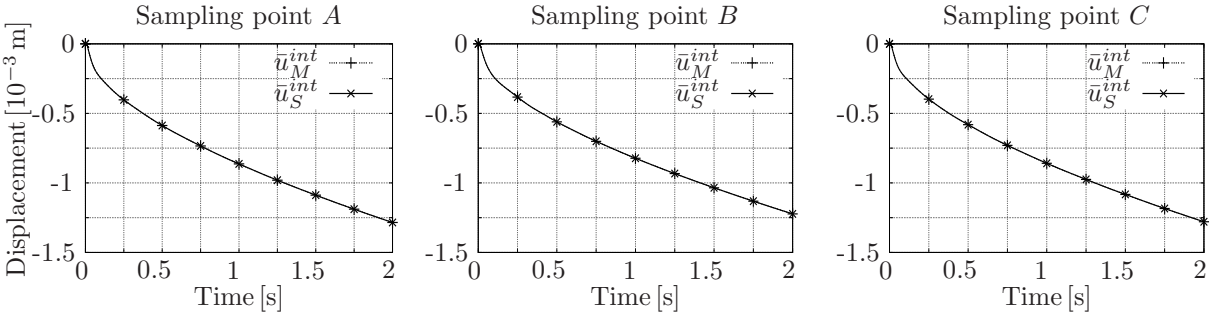

Figure 7.22: *Normal interface displacements of the mesh $\bar{u}_M^{int}$ in $\mathcal{X}^L$ and of the solid skeleton $\bar{u}_S^{int}$ in $\mathcal{X}^P$, calculated at the sampling points A, B and C.*

Chapter 8:
Conclusions and Outlook

To select a suitable solution strategy is certainly a vital step towards successful simulation of physical phenomena. Considering this, the presented study was set out to explore the important aspects regarding numerical treatment of mathematical models corresponding to the coupled multi-field phenomena in the framework of continuum mechanics. The mission to fulfil this goal included several specific tasks, such as reviewing and, subsequently, proposing a framework for classification of the coupled phenomena, studying various monolithic and decoupled solution strategies, providing several procedures for integration of the coupled systems of equations, gathering the important notions regarding the concept of stability of numerical solution schemes and presenting these in a unified manner, investigating various stability criteria, establishing their relation to one another and proposing a pragmatic stability analysis algorithm and, finally, demonstrating the applicability of the studied topics by solving several examples, including distinct surface- and volume-coupled problems.

In what follows, firstly, the process to achieve the above objectives is reviewed, the milestones are presented and the conclusions are drawn. Subsequently, the discussions and also the potentials for further expansion of the study are discussed in Section 8.2.

8.1 Summary and conclusions

Establishing a common language is undoubtedly the first step in facilitating a smooth conversation. Considering this, a framework for classification of the coupled physical phenomena and the corresponding mathematical models were firstly proposed and, for the sake of clarification, several examples from different fields were given.

In the next step, focusing on the continuum-mechanical modelling approach, the relevant concepts of the classical continuum mechanics and also of the Theory of Porous Media (TPM) were reviewed. It was seen that in this context, the mathematical models of the coupled phenomena take the form of coupled PDE or DAE systems. Then, recognising the algebraic constraints as a source of difficulty in numerical procedures, the concept of differential index as a measure for classification of the DAE systems was introduced, and the method of repeated differentiation as an option for index reduction was investigated. Moreover, the class of projection schemes (belonging to the family of the operator-splitting methods), and the penalty formulation (also known as the method of perturbed Lagrange multipliers) as two possibilities to overcome the differential constraints were studied. Apart from that, the controversial concept of stiffness of the differential equations was discussed, and a feasible definition for the stiff problems was presented.

After introduction to coupled systems of equations, the procedures for numerical solution of the differential equations in general, and those arising in the mathematical modelling of

coupled phenomena in particular, were explained. In this regard, and in order to avoid using an abstract equation system, a rheological model as a representative coupled physical system, and its corresponding governing equations as a representative coupled system of equations were introduced. Nevertheless, equations and relations were presented in such a way that the discussions may conveniently be extended to more practical applications. Using this model, various techniques for temporal integration of the generated systems of coupled equations were explained. This part was started with demonstrating the monolithic integration method, followed by presenting the rival decoupled solution strategies. In this context, after introducing selected staggered time-marching algorithms, spatial partitioning and operator splitting as two effective tools for decoupled solution of the coupled systems of equations were studied. In particular, several partitioning techniques, including the primal and the dual Schur complement methods, the global and the localised Lagrange-multiplier schemes, and also partitioning methods that follow a staggered integration were scrutinised and the relations between them were established. Furthermore, a convenient framework for presentation of the operator-splitting schemes was proposed, and the process of time integration in the methods belonging to this class of solution strategies was described. Apart from presenting the schemes, the advantages and disadvantages of the monolithic and the decoupled integrators were as well discussed. It was particularly mentioned that the monolithic methods, when combined with an implicit time-marching algorithm, yield unconditional stability. However, it was noted that, the monolithic solvers

i) enforce using identical time-step sizes for every part of the problem,
ii) require a special solution algorithm for each individual coupled system, and
iii) demand a holistic integration of the equation systems.

These three characteristics respectively call for special caution if

i) the system comprises components with drastically different evolution rates,
ii) there exist specialised solvers for the interacting components, or
iii) a large problem of practical size with too many DOF has to be considered.

It was mentioned that, exploiting a decoupled solution strategy is a feasible option to overcome these deficiencies of the monolithic integrators. Nevertheless, it was discussed that decoupling of the equation system, selection of the way of decoupling and the sequence of time integration of the subsystems can be detrimental to the stability of the scheme and can lead to conditional stability; a flaw that even in presence of an unconditionally stable, implicit time integrator within the subproblems persists to exist. Thus, dealing with the subject of stability analysis of the numerical schemes built the next milestone of the present study. In this regard, the related notions were introduced and their significance was explained. In particular, the terminologies, the stability criteria and the relation between them were reinterpreted in an application-related manner, where the explanations were supported by several examples. This study eventually led to the development of a stability analysis algorithm that can be employed to find the critical grid sizes in different scenarios with minimum difficulty and without any need to solve the whole problem.

In the final stage, several typical surface- and volume-coupled examples were introduced, where for each example the model problem of the case at hand was presented, selected

decoupled solution strategies were considered, the stability analysis was executed, and one or more benchmark numerical examples were given. These steps, especially, portrayed the applicability of the presented stability analysis algorithm in different scenarios (in all of the examples), the potency of the proposed framework for presentation of operator-splitting schemes (cf. the TED, PMD and multi-rate examples) the influence of the decoupling methodology on the stability of the resulting scheme (cf. the TED example), and the importance of the sequence of integration of subproblems (cf. the FSI and SSI examples). Furthermore, our attempt in employing the LLM method for partitioning of the surface-coupled problem of FPMI led to a parallel decoupled solution strategy, comprising a novel application of the concept of MED for describing the motion of a fluid body within moving boundaries, implementation of the penalty method for modelling of fluid as well as porous bodies using the FE-solver PANDAS, and generation of a workflow structure facilitating communication between existing modules of PANDAS.

8.2 Discussion and outlook

The present study was a successful attempt in investigating the fundamental issues related to the coupled problems in the mechanics of multi-physics and multi-phase materials. This is considering the great amount of effort invested in clear reinterpretation of the puzzling concepts, proposing comprehensible classification strategies, building a rational basis for designing and studying the numerical methods applied to the coupled mechanical problems, and providing several illustrative examples. Nevertheless, the enormously wide range of applications where the coupled problems arise makes it practically impossible to cover all of the related aspects. Furthermore, our discussions about merits and demerits of the monolithic and the decoupled solution methods showed that, to provide a global ultimate answer to the question of *"whether it is necessary to solve the whole equation system monolithically, or if decoupling methods can be applied yielding almost the same quality of the results but at lower numerical costs"* is rather impractical. Instead, one has to answer this question for each specific case via reaching a compromise between the criteria of stability, simplicity, efficiency, modularity, etc. Thus, further investigations should at best focus on specific applications. To this end, the material gathered within this monograph may be extended in various specialised directions. In this regard, one interesting option would be to design a systematic technique for investigating the dissipativity of the subproblems created through decoupling, in order to determine the stability of the solution scheme. Furthermore, the procedures presented for the spatial partitioning together with the framework provided for coupled execution of the existing physics of PANDAS open new opportunities for numerical treatment of more practical problems. For instance, implementing the partitioning schemes in the sense of domain decomposition provides an effective tool for breaking down the real-size 3-d problems into smaller subproblems, which can then be treated in a sequential or parallel manner. Another special case of interest would be to enhance the solution method proposed for the problem of FPMI, for example via including the fluid mass exchange between the bulk-fluid and the porous-medium subproblems. In this connection, several strategies for coupling of the free flow with the pore-fluid flow are proposed in the literature that shall be scrutinised.

Following that, a suitable method has to be adopted and appropriately integrated in the provided solution package. Moreover, the enhancement can be achieved through equipping the solver with a more efficient interface subroutine. To this end, the computational costs incurred by the matrix inversion operations shall be diminished. Apart from that, replacing the LLM method by a staggered integration technique leads to complete elimination of the interface subroutine and, hence, offers a potential alternative for a more efficient solution strategy.

Appendix A: Stability Analysis of the Isothermal Operator-Splitting Scheme

Recalling (6.10), one has

$$\left\{\begin{array}{rcl} \dfrac{u_j^{n+1}-u_j^n}{\Delta t} &=& v_j^{n+1/2}\,, \\ \dfrac{v_j^{n+1}-v_j^n}{\Delta t} &=& \dfrac{1}{\rho}\,\left[\dfrac{E}{\Delta x^2}\,(u_{j+1}^{n+1/2}-2\,u_j^{n+1/2}+u_{j-1}^{n+1/2})+\dfrac{m}{2\,\Delta x}\,(\vartheta_{j+1}^n-\vartheta_{j-1}^n)\right], \\ \dfrac{\vartheta_j^{n+1}-\vartheta_j^n}{\Delta t} &=& \dfrac{1}{c_v}\,\left[\dfrac{k}{\Delta x^2}\,(\vartheta_{j+1}^{n+1/2}-2\,\vartheta_j^{n+1/2}+\vartheta_{j-1}^{n+1/2})+\dfrac{\theta_0\,m}{2\,\Delta x}\,(v_{j+1}^{n+1}-v_{j-1}^{n+1})\right], \end{array}\right. \tag{A.1}$$

where following the trapezoidal rule (TR)

$$\mathfrak{u}_k^{n+1/2} := \frac{1}{2}\,(\mathfrak{u}_k^{n+1}+\mathfrak{u}_k^n) \quad \text{with} \quad \mathfrak{u}=\{u,v,\vartheta\} \quad \text{and} \quad k=\{j-1,j,j+1\}\,. \tag{A.2}$$

Moreover, the 1-d version of the inverse Fourier transform (5.71) reads

$$\mathfrak{u}_k^m = \frac{1}{\sqrt{2\pi}}\int_{-\pi/\Delta x}^{\pi/\Delta x} e^{I\,k\,\Theta}\hat{\mathfrak{u}}^m(\xi)\,\mathrm{d}\xi\,. \tag{A.3}$$

Inserting (A.3) in (6.10), the system of governing equations can be written as

$$\mathbf{A}\,\hat{\mathbf{u}}^{n+1}+\mathbf{B}\,\hat{\mathbf{u}}^n=\mathbf{0} \quad \rightarrow \quad \hat{\mathbf{u}}^{n+1}=-\mathbf{A}^{-1}\,\mathbf{B}\hat{\mathbf{u}}^n := \mathbf{G}\,\hat{\mathbf{u}}^n\,, \tag{A.4}$$

where $\hat{\mathbf{u}}^m$ is the Fourier transform of $\mathbf{u}_j^m$. Furthermore,

$$\mathbf{A} := \begin{bmatrix} \frac{1}{\Delta t} & -\frac{1}{2} & 0 \\ -\frac{E}{\Delta x^2}\,(\cos\Theta-1) & \frac{\rho}{\Delta t} & 0 \\ 0 & -\frac{\theta_0\,m}{\Delta x}\,I\,\sin\Theta & \frac{k}{\Delta x^2}\,(1-\cos\Theta)+\frac{c_v}{\Delta t} \end{bmatrix} \tag{A.5}$$

and

$$\mathbf{B} := \begin{bmatrix} -\frac{1}{\Delta t} & -\frac{1}{2} & 0 \\ \frac{E}{\Delta x^2}\,(1-\cos\Theta) & -\frac{\rho}{\Delta t} & -\frac{m}{\Delta x}\,I\,\sin\Theta \\ 0 & 0 & \frac{k}{\Delta x^2}\,(1-\cos\Theta)-\frac{c_v}{\Delta t} \end{bmatrix}. \tag{A.6}$$

Then, after some simplifications and following the procedure described in Section 5.4.2, the Hurwitz polynomial for the isothermal operator-splitting scheme reads

$$G_H(s) = \beta_3\, s^3 + \beta_2\, s^2 + \beta_1\, s + \beta_0 \tag{A.7}$$

with

$$\begin{aligned}
\beta_3 &= (1 - \cos^2\Theta)\,\theta_0\,\Delta t^2\,\Delta x^2\,m^2 - 4\,\Delta x^4\,\rho\,c_v\,,\\
\beta_2 &= (\cos\Theta - 1)\,\Delta t\,\Delta x^2\rho\,k\,,\\
\beta_1 &= (\cos^2\Theta - 1)\,\theta_0\,\Delta t^2\,\Delta x^2\,m^2 + 2\,(\cos\Theta - 1)\,E\,c_v\,\Delta t^2\,\Delta x^2\,,\\
\beta_0 &= (2\,\cos\Theta - 1 - \cos^2\Theta)\,E\,k\,\Delta t^3\,.
\end{aligned} \tag{A.8}$$

Investigating β_0 shows that

$$\beta_0 \le 0 \quad \forall\{E\,,k\,,\Delta t\} \ge 0 \quad \text{and} \quad \Theta \in [-\pi,\pi] \tag{A.9}$$

and, hence, $G_H(s)$ must be multiplied by -1. Doing so, the new coefficients of the Hurwitz polynomial read

$$\begin{aligned}
\beta_3 &= -(1 - \cos^2\Theta)\,\theta_0\,\Delta t^2\,\Delta x^2\,m^2 + 4\,\Delta x^4\,\rho\,c_v\,,\\
\beta_2 &= -(\cos\Theta - 1)\,\Delta t\,\Delta x^2\rho\,k\,,\\
\beta_1 &= -(\cos^2\Theta - 1)\,\theta_0\,\Delta t^2\,\Delta x^2\,m^2 - 2\,(\cos\Theta - 1)\,E\,c_v\,\Delta t^2\,\Delta x^2\,,\\
\beta_0 &= -(2\,\cos\Theta - 1 - \cos^2\Theta)\,E\,k\,\Delta t^3\,.
\end{aligned} \tag{A.10}$$

Moreover, based on the LCC and referring to Table 5.1, $\{\beta_0,\,\beta_1,\,\Delta_2,\,\beta_3\} \ge 0$ is the necessary stability condition for a 3rd-order Hurwitz polynomial. Accordingly, the second Hurwitz determinant Δ_2 for this case can be calculated from (5.88) and reads after some simplifications

$$\Delta_2 = \begin{vmatrix} \beta_1 & \beta_3 \\ \beta_0 & \beta_2 \end{vmatrix} = \sin^2\Theta\,\Delta x^2\,m^2\,\Delta t^3\,k\,\theta_0\left[\Delta t^2\,E\,(1-\cos\Theta)^2 + 2\,\Delta x^2\,\rho\,(1-\cos\Theta)\right]. \tag{A.11}$$

A careful investigation of (A.10) and (A.11) shows that

$$\{\beta_0,\,\beta_1,\,\beta_2,\Delta_2\} \ge 0 \quad \forall\Theta \in [-\pi,\pi]\,. \tag{A.12}$$

However,

$$\beta_3 \ge 0 \quad \Longleftrightarrow \quad \frac{\Delta t}{\Delta x} \le \frac{2\,\sqrt{\rho\,c_v/\theta_0}}{|m|} \tag{A.13}$$

and, consequently, (A.13) is the CFL condition for the isothermal operator-splitting scheme.

Appendix B: Stability Analysis of the LLM Method Applied to the Problem of FPMI

The system of governing equations for the FPMI problem as presented by (7.67) reads

$$
\begin{aligned}
\mathcal{X}^P: &\quad \begin{cases} (u_S)'_S = v_S\,, \\ \rho^S\,(v_S)'_S = H^S_A\,(u_S)_{,xx} + \dfrac{(n^F)^2\,\gamma^{FR}}{k^F}\,w_F + n^S\,\Gamma^P\,[n^S\,(v_S)_{,xx} + n^F(v_F)_{,xx}]\,, \\ \rho^F\,(v_F)'_S = -\dfrac{(n^F)^2\,\gamma^{FR}}{k^F}\,w_F + n^F\,\Gamma^P\,[n^S\,(v_S)_{,xx} + n^F(v_F)_{,xx}]\,, \end{cases} \\
\mathcal{X}^L: &\quad \rho^L\,(v_L)'_M = \Gamma^L\,(v_L)_{,xx}\,, \\
\mathcal{X}^\mathfrak{I}: &\quad \begin{cases} v_S^{int} - v_\mathfrak{I} = 0\,, \\ v_F^{int} - v_\mathfrak{I} = 0\,, \\ v_L^{int} - v_\mathfrak{I} = 0\,. \end{cases}
\end{aligned}
\tag{B.1}
$$

Spatial discretisation of the above equations via the CD scheme (7.68) accompanied by the temporal discretisation using the mid-point rule (4.22) generates the finite-difference stencil. Moreover, from the inverse Fourier transform, one has

$$
(\,\cdot\,)^n_h = \frac{1}{\sqrt{2\pi}} \int_{-\pi/\Delta x}^{\pi/\Delta x} e^{Ih\Theta}(\,\hat{\cdot}\,)^n(\xi_\beta)\,\mathrm{d}\xi_\beta\,, \tag{B.2}
$$

where $I := \sqrt{-1}$, $\Theta \in [-\pi, \pi]$ and $\xi_\beta := \Theta/\Delta x_\beta$. Subsequently, one finds the counterpart of (7.61) as

$$
\widetilde{\mathfrak{S}}_d\,\hat{\mathbf{u}}^{n+\frac{1}{2}} - \tilde{\mathbf{f}} = \mathbf{0}\,. \tag{B.3}
$$

Therein, $\hat{\mathbf{u}} := \Big[\hat{\boldsymbol{y}}_P\,, \hat{y}_L\,, \hat{y}_\mathfrak{I}\,, \hat{\boldsymbol{\ell}}^P\,, \hat{\ell}^L\Big]^T$, $\tilde{\mathbf{f}} := \Big[\tilde{\boldsymbol{f}}_P\,, \tilde{f}_L\,, 0\,, \mathbf{0}\,, 0\Big]^T$, and

$$
\widetilde{\mathfrak{S}}_d := \begin{bmatrix} \widetilde{\boldsymbol{\mathcal{K}}}_P & \mathbf{0} & \mathbf{0} & \frac{\Delta t}{2}\,\boldsymbol{\mathcal{B}}_P & \mathbf{0} \\ \mathbf{0} & \widetilde{\mathcal{K}}_L & 0 & \mathbf{0} & \frac{\Delta t}{2}\,\mathcal{B}_L \\ \mathbf{0} & 0 & 0 & \boldsymbol{\mathcal{L}}_P^T & \mathcal{L}_L \\ \boldsymbol{\mathcal{B}}_P^T & \mathbf{0} & -\boldsymbol{\mathcal{L}}_P & \mathbf{0} & \mathbf{0} \\ \mathbf{0} & \mathcal{B}_L & -\mathcal{L}_L & \mathbf{0} & 0 \end{bmatrix}. \tag{B.4}
$$

Therein, use has been made of the following notations:

$$\begin{aligned}
&\hat{\boldsymbol{y}}_P := [\hat{u}_S\,, \hat{v}_S\,, \hat{v}_F]^T\,, \quad \hat{y}_L := \hat{v}_L\,, \quad \hat{y}_\mathfrak{I} := \hat{v}_\mathfrak{I}\,, \quad \hat{\boldsymbol{\ell}}^P := [\hat{\ell}^S\,, \hat{\ell}^F]^T\,,\\
&\tilde{\boldsymbol{f}}_P := [\tilde{f}_{S1}\,, \tilde{f}_{S2}\,, \tilde{f}_F]^T = \boldsymbol{\mathcal{M}}_P\, \hat{\boldsymbol{y}}_P^n\,, \quad \tilde{f}_L = \mathcal{M}_L\, \hat{y}_L^n\,,\\
&\widetilde{\boldsymbol{\mathcal{K}}}_P := (\boldsymbol{\mathcal{M}}_P + \tfrac{\Delta t}{2}\, \boldsymbol{\mathcal{K}}_P)\,, \qquad \text{and} \quad \widetilde{\mathcal{K}}_L := (\mathcal{M}_L + \tfrac{\Delta t}{2}\, \mathcal{K}_L)\,,
\end{aligned} \tag{B.5}$$

where

$$\mathcal{M}_L = \rho^L\,, \quad \mathcal{K}_L = -r_L\, \Gamma^L\,, \tag{B.6}$$

and $\boldsymbol{\mathcal{M}}_P$ and $\boldsymbol{\mathcal{K}}_P$ are 3×3 matrices, where the only non-zero terms are

$$\begin{aligned}
&\mathcal{M}_{P11} = 1\,, \qquad \mathcal{M}_{P22} = \rho^S\,, \qquad \mathcal{M}_{P33} = \rho^F\,,\\
&\mathcal{K}_{P12} = -1\,, \qquad \mathcal{K}_{P21} = -r_P\, H_A^S\,,\\
&\mathcal{K}_{P22} = \frac{(n^F)^2\, \gamma^{FR}}{k^F} - r_P\, (n^S)^2\, \Gamma^P\,, \qquad \mathcal{K}_{P23} = -\frac{(n^F)^2\, \gamma^{FR}}{k^F} - r_P\, n^S\, n^F\, \Gamma^P\,,\\
&\mathcal{K}_{P32} = -\frac{(n^F)^2\, \gamma^{FR}}{k^F} - r_P\, n^F\, n^S\, \Gamma^P\,, \quad \mathcal{K}_{P33} = \frac{(n^F)^2\, \gamma^{FR}}{k^F} - r_P\, (n^F)^2\, \Gamma^P
\end{aligned} \tag{B.7}$$

with

$$r_\mathfrak{a} := \frac{2\,(\cos\Theta - 1)}{(\Delta\, x_\mathfrak{a})^2} \quad \text{for} \quad \mathfrak{a} = \{L\,, P\}\,. \tag{B.8}$$

Furthermore, $\boldsymbol{\mathcal{B}}_P$, $\mathcal{B}_L$, $\boldsymbol{\mathcal{L}}_P$ and $\mathcal{L}_L$ represent the coupling operators, where

$$\boldsymbol{\mathcal{B}}_P = \begin{bmatrix} 0 & 0 \\ \mathcal{B}_S & 0 \\ 0 & \mathcal{B}_F \end{bmatrix} \quad \text{and} \quad \boldsymbol{\mathcal{L}}_P = \begin{bmatrix} \mathcal{L}_S \\ \mathcal{L}_F \end{bmatrix}. \tag{B.9}$$

Therein, $\mathcal{B}_\beta$ and $\mathcal{L}_\beta$, $\beta = \{S\,, F\,, L\}$, are scalars in the range of 0 through 1, which determine the strength of coupling between the equations, such that setting these equal to zero renders (B.3) to a decoupled system of equations. Subsequently, and according to the solution algorithm of Section 7.3.2, solving the first two rows of (B.3) for the kinematic variables $\boldsymbol{y}_P$ and y_L yields

$$\hat{\boldsymbol{y}}_P^{n+\frac{1}{2}} = \widetilde{\boldsymbol{\mathcal{K}}}_P^{-1}\, \left[\boldsymbol{\mathcal{M}}_P\, \hat{\boldsymbol{y}}_P^n - \tfrac{\Delta t}{2}\, \boldsymbol{\mathcal{B}}_P\, (\hat{\boldsymbol{\ell}}^P)^{n+\frac{1}{2}}\right]\,, \; \hat{y}_L^{n+\frac{1}{2}} = \widetilde{\mathcal{K}}_L^{-1}\, \left[\mathcal{M}_L\, \hat{y}_L^n - \tfrac{\Delta t}{2}\, \mathcal{B}_L\, (\hat{\ell}^L)^{n+\frac{1}{2}}\right]. \tag{B.10}$$

Substituting these relations in the last three rows of (B.3) leads to the following equation system at the interface

$$\begin{bmatrix} \hat{\boldsymbol{\ell}} \\ \hat{y}_\mathfrak{I} \end{bmatrix} n + \frac{1}{2} = \underbrace{\boldsymbol{A}^{-1}\, \boldsymbol{B}}_{=:\, \mathbf{G}_\mathfrak{I}} \begin{bmatrix} \hat{\boldsymbol{y}}_P \\ \hat{y}_L \end{bmatrix}^n \tag{B.11}$$

with $\hat{\boldsymbol{\ell}} := [\hat{\boldsymbol{\ell}}^P, \hat{\ell}^L]^T$,

$$\boldsymbol{A} := \begin{bmatrix} \frac{\Delta t}{2}\,\boldsymbol{\mathcal{B}}_P^T\,\widetilde{\boldsymbol{\mathcal{K}}}_P^{-1}\,\boldsymbol{\mathcal{B}}_P & \mathbf{0} & \boldsymbol{\mathcal{L}}_P \\ \mathbf{0} & \frac{\Delta t}{2}\,\mathcal{B}_L\,\widetilde{\mathcal{K}}_L^{-1}\,\mathcal{B}_L & \mathcal{L}_L \\ \boldsymbol{\mathcal{L}}_P^T & \mathcal{L}_L & 0 \end{bmatrix} \tag{B.12}$$

and

$$\boldsymbol{B} := \begin{bmatrix} \boldsymbol{\mathcal{B}}_P^T\,\widetilde{\boldsymbol{\mathcal{K}}}_P^{-1}\,\boldsymbol{\mathcal{M}}_P & \mathbf{0} \\ \mathbf{0} & \mathcal{B}_L\,\widetilde{\mathcal{K}}_L^{-1}\,\mathcal{M}_L \\ \mathbf{0} & 0 \end{bmatrix}. \tag{B.13}$$

The matrix inversion in (B.11) could conveniently be done by partitioning $\boldsymbol{A}$ into block form:

$$\boldsymbol{A} = \begin{bmatrix} \boldsymbol{A}_{11} & \boldsymbol{A}_{12} \\ \boldsymbol{A}_{21} & \boldsymbol{A}_{22} \end{bmatrix}$$

$$\rightarrow \quad \boldsymbol{A}^{-1} = \begin{bmatrix} \boldsymbol{A}_{11}^{-1} + \boldsymbol{A}_{11}^{-1}\,\boldsymbol{A}_{12}\,\mathbf{S}_{\boldsymbol{A}_{11}}^{-1}\,\boldsymbol{A}_{21}\,\boldsymbol{A}_{11}^{-1} & -\boldsymbol{A}_{11}^{-1}\,\boldsymbol{A}_{12}\,\mathbf{S}_{\boldsymbol{A}_{11}}^{-1} \\ -\mathbf{S}_{\boldsymbol{A}_{11}}^{-1}\,\boldsymbol{A}_{21}\,\boldsymbol{A}_{11}^{-1} & \mathbf{S}_{\boldsymbol{A}_{11}}^{-1} \end{bmatrix} =: \begin{bmatrix} \bar{\boldsymbol{A}}_{11} & \bar{\boldsymbol{A}}_{12} \\ \bar{\boldsymbol{A}}_{21} & \bar{\boldsymbol{A}}_{22} \end{bmatrix}. \tag{B.14}$$

Therein, $\mathbf{S}_{\boldsymbol{A}_{11}} := \boldsymbol{A}_{22} - \boldsymbol{A}_{21}\boldsymbol{A}_{11}^{-1}\boldsymbol{A}_{12}$ represents the Schur complement of the block $\boldsymbol{A}_{11}$, and $\boldsymbol{A}_{ij}$ embodies the following 2×2 matrices:

$$\begin{aligned} &\boldsymbol{A}_{11} = \tfrac{\Delta t}{2}\,\boldsymbol{\mathcal{B}}_P^T\,\widetilde{\boldsymbol{\mathcal{K}}}_P^{-1}\,\boldsymbol{\mathcal{B}}_P\,, \quad \boldsymbol{A}_{12} = [\mathbf{0} \quad \boldsymbol{\mathcal{L}}_P]\,, \\ &\boldsymbol{A}_{21} = \boldsymbol{A}_{12}^T\,, \qquad\qquad \boldsymbol{A}_{22} = \begin{bmatrix} \frac{\Delta t}{2}\,\mathcal{B}_L\,\widetilde{\mathcal{K}}_L^{-1}\,\mathcal{B}_L & \mathcal{L}_L \\ \mathcal{L}_L & 0 \end{bmatrix}. \end{aligned} \tag{B.15}$$

Moreover, after expansion, $\boldsymbol{B}$ could also be written in the following block form

$$\boldsymbol{B} = \begin{bmatrix} \boldsymbol{B}_{11} & \boldsymbol{B}_{12} \\ \mathbf{0} & \boldsymbol{B}_{22} \end{bmatrix}, \tag{B.16}$$

where

$$\begin{aligned} &\boldsymbol{B}_{11} = \begin{bmatrix} \bar{\mathcal{K}}_{P21} & \bar{\mathcal{K}}_{P22}\,\mathcal{M}_{P22} \\ \bar{\mathcal{K}}_{P31} & \bar{\mathcal{K}}_{P32}\,\mathcal{M}_{P22} \end{bmatrix}, \quad \boldsymbol{B}_{12} = \begin{bmatrix} \bar{\mathcal{K}}_{P32}\,\mathcal{M}_{P33} & 0 \\ \bar{\mathcal{K}}_{P33}\,\mathcal{M}_{P33} & 0 \end{bmatrix}, \\ &\boldsymbol{B}_{22} = \begin{bmatrix} 0 & \mathcal{M}_L\,\widetilde{\mathcal{K}}_L^{-1} \\ 0 & 0 \end{bmatrix} \qquad \text{with} \quad [\bar{\mathcal{K}}_{Pij}] := \widetilde{\boldsymbol{\mathcal{K}}}_P^{-1}\,. \end{aligned} \tag{B.17}$$

Thus, the matrix $\mathbf{G}_{\mathfrak{J}} := \boldsymbol{A}^{-1}\,\boldsymbol{B}$ in conjunction with $(\text{B.14})_3$ and (B.16) reads

$$\mathbf{G}_{\mathfrak{J}} = \begin{bmatrix} \bar{\boldsymbol{A}}_{11}\,\mathbf{B}_{11} & \bar{\boldsymbol{A}}_{11}\,\mathbf{B}_{12} + \bar{\boldsymbol{A}}_{12}\,\mathbf{B}_{22} \\ \bar{\boldsymbol{A}}_{21}\,\mathbf{B}_{11} & \bar{\boldsymbol{A}}_{21}\,\mathbf{B}_{12} + \bar{\boldsymbol{A}}_{22}\,\mathbf{B}_{22} \end{bmatrix}. \tag{B.18}$$

Careful investigation of $\mathbf{G}_{\mathfrak{J}}$ reveals that this is actually a 4×4 matrix, the multiplication of which with the kinematic DOF of the subdomains at time $t = t_n$ updates both variables $\hat{\boldsymbol{\ell}}$ and $\hat{y}_{\mathfrak{J}}$. In particular,

$$\begin{bmatrix} \hat{\boldsymbol{\ell}}^P \\ \hat{\ell}^L \end{bmatrix}^{n+\frac{1}{2}} = \mathbf{G}_{\mathfrak{J}}^{\boldsymbol{\ell}} \begin{bmatrix} \hat{\boldsymbol{y}}_P \\ \hat{y}_L \end{bmatrix}^{n} \quad \text{with} \quad \mathbf{G}_{\mathfrak{J}}^{\boldsymbol{\ell}} := \begin{bmatrix} G_{\mathfrak{J}11} & \cdots & G_{\mathfrak{J}14} \\ . & \ddots & . \\ G_{\mathfrak{J}31} & \cdots & G_{\mathfrak{J}34} \end{bmatrix}. \tag{B.19}$$

Inserting this relation into two first rows of (B.3), one finds after rearrangement

$$\begin{bmatrix} \hat{\boldsymbol{y}}_P \\ \hat{y}_L \end{bmatrix}^{n+1} = \mathbf{G} \begin{bmatrix} \hat{\boldsymbol{y}}_P \\ \hat{y}_L \end{bmatrix}^{n}, \tag{B.20}$$

where $\mathbf{G}$ is the amplification matrix and reads

$$\mathbf{G} := 2\,\widetilde{\boldsymbol{\mathcal{K}}}^{-1}\,(\boldsymbol{\mathcal{M}} - \frac{\Delta t}{2}\,\boldsymbol{\mathcal{B}}\,\mathbf{G}_{\mathfrak{J}}^{\ell} - \frac{1}{2}\,\widetilde{\boldsymbol{\mathcal{K}}}) \tag{B.21}$$

with

$$\widetilde{\boldsymbol{\mathcal{K}}} := \begin{bmatrix} \widetilde{\boldsymbol{\mathcal{K}}}_P & \mathbf{0} \\ \mathbf{0} & \widetilde{\mathcal{K}}_L \end{bmatrix},\ \boldsymbol{\mathcal{M}} := \begin{bmatrix} \boldsymbol{\mathcal{M}}_P & \mathbf{0} \\ \mathbf{0} & \mathcal{M}_L \end{bmatrix},\ \boldsymbol{\mathcal{B}} := \begin{bmatrix} \boldsymbol{\mathcal{B}}_P & \mathbf{0} \\ \mathbf{0} & \mathcal{B}_L \end{bmatrix}. \tag{B.22}$$

Then, the scheme is stable, if the spectral radius of the amplification matrix, i. e., the biggest eigenvalue of $\mathbf{G}$ in the absolute form, is smaller than unity. This condition can be checked via the Liénard-Chipart Criterion (LCC). To this end, after assembling the amplification and subsequently the Hurwitz polynomials, one has to investigate the positivity of the corresponding parameters associated to the latter. In particular, for the present case, one ends up with a Hurwitz polynomial of order 3 with the following LCC parameters:

$$\begin{aligned} \beta_0 &= 1 - \cos\,\Theta\,, \\ \beta_1 &= (1 - \cos\,\Theta)\,(\Gamma^L + \Gamma^P)\,, \\ \beta_2 &= 16\,(\rho^S + \rho^F + \rho^L)\,. \end{aligned} \tag{B.23}$$

It is obvious that

$$\{\beta_0,\,\beta_1,\,\beta_2\} \geq 0 \quad \forall\,\Theta \in [-\pi, \pi] \quad \text{and} \quad \forall\,\Delta t\,, \Delta x_{\mathfrak{a}} > 0 \tag{B.24}$$

and, hence, the partitioned solution scheme applied to the equation system (7.67) is unconditionally stable.

Bibliography

[1] Aiken, R. C. (ed.): *Stiff Computation*. Oxford University Press, Oxford 1985.

[2] Allen, D. H.: *How Mechanics Shaped the Modern World*. Springer International Publishing, Switzerland 2014.

[3] Argyris, J.; Doltsinis, I. S.; Pimenta, P. & Wüstenberg, H.: Thermomechanical response of solids at high strains – natural approach. *Computer Methods in Applied Mechanics and Engineering* **32** (1982), 3–57.

[4] Armero, F. & Simo, J.: A new unconditionally stable fractional step method for non-linear coupled thermomechanical problems. *International Journal for Numerical Mehtods in Engineering* **35** (1992), 737–766.

[5] Ascher, U. M.: *Numerical Methods for Evolutionary Differential Equations*. SIAM, Philadelphia, PA 2008.

[6] Avci, O.: *Coupled Deformation and Flow Processes of Partially Saturated Soil: Experiments, Model Validation and Numerical Investigations*. Dissertation Thesis, Report No. II-26 of the Institute of Applied Mechanics (CE), University of Stuttgart 2013.

[7] Axelsson, O.: A class of A-stable methods. *BIT Numerical Mathematics* **9** (1969), 185–199.

[8] Banerjee, P. K.: *The Boundary Element Methods in Engineering*. 2nd edn. McGraw-Hill, London 1994.

[9] Bank, R. E.; Coughran, W. M.; Fichtner, W.; Grosse, E. H.; Rose, D. J. & Smith, R. K.: Transient simulation of silicon devices and circuits. *IEEE Transactions on Computer-Aided Design* **4** (1985), 436–451.

[10] Barry, D. A.; Bajracharya, K. & Miller, C. T.: Alternative split-operator approach for solving chemical reaction/groundwater transport models. *Advances in Water Resources* **19** (1996), 261–275.

[11] Barry, D. A.; Miller, C. T.; Culligan, P. J. & Bajracharya, K.: Analysis of split operator methods for nonlinear and multispecies groundwater chemical transport models. *Mathematics and Computers in Simulation* **43** (1997), 331–341.

[12] Bathe, K.-J.: *Finite Element Procedures*. 2nd edn. Prentice Hall, Englewood Cliffs, NJ 1996.

[13] Bathe, K.-J.; Zhang, H. & Ji, S.: Finite element analysis of fluid flows fully coupled with structural interactions. *Computers and Structures* **72** (1999), 1–16.

[14] Bathe, K.-J.; Zhang, H. & Wang, M. H.: Finite element analysis of incompressible and compressible fluid flows with free surfaces and structural interactions. *Computers and Structures* **56** (1995), 193–213.

[15] Bažant, Z. P. & Cedolin, L.: *Stability of Structures*. Oxford University Press, New York, NY 1991.

[16] Belvin, W. K. & Park, K. C.: Structural tailoring and feedback control synthesis – An interdisciplinary approach. *Journal of Guidance, Control, and Dynamics* **13** (1990), 424–429.

[17] Belytschko, T.; Liu, W. K. & Moran, B.: *Nonlinear Finite Elements for Continua and Structures*. John Wiley & Sons, Chichester 2000.

[18] Belytschko, T. & Mullen, R.: Stability of explicit-implicit mesh partitions in time integration. *International Journal for Numerical Methods in Engineering* **12** (1978), 1575–1586.

[19] Berger, M. J.: Stability of interfaces with mesh refinement. *Mathematics of Computation* **45** (1985), 301–318.

[20] Bernardi, C.; Maday, Y. & Patera, A. T.: Domain decomposition by the mortar element method. In Kaper, H. G. & Garbey, M. (eds.): *Asymptotic and Numerical Methods for Partial Differential Equations with Critical Parameters*. Springer-Verlag, Netherlands 1993, pp. 269–286.

[21] Bernardi, C.; Maday, Y. & Patera, A. T.: A new nonconforming approach to domain decomposition: The mortar element method. In Brezis, H. & Lions, J.-L. (eds.): *Nonlinear Partial Differential Equations and Their Applications, Vol. XI*. Longman Scientific & Technical, Harlow 1994, pp. 13–51.

[22] Bertsekas, D. P.: *Constrained Optimization and Lagrange Multiplier Methods*. Athena Scientific, Belmont, MA 1996.

[23] Biot, M. A.: General theory of three dimensional consolidation. *Journal of Applied Physics* **12** (1941), 155–164.

[24] Bjørstad, P. & Widlund, O.: Iterative methods for the solution of elliptic problems on regions partitioned into substructures. *SIAM Journal on Numerical Analysis* **23** (1986), 1097–1120.

[25] Blom, F. J.: A monolithical fluid-structure interaction algorithm applied to the piston problem. *Computer Methods in Applied Mechanics and Engineering* **167** (1998), 369–391.

[26] de Boer, R.: *Vektor- und Tensorrechnung für Ingenieure*. Springer-Verlag, Berlin 1982.

[27] de Boer, R. & Ehlers, W.: *Theorie der Mehrkomponentenkontinua mit Anwendung auf bodenmechanische Probleme*. Forschungsberichte aus dem Fachbereich Bauwesen, Heft 40, Universität-GH-Essen 1986.

[28] de Boer, R.; Ehlers, W. & Liu, Z.: One-dimensional transient wave propagation in fluid-saturated incompressible porous media. *Archiv of Applied Mechanics* **63** (1993), 59–72.

[29] Boerkoel, J. C. & Durfee, E. H.: A comparison of algorithms for solving the multi-agent simple temporal problem. In *Proceedings of the Twentieth International Conference on Automated Planning and Scheduling*, AAAI Press, Toronto 2010, pp. 26–33.

[30] Bowen, R. M.: Incompressible porous media models by use of the theory of mixtures. *International Journal of Engineering Science* **18** (1980), 1129–1148.

[31] Bowen, R. M.: Compressible porous media models by use of the theory of mixtures. *International Journal of Engineering Science* **20** (1982), 697–735.

[32] Boyer, C. B.: *A History of Mathematics*. John Wiley & Sons, New York, NY 1968.

[33] Braess, D.: *Finite Elemente*. Springer-Verlag, Berlin 1997.

[34] Brezina, C.: *Al-Khwarizmi: The Inventor of Algebra*. The Rosen Publishing Group, New York, NY 2006.

[35] Brezzi, F. & Fortin, M.: *Mixed and Hybrid Finite Element Methods*. Springer-Verlag, New York 1991.

[36] Brezzi, F. & Marini, L. D.: A three-field domain decomposition method. *Contemporary Mathematics* **157** (1994), 27–34.

[37] Bryant, J. D.; David, T.; Gaskell, P. H.; King, S. & Lond, G.: Rheology of bovine bone marrow. *Proceedings of the Institution of Mechanical Engineers. Part H, Journal of Engineering in Medicine* **203** (1989), 71–75.

[38] Burrage, K.: *Stability and Efficiency Properties of Implicit Runge-Kutta Methods*. Dissertation Thesis, Department of Mathematics, University of Auckland, Auckland 1978.

[39] Burrage, K.: *Parallel and Sequential Methods for Ordinary Differential Equations*. Clarendon Press, Oxford 1995.

[40] Burrage, K. & Butcher, J. C.: Stability criteria for implicit Runge-Kutta methods. *SIAM Journal on Numerical Analysis* **16** (1979), 46–57.

[41] Butcher, J. C.: Coefficients for the study of Runge-Kutta integration processes. *Journal of the Australian Mathematical Society* **3** (1963), 185–201.

[42] Butcher, J. C.: Implicit Runge-Kutta processes. *Mathematics of Computation* **18** (1964), 50–64.

[43] Butcher, J. C.: A stability property of implicit Runge-Kutta methods. *BIT Numerical Mathematics* **15** (1975), 358–361.

[44] Cai, X.-C. & Sarkis, M.: A restricted additive Schwarz preconditioner for general sparse linear systems. *SIAM Journal on Scientific Computing* **21** (1999), 792–797.

[45] Cao, Y.; Helmig, R. & Wohlmuth, B.: A two-scale operator-splitting method for two-phase flow in porous media. *Advances in Water Resources* **34** (2011), 1581–1596.

[46] Cartwright, J. H. E. & Piro, O.: The dynamics of Runge-Kutta methods. *International Journal of Bifurcation and Chaos* **2** (1992), 427–449.

[47] Chadwick, P.: *Continuum Mechanics: Concise Theory and Problems*. 2nd edn. Dover Publications, Mineola, NY 1999.

[48] Charney, J. G.; Fjörtoft, R. & von Neumann, J.: Numerical integration of the barotropic vorticity equation. *Tellus* **2** (1950), 237–254.

[49] Chen, C.: *Mapping Scientific Frontiers: The Quest for Knowledge Visualization*. Springer-Verlag, London 2013.

[50] Chen, W. K.: *Active Network Analysis*. World Scientific, Portland, OR 1991.

[51] Cheng, A.-D. & Detournay, E.: On singular integral equations and fundamental solutions of poroelasticity. *International Journal of Solids and Structures* **35** (1998), 4521–4555.

[52] Chorin, A.: A numerical method for solving incompressible viscous problems. *Journal of Applied Physics* **2** (1967), 12–26.

[53] Coelho, R. F.; Breitkopf, P. & Knopf-Lenoir, C.: Model reduction for multidisciplinary optimization – application to a 2D wing. *Structural and Multidisciplinary Optimization* **37** (2008), 29–48.

[54] Cooke, R. L.: *The History of Mathematics: A Brief Course*. John Wiley & Sons, Hoboken, NJ 2013.

[55] Corcoran, J.: Aristotle's prior analytics and Boole's laws of thought. *History and Philosophy of Logic* **24** (2003), 261–288.

[56] Courant, R.: *Dirichlet's principle, Conformal Mapping, and Minimal Surfaces*. Interscience, New York, NY 1950.

[57] Courant, R.; Friedrichs, K. O. & Lewy, H.: Über die partiellen Differenzengleichungen der mathematischen Physik. *Mathematische Annalen* **100** (1928), 32–74.

[58] Crouzeix, M.: Sur la B-stabilité des méthodes de Runge-Kutta. *Numerische Mathematik* **32** (1979), 75–82.

[59] Curtiss, C. F. & Hirschfelder, J. O.: Integration of stiff equations. *Proceedings of the National Academy of Sciences of the United States of America* **38** (1952), 235–243.

[60] Dahlquist, G.: A special stability problem for linear multistep methods. *BIT Numerical Mathematics* **3** (1963), 27–43.

[61] Dahlquist, G.: G-stability is equivalent to A-stability. *BIT Numerical Mathematics* **18** (1978), 384–401.

[62] Dechter, R.: Bucket elimination: A unifying framework for reasoning. *Artificial Intelligence* **113** (1999), 41–85.

[63] Degroote, J.; Bruggeman, P.; Haelterman, R. & Vierendeels, J.: Stability of a coupling technique for partitioned solvers in FSI applications. *Computers and Structures* **86** (2008), 2224–2234.

[64] Dekker, K. & Verwer, J. G.: *Stability of Runge-Kutta Methods for Stiff Nonlinear Differential Equations*. CWI Monographs, Amsterdam 1984.

[65] Der, R. & Martius, G.: *The Playful Machine*. Springer-Verlag, Berlin 2011.

[66] Diebels, S. & Ehlers, W.: Dynamic analysis of a fully saturated porous medium accounting for geometrical and material non-linearities. *International Journal for Numerical Methods in Engineering* **39** (1996), 81–97.

[67] Donea, J. & Huerta, A.: *Finite Element Methods for Flow Problems*. John Wiley & Sons, Chichester 2003.

[68] Dryja, M.: An additive Schwarz algorithm for two- and three-dimensional finite element elliptic problems. In Chan, T. F.; Glowinski, R.; Périaux, J. & Widlund, O. B. (eds.): *Domain Decomposition Methods*. SIAM, Philadelphia, PA 1989, pp. 168–172.

[69] Dryja, M. & Proskurowski, W.: On preconditioners for mortar discretization of elliptic problems. *Numerical Linear Algebra with Applications* **10** (2003), 65–82.

[70] Dryja, M. & Widlund, O. B.: Towards a unified theory of domain decomposition algorithms for elliptic problems. In Chan, T. F.; Glowinski, R.; Périaux, J. & Widlund, O. B. (eds.): *Proceedings of the Third International Symposium on Domain Decomposition Methods for Partial Differential Equations*, SIAM, Philidelphia, PA 1990, pp. 3–21.

[71] Dryja, M. & Widlund, O. B.: Additive Schwarz methods for elliptic finite element problems in three dimensions. In Keyes, D. E.; Chan, T. F.; Meurant, G.; Scroggs, J. S. & Voigt, R. G. (eds.): *Proceedings of the Fifth International Symposium on Domain Decomposition Methods for Partial Differential Equations*, SIAM, Philadelphia, PA 1992, pp. 3–18.

[72] DuChateau, P. & Zachmann, D.: *Applied partial differential equations*. Harper & Row, New York, NY 1989.

[73] Durant, W.: *The Story of Philosophy*. Simon and Schuster, New York, NY 1961.

[74] Dureisseix, D. & Bavestrello, H.: Information transfer between incompatible finite element meshes: Application to coupled thermo-viscoelasticity. *Computer Methods in Applied Mechanics and Engineering* **195** (2006), 6523–6541.

[75] Ehle, B. L.: High order A-stable methods for the numerical solution of systems of DE's. *BIT Numerical Mathematics* **8** (1968), 276–278.

[76] Ehle, B. L.: *On Padé Approximations to the Exponential function and A-Stable Methods for the Numerical Solution of Initial Value Problems*. Dissertation Thesis, University of Waterloo, Waterloo 1969.

[77] Ehlers, W.: *Poröse Medien – ein kontinuumsmechanisches Modell auf der Basis der Mischungstheorie*. Habilitation, Forschungsberichte aus dem Fachbereich Bauwesen, Heft 47, Universität-GH-Essen 1989.

[78] Ehlers, W.: Constitutive equations for granular materials in geomechanical context. In Hutter, K. (ed.): *Continuum Mechanics in Environmental Sciences and Geophysics*. CISM Courses and Lecture Notes No. 337, Springer-Verlag, Wien 1993, pp. 313–402.

[79] Ehlers, W.: Grundlegende Konzepte in der Theorie Poröser Medien. *Technische Mechanik* **16** (1996), 63–76.

[80] Ehlers, W.: *Vector and Tensor Calculus: An Introduction*. Lecture notes, Institute of Applied Mechanics (CE), Chair of Continuum Mechanics, University of Stuttgart 2000–2015.

[81] Ehlers, W.: Foundations of multiphasic and porous materials. In Ehlers, W. & Bluhm, J. (eds.): *Porous media: Theory, Experiments, and Numerical Applications*. Springer-Verlag, Berlin 2002, pp. 3–86.

[82] Ehlers, W.: Challenges of porous media models in geo- and biomechanical engineering including electro-chemically active polymers and gels. *International Journal of Advances in Engineering Sciences and Applied Mathematics* **1** (2009), 1–24.

[83] Ehlers, W.: Porous media in the light of history. In Stein, E. (ed.): *The History of Theoretical, Material and Computational Mechanics-Mathematics, Lecture Notes in Applied Mathematics and Mechanics 1*. Springer-Verlag, Berlin, Heidelberg 2014, pp. 211–227.

[84] Ehlers, W.; Ellsiepen, P.; Blome, P.; Mahnkopf, D. & Markert, B.: *Theoretische und numerische Studien zur Lösung von Rand- und Anfangswertproblemen in der Theorie Poröser Medien, Abschlußbericht zum DFG-Forschungsvorhaben Eh 107/6-2*. Bericht Nr. 99-II-1 aus dem Institut für Mechanik (Bauwesen), Universität Stuttgart 1999.

[85] Ehlers, W. & Wagner, A.: Multi-component modelling of human brain tissue: a contribution to the constitutive and computational description of deformation, flow and diffusion processes with application to the invasive drug-delivery problem. *Computer Methods in Biomechanics and Biomedical Engineering* **18** (2015), 861–879.

[86] Ehlers, W.; Zinatbakhsh, S. & Markert, B.: Stability analysis of finite difference schemes revisited: A study of decoupled solution strategies for coupled multifield problems. *International Journal for Numerical Methods in Engineering* **94** (2013), 758–786.

[87] Elaydi, S.: *An Introduction to Difference Equations*. Springer Science + Business Media, New York, NY 2005.

[88] Euler, L.: Principia motus fluidorum. *Novi Commentarii academiae scientiarum Petropolitanae* **6** (1761), 271–311.

[89] Farhat, C.: A saddle-point principle domain decomposition method for the solution of solid mechanics problems. In Keyes, D. E.; Chan, T. F.; Meurant, G.; Scroggs, J. S. & Voigt, R. G. (eds.): *Proceedings of the Fifth International Symposium on Domain Decomposition Methods for Partial Differential Equations*, SIAM, Philadelphia, PA 1992, pp. 271–292.

[90] Farhat, C.; Chen, P.-S. & Mandel, J.: A scalable Lagrange multiplier based domain decomposition method for time-dependent problems. *International Journal for Numerical Methods in Engineering* **38** (1995), 3831–3853.

[91] Farhat, C. & Lesoinne, M.: On the accuracy, stability, and performance of the solution of three-dimensional nonlinear transient aeroelastic problems by partitioned procedures. *AIAA Paper No. 96-1388* (1996), 629–641.

[92] Farhat, C. & Lesoinne, M.: Two efficient staggered algorithms for the serial and parallel solution of three-dimensional nonlinear transient aeroelastic problems. *Computer Methods in Applied Mechanics and Engineering* **182** (2000), 499–515.

[93] Farhat, C.; Lesoinne, M.; LeTallec, P.; Pierson, K. & Rixen, D.: FETI-DP: a dual-primal unified FETI method - part I: A faster alternative to the two-level FETI method. *International Journal for Numerical Methods in Engineering* **50** (2001), 1523–1544.

[94] Farhat, C.; Macedo, A.; Lesoinne, M.; Roux, F.-X.; Magoulès, F. & Bourdonnaie, A. d. L.: Two-level domain decomposition methods with Lagrange multipliers for the fast iterative solution of acoustic scattering problems. *Computer Methods in Applied Mechanics and Engineering* **184** (2000), 213–239.

[95] Farhat, C. & Mandel, J.: The two-level FETI method for static and dynamic plate problems - part I: An optimal iterative solver for biharmonic systems. *Computer Methods in Applied Mechanics and Engineering* **155** (1998), 129–151.

[96] Farhat, C.; Park, K. C. & Dubois-Pelerin, Y.: An unconditionally stable staggered algorithm for transient finite element analysis of coupled thermoelastic problems. *Computer Methods in Applied Mechanics and Engineering* **85** (1991), 349–365.

[97] Farhat, C. & Roux, F.-X.: A method of finite element tearing and interconnecting and its parallel solution algorithm. *International Journal for Numerical Methods in Engineering* **32** (1991), 1205–1227.

[98] Farhat, C. & Roux, F.-X.: Implicit parallel processing in structural mechanics. *Computational Mechanics Advances* **2** (1994), 1–124.

[99] Felippa, C. A. & Geers, T. L.: Partitioned analysis for coupled mechanical systems. *Engineering with Computers* **5** (1988), 123–133.

[100] Felippa, C. A. & Park, K. C.: Synthesis tools for structural dynamics and partitioned analysis of coupled systems. In Ibrahimbegovic, A. & Brank, B. (eds.): *Engineering Structures Under Extreme Conditions: Multi-Physics and Multi-Scale Computer Models in Non-Linear Analysis and Optimal Design*. IOS Press, Amsterdam 2005, pp. 50–110.

[101] Felippa, C. A.; Park, K. C. & Farhat, C.: Partitioned analysis of coupled mechanical systems. *Computer Methods in Applied Mechanics and Engineering* **190** (2001), 3247–3270.

[102] Ferziger, J. H.: *Numerical Methods for Engineering Application*. John Wiley & Sons, New York, NY 1998.

[103] Finn, J. M.: *Classical Mechanics*. Jones & Bartlett Publishers, Sudbury, MA 2010.

[104] Flemisch, B. & Wohlmuth, B. I.: Stable Lagrange multipliers for quadrilateral meshes of curved interfaces in 3D. *Computer Methods in Applied Mechanics and Engineering* **196** (2007), 1589–1602.

[105] Fourier, J.: *Théorie Analytique de la Chaleur*. Chez Firmin Didot, Père et Fils, Paris 1822.

[106] Fragakis, Y.: *Force and Displacement Duality in Domain Decomposition Methods for Solid and Structural Mechanics*. International Center for Numerical Methods in Engineering (CIMNE), Polytechnic University of Catalonia, Barcelona 2007.

[107] Fragakis, Y. & Papadrakakis, M.: The mosaic of high performance domain decomposition methods for structural mechanics: Formulation, interrelation and numerical efficiency of primal and dual methods. *Computer Methods in Applied Mechanics and Engineering* **192** (2003), 3799–3830.

[108] Fujiwara, M.: Über die algebraischen Gleichungen, deren Wurzeln in einem Kreise oder in einer Halbebene liegen. *Mathematische Zeitschrift* **24** (1926), 161–169.

[109] Gander, M. J.: Optimized Schwarz methods. *SIAM Journal on Numerical Analysis* **44** (2006), 699–731.

[110] Gander, M. J.: Schwarz methods over the course of time. *Electronic Transactions on Numerical Analysis* **31** (2008), 228–255.

[111] Gander, M. J. & Wanner, G.: The origins of the alternating Schwarz method. In Barth, T. J.; Griebel, M.; Keyes, D. E.; Nieminen, R. M.; Roose, D. & Schlick, T. (eds.): *Domain Decomposition Methods in Science and Engineering XXI, Lecture Notes in Computational Science and Engineering*. Springer International Publishing, Switzerland 2014, pp. 487–496.

[112] Gantmacher, F. R.: *The Theory of Matrices, Vol. II*. Chelsea Publications, New York, NY 1964.

[113] Gaul, L.; Kögl, M. & Wagner, M.: *Boundary Element Methods for Engineers and Scientists*. Springer-Verlag, Berlin 2003.

[114] Gear, C. W.: *Numerical Initial Value Problems in Ordinary Differential Equations*. Prentice Hall, Englewood Cliffs, NJ 1971.

[115] Glowinski, R. & Le Tallec, P.: Augmented Lagrangian interpretation of the nonoverlapping Schwarz alternating method. In Chan, T. F.; Glowinski, R.; Périaux, J. & Widlund, O. B. (eds.): *Proceedings of the Third International Symposium on Domain Decomposition Methods for Partial Differential Equations*, SIAM, Philidelphia, PA 1990, pp. 224–231.

[116] Glowinski, R.; Pan, T.-W.; Hesla, T. I. & Joseph, D. D.: A distributed Lagrange multiplier/fictitious domain method for particulate flows. *International Journal of Multiphase Flow* **25** (1999), 755–794.

[117] Godfrey-Smith, P.: *Theory and Reality: An Introduction to the Philosophy of Science*. University of Chicago Press, Chicago, IL 2003.

[118] Golnaraghi, M. F. & Kuo, B. C.: *Automatic Control Systems*. John Wiley & Sons, Hoboken, NJ 2010.

[119] Gossin, P.: *Encyclopedia of Literature and Science*. Greenwood Publishing Group, Westport, CT 2002.

[120] Gresho, P. M.: On the theory of semi-implicit projection methods for viscous incompressible flow and its implementation via a finite element method that also introduces a nearly consistent mass matrix. part 1: Theory. *International Journal for Numerical Methods in Fluids* **11** (1990), 587–620.

[121] Guermond, J.-L.; Minev, P. & Shen, J.: An overview of projection methods for incompressible flows. *Computer Methods in Applied Mechanics and Engineering* **195** (2006), 6011–6045.

[122] Guermond, J.-L. & Quartapelle, L.: On stability and convergence of projection methods based on pressure Poisson equation. *International Journal for Numerical Methods in Fluids* **26** (1998), 1039–1053.

[123] Gullberg, J.: *Mathematics: From the Birth of Numbers*. Norton & Company, New York, NY 1997.

[124] Gurtin, M. E.: *An Introduction to Continuum Mechanics*. 1st edn. Academic Press, New York, NY 1981.

[125] Gustafson, K. E.: *Introduction to Partial Differential Equations and Hilbert Space Methods*. 3rd edn. Dover Publications, Mineola, NY 2012.

[126] Gustafsson, B.; Kreiss, H.-O. & Oliger, J.: *Time-Dependent Problems and Difference Methods*. John Wiley & Sons, New York, NY 1995.

[127] Gustafsson, B.; Kreiss, H.-O. & Sundström, A.: Stability theory of difference approximations for mixed initial boundary value problems. II. *Mathematics of Computation* (1972), 649–686.

[128] Guthrie, W. K. C.: *A History of Greek Philosophy. II: The Presocratic Tradition from Parmenides to Democritus*. Cambridge University Press, Cambridge 1965.

[129] Hafstein, S. F.: A constructive converse Lyapunov theorem on asymptotic stability for nonlinear autonomous ordinary differential equations. *Dynamical Systems* **20** (2005), 281–299.

[130] Hairer, E.: Order conditions for numerical methods for partitioned ordinary differential equations. *Numerische Mathematik* **36** (1981), 431–445.

[131] Hairer, E.; Nørsett, S. P. & Wanner, G.: *Solving Ordinary Differential Equations I: Nonstiff Problems*. 2nd edn. Springer-Verlag, Berlin 1993.

[132] Hairer, E. & Wanner, G.: *Solving Ordinary Differential Equations II: Stiff and Differential-Algebraic Problems*. 2nd edn. Springer-Verlag, Berlin 1996.

[133] Hameyer, K.; Driesen, J.; De Gersem, H. & Belmans, R.: The classification of coupled field problems. *IEEE Transactions on Magnetics* **35** (1999), 1618–1621.

[134] Haupt, P.: *Continuum Mechanics and Theory of Materials*. Springer-Verlag, Berlin 2010.

[135] Haynsworth, E. V.: *On the Schur complement*. Basel Mathematical Notes, University of Basel, Basel 1968.

[136] Heath, T. L.: *A Manual of Greek Mathematics*. Dover Publications, Mineloa, NY 2003.

[137] Heider, Y.: *Saturated Porous Media Dynamics with Application to Earthquake Engineering*. Dissertation Thesis, Report No. II-25 of the Institute of Applied Mechanics (CE), University of Stuttgart 2012.

[138] Heider, Y.; Markert, B. & Ehlers, W.: Dynamic wave propagation in infinite saturated porous media half spaces. *Computational Mechanics* **49** (2012), 319–336.

[139] Heinrich, J. & Vionnet, C.: The penalty method for the Navier-Stokes equations. *Archive of Computational Methods in Engineering* **2** (1995), 51–65.

[140] Henrici, P.: *Discrete Variable Methods in Ordinary Differential Equations*. John Wiley & Sons, New York, NY 1962.

[141] Hestenes, M. R. & Stiefel, E.: Methods of conjugate gradients for solving linear systems. *Journal of Research of the National Bureau of Standards* **49** (1952), 409–436.

[142] Hirt, C. W.: Heuristic stability theory for finite-difference equations. *Journal of Computational Physics* **2** (1968), 339–355.

[143] Hofer, E.: A partially implicit method for large stiff systems of ODEs with only few equations introducing small time-constants. *SIAM Journal on Numerical Analysis* **13** (1976), 645–663.

[144] Holzapfel, G. A.: *Nonlinear Solid Mechanics: A Continuum Approach for Engineering*. John Wiley & Sons, Chichester 2001.

[145] Hübner, B.; Walhorn, E. & Dinkler, D.: A monolithic approach to fluid-structure interaction using space-time finite elements. *Computer Methods in Applied Mechanics and Engineering* **193** (2004), 2087–2104.

[146] Hughes, T. J. R.: *The Finite Element Method: Linear Static and Dynamic Finite Element Analysis*. Dover Publications, New York, NY 2000.

[147] Hughes, T. J. R.; Liu, W. & Brooks, A.: Finite element analysis of incompressible viscous flows by the penalty function formulation. *Journal of Computational Physics* **30** (1979), 1–60.

[148] Hughes, T. J. R. & Liu, W. K.: Implicit-explicit finite elements in transient analysis: stability theory. *Journal of Applied Mechanics* **45** (1978), 371–374.

[149] Hurwitz, A.: Über die Bedingungen, unter welchen eine Gleichung nur Wurzeln mit negativen reellen Theilen besitzt. *Mathematische Annalen* **46** (1895), 273–284.

[150] Iqbāl, M.: *Science and Islam*. Greenwood Publishing Group, Westport, CT 2007.

[151] Isaacson, E. & Keller, H. B.: *Analysis of Numerical Methods*. John Wiley & Sons, New York, NY 1966.

[152] Joosten, M. M.; Dettmer, W. G. & Perić, D.: Analysis of the block Gauss-Seidel solution procedure for a strongly coupled model problem with reference to fluid-structure interaction. *International Journal for Numerical Methods in Engineering* **78** (2009), 757–778.

[153] Jury, E. I.: *Inners and Stability of Dynamic Systems*. John Wiley & Sons, London 1974.

[154] van Kan, J.: A second-order accurate pressure-correction scheme for viscous incompressible flow. *SIAM Journal on Scientific Computing* **7** (1986), 870–891.

[155] Karajan, N.: *An Extended Biphasic Description of the Inhomogeneous and Anisotropic Intervertebral Disc*. Dissertation Thesis, Report No. II-19 of the Institute of Applied Mechanics (CE), University of Stuttgart 2009.

[156] Karajan, N.; Röhrle, O.; Ehlers, W. & Schmitt, S.: Linking continuous and discrete intervertebral disc models through homogenisation. *Biomechanics and Modeling in Mechanobiology* **12** (2013), 453–466.

[157] Karlsen, K. H. & Lie, K.-A.: An unconditionally stable splitting scheme for a class of nonlinear parabolic equations. *IMA Journal of Numerical Analysis* **19** (1999), 609–635.

[158] Kim, J.; Tchelepi, H. A. & Juanes, R.: Stability and convergence of sequential methods for coupled flow and geomechanics: Fixed-stress and fixed-strain splits. *Computer Methods in Applied Mechanics and Engineering* **200** (2011), 1591–1606.

[159] King, J. P.: *The Art of Mathematics*. Dover Publications, Mineola, NY 1992.

[160] Klawonn, A. & Widlund, O. B.: FETI and Neumann-Neumann iterative substructuring methods: connections and new results. *Communications on Pure and Applied Mathematics* **54** (2001), 57–90.

[161] Krause, R.; Schittler, D.; Waldherr, S.; Allgöwer, F.; Markert, B. & Ehlers, W.: Remodelling processes in bones: A biphasic porous media model. *PAMM* **12** (2012), 131–132.

[162] Kudryavtsev, L. D.: Dirichlet principle. In *Encyclopedia of Mathematics*. Kluwer Academic Publishers, Dordrecht 2002, URL `http://www.encyclopediaofmath.org/index.php?title=Dirichlet_principle&oldid=28181`.

[163] Kuhl, D.: *Modellierung und Simulation von Mehrfeldproblemen der Strukturmechanik*. Habilitation, Lehrstuhl für Statik und Dynamik, Ruhr-Universität Bochum 2005.

[164] Kunkel, P. & Mehrmann, V.: *Differential-Algebraic Equations: Analysis and Numerical Solution*. European Mathematical Society, Zurich 2006.

[165] Kutta, W.: Beitrag zur näherungsweisen Integration totaler Differentialgleichungen. *Zeitschrift für Mathematik und Physik* **46** (1901), 435–453.

[166] Lagrange, J. L.: *Mécanique Analytique*. Ve Courcier, Paris 1811.

[167] Lakshmikantham, V. & Trigiante, D.: *Theory of Difference Equations: Numerical Methods and Applications*. Academic Press, Boston, MA 1988.

[168] Lambert, J. D.: *Computational Methods in Ordinary Differential Equations*. John Wiley & Sons, New York, NY 1973.

[169] Lambert, J. D.: *Numerical Methods for Ordinary Differential Systems: The Initial Value Problem*. John Wiley & Sons, Chichester 1991.

[170] Larrosa, J.; Morancho, E. & Niso, D.: On the practical use of variable elimination in constraint optimization problems: 'Still-life' as a case study. *Journal of Artificial Intelligence Research* **23** (2005), 421–440.

[171] Lax, P. D. & Richtmyer, R. D.: Survey of the stability of linear finite difference equations. *Communications on Pure and Applied Mathematics* **9** (1956), 267–293.

[172] LeVeque, R. J.: *Finite Volume Methods for Hyperbolic Problems*. Cambridge University Press, New York, NY 2002.

[173] Lewis, R. W.: *Numerical Methods in Coupled Systems*. John Wiley & Sons, Chichester 1984.

[174] Lewis, R. W.; Majorana, C. E. & Schrefler, B. A.: A coupled finite element model for the consolidation of nonisothermal elastoplastic porous media. *Transport in Porous Media* **1** (1986), 155–178.

[175] Lewis, R. W.; Schrefler, B. A. & Simoni, L.: Coupling versus uncoupling in soil consolidation. *International Journal for Numerical and Analytical Methods in Geomechanics* **15** (1991), 533–548.

[176] Liénard, A. & Chipart, M. H.: Sur la signe de la partie reelle des racines d'une équation algebrique. *Journal de Mathématiques Pures et Appliqués* **10** (1914), 291–346.

[177] Lin, F.-H.; Liu, C. & Zhang, P.: On a micro-macro model for polymeric fluids near equilibrium. *Communications on Pure and Applied Mathematics* **60** (2007), 838–866.

[178] Lin, T. & Farhat, C.: *Transient Aeroelastic Computations Using Multiple Moving Frames of Reference*. Report No. AIAA-90-3053-CP of the Center for Aerospace Structures, University of Colorado, Boulder, CO 1990.

[179] Lions, P.-L.: On the Schwarz alternating method. I. In Glowinski, R. (ed.): *Proceedings of the First International Symposium on Domain Decomposition Methods for Partial Differential Equations*, SIAM, Philadelphia, PA 1988, pp. 1–42.

[180] Lions, P.-L.: On the Schwarz alternating method. III: a variant for nonoverlapping subdomains. In Chan, T. F.; Glowinski, R.; Périaux, J. & Widlund, O. B. (eds.): *Proceedings of the Third International Symposium on Domain Decomposition Methods for Partial Differential Equations*, SIAM, Philadelphia, PA 1990, pp. 202–223.

[181] Lui, S. H.: *Numerical Analysis of Partial Differential Equations*. John Wiley & Sons, Hoboken, NJ 2011.

[182] Lyapunov, A. M.: *The General Problem of the Stability of Motion*. Translated by A. T. Fuller, Taylor & Francis, London 1992.

[183] Maday, Y.; Patera, A. T. & Rønquist, E. M.: An operator-integration-factor splitting method for time-dependent problems: application to incompressible fluid flow. *Journal of Scientific Computing* **5** (1990), 263–292.

[184] Mandel, J.: Balancing domain decomposition. *Communications in Numerical Methods in Engineering* **9** (1993), 233–241.

[185] Mandel, J. & Brezina, M.: Balancing domain decomposition for problems with large jumps in coefficients. *Mathematics of Computation of the American Mathematical Society* **65** (1996), 1387–1401.

[186] Marchuk, G. I.: *Methods of Numerical Analysis*. Springer-Verlag, New York, NY 1975.

[187] Markert, B.: *Porous Media Viscoelasticity with Application to Polymeric Foams*. Dissertation Thesis, Report No. II-12 of the Institute of Applied Mechanics (CE), University of Stuttgart 2005.

[188] Markert, B.: *Weak or Strong: On Coupled Problems in Continuum Mechanics*. Habilitation Thesis, Report No. II-20 of the Institute of Applied Mechanics (CE), University of Stuttgart 2010.

[189] Markert, B.: A survey of selected coupled multifield problems in computational mechanics. *Journal of Coupled Systems and Multiscale Dynamics* **1** (2013), 22–48.

[190] Markert, B.; Heider, Y. & Ehlers, W.: Comparison of monolithic and splitting solution schemes for dynamic porous media problems. *International Journal for Numerical Methods in Engineering* **82** (2010), 1341–1383.

[191] Markert, B.; Monastyrskyy, B. & Ehlers, W.: Fluid penetration effects in porous media contact. *Continuum Mechanics and Thermodynamics* **20** (2008), 303–315.

[192] Matthies, H. G.; Niekamp, R. & Steindorf, J.: Algorithms for strong coupling procedures. *Computer Methods in Applied Mechanics and Engineering* **195** (2006), 2028–2049.

[193] Matthies, H. G. & Steindorf, J.: Strong coupling methods. In Wendland, W. L. & Efendiev, M. (eds.): *Analysis and Simulation of Multifield Problems*. Springer-Verlag, Berlin 2003, pp. 13–36.

[194] Maxwell, J. C.: A dynamical theory of the electromagnetic field. *Proceedings of the Royal Society of London* **13** (1864), 531–536.

[195] McLachlan, R. I. & Quispel, G. R. W.: Splitting methods. *Acta Numerica* (2002), 341–434.

[196] Meri, J. W.: *Medieval Islamic Civilization: An Encyclopedia*. Taylor & Francis, Abingdon 2006.

[197] Michler, C.; Hulshoff, S. J.; van Brummelen, E. H. & de Borst, R.: A monolithic approach to fluid-structure interaction. *Computer and Fluids* **33** (2004), 839–848.

[198] Miller, C. T. & Rabideau, A. J.: Development of split-operator, Petrov-Galerkin methods to simulate transport and diffusion problems. *Water Resources Research* **29** (1993), 2227–2240.

[199] Mitchell, A. R. & Craggs, J. W.: Stability of difference relations in the solution of ordinary differential equations. *Mathematics of Computation* **7** (1953), 127–129.

[200] Mitchell, A. R. & Griffiths, D. F.: *The Finite Difference Method in Partial Differential Equations*. John Wiley & Sons, Chichester 1980.

[201] Mohandas, K. P.: *Modern Control Engineering*. Sanguine Technical Publishers, Bangalore 2006.

[202] Morand, H. & Ohayon, R.: *Fluid-Structure Interaction.* John Wiley & Sons, Chichester 1995.

[203] Morton, K. W. & Mayers, D. F.: *Numerical Solution of Partial Differetial Equations, an Introduction*. 2nd edn. Cambridge University Press, Cambridge 2005.

[204] Newmark, N. M.: *Computation of Dynamic Structural Response in the Range Approaching Failure*. Report No. NR-064-183 of the Department of Civil Engineering, University of Illinois, Urbana, IL 1952.

[205] Newmark, N. M.: A method of computation for structural dynamics. *ASCE Journal of Engineering Mechanics* **85** (1959), 67–94.

[206] Nørsett, S. P.: *Semi-Explicit Runge-Kutta Methods*. Dissertation Thesis, Report No. 6/74 of the Department of Mathematics, University of Trondheim, Trondheim 1974.

[207] O'Regan, G.: *A Brief History of Computing*. Springer-Verlag, London 2012.

[208] Öttinger, H. C.: *Stochastic Processes in Polymeric Fluids: Tools and Examples for Developing Simulation Algorithms*. Springer-Verlag, New York, NY 1996.

[209] Padula, S. L.; Korte, J. J.; Dunn, H. J. & Salas, A. O.: *Multidisciplinary Optimization Branch Experience Using iSIGHT Software*. Report No. TM-1999-209714 of the NASA Langley Research Center, Hampton, VA 1999.

[210] Park, K. C.: Partitioned transient analysis procedures for coupled-field problems: stability analysis. *Journal of Applied Mechanics* **47** (1980), 370–376.

[211] Park, K. C.: Stabilization of partitioned solution procedure for pore fluid-soil interaction analysis. *International Journal For Numerical Methods in Engineering* **19** (1983), 1669–1673.

[212] Park, K. C.: Locking, spurious mechanisms, and pressure divergence in penalty finite element methods for stokes flow problems. *Computer Methods in Applied Mechanics and Engineering* **47** (1984), 315–330.

[213] Park, K. C. & Belvin, W. K.: Partitioned solution procedure for control-structure interaction simulations. *Journal of Guidance, Control, and Dynamics* **14** (1991), 59–67.

[214] Park, K. C. & Felippa, C. A.: *A Variatioinal Principle for the Formulation of Partitioned Structural Systems*. Report No. CU-CAS-99-02 of the Center for Aerospace Structures, University of Colorado, Boulder, CO 1999.

[215] Park, K. C.; Felippa, C. A. & DeRuntz, J. A.: Stabilization of staggered solution procedures for fluid-structure interaction analysis. *Computational Methods for Fluid-Structure Interaction Problems* (1977), 95–124.

[216] Park, K. C.; Felippa, C. A. & Ohayon, R.: Partitioned formulation of internal fluid-structure interaction problems by localized Lagrange multipliers. *Computer Methods in Applied Mechanics and Engineering* **190** (2001), 2989–3007.

[217] Park, K. C.; Felippa, C. A. & Rebel, G.: A simple algorithm for localized construction of non-matching structural interfaces. *International Journal for Numerical Methods in Engineering* **53** (2002), 2117–2142.

[218] Paulos, J. A.: *Beyond Numeracy: Ruminations of a Numbers Man*. Random House, New York, NY 1997.

[219] Pavarino, L. F. & Widlund, O. B.: Balancing Neumann-Neumann methods for incompressible stokes equations. *Communications on Pure and Applied Mathematics* **55** (2002), 302–335.

[220] Peet, Y. T. & Fischer, P. F.: Stability analysis of interface temporal discretization in grid overlapping methods. *SIAM Journal on Numerical Analysis* **50** (2012), 3375–3401.

[221] Perry, M.: *Sources of the Western Tradition: Volume I: From Ancient Times to the Enlightenment*. 9th edn. Wadsworth, Cengage Learning, Boston, MA 2014.

[222] Perry, M.; Chase, M.; Jacob, J. R.; Jacob, M. C. & von Laue, T. H.: *Western Civilization: Ideas, Politics, and Society, Volume I: To 1789*. 10th edn. Wadsworth, Cengage Learning, Boston, MA 2013.

[223] Piperno, S. & Farhat, C.: Design of efficient partitioned procedures for the transient solution of aeroelastic problems. *Revue Européenne des Éléments Finis* **9** (2000), 655–680.

[224] Piperno, S. & Farhat, C.: Partitioned procedures for the transient solution of coupled aeroelastic problems – Part II: Energy transfer analysis and three dimensional applications. *Computer Methods in Applied Mechanics and Engineering* **190** (2001), 3147–3170.

[225] Piperno, S.; Farhat, C. & Larrouturou, B.: Partitioned procedures for the transient solution of coupled aeroelastic problems Part I: Model problem, theory and two-dimensional application. *Computer Methods in Applied Mechanics and Engineering* **124** (1995), 79–112.

[226] Pironneau, O.: On the transport-diffusion algorithm and its applications to the Navier-Stokes equations. *Numerische Mathematik* **38** (1982), 309–332.

[227] Prohl, A.: *Projection and Quasi-Compressibility Methods for Solving the Incompressible Navier-Stokes Equations*. Teubner, Stuttgart 1997.

[228] Przemieniecki, J. S.: Matrix structural analysis of substructures. *AIAA Journal* **1** (1963), 138–147.

[229] Rannacher, R.: Finite element methods for the incompressible Navier-Stokes equations. In Galdi, P.; Heywood, J. & Rannacher, R. (eds.): *Fundamental Directions in Mathematical Fluid Mechanics*. Birkhäuser, Basel 2000, pp. 191–293.

[230] Richtmyer, R. D. & Morton, K. W.: *Difference Methods for Initial-value Problems*. Interscience Publishers, New York, NY 1967.

[231] Riedweg, C.: *Pythagoras: His life, Teaching, and Influence*. Cornell University Press, New York, NY 2005.

[232] Riemann, B.: *Grundlagen für eine allgemeine Theorie der Functionen einer veränderlichen complexen Grösse*. Inauguraldissertation, Göttingen 1851.

[233] Rivera-Gallego, W.: Stability analysis of numerical boundary conditions in domain decomposition algorithms. *Applied Mathematics and Computation* **137** (2003), 375–385.

[234] Ropp, D. L. & Shadid, J. N.: Stability of operator splitting methods for systems with indefinite operators: reaction-diffusion systems. *Journal of Computational Physics* **203** (2005), 449–466.

[235] Ross, M. R.; Felippa, C. A.; Park, K. C. & Sprague, M. A.: Treatment of acoustic fluid-structure interaction by localized Lagrange multipliers: formulation. *Computer Methods in Applied Mechanics and Engineering* **197** (2008), 3057–3079.

[236] Ross, M. R.; Sprague, M. A.; Felippa, C. A. & Park, K. C.: Treatment of acoustic fluid–structure interaction by localized Lagrange multipliers and comparison to alternative interface-coupling methods. *Computer Methods in Applied Mechanics and Engineering* **198** (2009), 986–1005.

[237] Routh, E. J.: *A Treatise on the Stability of a Given State of Motion*. Macmillan and Co., London 1877.

[238] Runge, C.: Über die numerische Auflösung totaler Differentialgleichungen. *Nachrichten von der Gesellschaft der Wissenschaften zu Göttingen, Mathematisch-Physikalische Klasse* (1895), 252–257.

[239] Ryu, D. & Jones, T. W.: Numerical magnetohydrodynamics in astrophysics: algorithm and tests for one-dimensional flow. *The Astrophysical Journal* **442** (1995), 228–258.

[240] Schanz, M.: Poroelastodynamics: linear models, analytical solutions, and numerical methods. *Applied Mechanics Reviews* **62** (2009), 030803–1–030803–15.

[241] Schanz, M. & Cheng, A.-D.: Transient wave propagation in a one-dimensional poroelastic column. *Acta Mechanica* **145** (2000), 1–18.

[242] Scherer, R.: A necessary condition for B-stability. *BIT Numerical Mathematics* **19** (1979), 111–115.

[243] Schrefler, B. A.: A partitioned solution procedure for geothermal reservoir analysis. *Communications in Applied Numerical Methods* **1** (1985), 53–56.

[244] Schrefler, B. A.; Simoni, L. & Turska, E.: Standard staggered and staggered Newton schemes in thermo-hydro-mechanical problems. *Computer Methods in Applied Mechanics and Engineering* **144** (1997), 93–109.

[245] Schuler, J. J. & Felippa, C. A.: Superconducting axisymmetric finite elements based on a gauged potential variational principle – I. Formulation. *Computing Systems in Engineering* **5** (1994), 215–225.

[246] Schuler, J. J. & Felippa, C. A.: Superconducting axisymmetric finite elements based on a gauged potential variational principle – II. Solution and numerical results. *Computing Systems in Engineering* **5** (1994), 227–237.

[247] Schur, I.: Über Potenzreihen, die im Innern des Einheitskreises beschränkt sind. *Journal für die reine und angewandte Mathematik* **147** (1917), 205–232.

[248] Schwarz, H. A.: Ueber einen Grenzübergang durch alternierendes Verfahren. *Vierteljahrsschrift der Naturforschenden Gesellschaft in Zürich* **15** (1870), 272–286.

[249] Selvadurai, A.: The analytical method in geomechanics. *Applied Mechanics Reviews* **60** (2007), 87–106.

[250] Siim Sepp: "Sand from Gobi Desert". Licensed under CC BY-SA 3.0 via Wikimedia Commons. (2011), URL `https://commons.wikimedia.org/wiki/File:Sand_from_Gobi_Desert.jpg#mediaviewer/File:Sand_from_Gobi_Desert.jpg`.

[251] Shi, J.: *A simplified von Neumann method for linear stability analysis*. Report No. 9310 of the Department of Aerospace Science, College of Aeronautics, Cranfield Institute of Technology, Bedford 1993.

[252] Simo, J. & Miehe, C.: Associative coupled thermoplasticity at finite strains: formulation, numerical analysis and implementation. *Computer Methods in Applied Mechanics and Engineering* **98** (1992), 41–104.

[253] Simoni, L. & Schrefler, B. A.: A staggered finite-element solution for water and gas flow in deforming porous media. *Communications in Applied Numerical Methods* **7** (1991), 213–223.

[254] Smolinski, P.; Belytschko, T. & Neal, M.: Multi-time-step integration using nodal partitioning. *International Journal for Numerical Methods in Engineering* **26** (1988), 349–359.

[255] Spilker, R. & Maxian, T.: A mixed-penalty finite element formulation of the linear biphasic theory for soft tissues. *International Journal for Numerical Methods in Engineering* **30** (1990), 1063–1082.

[256] Steinhauser, M. O.: *Computational Multiscale Modeling of Fluids and Solids*. Springer-Verlag, Berlin 2008.

[257] Stetter, H. J.: *Analysis of Discretization Methods for Ordinary Differential Equations*. Springer-Verlag, Berlin 1973.

[258] Strang, G.: On the construction and comparison of difference schemes. *SIAM Journal on Numerical Analysis* **5** (1968), 506–517.

[259] Strganac, T. W. & Mook, D. T.: Numerical model of unsteady subsonic aeroelastic behavior. *AIAA Journal* **28** (1990), 903–909.

[260] Strikwerda, J. C.: *Finite Difference Schemes and Partial Differential Equations*. 2nd edn. SIAM, Philadelphia, PA 2004.

[261] Suh, J.; Spilker, R. & Holmes, M.: A penalty finite element analysis for nonlinear mechanics of biphasic hydrated soft tissue under large deformation. *International Journal for Numerical Methods in Engineering,* **32** (1991), 1411–1439.

[262] Süli, E. & Mayers, D. F.: *An Introduction to Numerical Analysis*. Cambridge University Press, Cambridge 2006.

[263] Thomas, J. W.: *Numerical Partial Differential Equations: Finite Difference Methods*. Springer-Verlag, New York, NY 1995.

[264] Timmermans, L.; Van de Vosse, F. & Minev, P.: Taylor-Galerkin-based spectral element methods for convection-diffusion problems. *International Journal for Numerical Methods in Fluids* **18** (1994), 853–870.

[265] Truesdell, C.: *Essays in the History of Mechanics*. Springer-Verlag, Berlin 1968.

[266] Truesdell, C.: *An Idiot's Fugitive Essays on Science: Methods, Criticism, Training, Circumstances*. Springer-Verlag, New York, NY 1984.

[267] Truesdell, C. & Noll, W.: The nonlinear field theories of mechanics. In Flügge, S. (ed.): *Handbuch der Physik, Vol. III(3)*. Springer-Verlag, Berlin 1965.

[268] Truesdell, C. & Toupin, R. A.: The classical field theories. In Flügge, S. (ed.): *Handbuch der Physik, Vol. III(1)*. Springer-Verlag, Berlin 1960, pp. 226–902.

[269] Truesdell, C. A.: Sulle basi della termomeccanica. *Rendiconti Lincei* **22** (1957), 33–38.

[270] Turska, E. & Schrefler, B. A.: On convergence conditions of partitioned solution procedures for consolidation problems. *Computer Methods in Applied Mechanics and Engineering* **106** (1993), 51–63.

[271] Turska, E.; Wisniewski, K. & Schrefler, B. A.: Error propagation of staggered solution procedures for transient problems. *Computer Methods in Applied Mechanics and Engineering* **114** (1994), 177–188.

[272] Varga, R. S.: *Matrix Iterative Analysis*. Prentice Hall, Englewood Cliffs, NJ 1962.

[273] Versteeg, H. & Malalasekera, W.: *An Introduction to Computational Fluid Dynamics: The Finite Volume Method*. 2nd edn. Prentice Hall, Harlow 2007.

[274] Wagner, A.: *Extended Modelling of the Multiphasic Human Brain Tissue with Application to Drug-Infusion Processes*. Dissertation Thesis, Report No. II-27 of the Institute of Applied Mechanics (CE), University of Stuttgart 2014.

[275] Wall, W. A.: *Fluid-Struktur-Interaktion mit stabilisierten Finiten Elementen*. Dissertation, Bericht Nr. 31 aus dem Institut für Baustatik, Universität Stuttgart 1999.

[276] Weeratunga, S. & Pramono, E.: Direct coupled aeroelastic analysis through concurrent implicit time integration on a parallel computer. *AIAA Paper No. 94-1550-CP* (1994).

[277] Weickert, J.; Romeny, B. M. t. H. & Viergever, M. A.: Efficient and reliable schemes for nonlinear diffusion filtering. *IEEE Transactions on Image Processing* **7** (1998), 398–410.

[278] Weinan, E.: *Principles of Multiscale Modeling*. Cambridge University Press, New York, NY 2011.

[279] Wellmann, C. & Wriggers, P.: A two-scale model of granular materials. *Computer Methods in Applied Mechanics and Engineering* **205** (2012), 46–58.

[280] Weston, R. P.; Townsend, J. C.; Eidson, T. M. & Gates, R. L.: *A Distributed Computing Environment for Multidisciplinary Design*. NASA Langley Technical Report Server 1994, URL `http://www.ncstrl.org:8900/ncstrl/servlet/search?formname=detail\&id=oai%3ALTRS%3Aaiaa-94-4372`.

[281] Widlund, O. B.: A note on unconditionally stable linear multistep methods. *BIT Numerical Mathematics* **7** (1967), 65–70.

[282] Wohlmuth, B. I.: A mortar finite element method using dual spaces for the Lagrange multiplier. *SIAM Journal on Numerical Analysis* **38** (2000), 989–1012.

[283] Wrobel, L. C. & Aliabadi, M. H.: *The Boundary Element Method*. John Wiley & Sons, Chichester 2002.

[284] Yanenko, N. N.: *The Method of Fractional Steps*. Springer-Verlag, New York, NY 1971.

[285] Yang, B. & Pope, S. B.: An investigation of the accuracy of manifold methods and splitting schemes in the computational implementation of combustion chemistry. *Combustion and Flame* **112** (1998), 16–32.

[286] Yeh, K.-H. & Lu, H.-C.: Robust stability analysis for two-dimensional systems via eigenvalue sensitivity. *Multidimensional Systems and Signal Processing* **6** (1995), 223–236.

[287] Zienkiewicz, O. C.: Coupled problems and their numerical solution. In Lewis, R. W.; Bettess, P. & Hinton, E. (eds.): *Numerical Methods in Coupled Systems*. John Wiley & Sons, Chichester 1984, pp. 35–58.

[288] Zienkiewicz, O. C.; Paul, D. K. & Chan, A. H. C.: Unconditionally stable staggered solution procedure for soil-pore fluid interaction problems. *International Journal for Numerical Methods in Engineering* **26** (1988), 1039–1055.

[289] Zienkiewicz, O. C.; Qu, S.; Taylor, R. L. & Nakazawa, S.: The patch test for mixed formulations. *International Journal for Numerical Methods in Engineering* **23** (1986), 1873–1883.

[290] Zienkiewicz, O. C. & Taylor, R. L.: *The Finite Element Method. The Basis, Vol. 1*. Butterworth Heinemann, Oxford 2000.

Curriculum Vitae

Personal Data:

Name:	Seyedmohammad Zinatbakhsh
Date of birth:	22 August, 1980
Place of birth:	Shiraz, Iran
Nationality:	Iranian
Parents:	Seyedabdolreza Zibsiratbakhsh and Afsaneh Hashemi
Sibling:	Seyed Mansour Zinatbakhsh
Marital status:	married with Maryam Jamei

Education:

09/1986 – 06/1991	elementary school, Shiraz, Iran
09/1991 – 06/1994	middle school, Shiraz, Iran
09/1994 – 06/1998	high school, Shiraz, Iran
09/1998 – 07/2004	studies in mechanical engineering at the School of Mechanical Engineering, University of Shiraz, Iran
07/2004	degree: "Bachelor of Science (B. Sc.) in Mechanical Engineering"
09/2006 – 07/2008	studies in Computational Mechanics of Materials and Structures (COMMAS) at the Universität Stuttgart, Germany
07/2008	degree: "Master of Science (M. Sc.) in COMMAS"

Professional Occupation:

since 09/2008	teaching assistant and research associate at the Institute of Applied Mechanics (Civil Engineering), Universität Stuttgart, Germany

Temporary Stay Abroad:

04/2012 – 05/2012	University of Colorado at Boulder, CO, USA

Released Report Series

II-1 Gernot Eipper: *Theorie und Numerik finiter elastischer Deformationen in fluidgesättigten porösen Festkörpern*, 1998.

II-2 Wolfram Volk: *Untersuchung des Lokalisierungsverhaltens mikropolarer poröser Medien mit Hilfe der Cosserat-Theorie*, 1999.

II-3 Peter Ellsiepen: *Zeit- und ortsadaptive Verfahren angewandt auf Mehrphasenprobleme poröser Medien*, 1999.

II-4 Stefan Diebels: *Mikropolare Zweiphasenmodelle: Formulierung auf der Basis der Theorie Poröser Medien*, 2000.

II-5 Dirk Mahnkopf: *Lokalisierung fluidgesättigter poröser Festkörper bei finiten elastoplastischen Deformationen*, 2000.

II-6 Heiner Müllerschön: *Spannungs-Verformungsverhalten granularer Materialien am Beispiel von Berliner Sand*, 2000.

II-7 Stefan Diebels (Ed.): *Zur Beschreibung komplexen Materialverhaltens: Beiträge anläßlich des 50. Geburtstages von Herrn Prof. Dr.-Ing. Wolfgang Ehlers*, 2001.

II-8 Jack Widjajakusuma: *Quantitative Prediction of Effective Material Parameters of Heterogeneous Materials*, 2002.

II-9 Alexander Droste: *Beschreibung und Anwendung eines elastisch-plastischen Materialmodells mit Schädigung für hochporöse Metallschäume*, 2002.

II-10 Peter Blome: *Ein Mehrphasen-Stoffmodell für Böden mit Übergang auf Interface-Gesetze*, 2003.

II-11 Martin Ammann: *Parallel Finite Element Simulations of Localization Phenomena in Porous Media*, 2005.

II-12 Bernd Markert: *Porous Media Viscoelasticity with Application to Polymeric Foams*, 2005.

II-13 Saeed Reza Ghadiani: *A Multiphasic Continuum Mechanical Model for Design Investigations of an Effusion-Cooled Rocket Thrust Chamber*, 2005.

II-14 Wolfgang Ehlers & Bernd Markert (Eds.): *Proceedings of the 1st GAMM Seminar on Continuum Biomechanics*, 2005.

II-15 Bernd Scholz: *Application of a Micropolar Model to the Localization Phenomena in Granular Materials: General Model, Sensitivity Analysis and Parameter Optimization*, 2007.

II-16 Wolfgang Ehlers & Nils Karajan (Eds.): *Proceedings of the 2nd GAMM Seminar on Continuum Biomechanics*, 2007.

II-17 Tobias Graf: *Multiphasic Flow Processes in Deformable Porous Media under Consideration of Fluid Phase Transitions*, 2008.

II-18 Ayhan Acartürk: *Simulation of Charged Hydrated Porous Materials*, 2009.

II-19 Nils Karajan: *An Extended Biphasic Description of the Inhomogeneous and Anisotropic Intervertebral Disc*, 2009.

II-20 Bernd Markert: *Weak or Strong – On Coupled Problems In Continuum Mechanics*, 2010.

II-21 Wolfgang Ehlers & Bernd Markert (Eds.): *Proceedings of the 3rd GAMM Seminar on Continuum Biomechanics*, 2012.

II-22 Wolfgang Ehlers: *Poröse Medien – ein kontinuumsmechanisches Modell auf der Basis der Mischungstheorie*, 2012. Nachdruck der Habilitationsschrift aus dem Jahr 1989 (Forschungsberichte aus dem Fachbereich Bauwesen der Universität-GH-Essen **47**, Essen 1989).

II-23 Hans-Uwe Rempler: *Damage in multi-phasic Materials Computed with the Extended Finite-Element Method*, 2012.

II-24 Irina Komarova: *Carbon-Dioxide Storage in the Subsurface: A Fully Coupled Analysis of Transport Phenomena and Solid Deformation*, 2012.

II-25 Yousef Heider: *Saturated Porous Media Dynamics with Application to Earthquake Engineering*, 2012.

II-26 Okan Avci: *Coupled Deformation and Flow Processes of Partial Saturated Soil: Experiments, Model Validation and Numerical Investigations*, 2013.

II-27 Arndt Wagner: *Extended Modelling of the Multiphasic Human Brain Tissue with Application to Drug-Infusion Processes*, 2014.

II-28 Joffrey Mabuma: *Multi-Field Modelling and Simulation of the Human Hip Joint*, 2014.

II-29 Robert Krause: *Growth, Modelling and Remodelling of Biological Tissue*, 2014.

II-30 Seyedmohammad Zinatbakhsh: *Coupled Problems in the Mechanics of Multi-Physics and Multi-Phase Materials*, 2015.

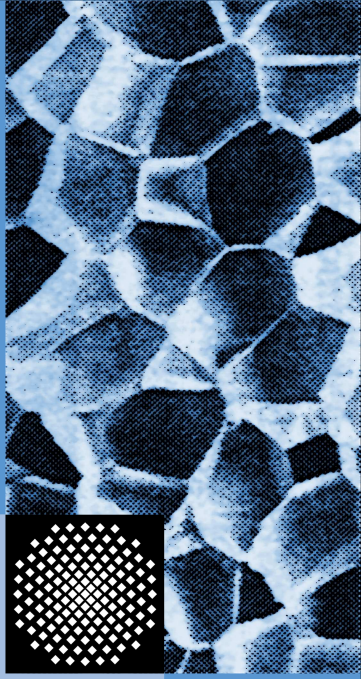

ISBN 978-3-937399-30-5
(D 93 – Dissertation, Universität Stuttgart)